

# JPTM

Journal of Pathology  
and Translational Medicine

May 2017  
Vol. 51 / No.3  
jpatholm.org  
pISSN: 2383-7837  
eISSN: 2383-7845



*Good Laboratory Standards  
for Clinical Next-Generation  
Sequencing Cancer Panel Tests*

*Molecular Testing of Brain  
Tumor, Lymphoproliferative  
Disorders, and Lung Cancers*

## Aims & Scope

The *Journal of Pathology and Translational Medicine* is an open venue for the rapid publication of major achievements in various fields of pathology, cytopathology, and biomedical and translational research. The Journal aims to share new insights into the molecular and cellular mechanisms of human diseases and to report major advances in both experimental and clinical medicine, with a particular emphasis on translational research. The investigations of human cells and tissues using high-dimensional biology techniques such as genomics and proteomics will be given a high priority. Articles on stem cell biology are also welcome. The categories of manuscript include original articles, review and perspective articles, case studies, brief case reports, and letters to the editor.

## Subscription Information

To subscribe to this journal, please contact the Korean Society of Pathologists/the Korean Society for Cytopathology. Full text PDF files are also available at the official website (<http://jpatholtm.org>). *Journal of Pathology and Translational Medicine* is indexed by Emerging Sources Citation Index (ESCI), PubMed, PubMed Central, Scopus, KoreaMed, KoMCI, WPRIM, Directory of Open Access Journals (DOAJ), and CrossRef. Circulation number per issue is 700.

## Editors-in-Chief

Hong, Soon Won, MD (Yonsei University, Korea)

Kim, Chong Jai, MD (University of Ulsan, Korea)

## Associate Editors

Jung, Chan Kwon, MD (The Catholic University of Korea, Korea)

Park, So Yeon, MD (Seoul National University, Korea)

Shin, Eunah, MD (CHA University, Korea)

Kim, Haeryoung, MD (Seoul National University, Korea)

## Editorial Board

Ali, Syed Z. (Johns Hopkins Hospital, U.S.A.)

Avila-Casado, Maria del Carmen (University of Toronto, Toronto General Hospital UHN, Canada)

Bae, Young Kyung (Yeungnam University, Korea)

Bongiovanni, Massimo (Centre Hospitalier Universitaire Vaudois, Switzerland)

Cho, Kyung-Ja (University of Ulsan, Korea)

Choi, Yeong-Jin (The Catholic University of Korea, Korea)

Choi, Yoo Duk (Chonnam National University, Korea)

Chung, Jin-Haeng (Seoul National University, Korea)

Gong, Gyungyub (University of Ulsan, Korea)

Fadda, Guido (Catholic University of the Sacred Heart, Italy)

Grignon, David J. (Indiana University, U.S.A.)

Ha, Seung Yeon (Gachon University, Korea)

Han, Jee Young (Inha University, Korea)

Jang, Se Jin (University of Ulsan, Korea)

Jeong, Jin Sook (Dong-A University, Korea)

Kang, Gyeong Hoon (Seoul National University, Korea)

Katoh, Ryohei (University of Yamaguchi, Japan)

Kerr, Keith M. (Aberdeen University Medical School, U.K.)

Kim, Aeree (Korea University, Korea)

Kim, Jang-Hee (Ajou University, Korea)

Kim, Jung Ho (Seoul National University, Korea)

Kim, Kyoung Mee (Sungkyunkwan University, Korea)

Kim, Kyu Rae (University of Ulsan, Korea)

Kim, Se Hoon (Yonsei University, Korea)

Kim, Woo Ho (Seoul National University, Korea)

Kim, Youn Wha (Kyung Hee University, Korea)

Ko, Young Hye (Sungkyunkwan University, Korea)

Koo, Ja Seung (Yonsei University, Korea)

Lee, C. Soon (University of Western Sydney, Australia)

Lee, Hye Seung (Seoul National University, Korea)

Lee, Kyung Han (Sungkyunkwan University, Korea)

Lee, Sug Hyoung (The Catholic University of Korea, Korea)

Lkhagvadorj, Sayamaa (Mongolian National University of Medical Sciences, Mongolia)

Moon, Woo Sung (Chonbuk University, Korea)

Ngo, Quoc Dat (Ho Chi Minh University of Medicine and Pharmacy, VietNam)

Park, Young Nyun (Yonsei University, Korea)

Ro, Jae Y. (Cornell University, The Methodist Hospital, U.S.A.)

Romero, Roberto (National Institute of Child Health and Human Development, U.S.A.)

Schmitt, Fernando (IPATIMUP [Institute of Molecular Pathology and Immunology of the University of Porto], Portugal)

Shahid, Pervez (Aga Khan University, Pakistan)

Sung, Chang Ohk (University of Ulsan, Korea)

Tan, Puay Hoon (National University of Singapore, Singapore)

Than, Nandor Gabor (Semmelweis University, Hungary)

Tse, Gary M. (Prince of Wales Hospital, Hongkong)

Vielh, Philippe (International Academy of Cytology Gustave Roussy Cancer Campus Grand Paris, France)

Wildman, Derek (University of Illinois, U.S.A.)

Yatabe, Yasushi (Aichi Cancer Center, Japan)

Yoon, Bo Hyun (Seoul National University, Korea)

Yoon, Sun Och (Yonsei University, Korea)

## Statistics Editors

Kim, Dong Wook (National Health Insurance Service Ilsan Hospital, Korea)

Lee, Hye Sun (Yonsei University, Korea)

## Manuscript Editor

Chang, Soo-Hee (InfoLumi Co., Korea)

## Contact the Korean Society of Pathologists/the Korean Society for Cytopathology

**Publishers:** Han Kyeom Kim, MD, Hye Kyoung Yoon, MD

**Editors-in-Chief:** Soon Won Hong, MD, Chong Jai Kim, MD

**Published by the Korean Society of Pathologists/the Korean Society for Cytopathology**

## Editorial Office

Room 1209 Gwanghwamun Officia, 92 Saemunan-ro, Jongno-gu,

Seoul 03186, Korea/#406 Lilla Swami Bldg, 68 Dongsan-ro,

Seocho-gu, Seoul 06784, Korea

Tel: +82-2-795-3094/+82-2-593-6943

Fax: +82-2-790-6635/+82-2-593-6944

E-mail: [office@jpatholtm.org](mailto:office@jpatholtm.org)

**Printed by** iMiS Company Co., Ltd. (JMC)

Jungang Bldg. 18-8 Wonhyo-ro 89-gil, Yongsan-gu, Seoul 04314, Korea

Tel: +82-2-717-5511 Fax: +82-2-717-5515 E-mail: [ml@smileml.com](mailto:ml@smileml.com)

**Manuscript Editing by** InfoLumi Co.

210-202, 421 Pangyo-ro, Bundang-gu, Seongnam 13522, Korea

Tel: +82-70-8839-8800 E-mail: [infolumi.chang@gmail.com](mailto:infolumi.chang@gmail.com)

Front cover image: Intravascular Large B-Cell Lymphoma with Concomitant Extravascular Central Nervous System (CNS) Involvement (Fig. 2, 3). p287-288.

© Copyright 2017 by the Korean Society of Pathologists/the Korean Society for Cytopathology

© Journal of Pathology and Translational Medicine is an Open Access journal under the terms of the Creative Commons Attribution Non-Commercial License (<http://creativecommons.org/licenses/by-nc/4.0>).

© This paper meets the requirements of KS X ISO 9706, ISO 9706-1994 and ANSI/NISO Z.39.48-1992 (Permanence of Paper).

This journal was supported by the Korean Federation of Science and Technology Societies Grant funded by the Korean Government.

## CONTENTS

---

### REVIEWS

- 191 **Good Laboratory Standards for Clinical Next-Generation Sequencing Cancer Panel Tests**  
Jihun Kim, Woong-Yang Park, Nayoung K. D. Kim, Se Jin Jang, Sung-Min Chun, Chang-Ohk Sung, Jene Choi, Young-Hyeh Ko, Yoon-La Choi, Hyo Sup Shim, Jae-Kyung Won, The Molecular Pathology Study Group of Korean Society of Pathologists
- 205 **Molecular Testing of Brain Tumor**  
Sung-Hye Park, Jaekyung Won, Seong-Ik Kim, Yujin Lee, Chul-Kee Park, Seung-Ki Kim, Seung-Hong Choi
- 224 **Molecular Testing of Lymphoproliferative Disorders: Current Status and Perspectives**  
Yoon Kyung Jeon, Sun Och Yoon, Jin Ho Paik, Young A Kim, Bong Kyung Shin, Hyun-Jung Kim, Hee Jeong Cha, Ji Eun Kim, Jooryung Huh, Young-Hyeh Ko, The Hematopathology Study Group of the Korean Society of Pathologists, The Molecular Pathology Study Group of Korean Society of Pathologists
- 242 **Molecular Testing of Lung Cancers**  
Hyo Sup Shim, Yoon-La Choi, Lucia Kim, Sunhee Chang, Wan-Seop Kim, Mee Sook Roh, Tae-Jung Kim, Seung Yeon Ha, Jin-Haeng Chung, Se Jin Jang, Geon Kook Lee, The Korean Cardiopulmonary Pathology Study Group, The Korean Molecular Pathology Study Group

### ORIGINAL ARTICLES

- 255 **Clinicopathological Study of 18 Cases of Inflammatory Myofibroblastic Tumors with Reference to ALK-1 Expression: 5-Year Experience in a Tertiary Care Center**  
Ramesh Babu Telugu, Anne Jennifer Prabhu, Nobin Babu Kalappurayil, John Mathai, Birla Roy Gnanamuthu, Marie Therese Manipadam
- 264 **Characteristic Changes in Decidual Gene Expression Signature in Spontaneous Term Parturition**  
Haidy El-Azzamy, Andrea Balogh, Roberto Romero, Yi Xu, Christopher Lajeunesse, Olesya Plazyo, Zhonghui Xu, Theodore G. Price, Zhong Dong, Adi L. Tarca, Zoltan Papp, Sonia S. Hassan, Tinnakorn Chaiworapongsa, Chong Jai Kim, Nardhy Gomez-Lopez, Nandor Gabor Than
- 284 **A Small Case Series of Intravascular Large B-Cell Lymphoma with Unexpected Findings: Subset of Cases with Concomitant Extravascular Central Nervous System (CNS) Involvement Mimicking Primary CNS Lymphoma**  
Kate Poropatich, Dave Dittmann, Yi-Hua Chen, Kirtee Raparia, Kristy Wolniak, Juehua Gao
- 292 **An Experimental Infarct Targeting the Internal Capsule: Histopathological and Ultrastructural Changes**  
Chang-Woo Han, Kyung-Hwa Lee, Myung Giun Noh, Jin-Myung Kim, Hyung-Seok Kim, Hyung-Sun Kim, Ra Gyung Kim, Jongwook Cho, Hyoung-Ihl Kim, Min-Cheol Lee

- 
- 306 **Overexpression of POSTN in Tumor Stroma Is a Poor Prognostic Indicator of Colorectal Cancer**  
Hyeon Jeong Oh, Jeong Mo Bae, Xian-Yu Wen, Nam-Yun Cho, Jung Ho Kim, Gyeong Hoon Kang
- 314 **Comparison of Unsatisfactory Samples from Conventional Smear versus Liquid-Based Cytology in Uterine Cervical Cancer Screening Test**  
Hoiseon Jeong, Sung Ran Hong, Seoung-Wan Chae, So-Young Jin, Hye Kyoung Yoon, Juhie Lee, Eun Kyung Kim, Sook Tai Ha, Sung Nam Kim, Eun-Jung Park, Jong Jae Jung, Sun Hee Sung, Sung-Chul Lim

## CASE REPORTS

- 320 **Unusual Histology of Eosinophilic Myenteric Ganglionitis: A Case Report**  
HyeKyung Lee, Dongwook Kang, Heejin Kim, ByungSun Cho, Jeho Jang
- 325 **Clear Cell Renal Cell Carcinoma with Intratumoral Granulomatous Reaction: A Case Report and Review of the Literature**  
Hayeon Kim, Jong Wook Kim, Aeree Kim, HyeYoon Chang
- 329 **Human Papillomavirus Infection–Associated Adenoid Cystic Carcinoma of the Hard Palate**  
Arthur Minwoo Chung, Dong Il Sun, Eun Sun Jung, Youn Soo Lee
- 332 **A Rare Case of Nodular Mucinosis of the Breast**  
Hyun Min Koh, Young Hee Maeng, Bo Geun Jang, Jae Hyuk Choi, Chang Lim Hyun
- 335 **Cerebellar Liponeurocytoma: Relevant Clinical Cytogenetic Findings**  
Alexander Tucker, Kritsanapol Boon-Unge, Nancy McLaughlin, Hassana Ibrahim, Nagesh Rao, Neil Martin, Richard Everson, Négar Khanlou

**Instructions for Authors** for *Journal of Pathology and Translational Medicine* are available at <http://jpatholtm.org/authors/authors.php>

## Good Laboratory Standards for Clinical Next-Generation Sequencing Cancer Panel Tests

Jihun Kim<sup>1,2\*</sup> · Woong-Yang Park<sup>3\*</sup>  
Nayoung K. D. Kim<sup>3</sup> · Se Jin Jang<sup>1,2</sup>  
Sung-Min Chun<sup>1,2</sup> · Chang-Ohk Sung<sup>1,2</sup>  
Jene Choi<sup>1</sup> · Young-Hyeh Ko<sup>4</sup>  
Yoon-La Choi<sup>4</sup> · Hyo Sup Shim<sup>5</sup>  
Jae-Kyung Won<sup>6</sup> · The Molecular  
Pathology Study Group of Korean  
Society of Pathologists

<sup>1</sup>Department of Pathology, Asan Medical Center, University of Ulsan College of Medicine, Seoul; <sup>2</sup>Center for Cancer Genome Discovery, Asan Institute for Life Sciences, Seoul; <sup>3</sup>Samsung Genome Institute, Sungkyunkwan University School of Medicine, Seoul; <sup>4</sup>Department of Pathology, Samsung Medical Center, Sungkyunkwan University School of Medicine, Seoul; <sup>5</sup>Department of Pathology, Yonsei University College of Medicine, Seoul; <sup>6</sup>Department of Pathology, Seoul National University College of Medicine, Seoul, Korea

Received: February 20, 2017  
Accepted: March 14, 2017

### Corresponding Author

Jihun Kim, MD, PhD  
Department of Pathology, Asan Medical Center,  
University of Ulsan College of Medicine, 88  
Olympic-ro 43-gil, Songpa-gu, Seoul 05505, Korea  
Tel: +82-2-3010-4556  
Fax: +82-2-472-7898  
E-mail: jihunkim@amc.seoul.kr

\*Jihun Kim and Woong-Yang Park contributed equally to this work as co-first authors.

Next-generation sequencing (NGS) has recently emerged as an essential component of personalized cancer medicine due to its high throughput and low per-base cost. However, no sufficient guidelines for implementing NGS as a clinical molecular pathology test are established in Korea. To ensure clinical grade quality without inhibiting adoption of NGS, a taskforce team assembled by the Korean Society of Pathologists developed laboratory guidelines for NGS cancer panel testing procedures and requirements for clinical implementation of NGS. This consensus standard proposal consists of two parts: laboratory guidelines and requirements for clinical NGS laboratories. The laboratory guidelines part addressed several important issues across multi-step NGS cancer panel tests including choice of gene panel and platform, sample handling, nucleic acid management, sample identity tracking, library preparation, sequencing, analysis and reporting. Requirements for clinical NGS tests were summarized in terms of documentation, validation, quality management, and other required written policies. Together with appropriate pathologist training and international laboratory standards, these laboratory standards would help molecular pathology laboratories to successfully implement NGS cancer panel tests in clinic. In this way, the oncology community would be able to help patients to benefit more from personalized cancer medicine.

**Key Words:** High-throughput nucleotide sequencing; Molecular pathology; Neoplasms; Quality control; Practice guidelines as topic

By virtue of completion of the human genome project, a set of technologies that are referred to as next-generation sequencing (NGS) has been developed.<sup>1,2</sup> Being able to sequence millions of short fragments of DNA simultaneously, NGS technologies have achieved unprecedented high-throughput and low per-base cost. The combination of its powerful analytic performances and the rapidly dropping cost of NGS rapidly brought NGS to clinic. However, the amount and complexity of sequencing data, especially for cancer genome sequencing, raised concerns

about the reliability of NGS cancer panels. Regarding this issue, several working groups, including the College of American Pathologists (CAP) or the American College of Medical Genetics and Genomics (ACMG), issued guidelines on NGS clinical tests.<sup>3,4</sup> Yet, there is no reliable guideline for NGS cancer panel tests that accommodates the regulatory environment in Korea. Considering that NGS-based testing is rapidly evolving and improving, the Molecular Pathology Study Group aimed to establish a necessary regulatory framework for clinical NGS

tests without inhibiting further upgrade of NGS-based technologies.

Unlike traditional single gene-based sequencing tests, the NGS cancer panel involves a complex two-step process: (1) wet bench process and (2) bioinformatics analysis of sequence data. The wet bench process includes the handling of patient samples, extraction of nucleic acids, fragmentation and barcoding, target enrichment, adaptor ligation, library preparation, and generation of sequence reads. Bioinformatics analysis includes mapping sequence reads to the human reference genome, variant calling, annotation, and reviewing data in the right clinical context. We regarded these two steps as distinct processes requiring separate standards because some laboratories might use external facilities to perform either portion of the NGS cancer panel tests. This report aims to provide a general guidance for developing more detailed NGS checklists, that will be done by a separate working group involving regulatory agencies in the near future.

## LABORATORY GUIDELINES FOR NEXT-GENERATION SEQUENCING CANCER PANEL TESTS

### Choice of genes to be tested and test platforms

Traditionally, only a limited number of clinically validated predictive or prognostic biomarkers have been approved as clinical tests. However, accumulating genomic data obtained from multiple tumor types and expansion of genome-based clinical trials suggest that many of the future anti-cancer treatments and clinical trials will require comprehensive diagnostic panels that allow the detection of multiple mutations at the same time. Such tests might involve either probe-based capture or primer-based amplification for the enrichment of genomic regions to be tested.

The number and scope of genes to be tested depend on the purpose of the test. If the purpose is limited to companion diagnostics for current standard care, the number of genes would be very limited. However, if there is a need for clinical trials for which NGS-based tests are required to stratify patients, a broader range of genes should be interrogated. In this context, the currently used cancer panel tests are mainly focused on clinically actionable genomic alterations at selected protein-coding regions that are defined by the availability of approved drugs and pathogenomic molecular features. However, there is an increasing need for adding genomic alterations associated with resistance to molecularly targeted therapies or predicted response to investigational drugs. Furthermore, genomic data could be used to

refine pathological diagnosis. For example, mutations in *IDH1* or *IDH2* and co-deletion of chromosome 1p and 19q are already incorporated in recently revised pathological diagnosis of diffuse glioma.<sup>5</sup>

There are several NGS platforms such as Illumina, Ion Torrent, and Roche 454, and all of which have been reported to be as reliable as the current standard genotyping tools at least for the important cancer genes provided that laboratories perform adequate quality control.<sup>6-8</sup> Thus, pathology laboratories may choose their preferred platforms based on their individual requirements, such as expected sample status (i.e., small biopsies, resected tissue samples, or liquid biopsies, etc.), expected number of samples, and/or types of variants to be analyzed (e.g., copy-number analysis might be limited in platforms that use primer-based amplification during target enrichment). It is important for laboratories to be aware of platform characteristics and perform adequate quality controls depending on the platform characteristics.

### Specimen handling

#### *Sample transportation, receipt, and storage*

Adequate processing of tissue samples is essential in a reliable NGS cancer panel test. Required specimen handling procedures are nearly the same as those required for traditional single-gene tests. Briefly, the quality and the amount of neutral buffered formalin relative to the size of the specimen should be monitored. The time interval from specimen acquisition to fixation should be minimized, and optimal fixation duration should be monitored.<sup>9</sup> The optimal fixation duration depends on the dimension of each sample because formalin penetrates tissue at a rate of approximately 1 mm per hour. The rule of thumb for recommended fixation duration for surgically resected specimen is 24 hours.<sup>10</sup>

#### *Morphological assessment and designation of ideal tumor area*

Correct pathologic diagnosis and assessment of the fraction of neoplastic cell nuclei in tumor area by pathologists are crucial for the interpretation of NGS results. Once the diagnosis and tumor purity are established, it is strongly recommended that the pathologists circle an area from which nucleic acid is extracted so that neoplastic cells are enriched to the appropriate level of tumor purity. The minimum requirement of tumor purity can be established in the initial validation of test performances (see "Validation" section). The estimated tumor purity of a selected area should be documented. When tumor purity is assessed, the

pathologists should be aware of the fact that the relative number of tumor cell nuclei reflects tumor purity rather than occupied tumor area. Thus, an area with heavy inflammatory cell infiltration should be avoided (Fig. 1A, B). Also, to ensure DNA quality, pathologists should try to avoid necrotic areas (Fig. 1C) and areas with extensive extracellular mucin (Fig. 1D).

#### Nucleic acid extraction, quantification, and storage

For clinical tests, DNA extraction kits should have a high level of performance specification to obtain DNA of sufficient quality and quantity for intended NGS tests from formalin-fixed paraffin embedded (FFPE) samples. In addition, DNA extraction procedures should have appropriate mechanisms by which sample contamination or misidentification could be avoided. Several commercially available kits that use silica-based or magnetic bead-based extraction protocols meet such require-

ments.

A major cause of sequence artifacts is deamination of cytosine resulting in C to T transitions during amplification.<sup>11-14</sup> Formalin fixation and longer storage period contribute to this process.<sup>15</sup> Since those sequence artifacts are usually present at a very low frequency, such artifacts are unlikely to affect test results if sufficient amounts of unique DNA molecules are available. However, if the DNA input amount is too small or if the purpose is to detect variants with low allelic fraction, these artifacts would be a problem. In addition, amplicon-based methods are more susceptible to these artifacts than hybridization capture-based methods.<sup>11</sup> Thus, laboratories may choose DNA extraction protocols with enzymatic removal of uracil-containing templates when they interrogate FFPE samples with highly fragmented DNA or with low tumor purity by amplicon-based methods. In the case of decalcified specimens, DNA quality or quantity is inferior to

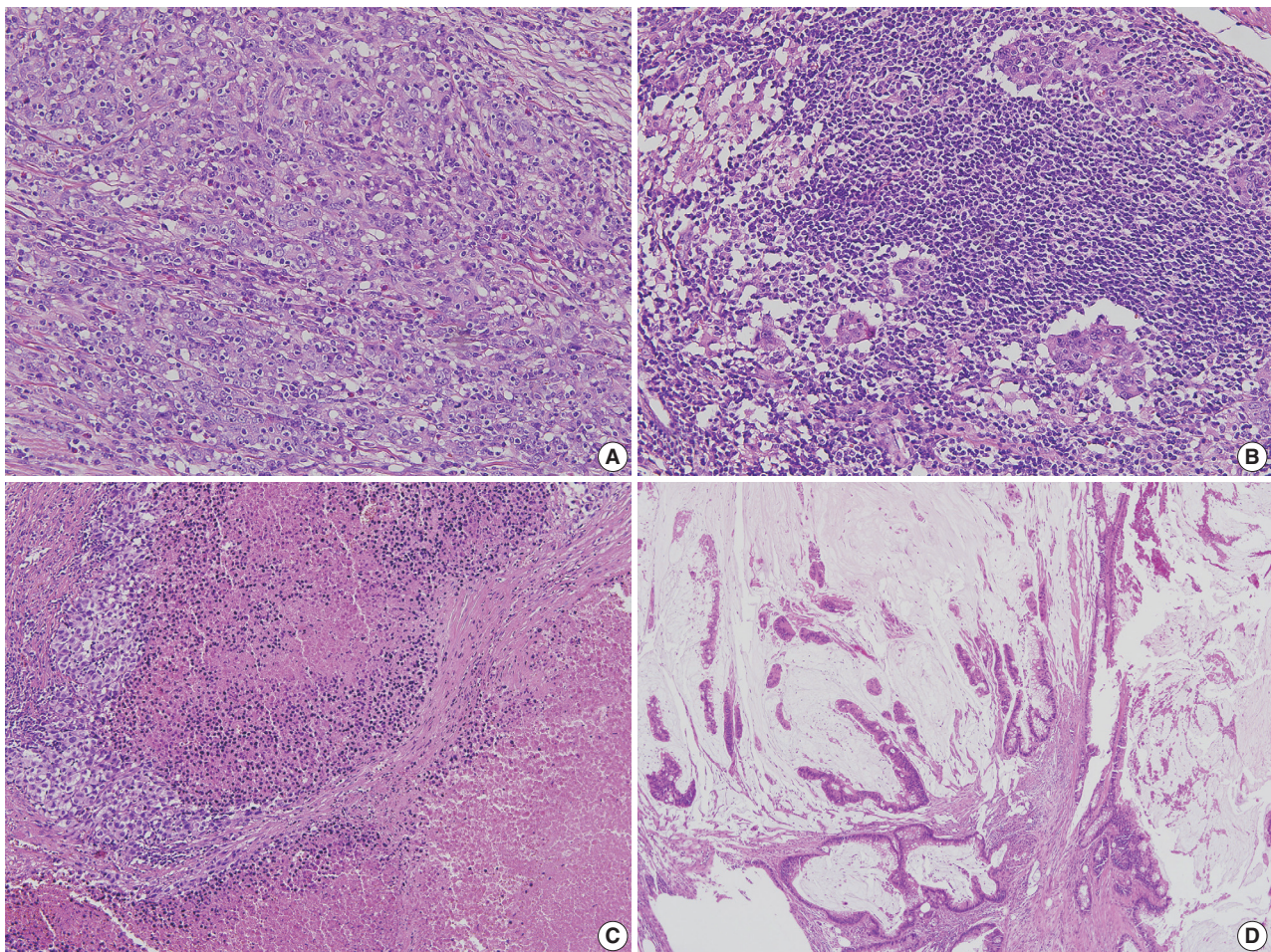


**Fig. 1.** Varying tissue conditions to be considered for next-generation sequencing analysis. (A) Gastric carcinoma with lymphoid stroma with acceptable tumor content although many intraepithelial lymphocytes are seen. (B) The same case as (A) but this area has unacceptable tumor content due to heavy lymphoid cell infiltration. (C) This poorly differentiated carcinoma shows extensive necrosis. (D) Mucinous adenocarcinoma of the colon shows a large area of extracellular mucin.

those of the specimens without decalcification. Regarding this, it has been reported that a decalcification protocol involving ethylenediaminetetraacetic acid might be better than that involving hydrochloric acid in terms of usable nucleic acid for subsequent NGS analysis.<sup>16</sup>

Quantitation of extracted nucleic acids can be done by Nano-Drop, Qubit, or the Picogreen method. Among them, Nano-Drop is not recommended because it also detects nucleic acids that are not suitable for downstream analyses. Nucleic acids should be stored under highly controlled conditions in order to maintain sample identity and integrity. Extracted DNA is to be stored at  $-20^{\circ}\text{C}$  and RNA at  $-80^{\circ}\text{C}$ . Sequencing libraries and polymerase chain reaction (PCR) products may be stored in  $-20^{\circ}\text{C}$  but should be separated from pre-amplification materials to prevent them from contaminating pre-amplification materials.

### Sample identity tracking

Like other single gene-based tests, verification of sample identity is the most basic and important aspect in clinical NGS test. The NGS cancer panel tests involve many steps, making them inherently subject to sample mix-up or swapping. Thus, test procedures should have an appropriate system to minimize such critical events. For example, panels could be designed to include a number of single nucleotide polymorphism (SNP) markers that allow molecular barcoding of patient samples<sup>17</sup> so that sample identity can be traced. In addition, an electronic laboratory information management system could be useful for this purpose. With any tool in place, it is important to enable end-to-end sample tracking in clinical NGS cancer panel tests.

### Library preparation

Library preparation is the step where extracted nucleic acids are prepared for the sequencing reaction. It involves DNA fragmentation, adaptor ligation, and enrichment of the target of interest. Target enrichment can be done either by an amplicon-based approach or by hybridization-based capture. Molecular barcodes are usually introduced to enable sample identification and pooling of multiple samples in a single flow cell lane. To avoid contamination, all steps before amplification should be done in a separate space. In addition, extra-caution should be in place during sample transportation from pre-PCR area to post-PCR area. After library preparation, appropriate quality controls should be applied to determine whether the rest of the procedures should be continued. Quality controls include quantitation, fragment size analysis, and quantitative PCR using adaptor sequences for priming.

### Data analysis of sequence reads

Bioinformatics pipelines used for the analysis of NGS data consists of multiple steps, such as de-multiplexing, read alignment, de-duplication, base calibration, variant calling, filtering, and annotation. Currently, no single “gold-standard” algorithm exists. Therefore, laboratories should choose the most suitable algorithm for the types of variants to be reported and optimize them. In the absence of a “gold standard,” it is important to validate the analytic performance of the bioinformatics pipelines.<sup>18-20</sup> It is also important to make sure that all versions of algorithms are traceable and properly updated (see “Validation” section).

### Sequencing read

The initial step after sequencing includes converting the base intensities in a sequencer to digital-level nucleotide sequences, called FASTQ. Although the types of signals differ among various sequencing platforms, most have their internal software for translating base calling into the compressed and de-multiplexed FASTQ files. The nucleotides in FASTQ have corresponding base quality scores that are in a form of logarithmic scales indicating the probabilistic confidence level of the bases. Appropriate quality control should be done to confirm the general integrity of the sequencing data, such as the total number of bases, sequence contents (including GC contents), per base sequence quality, etc. Read trimming is recommended if the base quality or composition does not meet the quality control threshold that each laboratory has empirically set up or that the sequencer manufacturer has recommended.

### Alignment

This step is to find where the short read sequences are located. In general, single or pair-end reads are first aligned (mapped) to a human genome reference. It is essential to include the version of the human reference sequence in the clinical report. Since poorly mapped sequences may lead to compromise the reliability of called variants, especially in solid tumors with low tumor content, sequencing reads should be filtered based on mapping quality score so that only confidently mapped reads are processed further. After the initial mapping, read duplicates should be removed, because unwanted clonal amplification of reads with sequence artifacts may lead to false-positive variant calls. Alignment is often challenging when the sequence reads come from genomic regions having large insertions or deletions, repetitive regions, pseudogenes, or homologous genes because there can be several other similar-looking genomic regions across the reference genome. Realignment using known references that

have the suspected insertions or deletions may be necessary in such cases.

*Variant calling: single nucleotide variation, insertion/deletion, copy-number variation, and translocation*

Somatic variants can be identified by subtracting variants found in non-neoplastic cells from those found in cancer. If a laboratory chooses not to sequence the corresponding normal samples, it should be noted that some germline variations might exist in the result. Laboratories should consider the implementation of modular analysis pipelines, in which different algorithms or settings are used to call different types of variants: single nucleotide variations (SNVs), insertion/deletion (Indels), copy-number variations (CNVs), and translocations.

*SNV/Indel*

The quality of variant calls is strongly related to the quality of alignment. The key challenge of variant calling is to distinguish real variants from sequencing errors. In general, the more times the variant is sequenced, the more reliable the variant call is. The minimum depth of coverage depends on the required sensitivity of the intended assay, the sequencing platform and the types of mutations to be detected. Although sensitivity is increased in proportion to sequencing depth, false-positive calls may also be increased especially in cases with low tumor content. There are various reasons for false-positive variant calls; they often result from PCR errors, sequencing errors, mis-mapped reads on repetitive sequences or homologous regions and so forth. Because each variant calling algorithm uses different strategies to filter out false calls, different algorithms sometimes generate discrepant results. Thus, laboratories should find optimal parameter settings during assay development and validation to minimize algorithm-dependent result variability.

Reliable identification of Indels is particularly challenging because sequence reads containing this type of variants are not often accurately mapped. Thus, the sensitivity and specificity for this type of variants is often reduced. With regard to this, laboratories should identify clinically important Indels and validate assay performances to establish reasonable sensitivity and positive predictive value for the identification of those Indels. Due to the high rate of false-positives, manual review by using visualization tools and comparison with the same regions in other samples on the same run is recommended for all Indel calls.

*Copy-number variation*

The reliable identification of CNV is quite difficult in NGS

cancer panel sequencing because of the uneven target coverage related to hybridization capturing steps, the absence of matched normal data, or the lack of coverage uniformity.<sup>21</sup> Although algorithms for detecting CNV in targeted NGS tests are improving,<sup>22</sup> the inherent limitations in cancer panel sequencing of clinical FFPE samples require robust validation of test performance. This type of validation can be done by testing characterized cancer cell lines or clinical samples with known CNV profiles (see “Validation” section),<sup>23</sup> although there is no agreement upon the minimal number of samples for appropriate validation.

*Translocation*

Translocation can be identified based on the DNA level, using discordant or split sequencing reads. However, the inherent limitations of short-reads in terms of alignment can result in many false positive calls. Therefore, the test performance should be appropriately validated using reference materials with known translocations across targeted genomic regions that have been confirmed by the current gold standard. Furthermore, it is highly recommended that all translocation calls be manually reviewed by using genome visualization tools such as the Integrative Genomics Viewer. Finally, it should be noted that a translocation can be missed if the breakpoint of fusion (may be somewhere in the introns not covered by the panel) is not included in targeted genomic regions, even though protein-coding regions of the translocation partners are included in the panel.

*Variant annotation and filtering*

Variant annotation determines if a sequence variant is real and provides predicted resulting amino acid changes. To identify true somatic variants, false variants should be properly filtered. Important sources of false variants include cytosine deamination, amplification errors, and sequencing errors. Cytosine deaminations are introduced *ex vivo*; these variants are not copied to the opposite strand, meaning that the artifacts are only present on one strand. To facilitate the detection of cytosine deamination artifacts, laboratories may use techniques such as molecular inversion probe and HaloPlex and Duplex sequencing, to enrich and sequence both the sense and antisense DNA strands.<sup>24</sup> Amplification errors can be introduced due to DNA polymerase errors during amplification steps of library enrichment. These errors might be minimized by the application of unique barcodes to individual DNA molecules during library enrichment. If the same variant is detected in multiple unique molecules, the variant might be real because it is unlikely that individual molecules acquire the same polymerase error during amplification. Sequenc-

ing errors are highly dependent on the sequencing platform and sequencing chemistry. The ability to call SNVs and Indels is known to be similarly accurate for data generated on the PGM and Illumina platform, provided that there is sufficient coverage.<sup>24</sup>

#### Interpretation of computational output

Depending on the types of variants (e.g., missense, nonsense, etc.) and the types of genes (e.g., hotspots in oncogenes vs randomly distributed mutations in tumor suppressor genes), interpretation of detected variants can be simple or quite complicated. Basically, the ACMG strongly recommends that interpretation is performed by trained staffs such as clinical molecular geneticists or molecular pathologists.<sup>4</sup> A multi-disciplinary sequencing data analysis team with various scientific backgrounds including clinical oncology, genomics, bioinformatics, and pathology, is recommended for accurate interpretation.

For variants that are not hotspot mutations, germline variants should be excluded first. Since most cancer panel tests do not analyze matched non-neoplastic tissue, laboratories should prepare mechanisms to filter out potential germline variants based on the genetic polymorphism data on the population to which the tested patient belongs. In most instances, laboratories use public databases on germline polymorphism such as the 1000 Genomes Project, ExAC, or dbSNP (Table 1), but ideally, these data should be derived from the same ethnic group as the tested patient.

Since the clinical and biological significance of cancer-related genomic variants are increasingly characterized, many variants detected in most cancer panel tests have related information in public databases (see “Reporting” section for details). However, previously uncharacterized variants may also be detected

considering the characteristics of NGS tests. Potential biological significance, or pathogenicity, could be inferred from the archived genotype-phenotype correlation data such as ClinVar, Human Gene Mutation Database, and Leiden Open Variation Database (Table 1). In addition, the *in silico* prediction of functional impacts is available in dbNSFP or Ensembl Variant Effector (Table 1). Since no single database is perfect, it is essential to refer to multiple resources for appropriate interpretation. Finally, knowledge about variants will be continuously improved with the accumulation of each lab’s experiences and feedbacks from clinicians.

## Reporting

#### General format

Reporting of NGS cancer panel test results should follow the general professional organizations’ recommendations and guidelines.<sup>25</sup> There are two major essential parts of a report: proper patient identification and detected actionable variants. The patient identification part is the same as that in the current standard single gene-based tests, but the detected variant part is more complex and sophisticated in clinical NGS cancer panel tests because typical NGS cancer panel tests detect multiple variants at the same time. The clinical NGS report should include the essential information listed in Table 2, and the most pertinent information, such as actionable variants and a critical summary of those variants, should be placed in a clearly visible section on the first page. Detected sequence variants should be annotated in concordance with the Human Genome Variation Society mutation nomenclature and the version of the human reference sequence to which sequence reads were aligned should also be

**Table 1.** Useful online resources for variant interpretation

Subject	Database/Algorithm	URL
Germline polymorphism	dbSNP, dbVar 1000 Genomes Project ExAC	<a href="https://www.ncbi.nlm.nih.gov/projects/SNP/">https://www.ncbi.nlm.nih.gov/projects/SNP/</a> <a href="http://browser.1000genomes.org/">http://browser.1000genomes.org/</a> <a href="http://exac.broadinstitute.org">http://exac.broadinstitute.org</a>
Cancer-specific somatic variants	COSMIC cBioPortal My Cancer Genome CIVIC Personalized Cancer Therapy, MD Anderson Cancer Center	<a href="http://cancer.sanger.ac.uk/cosmic">http://cancer.sanger.ac.uk/cosmic</a> <a href="http://www.cbioportal.org/">http://www.cbioportal.org/</a> <a href="https://www.mycancergenome.org/">https://www.mycancergenome.org/</a> <a href="https://civic.genome.wustl.edu/#/home">https://civic.genome.wustl.edu/#/home</a> <a href="https://pct.mdanderson.org/#/">https://pct.mdanderson.org/#/</a>
Genotype-phenotype association, not limited to cancer	ClinVar Human Gene Mutation Database Leiden Open Variation Database	<a href="https://www.ncbi.nlm.nih.gov/clinvar/">https://www.ncbi.nlm.nih.gov/clinvar/</a> <a href="http://www.hgmd.cf.ac.uk/ac/index.php">http://www.hgmd.cf.ac.uk/ac/index.php</a> <a href="http://www.lovd.nl/3.0/home">http://www.lovd.nl/3.0/home</a>
<i>In silico</i> functional prediction	dbNSFP (pre-computed <i>in silico</i> functional prediction and annotation of non-synonymous SNVs) Ensembl Variant Effector Predictor	<a href="http://sites.google.com/site/jpopgen/dbNSFP">http://sites.google.com/site/jpopgen/dbNSFP</a> <a href="http://www.ensembl.org/info/docs/tools/vep/index.html">http://www.ensembl.org/info/docs/tools/vep/index.html</a>

This list is not comprehensive and only provides some examples. All websites were last accessed on January 3, 2017.

ExAC, Exome Aggregation Consortium; COSMIC, Catalog of Somatic Mutations in Cancer; CIVIC, Clinical Interpretations of Variants in Cancer; NSFP, non-synonymous functional prediction; SNV, single nucleotide variation.

included in the report. Variants, which are not clinically actionable but are potentially useful for future practice, might follow the actionable variants. Then, detailed information about the detected variants (see the “Interpretation” section) and essential technical information, such as genes or genomic regions included in the panel and key quality control metrics, may be listed. Inclusion of granular details of technical information is not recommended, but a description of how clinicians can obtain the details may be included.<sup>26</sup>

#### Presentation of detected variants and clinical translation

Since typical cancer panel results include several cancer-related genomic variants with different levels of clinical or biological evidences, variants should be classified and reported according to the level of evidences. Several leading institutions use their own variant classification system and each institution may discuss with clinicians about which variant classification system should be used. However, a recently published related guideline is a good example<sup>27</sup>: (1) Tier 1, strong clinical significance such as Food and Drug Administration (FDA)–approved therapies, professional guidelines, prognostic and diagnostic markers based on well-powered studies with expert consensus; (2) Tier 2, potential clinical significance such as FDA-approved therapies for different tumor types, investigational therapies, prognostic and diagnostic markers based on small published studies with some consensus and preclinical trials or case reports without consensus; (3) Tier 3, unknown clinical significance; and (4) Tier 4, benign or likely benign. Tier 1 to 3 variants should be included in the clinical NGS report in a decreasing order of clinical significance and it is not recommended to include Tier 4 variants in clinical NGS report.

Interpretation of detected variants in terms of their clinical

impact and pathogenicity is a daunting task. As mentioned in the “Interpretation of computational output” section, many information sources such as public databases, published guidelines, and computational prediction algorithms should be integrated for proper interpretation. In addition to the previously mentioned public databases on germline polymorphism, *in silico* prediction of the functional impacts, genotype-phenotype relationship, and several cancer-specific mutation databases are available online (Table 1). These resources are very useful in the interpretation of variants in the context of cancer, but it is important to make sure that the database is properly curated, referenced and updated in a regular basis. Regarding this, FDA guidance suggested that appropriate databases should implement decision matrices with published details of each variant’s interpretation and have documented standard operating procedures (SOPs) for the curation and update of this information.<sup>28</sup>

When assigning variants to each tier, it is essential that they should be interpreted in the context of both variant details (e.g., *BRAF* V600E) and patient tumor type (e.g., malignant melanoma vs colorectal cancer). This is because different variants in a single gene may have different clinical impacts and the clinical significance of a particular variant may vary depending on the tumor type. For tier 1 variants, a clear statement on their clinical relevance and any appropriate action should be included. Also, it might be helpful to clarify the absence of other variants that are important in the patient tumor type. For tier 2 variants, advising the ordering physician about available clinical trials may be useful. In addition, tier information is subject to change as new evidences and therapeutic options are continuously emerging.

In cases where only limited interpretation can be made and full quality control standards could not be met, it is essential that pathologists make a professional judgment on whether the

**Table 2.** Information to be included in the clinical NGS report

Element	Example
Patient identification	Registration number, age, gender, ordering physician
Specimen type	FFPE, fresh frozen
Pathologic diagnosis	Lung adenocarcinoma, colorectal cancer
Tissue sample identification	Specimen number, block number
Important dates	Date on reception or on report
Percentage of tumor nuclei of the sample used	30%
Variants found	Variant details according to HGVS mutation nomenclature
Version of reference genome used	hg19 build 36
NGS method used	Amplicon-based or hybridization capture-based
Key quality control metrics	Mean target coverage, percentage of selected bases, duplication rate
Genes or genomic regions included in the panel	Exonic regions of gene A, B, C, etc.
Interpretation and summary	<i>EGFR</i> L858R variants predict response to <i>EGFR</i> tyrosine kinase inhibitors (Erlotinib or Gefitinib)

NGS, next-generation sequencing; FFPE, formalin-fixed paraffin embedded; HGVS, Human Genome Variation Society; *EGFR*, epidermal growth factor receptor.

result should be reported. Also, any limitation of the analysis should be clarified in the report. For example, negative results in samples with low neoplastic cell content at near or below the established sample rejection criteria should be accompanied by a note on potential false negatives. Furthermore, clinical NGS laboratories should have clearly defined protocols about when additional confirmatory tests should be advised, as well as performance validation data in cases where those confirmatory tests are not necessary.

## REQUIREMENTS FOR CLINICAL NEXT-GENERATION SEQUENCING LABORATORIES

### Wet Bench Analytic Process

#### *Documentation*

The detailed documentation of SOPs is critical for quality assurance of a complex, multi-step wet bench process. All SOPs of each step of the wet bench process must be documented so that each step can be traced. This includes documentation of all methods, reagents, instruments and controls (if applicable). Most of the documentations should be similar to those of current standard single gene testing, but those specific to NGS testing include detailed information regarding captured regions, such as genomic coordinates of captured probes and lists of genes and target enrichment protocols. Clinical laboratories that process different types of samples, such as FFPE samples or blood, should establish SOPs for each validated sample type. Metrics for quality control to assess run status must also be documented. Examples include mean target coverage, percentage of reads that map to target regions, and the fraction of bases meeting specified quality and coverage thresholds. Laboratories must define and document acceptance or rejection criteria for each step of the wet bench process, such as DNA extraction, library preparation, and sequencing.

#### *Validation*

Before testing patient samples, clinical NGS laboratories must establish the analytical validity of the intended tests. If the intended test is approved by the Ministry of Food and Drug Safety (MFDS), laboratories can verify the performance specifications established by the manufacturer. If the intended test is not approved by the MFDS, i.e., a laboratory-developed test, laboratories must establish performance characteristics such as accuracy, precision, sensitivity, specificity, and reportable range.

Because NGS cancer panel tests involve complex, multistep processes, each step needs to be empirically optimized to determine optimal assay conditions. Once those optimizations are done, an analytic validation should be performed for a whole test in a “beginning to end” fashion. Test performance should be separately validated for different types of samples, such as FFPE or blood.

For “beginning to end” validation, a number of samples should be analyzed to assess the test performance. There is no general agreement on how many samples are required for this type of validation. With regard to this issue, the CAP concluded that adding a minimum number of samples for validation is premature given the ongoing evolution of NGS technologies and the diversity of diagnostic applications.<sup>3</sup> Literature review revealed that the sample number for validation varied with a range of 20–80 samples.<sup>29–32</sup> The minimum number of samples needed for an appropriate validation might be affected by the size of the test, i.e., a larger gene panel will require more extensive validation, and by the range of samples to be tested, i.e., FFPE samples with variable tumor content. Here, we suggest the general principles of validation in terms of several important analytic performance parameters.

Considering the inherent characteristics of NGS cancer panel tests, it is important to evaluate as many different genomic regions as possible because sequence context can influence sequencing results. In addition, laboratories should determine analytic performances for all variant types relevant to the intended test (e.g., SNV, Indel, CNV, and translocations). Since NGS-based tests interrogate multiple variants at the same time, the validation of test performances involves two parts: method-specific (detection of as many variants as possible in a single sample) and analyte-specific (detection of a certain genomic variant in multiple samples). Laboratories can establish the test performances by combining those two approaches.

Accuracy validation is a “method-specific” way of validation. For this type of validation, laboratories might use well-characterized cancer cell line samples to interrogate whether the intended test accurately detects all known variants within the genomic regions covered by the panel. In this case, reference cell line samples should be periodically monitored for identity and passage number to prevent a significant genetic drift. In addition, laboratories might use well-characterized HapMap samples (NA12878 and NA19240), variants of which are readily available on the web.<sup>33,34</sup> Details of available reference materials are summarized in Table 3. Evaluation of these reference samples might be quite useful to validate the accuracy across a wide range of genomic

regions.<sup>23</sup> During this type of validation, an adequate depth of coverage threshold<sup>35</sup> necessary to accurately call all expected variants can be empirically established by plotting false-positives and false-negatives as a function of coverage.

Analytic sensitivity can be evaluated by comparing NGS test results with the current gold standard test results for known genetic variants in reference materials. To this end, laboratories may use historical controls such as accumulated clinical samples with well-characterized genomic variants by gold standard methods, provided that the gold standard tests were done in an appropriately accredited environment.

Analytic specificity is theoretically calculated by determining the fraction of test negatives (wild type sequence calls by the intended test) per true-negatives (samples that are known to have wild type sequences by the gold standard method). However, this concept often does not work well for NGS-based tests because too many potential variants are included in typical cancer panels. For most laboratories, it might be reasonable to leverage specificity by determining the average number of false-positive calls for the regions tested in a number of well-characterized clinical samples.

The limit of detection can be determined by cell line “mixing” experiments, in which a cell line with known genetic variants is serially diluted with another cell line without such variants to have different mixture ratios, which are then tested to determine whether the intended test accurately detects all specified variants under a certain coverage threshold. Alternatively, laboratories may determine the limit of detection by using the HapMap samples (NA12878 and NA19240) mentioned earlier by mixing them in various ratios and interrogating variants that differ between the two different HapMap samples.

Precision (repeatability for intra-run and reproducibility for inter-run variability) can be determined by repeating the same samples in the same run (repeatability) or by repeating the same sample in a different run (on a different day by a different operator). Ideally, testing at least three samples is recommended to adequately establish precision adequately.<sup>3</sup>

Any changes to a clinical NGS test, such as changes in instruments, specimen types, reagents, or software, require that performance specifications be re-established or be shown to be unchanged. For example, inclusion of new genes to an existing gene panel requires revalidation to make sure that new sequence variations are reliably detected without compromising the quality of the original assay. The extent of re-validation depends on the predicted influence on the test performance related to the change. For example, if only the bioinformatics pipeline is updated, it may not be necessary to re-validate all steps before data analysis.

#### Quality management

Clinical NGS laboratories should establish and follow a quality management plan. This plan should be integrated within the institution’s overall quality assurance program. Components of the NGS quality management program are not much different from the traditional single gene-based tests. Once laboratories establish an initial validation of test performances, laboratories must perform internal quality controls daily and external quality controls periodically. Each component of the quality assurance program specific to NGS cancer panel tests is discussed in detail below.

#### Internal quality assurance program

Recently, guidelines for quality control and recommenda-

**Table 3.** Reference materials for NGS: advantages and disadvantages

Type of material	Advantage	Disadvantage
Genomic DNA from cell line	Large amount available Similar complexity to patient’s DNA May have well-characterized variants	May have heterogeneity associated with cell line maintenance Possible genomic instability over time
Genomic DNA from patient’s sample	Identical condition to real samples	Not necessarily renewable Limited amount of DNA Well characterized genetic information may be limited
Synthetic DNA	Can synthesize a broad range of sequences and variations Can make sequence templates with complex regions (deletions or duplications) Large amount available	Does not represent actual human cancer genome May not perform as actual human cancer DNA due to differences in sequence complexity Will not cover all regions of tested genome May exhibit higher variant calls due to errors in synthesis
Electronic reference data files	Can engineer any wanted sequence files	Reference only for data analysis step Requires many reference datasets to mimick many types of sequence data Data files may not be interoperable among different platforms

Adapted by permission from Macmillan Publishers Ltd: [Nature Biotechnology] Gargis *et al.* 2012;30:1033-6,<sup>36</sup> copyright (2012). NGS, next-generation sequencing.

tions for the use of NGS in different applications have been published<sup>3,4,25,36-42</sup> and are summarized in Table 4. This guidance will work as a checklist for each component of the intended NGS test and related quality control metrics that require reviewing in order to feel confident about the quality of results. It is impractical to include multiple positive controls with different variant types during each run due to unacceptable cost and time. Instead, a single characterized external control with known variants in each run may be sufficient to demonstrate that the procedure is successful.<sup>36</sup> Typically, this can be done by preparing a number of DNA aliquots from a large FFPE sample block whose genome has already been well-characterized genomically and include those aliquots in each run of patient samples.

Externally and include those aliquots in each run of patient samples.

External quality assurance program: proficiency testing and alternate assessment

The Clinical Laboratory Improvement Amendment (CLIA) requires participation in a proficiency testing (PT) program twice a year for most clinical tests. For any clinical tests without such PT requirements, laboratories must verify test performance twice a year.<sup>24</sup> Since PT programs specific to NGS cancer panel tests do not currently exist, laboratories may verify their test performance by using alternate assessment (AA), where de-identified patient samples are exchanged and re-tested between

**Table 4.** Recommended items to check prior to releasing NGS results for diagnostic use and QC metrics

Item	Checklist	Consequences of non-conformity	Improvement suggestions
Tissue sample adequacy	Criteria for inadequate specimen Minimum tumor content Appropriate sample handling including fixation and transportation	Testing inadequate specimens may lead to a waste of time and money or depletion of available samples. Inadequate amount or tumor content can lead to false-negative test results.	Check sample adequacy rigorously before testing. Request further sampling in case of inadequate samples.
Nucleic acid extraction	DNA quantity and quality in terms of amplifiable DNA	DNA with suboptimal quality may inhibit sequencing reaction. Small amount or fragmentation of DNA may lead to poor quality sequencing data with insufficient or uneven coverage and/or high duplication rate.	Failed samples should be reported as such and further material might be requested with specified requirement. Trying another validated extraction method may often helps.
Sample identification	Sample identity tracking throughout all steps	Misidentification of samples could lead to incorrect patient management.	If there is any concern about sample identity, starting over from DNA extraction may be necessary. Introduction of polymorphic SNP markers into gene panel and running another genotyping method with the same marker set might be helpful.
Library preparation	Minimum library concentration	Poor sequencing library may lead to insufficient or uneven coverage. Libraries with poor complexity or bias may result in false-negatives. False-positives may also occur due to potential amplification bias.	Consider modification of library preparation method or an alternative method to verify any uncertain results.
Sequencing	Criteria for minimum sequencing depth and other quality metrics (% reads mapped to target regions, % of targets with specified coverage, duplication rate)	Inadequate coverage is associated with higher levels of uncertainty of the test results. Genomic regions with insufficient local coverage may lead to inaccurate results for variants located in those regions.	Repeat sequencing with existing library or start over from DNA extraction step. Verification of uncertain results with another method may be helpful, especially, in case of actionable variants.
Variant detection and review	Variant allele frequency, local sequencing depth and quality score Presence of the same variant in forward and reverse strands Mapping quality of sequencing reads Potential sequencing artifacts	Failure to filter out sequencing artifacts may lead to false-positive results. Clinically important variants may sometimes be missed.	Manually review of clinically important variants even if computational algorithms called no mutation on them. Any ambiguous or unexpected results should be reviewed by laboratory scientists and pathologists. Verify variants with another method, if applicable.
Bioinformatics	Correct pipeline and version Appropriate version and build of human reference sequence Cross-contamination?	Using outdated or inadequate software can lead to false-positive or false-negative results.	Update software on a regular basis.
Reporting	Endorsed by an authorized competent pathologist?	Variants with clinical significance may be reported erroneously, leading to inappropriate treatment.	Responsible pathologists should be given enough time and opportunities for education and training.

NGS, next-generation sequencing; QC, quality control.

different laboratories until formal PT programs are set.<sup>24</sup> A Korean guideline published by the MFDS follows the same principle and requires documentation of all procedures related to PT or AA.<sup>45</sup> There is no general agreement upon the number of reference materials per one round of PT or AA but analysis of two samples has been recommended.<sup>36</sup>

#### *Policies: confirmatory testing, laboratory records, upgrades*

As NGS cancer panel tests with appropriate quality controls are reported to meet a clinical grade performance,<sup>23,44-47</sup> routine confirmatory testing is not recommended. However, laboratories should have a policy that clearly documents both any indication for confirmatory testing as well as any performance validation data upon which they decided that such confirmatory testing is not necessary. In addition, the CAP is flexible regarding the methods used for any needed confirmatory testing.

Keeping comprehensive laboratory records is essential in monitoring complex, multi-step NGS cancer panel tests. In this regard, such records should be maintained in such a way that all detailed information about test procedures including reagents, sequencing runs, wet lab, and bioinformatics procedures and responsible technicians is traceable. While all details need not be included in the clinical report, laboratories should maintain a database from which detailed information regarding the analysis of individual specimen can be obtained.

Laboratories must be prepared for upgrades to make sure that they are not using obsolete methods. A policy for the upgrade of instruments, sequencing chemistries, and reagents or kits, as well as subsequent post-upgrade validation of test performances should be in place. The policy may include specified intervals for upgrade and required validation processes, depending on the type or extent of upgrade.

## Bioinformatics process

### *Documentation*

Laboratories should document all bioinformatics processes, including all data files, variant caller's parameters, and versions of the bioinformatics algorithms. Sources and versions of all bioinformatics algorithms should be documented and updated properly. Quality control information on bioinformatics analysis, such as the cut-off of read depth, base quality score, and mapping quality, should also be documented.

### *Validation and quality management*

General validation principles were already discussed in the

Validation portion of the “Wet Bench Analytic Process” section. Briefly, for bioinformatics pipelines, laboratories should iteratively find parameters for optimal performance of computational algorithms before applying it to the lab process. Once the pipeline is initially validated, variations between sequencing runs should be monitored daily. Principles of the quality management were already discussed in the “Wet Bench Analytic Process” section. In short, laboratories should monitor any deviation from established performance characteristics in terms of quality metrics and analysis results. For any deviation, laboratories should document the investigational measures and corrective actions made to resolve the deviation. Essential quality metrics for bioinformatics performance verification include depth of coverage, uniformity of coverage and base call quality scores. In addition, GC bias, proportion of reads that map to nontargeted regions, and percentage of duplicated reads could also be used to monitor performances of sequencing reaction and subsequent bioinformatics analyses (Table 5).

### *Policies: upgrades, storage, and data management*

The bioinformatics pipeline should be revalidated upon any changes in operating systems, software, or overall pipelines, which may otherwise affect its analytic performance. Since a huge amount of data files are generated from the bioinformatics pipeline, it is impractical to store all sorts of files considering the significant cost. Instead, the CAP NGS workgroup recommended that some important file formats, such as FASTQ, BAM, and VCF, should be stored for quality controls or investigational use.<sup>3</sup> There is no general agreement on the required storage period, but it is important for laboratories to set their own storage policies in accordance with local or national requirements (if any) and inform clients of those policies.

## CONCLUSION

Although the advancement of NGS technologies unraveled the genomic landscape of human malignancies and opened an era of genome-guided anti-cancer therapies, the complexity of NGS technologies made it especially difficult to set up regulatory or professional standards for assuring analytical validity of test results. In this report, the workgroup addressed general guidelines related to the test procedures and proposed requirements for clinical NGS cancer panel tests such as test validation, quality controls, reference materials and participation in PT or AA. Due to space limitations and the clinical implementation of NGS cancer panel tests being in its infancy, granular

**Table 5.** Metrics needed to validate and monitor performances of NGS sequencing runs and bioinformatics pipeline

Quality metrics	General considerations upon validation	Actions to be considered during quality controls
Depth of coverage	Minimum coverage threshold required for desired sensitivity and specificity across targeted regions should be established.	When the coverage threshold could not be met in a suspicious variant call, additional validation by an alternate method (e.g., Sanger sequencing) should be considered.
Uniformity of coverage	Coverage across targeted regions should be as uniform as possible to produce reliable results across all targeted genomic regions.	Uniformity of coverage often decreases with samples having low DNA amount or highly degraded DNA. When coverage uniformity significantly deviates from that established during initial validation, this may indicate potential analytical errors.
GC bias	GC content affects the efficiency of the sequencing reactions and will affect the uniformity of coverage. The amount of GC bias should be established across the targeted genomic regions.	GC bias should be monitored in every run to detect any change in test performance.
Base call quality scores	Informatics filters should be in place to eliminate any reads having a base call quality score below the acceptable quality score.	Quality scores are not readily comparable from one sequencing platform to another.
Mapping quality	During validation, it is important to make sure that the test analyzes the reads that map specifically to the targeted genomic regions. Informatics filters should be in place to eliminate any reads that map to non-targeted regions.	The proportion of reads that do not map to targeted regions should be monitored during each run. Poor mapping quality may come from non-specific amplification, capture of off-target DNA, or contamination.
Proportion of duplicated reads	Informatics filters should be in place to eliminate duplicate reads resulting from clonal amplification during alignment.	The amount of duplicate reads should be monitored to prevent skewing of allelic fractions.

Adapted by permission from Macmillan Publishers Ltd: [Nature Biotechnology] Gargis *et al.* 2012;30:1033-6,<sup>36</sup> copyright (2012). NGS, next-generation sequencing.

details were not covered in this review and those details should be addressed in further publications.

As clinical experiences accumulate and technologies evolve, more refined recommendations or guidelines could be published in the near future. In addition, good clinical decision support systems or knowledge bases need to be developed to help patients in terms of benefits from personalized FDA-approved or investigational therapies and prognostic information. To realize personalized cancer medicine in the end, it is important for medical communities to share information on genotype (oncogenic variants in patients' samples)–phenotype (drug response or prognosis) relationships, and all these efforts start with accurate genomic profiling of cancer tissue. To ensure reliability of NGS-based genomic profiling, a multi-disciplinary team approach, involving clinicians, pathologists, laboratory scientists, bioinformaticians, manufacturers, professional organizations, and government agencies, is essential.

### Conflicts of Interest

No potential conflict of interest relevant to this article was reported.

### Acknowledgments

The study was supported by a grant from Ministry of Food and Drug Safety, Republic of Korea, in 2016 (grant No. 16173

MFDS004; to W.-Y.P.).

The study was supported by the Korean Society of Pathologists Grant (2016).

## REFERENCES

- Bentley DR, Balasubramanian S, Swerdlow HP, *et al.* Accurate whole human genome sequencing using reversible terminator chemistry. *Nature* 2008; 456: 53-9.
- Metzker ML. Sequencing technologies: the next generation. *Nat Rev Genet* 2010; 11: 31-46.
- Aziz N, Zhao Q, Bry L, *et al.* College of American Pathologists' laboratory standards for next-generation sequencing clinical tests. *Arch Pathol Lab Med* 2015; 139: 481-93.
- Rehm HL, Bale SJ, Bayrak-Toydemir P, *et al.* ACMG clinical laboratory standards for next-generation sequencing. *Genet Med* 2013; 15: 733-47.
- Louis DN, Ohgaki H, Wiestler OD, Cavenee WK. WHO classification of tumours of the central nervous system. Revised 4th ed. Lyon: IARC Press, 2016.
- Burghel GJ, Hurst CD, Watson CM, *et al.* Towards a next-generation sequencing diagnostic service for tumour genotyping: a comparison of panels and platforms. *Biomed Res Int* 2015; 2015: 478017.
- Hinrichs JW, van Blokland WT, Moons MJ, *et al.* Comparison of next-generation sequencing and mutation-specific platforms in

- clinical practice. *Am J Clin Pathol* 2015; 143: 573-8.
8. McCourt CM, McArt DG, Mills K, *et al.* Validation of next generation sequencing technologies in comparison to current diagnostic gold standards for *BRAF*, *EGFR* and *KRAS* mutational analysis. *PLoS One* 2013; 8: e69604.
  9. Hicks DG, Boyce BF. The challenge and importance of standardizing pre-analytical variables in surgical pathology specimens for clinical care and translational research. *Biotech Histochem* 2012; 87: 14-7.
  10. Howat WJ, Wilson BA. Tissue fixation and the effect of molecular fixatives on downstream staining procedures. *Methods* 2014; 70: 12-9.
  11. Do H, Dobrovic A. Sequence artifacts in DNA from formalin-fixed tissues: causes and strategies for minimization. *Clin Chem* 2015; 61: 64-71.
  12. Do H, Wong SQ, Li J, Dobrovic A. Reducing sequence artifacts in amplicon-based massively parallel sequencing of formalin-fixed paraffin-embedded DNA by enzymatic depletion of uracil-containing templates. *Clin Chem* 2013; 59: 1376-83.
  13. Lin MT, Mosier SL, Thiess M, *et al.* Clinical validation of *KRAS*, *BRAF*, and *EGFR* mutation detection using next-generation sequencing. *Am J Clin Pathol* 2014; 141: 856-66.
  14. Serizawa M, Yokota T, Hosokawa A, *et al.* The efficacy of uracil DNA glycosylase pretreatment in amplicon-based massively parallel sequencing with DNA extracted from archived formalin-fixed paraffin-embedded esophageal cancer tissues. *Cancer Genet* 2015; 208: 415-27.
  15. Marchetti A, Felicioni L, Buttitta F. Assessing *EGFR* mutations. *N Engl J Med* 2006; 354: 526-8.
  16. Choi SE, Hong SW, Yoon SO. Proposal of an appropriate decalcification method of bone marrow biopsy specimens in the era of expanding genetic molecular study. *J Pathol Transl Med* 2015; 49: 236-42.
  17. Pengelly RJ, Gibson J, Andreoletti G, Collins A, Mattocks CJ, Ennis S. A SNP profiling panel for sample tracking in whole-exome sequencing studies. *Genome Med* 2013; 5: 89.
  18. Brownstein CA, Beggs AH, Homer N, *et al.* An international effort towards developing standards for best practices in analysis, interpretation and reporting of clinical genome sequencing results in the CLARITY Challenge. *Genome Biol* 2014; 15: R53.
  19. Cornish A, Guda C. A comparison of variant calling pipelines using genome in a bottle as a reference. *Biomed Res Int* 2015; 2015: 456479.
  20. Hwang S, Kim E, Lee I, Marcotte EM. Systematic comparison of variant calling pipelines using gold standard personal exome variants. *Sci Rep* 2015; 5: 17875.
  21. Teo SM, Pawitan Y, Ku CS, Chia KS, Salim A. Statistical challenges associated with detecting copy number variations with next-generation sequencing. *Bioinformatics* 2012; 28: 2711-8.
  22. Onsongo G, Baughn LB, Bower M, *et al.* CNV-RF is a random forest-based copy number variation detection method using next-generation sequencing. *J Mol Diagn* 2016; 18: 872-81.
  23. Frampton GM, Fichtenholtz A, Otto GA, *et al.* Development and validation of a clinical cancer genomic profiling test based on massively parallel DNA sequencing. *Nat Biotechnol* 2013; 31: 1023-31.
  24. Deans ZC, Costa JL, Cree I, *et al.* Integration of next-generation sequencing in clinical diagnostic molecular pathology laboratories for analysis of solid tumours; an expert opinion on behalf of IQN Path ASBL. *Virchows Arch* 2017; 470: 5-20.
  25. ISO 15189: 2012 Medical laboratories: requirements for quality and competence [Internet]. Geneva: International Organization for Standardization, c2012-2017 [cited 2017 Jan 31]. Available from: <https://www.iso.org/obp/ui/#iso:std:iso:15189:ed-3:v2:en>.
  26. Nomenclature for the description of sequence variants [Internet]. Melbourne: Human Genome Variation Society, c2010-2017 [cited 2017 Jan 31]. Available from: <http://www.hgvs.org/mutnomen/>.
  27. Li MM, Datto M, Duncavage EJ, *et al.* Standards and guidelines for the interpretation and reporting of sequence variants in cancer: a joint consensus recommendation of the Association for Molecular Pathology, American Society of Clinical Oncology, and College of American Pathologists. *J Mol Diagn* 2017; 19: 4-23.
  28. Use of standards in FDA regulatory oversight of next generation sequencing (NGS)-based in vitro diagnostics (IVDs) used for diagnosing germline diseases [Internet]. Rockville: US Department of Health and Services, Food and Drug Administration, c2016-2017 [cited 2017 Jan 31]. Available from: <http://www.fda.gov/downloads/MedicalDevices/DeviceRegulationandGuidance/GuidanceDocuments/UCM509838.pdf>.
  29. Chin EL, da Silva C, Hegde M. Assessment of clinical analytical sensitivity and specificity of next-generation sequencing for detection of simple and complex mutations. *BMC Genet* 2013; 14: 6.
  30. Cottrell CE, Al-Kateb H, Bredemeyer AJ, *et al.* Validation of a next-generation sequencing assay for clinical molecular oncology. *J Mol Diagn* 2014; 16: 89-105.
  31. Hagemann IS, Cottrell CE, Lockwood CM. Design of targeted, capture-based, next generation sequencing tests for precision cancer therapy. *Cancer Genet* 2013; 206: 420-31.
  32. Williams ES, Hegde M. Implementing genomic medicine in pathology. *Adv Anat Pathol* 2013; 20: 238-44.
  33. Zook JM, Chapman B, Wang J, *et al.* Integrating human sequence data sets provides a resource of benchmark SNP and indel genotype calls. *Nat Biotechnol* 2014; 32: 246-51.

34. National Center for Biotechnology Information. GeT-RM Homo sapiens [Internet]. Bethesda: US National Library of Medicine, c2017 [cited 2017 Jan 31]. Available from: <https://www.ncbi.nlm.nih.gov/variation/tools/get-rm/>.
35. Ajay SS, Parker SC, Abaan HO, Fajardo KV, Margulies EH. Accurate and comprehensive sequencing of personal genomes. *Genome Res* 2011; 21: 1498-505.
36. Gargis AS, Kalman L, Berry MW, *et al.* Assuring the quality of next-generation sequencing in clinical laboratory practice. *Nat Biotechnol* 2012; 30: 1033-6.
37. Gargis AS, Kalman L, Bick DP, *et al.* Good laboratory practice for clinical next-generation sequencing informatics pipelines. *Nat Biotechnol* 2015; 33: 689-93.
38. Association for Molecular Pathology. Clinical practice guidelines [Internet]. Bethesda: Association for Molecular Pathology, c2009-2017 [cited 2017 Jan 31]. Available from: [https://www.amp.org/committees/clinical\\_practice/AMPclinicalpracticeguidelines.cfm](https://www.amp.org/committees/clinical_practice/AMPclinicalpracticeguidelines.cfm).
39. ESMO clinical practice guidelines [Internet]. Viganello-Lugano: European Society for Medical Oncology, c2017 [cited 2017 Jan 31]. Available from: <http://www.esmo.org/Guidelines>.
40. Cree IA, Deans Z, Ligtenberg MJ, *et al.* Guidance for laboratories performing molecular pathology for cancer patients. *J Clin Pathol* 2014; 67: 923-31.
41. Luthra R, Chen H, Roy-Chowdhuri S, Singh RR. Next-generation sequencing in clinical molecular diagnostics of cancer: advantages and challenges. *Cancers (Basel)* 2015; 7: 2023-36.
42. Schrijver I, Aziz N, Farkas DH, *et al.* Opportunities and challenges associated with clinical diagnostic genome sequencing: a report of the Association for Molecular Pathology. *J Mol Diagn* 2012; 14: 525-40.
43. Next generation sequence analysis (NGS). Clinical laboratory certification guidelines [Internet]. Cheongju: Ministry of Food and Drug Safety, c2016 [cited 2017 Jan 31]. Available from: <http://www.mfds.go.kr/index.do?mid=1161&seq=11001&cmd=v>.
44. Cheng DT, Mitchell TN, Zehir A, *et al.* Memorial Sloan Kettering-Integrated Mutation Profiling of Actionable Cancer Targets (MSK-IMPACT): a hybridization capture-based next-generation sequencing clinical assay for solid tumor molecular oncology. *J Mol Diagn* 2015; 17: 251-64.
45. Fisher KE, Zhang L, Wang J, *et al.* Clinical validation and implementation of a targeted next-generation sequencing assay to detect somatic variants in non-small cell lung, melanoma, and gastrointestinal malignancies. *J Mol Diagn* 2016; 18: 299-315.
46. Pritchard CC, Salipante SJ, Koehler K, *et al.* Validation and implementation of targeted capture and sequencing for the detection of actionable mutation, copy number variation, and gene rearrangement in clinical cancer specimens. *J Mol Diagn* 2014; 16: 56-67.
47. Sikkema-Raddatz B, Johansson LF, de Boer EN, *et al.* Targeted next-generation sequencing can replace Sanger sequencing in clinical diagnostics. *Hum Mutat* 2013; 34: 1035-42.

## Molecular Testing of Brain Tumor

Sung-Hye Park<sup>1,2</sup> · Jaekyung Won<sup>1</sup>  
Seong-Ik Kim<sup>1</sup> · Yujin Lee<sup>1</sup>  
Chul-Kee Park<sup>3</sup> · Seung-Ki Kim<sup>3</sup>  
Seung-Hong Choi<sup>4</sup>

<sup>1</sup>Department of Pathology, <sup>2</sup>Neuroscience Institute, Departments of <sup>3</sup>Neurosurgery and <sup>4</sup>Radiology, Seoul National University, College of Medicine, Seoul, Korea

Received: February 19, 2017  
Accepted: March 8, 2017

### Corresponding Author

Sung-Hye Park, MD, PhD  
Department of Pathology, Seoul National University Hospital, Seoul National University College of Medicine, 103 Daehak-ro, Jongno-gu, Seoul 03080, Korea  
Tel: +82-2-2072-3090  
Fax: +82-2-743-5530  
E-mail: shparknp@snu.ac.kr

The World Health Organization (WHO) classification of central nervous system (CNS) tumors was revised in 2016 with a basis on the integrated diagnosis of molecular genetics. We herein provide the guidelines for using molecular genetic tests in routine pathological practice for an accurate diagnosis and appropriate management. While astrocytomas and IDH-mutant (secondary) glioblastomas are characterized by the mutational status of *IDH*, *TP53*, and *ATRX*, oligodendrogliomas have a 1p/19q codeletion and mutations in *IDH*, *CIC*, *FUBP1*, and the promoter region of telomerase reverse transcriptase (*TERTp*). IDH-wildtype (primary) glioblastomas typically lack mutations in *IDH*, but are characterized by copy number variations of *EGFR*, *PTEN*, *CDKN2A/B*, *PDGFRA*, and *NF1* as well as mutations of *TERTp*. High-grade pediatric gliomas differ from those of adult gliomas, consisting of mutations in *H3F3A*, *ATRX*, and *DAXX*, but not in *IDH* genes. In contrast, well-circumscribed low-grade neuroepithelial tumors in children, such as pilocytic astrocytoma, pleomorphic xanthoastrocytoma, and ganglioglioma, often have mutations or activating rearrangements in the *BRAF*, *FGFR1*, and *MYB* genes. Other CNS tumors, such as ependymomas, neuronal and glioneuronal tumors, embryonal tumors, meningothelial, and other mesenchymal tumors have important genetic alterations, many of which are diagnostic, prognostic, and predictive markers and therapeutic targets. Therefore, the neuropathological evaluation of brain tumors is increasingly dependent on molecular genetic tests for proper classification, prediction of biological behavior and patient management. Identifying these gene abnormalities requires cost-effective and high-throughput testing, such as next-generation sequencing. Overall, this paper reviews the global guidelines and diagnostic algorithms for molecular genetic testing of brain tumors.

**Key Words:** Brain neoplasms; Molecular biology; Next generation sequencing; Pathological diagnosis

The central nervous system (CNS) tumors are those of the brain and spinal cord including the meninges, pituitary gland, pineal gland, and nerves according to the 3rd edition of the International Classification of Diseases for Oncology (ICD-O-3) (<http://codes.iarc.fr/>). The incidence rate of all primary malignant and nonmalignant CNS tumors in the United States was 22.36 cases per 100,000 (5.67/100,000 for 0–14 years, 5.71/100,000 for 0–19 years) according to the U.S. Central Brain Tumor Registry (CBTRUS; <http://www.cbtrus.org/factsheet/factsheet.html>). The proportion of women with CNS tumors is higher than that of men (1.2:1). In the United States, the number of newly diagnosed primary malignant and nonmalignant CNS tumors is expected to reach 79,270 (26,070 cases of primary malignant and 53,200 cases of nonmalignant tumors) by 2017. The average annual mortality rate in the United States between 2009 and 2013 is 4.32 per 100,000 and with 73,450 deaths attributed to primary malignant brain and other CNS tumors. If we extrapolate the U.S. data with its incidence rate to the

Korean population, per year we would expect about 12,500 new cases of primary CNS tumors and 2,160 deaths. According to the nationwide cancer registration (hospital based Korean Central Cancer Registry [KCCR], [http://www.iacr.com.fr/index.php?option=com\\_comprofiler&task=userprofile&user=973&Itemid=498](http://www.iacr.com.fr/index.php?option=com_comprofiler&task=userprofile&user=973&Itemid=498), <http://ncc.re.kr/cancerStatsView.ncc?bbsnum=358&searchKey=total&searchValue=&pageNum=1>), 10,004 patients were diagnosed with primary CNS tumors in Korea in 2010, which means that the incidence of brain tumors in Korea is lower than that of United States.<sup>1,2</sup> Similar to the United States, CNS tumors occurred more frequently in female (female:male, 1.59:1). The four most common tumors were meningioma (35.5%), pituitary tumors (18.7%), gliomas (15.1%), and nerve sheath tumors (10.3%). Glioblastoma (GBM) is the most common and the most malignant glioma, which comprises 34.6% of all gliomas. In children (0–19 years), sellar region tumors (pituitary adenoma and craniopharyngiomas), pilocytic astrocytomas, germ cell tumor, and embryonal tumors/medulloblastoma were

the most common brain tumors.<sup>2</sup>

The 5-year relative survival rate in the United States after the diagnosis of brain or other CNS tumors that are either primary malignant or nonmalignant is 34.7% and 90.4%, respectively. The survival rate of patients with malignant CNS tumors depends on onset age, histologic and molecular diagnosis, and the tumor grade. The overall survival rate decreases with age (0–19 years, 73.8%; 20–44 years, 61.5%; 45–54 years, 33.5%; 55–64 years, 18.5%; 65–74 years, 11.2%; 75 or older: 6.3%). Therefore, children are more likely to survive than adults after malignant CNS tumors develop. Thus, advances must be made to improve the survival rates of young patients with CNS tumors.

The completion of the human genome project led to two powerful tools: the human genome sequence and advanced molecular technologies. Over the past few decades, investigators have been constantly searching for causes of cancer. Through high-throughput studies such as the Cancer Genome Atlas (TCGA) project (<https://cancergenome.nih.gov/>) or the cBioPortal project (<http://www.cbioportal.org/>), a large number of brain tumors have been sequenced and major genetic alterations in brain tumors have been identified,<sup>3</sup> thus allowing for the classification of gliomas. The signaling pathways that are mainly involved in GBM are RTK/RAS/phosphoinositide 3-kinase (PI3K) signaling, p53 signaling, and Rb signaling, which were identified through analyses of common mutations and copy number variations (CNV) in gliomas.<sup>4</sup> In addition, according to the molecular classification by global mRNA expression and DNA methylation, GBMs can be categorized into neural, proneural, classical, and mesenchymal transcriptomic subtypes.<sup>5</sup>

One of the most prominent molecular discoveries was made in 2008 in the genomics of diffuse gliomas. Mutations in *IDH1* and *IDH2* were discovered by whole exome sequencing (WES) of GBMs, thus altering the classification of gliomas.<sup>6</sup> *IDH1* or *IDH2* mutations are found in both astrocytic and oligodendroglial tumors since they act as a starting point for gliomagenesis. Therefore, the 2016 World Health Organization (WHO) classification guidelines combined astrocytic tumors and oligodendroglial tumors into one category.<sup>7–10</sup> Furthermore, each tumor has a typical genetic signature. For example, oligodendrogliomas are characterized by a codeletion in 1p/19q, mutations in *IDH*, and the promoter region of the gene encoding telomerase reverse transcriptase (*TERT*). Furthermore, grade 2 and grade 3 astrocytic tumors are characterized by *ATRX* and *TP53* mutations, while *IDH*-wildtype (primary) GBMs are characterized by the CNV of *EGFR*, *PTEN*, *CDKN2A/B*, *PDGFRA*, and *MET* genes, in addition to a lack of mutations

in *IDH* and a codeletion in 1p/19q.<sup>11–13</sup>

Even in tumors that are morphologically similar, those with mutations in *IDH* and a codeletion in 1p/19q differ in the treatment response and prognosis compared with tumors without these two molecular alterations.<sup>11,14–19</sup> Since only gliomas with mutations in *IDH* and a codeletion in 1p/19q are considered oligodendrogliomas, the so-called pediatric-type oligodendroglioma lacking these two alterations is not considered an oligodendroglioma. The molecular differences of primary *IDH*-wildtype and *IDH*-mutant (secondary) GBMs are well summarized in the paper by Cachia et al.<sup>20</sup> The genetic abnormalities of the *IDH*-mutant GBMs are similar to grade II/III astrocytomas. In other words, they more likely have mutations in *IDH*, *ATRX*, and *TP53*.

Since the prognosis of each tumor depends on the mutational status of *IDH1* and *IDH2*, astrocytic tumors are also classified according to this metric (Fig. 1).<sup>6,8,21</sup> Pediatric GBMs and high-grade gliomas differ from those of adults. No genetic abnormalities in *IDH1* and *IDH2* are found in pediatric GBMs, but mutations are generally found in *H3F3A*, *ATRX* and *DAXX* (Fig. 2). The K27M in *H3F3A* is a major mutation found in diffuse midline gliomas.<sup>22–25</sup> Additionally, a *C11orf95-RELA* fusion was found in supratentorial ependymomas.<sup>26–34</sup> A V600E mutation in *BRAF* was found in circumscribed gliomas, such as pleomorphic xanthoastrocytoma (PXA) (66%),<sup>35–38</sup> gangliogliomas (25%),<sup>35,38</sup> and pilocytic astrocytomas (15%).<sup>35,38</sup> Furthermore, a *BRAF-TIAA1549* fusion was discovered in pilocytic astrocytoma (more than 70%) (Fig. 2).<sup>39–43</sup> *SMARCB1* (*INI1*) or *SMARCA4* (*BRG1*) gene mutations or deletions were observed in atypical teratoid/rhabdoid tumors (AT/RT),<sup>44–46</sup> and a *NAB2-STAT6* fusion was present in solitary fibrous tumor/hemangiopericytomas.<sup>47–49</sup> Meningiomas also have typical gene mutations according to the tumor type and grade. Sixty percent of the sporadic meningiomas have mutations in *TRAF7*, *KLF4*, *AKT1*, *SMO*, and *PIK3CA*.<sup>50–52</sup> Among them, mutations in *TRAF7* and *KLF4* are found in secretory-type meningiomas and mutations in *TRAF7/AKT1/PIK3CA* are found in meningotheial and transitional-type meningiomas.<sup>52,53</sup> Mutations in *TRAF7* are the most common genomic aberrations and are found in 12%–15% of sporadic meningiomas, preferentially fibrous and transitional subtype, which are found concurrently with mutations in *KLF4*, *AKT1*, or *PIK3CA*, but are mutually exclusive with mutations in *SMO* and neurofibromatosis type 2 (*NF2*).<sup>53</sup> *NF2*-associated meningiomas have mutations in *NF2*. Atypical and anaplastic meningiomas usually have mutations in *TERT* or marked copy number aberrations and loss of *CDKN2A/2B*.<sup>53</sup>

These findings demonstrate that tumors are genetic disorders and that certain mutations can represent different biological behaviors and result in different prognoses.

Molecular testing, such as molecular profiling of brain tumors, improves diagnostic accuracy, allows for predictive prognosis, and enables target identification. At present, target therapy has become one of the most promising treatment options for many tumors. Here, we summarize and provide guidelines for the molecular testing of brain tumors. High-throughput genomic studies, such as next-generation sequencing (NGS), can be useful financially and practically by rapidly replacing time-consuming and labor-intensive conventional methods since multiple molecular genetic abnormalities must be studied in order to diagnose various brain tumors.

## IMPORTANT MOLECULAR GENETICS FOUND IN BRAIN TUMORS

The indications and methods of each genetic study common to brain tumors are summarized in Tables 1–6. Integration of morphological criteria and genetic alterations is the guideline for an accurate diagnosis, risk classification, and development of therapeutic strategies.

### Mutations in *IDH1/2*

The discovery of mutations affecting the enzymatic function of IDH in gliomas provided a fundamentally new insight into the biology of gliomagenesis and triggered molecular classification of gliomas by a somatic mutation. IDH catalyzes the oxidative decarboxylation of isocitrate to produce  $\alpha$ -ketoglutarate

**Table 1.** Mutation rate in various genes commonly mutated in brain tumors<sup>3,41,55-61</sup>

	WHO grade	Altered genes	Genomic alteration (%)
Astrocytoma	II, III	<i>IDH</i> mutation	65
		<i>P53</i> mutation	96
		<i>ATRX</i> mutation	96
Glioblastoma	IV	<i>EGFR</i> amplification	57
		<i>PDGFRA</i> amplification	13
		<i>EGFRvIII</i> mutation	20
		<i>PTEN</i> homozygous deletion	25–35
		<i>CDKN2A</i> homozygous deletion	61
		<i>BRAF</i> V600E mutation	1–2 (epithelioid GBM)
Oligodendroglioma	II, III	<i>IDH</i> mutation	100
		1p/19q codeletion	100
		<i>CIC/FUBP1</i> mutation	56/29
		<i>TERTp</i> mutation	80–96
Subependymal giant cell astrocytoma	I	<i>TSC1</i> and <i>TSC2</i> mutation	100
Pilocytic astrocytoma	I	<i>BRAF-KIAA1549</i> fusion	75 (cerebellar tumor)
		<i>BRAF</i> V600E mutation	13–15
Pleomorphic xanthoastrocytoma	II, III	<i>BRAF</i> V600E mutation	66
		<i>CDKN2A</i> homozygous deletion	50
Angiocentric glioma	I	<i>MYB-QK1</i> fusion	100
Ganglioglioma	I, III	<i>BRAF</i> V600E mutation	25
		<i>TSC1</i> and <i>TSC2</i> mutation	Unknown
Craniopharyngioma, papillary type	I	<i>BRAF</i> V600E mutation	100
Craniopharyngioma, adamantinomatous type	I	<i>CTNNB1</i> mutation	100
AT/RT	IV	<i>SMARCB1</i> deletion/mutation	>95
	IV	<i>SMARCA4</i> mutation	<5
Cribriform tumor		<i>SMARCB1</i> deletion/mutation	100
Meningioma, fibrous type		<i>NF2</i> inactivation mutation (no hot spot)	45–55 <sup>50</sup>
		<i>TRAF7/KLF4</i> mutation	100 (secretory meningioma)
		<i>AKT1</i> (p.Glu17Lys) mutation	2.5
		<i>SMO</i> (p.Trp535Leu) mutation	5
		<i>TERTp</i> mutation	10
Langerhans cell histiocytosis	I, III	<i>BRAF</i> V600E mutation	50–57 <sup>54</sup>

WHO, World Health Organization; GBM, glioblastoma; TSC, tuberous sclerosis complex; AT/RT, atypical teratoid/rhabdoid tumor.

**Table 2.** Common pediatric molecular subgroups with molecular features<sup>7,23,30,43,56,62,66</sup>

Tumor	Molecular subgroup	Molecular feature	Prognosis
LGG	<i>BRAFV600E</i>	70% of PXA, GG, DA	Good
	<i>KIAA-BRAF</i> fusion; <i>BRAF</i> duplication	90% of PA	Good
	<i>MYB-QKI</i> rearrangement	High proportion of AG	Good
	<i>FGFR1</i> duplication	PA, DA, DNT	Good
HGG	K27M-mutant	H3.1 and H3.3 K27 mutation, <i>PDGFRA</i> focal amplification, <i>TP53</i> mutation, <i>ACVR1</i> mutation	Poor
	G34R/V-mutant	H3.3 G3 and <i>TP53</i> mutation	Poor
	<i>RTK1</i> amplified	<i>PDGFRA</i> and <i>EGFR</i> focal amplification, <i>CDKN2A/2B</i> homozygous deletion	Poor
	Mesenchymal	<i>NFI</i> mutation, <i>PDGFRA</i> and <i>EGFR</i> focal amplification, <i>CDKN2A/2B</i> homozygous deletion	-
Ependymoma	C11orf95- <i>RELA</i> + (70% of ST E)	<i>RELA</i> fusion transcripts	Poor
	<i>RELA</i> fusion – (30% of ST E)	Possibly <i>YAP1</i> fusion transcripts	Good
	Posterior fossa E	Group A: <i>LAMA2</i> overexpression, Group B: <i>NELL2</i> overexpression	Poor Good
	Spinal cord E (10% of child E)	<i>NF2</i> mutation, myxopapillary histology	Good
Medulloblastoma	WNT (10%)	Nuclear $\beta$ -catenin positive, <i>CTNNT1</i> mutations in exon 3, monosomy 6	Excellent
	SHH (30%)	Heterogeneous molecular features depending on age of presentation; <i>PTCH1</i> , <i>SMO</i> , and <i>SUFU</i> mutations, <i>GLI2</i> and <i>MYCN</i> amplification; germline <i>TP53</i> mutations	Intermediate (except in infants who have a good prognosis)
	Group 3 (25%)	By some unknown mechanism; <i>MYC</i> amplification and over expression	Poor
	Group 4 (35%)	i(17)q; <i>MYCN</i> amplification	Intermediate
AT/RT		<i>SMARCB1/SHARCA4</i> mutation	Poor
ETMR		<i>C19MC</i> amplification	Poor

LGG, low grade glioma; PXA, pleomorphic xanthoastrocytoma; GG, ganglioglioma; DA, diffuse astrocytoma; PA, pilocytic astrocytoma; AG, angiocentric glioma; DNT, dysembryoplastic neuroepithelial tumor; HGG, high grade glioma; ST, supratentorial; PF, posterior fossa; E, ependymoma; WNT, wntless signaling pathway; i, isochromosome; AT/RT, atypical teratoid/rhabdoid tumor; ETMR, embryonal tumor with multilayer rosettes.

( $\alpha$ -KG) and CO<sub>2</sub>, but mutant *IDH1/2* has a preferential affinity for  $\alpha$ -KG instead of isocitrate outside of the citric acid cycle, thus leading to the production and accumulation of the oncometabolite 2-hydroxyglutarate (2HG).<sup>67-70</sup> Dang et al.<sup>68</sup> hypothesized that 2HG induces redox stress due to damage to the respiratory chain, which subsequently promotes the mutagenesis and development of gliomas. The  $\alpha$ -KG-dependent prolyl hydroxylases modulate HIF1 $\alpha$  levels and changes in the HIF1 $\alpha$  downstream pathway, leading to an increase in reactive oxygen species levels and potentially contributing to the risk of cancer.<sup>71</sup>

The glioma-CpG island methylator phenotype (G-CIMP) subset is distinctively and invariably found in the gliomas with mutant *IDH*, which is the proneural transcriptional group.<sup>72</sup> 2HG, the oncometabolite produced by mutant *IDH1/2*, inhibits  $\alpha$ -KG-dependent dioxygenases including histone demethylases and the Ten-Eleven Translocation (*TET*) family of histone 5-methylcytosine hydroxylase, which directly induce the hypermethylated state.<sup>73</sup> The G-CIMP subgroup of GBMs is common in younger patients and has a longer lifespan.<sup>13,17,30,67,74-76</sup>

All *IDH1/2* mutations are common in 70%–80% of type II and III infiltrating gliomas and are found in 100% of oligodendroglomas and IDH-mutant GBMs.<sup>67</sup>

droglomas and IDH-mutant GBMs.<sup>67</sup>

#### *TP53* mutation

*TP53* is a typical tumor suppressor gene located in 17p13.1, which encodes the nuclear protein p53. The p53 protein responds to diverse cellular stresses to regulate the expression of its target genes, thereby inducing cell cycle arrest, apoptosis, senescence, DNA repair, or metabolic changes. Mutated *TP53* genes and overexpressed abnormal p53 protein, which has a longer half-life than wild type p53, are associated with a variety of human cancers, including Li-Fraumeni syndrome and many hereditary gliomas. As mentioned in the introduction, the p53 signaling pathway is one of the major abrogated pathways of astrocytic tumors including GBMs. WHO class II and III astrocytic tumors show high levels of *TP53* mutations (94%) and/or p53 overexpression (Tables 3, 4).<sup>3</sup> However, these alterations are rare in oligodendroglomas, well-circumscribed astrocytic tumors including pilocytic astrocytomas, pleomorphic xanthoastrocytomas, and subependymal giant cell astrocytomas, ependymomas, and embryonal tumors such as medulloblastoma, except for the SHH-type, p53-activated subgroup.

**Table 3.** Mutation rate of commonly mutated genes in various brain tumors<sup>7,9,48,55-57,63,77-81</sup>

Genes and molecules	Biomarker type	PA (%)	PXA (%)	DA/AA (%)	IDH-wildtype GBM (%)	IDH-mutant GBM (%)	DMG, H3 K27M (%)	ODG (%)	Epen (%)	MB (%)	AT/RT (%)	Test method
WHO grade		I	II, III	II, III	IV	IV	IV	II/III	II/III	IV	IV	
<i>IDH1</i> mutation	Diagnostic and prognostic	0	-	>80	5–6	>95	0	98	0	0	0	IHC, sequencing
<i>IDH2</i> mutation	Diagnostic and prognostic	0	-	-	-	2–5	0	2	0	0	0	Sequencing
<i>TP53</i> mutation	Diagnostic and prognostic	0	6	94	25–35	62–65	45–50	9–44	0	-	0	Sequencing, IHC
<i>ATRX</i> mutation	Diagnostic and prognostic		-	86	0	90–95	50	-	0	-	0	IHC, sequencing
Histone K27M mutation	Diagnostic and prognostic	0	-	0	Pediatric HGG	0	100	0	0	0	0	IHC, sequencing
Histone G34 mutation	Diagnostic and prognostic	0	-	-	Uncertain	-	-	0	0	-	-	Sequencing
Histone K36 mutation	Diagnostic and prognostic	0	-	-	-	-	-	0	0	-	-	Sequencing
1p/19q codeletion	Diagnostic, prognostic, and predictive	0	0	0	0	0	0	100	0	0	0	FISH, CGH
<i>CIC</i> mutation	Diagnostic, prognostic, and predictive	0	-	-	-	-	-	49	0	-	-	Sequencing, IHC
<i>FUBP1</i> mutation	Diagnostic, prognostic, and predictive	0	-	-	-	-	-	29	0	-	-	Sequencing, IHC
<i>EGFR</i> amp	Prognostic	0	-	-	35–45	4	-	-	0	-	-	FISH, CGH, IHC
<i>PDGFRA</i> amp	Diagnostic		-	-	13	-	50	-	-	-	-	FISH, CGH, IHC
<i>PTEN</i> HoD	Prognostic	0	-	-	25–35	5	-	-	0	-	-	FISH, CGH, IHC
<i>CDKN2A</i> HoD	Predictive	0	60	11	35–50	-	<5	-	0	-	-	FISH, CGH, IHC
<i>BRAF</i> V600E mutation	Diagnostic and prognostic	15	67	0	1–2	0	0	0	0	0	0	Sequencing, IHC
<i>BRAF-KIAA1549</i> fusion	Diagnostic and prognostic	70	-	-	-	-	-	-	-	-	-	RT-PCR, FISH (gain)
<i>TERT</i> promoter mutation	Diagnostic and prognostic	-	-	-	>80	26	-	96	0	21	-	Sequencing
<i>C11orf95-RELA</i> fusion	Diagnostic and prognostic	0	-	-	-	-	-	-	<5	-	-	RT-PCR, IHC, RNA seq
$\beta$ -Catenin mutation	Diagnostic and prognostic	0	-	-	-	-	-	-	0	6–9	-	IHC, sequencing
<i>MYC</i> amp	Prognostic	0	-	-	-	-	-	-	-	10–15	-	FISH, CGH, IHC
<i>MYCN</i> amp	Prognostic	0	-	-	-	-	-	-	-	10–15	-	FISH, CGH
<i>SMARCB1</i> mutation	Diagnostic and prognostic	0	-	-	-	-	-	-	0	0	98	IHC, sequencing
<i>SMARCA4</i> mutation	Diagnostic and prognostic	0	-	-	-	-	-	-	0	0	1–2	IHC, sequencing
<i>MGMT</i> methylation	Predictive	-	-	78.5	48.5	60–80	-	85	0	0	0	MSP-PCR, pyrosequencing, IHC

PA, pilocytic astrocytoma; PXA, pleomorphic xanthoastrocytoma; DA, diffuse astrocytoma; AA, anaplastic astrocytoma; GBM, glioblastoma; DMG, diffuse midline glioma; HGG, high grade glioma; ODG, oligodendroglioma; MB, medulloblastomas; AT/RT, atypical teratoid/ rhabdoid tumor; WHO, World Health Organization; IHC, immunohistochemistry; FISH, fluorescent *in situ* hybridization; CGH, comparative genomic hybridization; RT-PCR, reverse transcription polymerase chain reaction; -, not known; MSP-PCR, methylation-specific polymerase chain reaction.

### *ATRX* is an X-linked gene of $\alpha$ -thalassemia and mental retardation syndrome

*ATRX* is located in Xq21.1, encodes a 280-kDa nuclear protein, and has been shown to be involved in a wide range of cellular functions such as DNA recombination, repair, and transcription regulation.<sup>82</sup> It binds strongly within the promyelocytic leukemia body of the nucleus. When *ATRX* interacts with *DAXX*, this complex functions as a histone chaperone complex for the deposition of histone variant H3.3 into heterochromatic

repeats including pericentric, telomeric, and ribosomal DNA repeat sequences.<sup>83</sup> Functional mutations of this gene have been associated with sister chromatid clumps and defects, abnormal DNA methylation, and the maintenance of telomerase-independent telomeres, resulting in an alternative lengthening of telomeres (ALT). Decreased nuclear expression of *ATRX* and *ATRX* mutations are observed in grade 2 and 3 astrocytic tumors including *IDH* mutant gliomas (86%), *IDH*-mutant GBMs (85%), and pediatric high grade gliomas such as diffuse midline

**Table 4.** Summary of the mutation specific antibodies and their indication in glioma diagnosis<sup>12,36,48,81,84</sup>

Antibody	Positive loci	Mutated gene status	Positive result	Tumors
ATRX	Nucleus	Loss of function mutation	Negative	Diffuse and anaplastic astrocytoma
β-Catenin	Nucleus	Gain of function mutation	Focal positive	WNT type medulloblastoma, adamantinomatous craniopharyngioma
BRAF VE1 (BRAF V600E)	Cytoplasm	Gain of function mutation	Positive	Pleomorphic xanthoastrocytoma, ganglioglioma, pilocytic astrocytoma, epithelioid glioblastoma, papillary craniopharyngioma
BRG1	Nucleus	Gain of function mutation	Negative	Atypical teratoid rhabdoid tumor
CIC	Nucleus	Loss of function mutation	Negative	Oligodendroglioma (47%) <sup>15</sup>
c-MET	Membrane	Overexpression	Positive	Glioblastoma, anaplastic astrocytoma
EGFR	Membrane	Overexpression	Positive	Glioblastoma, anaplastic astrocytoma
EGFRvIII	Membrane	Overexpression	Positive	Glioblastoma, anaplastic astrocytoma
H3 K27M	Nucleus	Gain of function mutation	Positive	Diffuse midline glioma
FUBP1	Nucleus	Loss of function mutation	Negative	Oligodendroglioma (16%) <sup>15</sup>
IDH1 (H09)	Nucleus and cytoplasm	Gain of function mutation	Positive	Astrocytoma and oligodendroglioma
INI1	Nucleus	Loss of function mutation	Negative	Atypical teratoid rhabdoid tumor
P16	Nucleus and cytoplasm	Loss of function mutation	Negative	High grade glioma
P53	Nucleus	Overexpression	Positive	Astrocytic tumors
PDGFRA	Membrane	Overexpression	Positive	Glioblastoma, anaplastic astrocytoma
PTEN	Cytoplasm	Loss of function mutation	Negative	Glioblastoma
RELA (NFκB3)	Cytoplasm	Gain of function mutation	Positive	Cerebral ependymoma
STAT6	Nucleus	Gain of function mutation	Positive	Solitary fibrous tumor/hemangiopericytoma
MLH1	Nucleus	Loss of function mutation	Negative	Gliomas
MSH2	Nucleus	Loss of function mutation	Negative	Gliomas
PMS2	Nucleus	Loss of function mutation	Negative	Gliomas
Ki67	Nucleus	Overexpression	Positive	Brain tumors (for an ancillary test for tumor grading)
pHH3	Nucleus	Overexpression	Positive	Brain tumors (for counting mitoses)
GFAP	Nucleus	Expression	Positive	Astrocytic tumors
Olig2	Nucleus	Expression	Positive	Gliomas including astrocytomas and oligodendroglioma Neither neuronal nor ependymal tumors

gliomas (DMGs) (Figs. 1, 2).<sup>3</sup>

### Histone *H3F3A* (K27M, K36, and G34) mutations

Histone protein H3.1 and H3.2 are expressed only in the S phase and are integrated into the chromatin by chaperone CAF1 during DNA replication only, but H3.3 is expressed at all stages of the cell cycle and can be integrated into the chromatin independently of DNA replication. H3.3 is associated with active chromatin such as H3K4 trimethylation, which promotes open chromatin structure for the binding of co-factors and transcription factors to activate transcription.<sup>85</sup> Recurrent mutations in *H3F3A*, which encodes the replication-independent histone 3 variant H3.3, were first detected in the pediatric diffuse infiltrating pontine glioma (DIPG) by a comprehensive WES analysis. DIPG was later renamed as DMG and is considered a H3 K27M mutation in the new 2016 WHO classification (Fig. 2).<sup>7,23</sup> Eighty percent of pontine gliomas (DIPG) and 70% of other loci DMGs contain a mutation in one allele of the *H3F3A* gene, which is a mutation on the histone tail (K27M, K36, G34R/G34V), an important post-translational modification factor.<sup>25</sup>

The histone *H3F3A* mutant gliomas have a poor prognosis

regardless of histopathological grade. K27M-H3.3 mutations occur mainly in young patients (median age, 11 years) and G34R/V-H3.3 mutations occur in older children and young adults (median age, 20 years).<sup>22</sup> All of the cases with G34-H3.3 mutations are in pediatric GBMs (13/13), and especially associated with mutations in *ATRX* and *DAXX*.<sup>22</sup> Loss of *ATRX* is associated with the *ALT* phenotype; thus, *ALT* often coexists with mutations in *ATRX/H3F3A/TP53*.<sup>22</sup>

### Codeletion of chromosome 1p/19q and mutations in *CIC* and *FUBP1*

Simultaneous deletion of chromosome 1p/19q is a characteristic and early genetic event in oligodendroglial tumors, which is associated with better prognosis and is also a good indicator of the patient response to specific combination chemotherapy of procarbazine, lomustine, and vincristine (PCV). Recurrent mutations in *CIC* and *FUBP1* were found in 46%–53% and 15%–24% of oligodendroglomas, respectively, in addition to a codeletion in 1p/19q and mutations in *IDH1* or *IDH2* (Fig. 1).<sup>86-88</sup>

*FUBP1* is located in 1p31.1, and mutations in *FUBP1* are predicted to disrupt *FUBP1* protein function (Table 1). *FUBP1*

acts as an RNA binding protein and alterations of its normal function can lead to tumorigenesis, which has been suggested to act either as a protooncogene or a tumor suppressor gene depending on the tumor type.<sup>36,87</sup> Through the c-Myc pathway, *FUBP1* promotes cell migration and protects cells from apoptosis.

The *CIC* gene on chromosome 19q13.2 represses genes induced by RTK pathway activation.<sup>89</sup> Although the function of

human *CIC* protein is not known, a recent study in cultured cells demonstrated that *CIC* acts together with *IDH1* to regulate citrate levels in the cytoplasm. *CIC* mutations promote the accumulation of 2HG and reduce clonogenicity in the setting of *IDH1* mutations. Loss of 19q in oligodendroglial tumors unmasks mutations in the *CIC* gene.<sup>87,90</sup> In this regard, the co-existence of *IDH1* with *CIC* or *FUBP1* mutations may partially

**Table 5.** The current sequencing conditions commonly used for brain tumor diagnosis<sup>35,45,59,68,84,91,92</sup>

Gene	Full name	Gene location	Forward primer	Reverse primer	Product (bp)	Indication	Function
<i>IDH1</i>	Isocitrate dehydrogenase 1	2q33.3	5'-M13-GTA AAA CGA CGG CCA GTC GGT CTT CAG AGA AGC CA-3'	5'-GCG GAT AAC AAT TTC ACA CAG GGC AAA ATC ACA TTA TTG C-3'	180–190	Astrocytic and ODG	Affect citrate metabolism, leading to 2-HG metabolite
<i>IDH2</i>	Isocitrate dehydrogenase 2	15q26.1	5'-GCT GCA GTG GGA CCA CTA TT-3'	5'-TGT GGC GTT GTA CTG CAG AG-3'	295–305	Astrocytic and ODG	Same with <i>IDH1</i>
<i>H3F3A</i> (K27M/K36/G34)	H3 Histone family 3A	1q42.12	5'-CTG GTA AAG CAC CCA GGA AGC-3'	5'-CAT GGA TAG CAC ACA GGT TGG T-3'	330–340	DMG	Chromatin structure, gene transcription
<i>BRAF</i> V600E	V-RAF murine sarcoma viral oncogene homolog B1	7q34	1st: 5'-GCT TGC TCT GAT AGG AAA ATG AG-3' 2nd: 5'-TCA TAA TGC TTG CTC TGA TAG GA-3'	1st: 5'-GTA ACT CAG CAG CAT CTC AGG-3' 2nd: 5'-GGC CAA AAA TTT AAT CAG TGG A-3'	245–255 230–235	Gliomas including PXA, GG, PA, epithelioid GBM	MAPK signaling
<i>CTNNB1</i>	Catenin, beta-1	3p22.1	5'-GAT TTG ATG GAG TTG GAC ATG G-3'	5'-TGT TCT TGA GTG AAG GAC TGA G-3'	230–235	Medulloblastoma, WNT subtype, craniopharyngioma, adamantinomatous type	The transmission of the 'contact inhibition' signal
<i>TERTp</i>	Telomerase reverse transcriptase	5p15.33	5'-M13-GGC CGA TTC GAC CTC TCT-3' (M13: TGT AAA ACG ACG GCC AGT)	5'-AGC ACC TCG CGG TAG TGG-3' (M13: GCG GAT AAC AAT TTC ACA CA)	300–310	Gliomas, especially ODG and GBM	Telomerase maintenance
<i>MGMT</i>	O6 methylguanine-DNA methyltransferase	10q26.3	5'-TTT CGA CGT TCG TAG GTT TTC GC-3'	5'-GCA CTC TTC CGA AAA CGA AAC G-3'	80–90	Gliomas	Promoter methylation

ODG, oligodendroglioma; 2-HG, 2-hydroxyglutamate; DMG, diffuse midline glioma; PXA, pleomorphic xanthoastrocytoma; GG, ganglioglioma; PA, pilocytic astrocytoma; GBM, glioblastoma; MAPK, mitogen-activated protein kinase.

**Table 6.** Probes and reading criteria of FISH studies used for brain tumor diagnosis

	Target probe	Control	Cut off	Indication	Biomarker
1p deletion	Chr1p36	1q25	1p < 0.8 and Deleted nuclei > 50%	ODG	Diagnostic, prognostic, and predictive
19q deletion	Chr19q13	19p13	19q < 0.8 and Deleted nuclei > 50%	ODG, HGG	Diagnostic, prognostic, and predictive
<i>BRAF</i> gain	Chr7q34	CEP7	Gold signal > 3	PA	Diagnostic, prognostic, and predictive
<i>CDKN2A</i> (9p21.3) homozygous/hemizygous deletion	Chr9p21.3	CEP9	HoD ≥ 10% HeD ≥ 50%	HGG	Diagnostic and prognostic
<i>EGFR</i> amplification	Chr711.2	CEP7	Ratio ≥ 2.0	HGG	Diagnostic and prognostic
<i>PTEN</i> HoD /HeD	Chr10q23.31	CEP10	HoD ≥ 10% HeD ≥ 50%	HGG	Diagnostic and prognostic
<i>RELA-C11orf95</i> fusion	Chr11q13.1	CEP11	Break apart	S-ependymoma	Diagnostic and prognostic
<i>C19MC</i> amplification	Chr19	CEP19	Ratio ≥ 2.0	ODG, GBM	Diagnostic and prognostic
<i>SMARCB1</i>	Chr22q11.23	CEP22	NF2 < 0.8	AT/RT	Diagnostic and prognostic

FISH, fluorescent *in situ* hybridization; Chr, chromosome; ODG, oligodendroglioma; HGG, high grade glioma; PA, pilocytic astrocytoma; HoD, homozygous deletion; HeD, hemizygous deletion; S-ependymoma, supratentorial ependymoma; GBM, glioblastoma; AT/RT, atypical teratoid/rhabdoid tumor.

explain the slower tumor growth and longer survival of oligodendrogliomas with mutations in *IDH1* and a codeletion of 1p/19q when compared to other diffuse gliomas.<sup>90</sup> The overall survival rate of patients with oligodendrogliomas with *CIC* mutations was lower than that of patients without *CIC* mutations, and the *FUBP1* mutation was significantly associated with unfavorable progression-free survival.<sup>15</sup> However, oligodendrogliomas cannot be diagnosed with *CIC* or *FUBP1* mutations only.<sup>15</sup>

**EGFR amplification and EGFRvIII truncation mutations**

*EGFR*, also called *Erb1* or *HER1*, is located on chromosome 7q12 and acts as an *ErbB* family receptor tyrosine kinase. *EGFR* amplification is closely related to *EGFR* overexpression. *EGFRvIII*-positive tumor cells exhibit particularly high levels of *mTOR* signal and exhibit the most proliferative and aggressive phenotype similar to GBMs (Fig. 1). The *EGFRvIII* mutation is a 801 bp frame deletion from exons 2 to 7 of the *EGFR* gene, which is associated with *EGFR* amplification and the response to antibody therapy as well as poor prognosis.<sup>93</sup> In addition to *EGFR* amplification, *EGFRvIII*-positive GBM cell lines are sensitively suppressed by first-generation *EGFR* inhibitors (erlotinib, gefitinib, vandetanib) and second-generation *EGFR* inhibitors (NT113) as compared to GBM cell lines in which *PTEN*

tumor suppressor genes are lost *in vitro*.<sup>94</sup>

*EGFR* immunohistochemistry is usually uniform in tumors expressing high levels of the protein, however, *EGFRvIII* staining is heterogeneous and usually present in only a subset of tumor cells. Therefore, representative sampling of tumor tissue is important to avoid false-negative results.<sup>56,57</sup>

Unlike *EGFR* point mutations, *EGFR* fusions with *SEPT14*, *PSPH*, or *SEC61G* has also been shown to play a role in GBMs, offering a unique opportunity to investigate fused oncogene dependencies.<sup>94</sup>

**Deletions in CDKN2A/2B**

*CDKN2A/2B* is a tumor suppressor gene located on chromosome 9p21.3, because it encodes a cyclin-dependent kinase inhibitor (p16) and is a cell cycle regulator of the *Rb* pathway. In 60% of GBMs and 11% of low-grade gliomas including oligodendroglioma, pleomorphic xanthoastrocytoma, and pilocytic astrocytoma, the loss or inactivation of p16 protein as a result of a homozygous deletion or promoter methylation of *CDKN2A/2B* is observed (Fig. 1).<sup>55</sup> It is also one of the more commonly altered genes in PXA and high grade gliomas in both adults and children (Fig. 2).<sup>55,95</sup> After adjusting for the *IDH* mutational status, sex, and age, *CDKN2A* deletions were strongly associated with poorer overall survival in astrocytomas but not in oligodendrogliomas.<sup>18</sup>

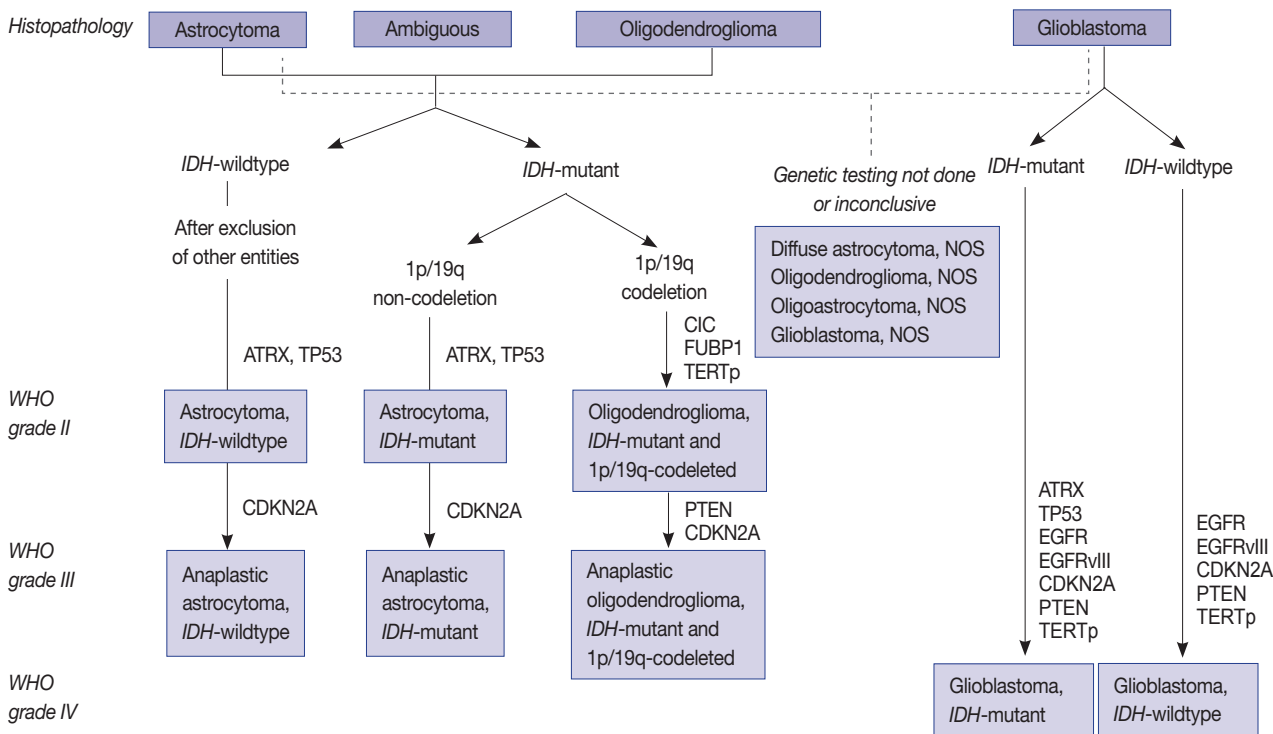
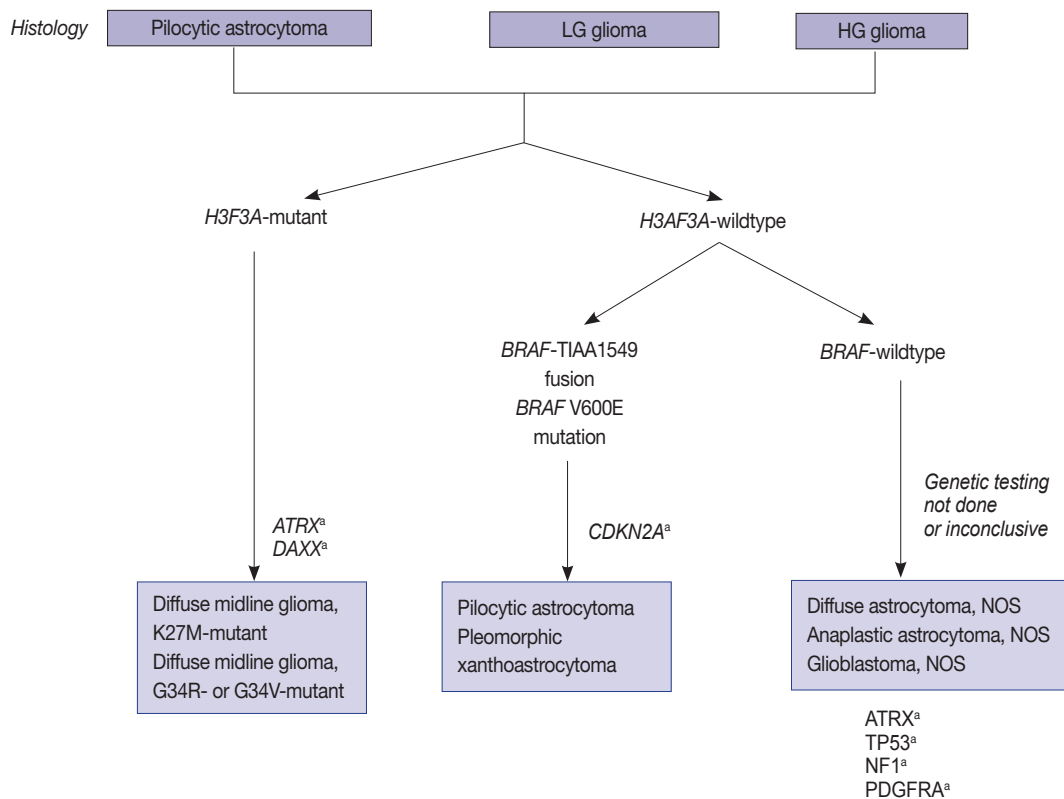


Fig. 1. Schematic view of the classification of adult diffuse glioma according to the status of key genes.



**Fig. 2.** Schematic view of the classification of pediatric diffuse gliomas according to the status of key genes. LG, low grade; HG, high grade; NOS, not otherwise specified. <sup>a</sup>Characteristic but not required for diagnosis.

### BRAF mutations and BRAF-KIAA1549 fusions

*BRAF* V600E mutations and fusions of *BRAF* with *KIAA1549* or *FAM131B* are characteristics of pilocytic astrocytomas. In 2008, a tandem duplication was confirmed in 7q34, and a new fusion gene was found to be generated by a fusion between the *KIAA1549* gene and *BRAF* genes, which was previously uncharacterized in pilocytic astrocytomas.<sup>58</sup> Fusions between *KIAA1549* exon 15 and *BRAF* exon 9 and those between *FAM131B* exon 2 and *BRAF* exon 9 are derived from a 2.0 Mb tandem duplication in chromosome band 7q34, which can be detected by real-time polymerase chain reaction (PCR) or fluorescent *in situ* hybridization (FISH) (Fig. 2).<sup>62</sup>

The *BRAF* V600E mutation was found in two-thirds of all pleomorphic xanthoastrocytomas, one-fourth of gangliogliomas, and one-seventh of pilocytic astrocytomas.<sup>35</sup>

In children, *CDKN2A* deletions and *BRAF* mutations are early events in low-grade gliomas (pediatric low-grade glioma [PLGG]) undergoing malignant transformation (Fig. 2).<sup>96</sup> The *BRAF* V600E mutant PLGG has longer transformation latency periods than the *BRAF* wild type PLGG (median latency period, 6.65 years vs 1.59 years, respectively).<sup>96</sup> As a result, all of the

patients with secondary high-grade glioma (sHGGs) containing mutant *BRAF* were diagnosed at age 9 or older.<sup>96</sup> The sHGG in children showed recurrent changes of *BRAF* V600E mutations and *CDKN2A* deletions in 39% and 57%, respectively.

### TERTp mutations

Human telomerase is a ribonucleoprotein that regulates the length of telomeric DNA at the ends of chromosomes; therefore, it plays an important role in cellular immortalization and oncogenesis.<sup>13</sup> Mutations in *TERTp* are molecular hallmarks of glioma, occurring in more than 80%–96% of IDH-wildtype GBMs and oligodendrogliomas, but less frequently present in grade II and III astrocytomas (38.5%) (Table 1, Fig. 1).<sup>97</sup> Chan *et al.* (2015)<sup>98</sup> found that mutations in *TERTp* are present in 41 of 142 (28.9%) grade II gliomas and 20 of 72 (27.8%) grade III gliomas. The mutations were always found in two hotspots (chr5: 1 295 228 C > T and 1 295 250 C > T), resulting in a somatic gain-of-function mutation and an enhancement of *TERTp* activity.<sup>99</sup> A relative telomere length is strongly correlated with *TERTp* mutations. These two hot spot mutations are mutually exclusive in gliomas and *TP53* mutations, but coincident with

a 1p/19q codeletion.<sup>100</sup>

The prognostic effect of the *TERT* mutation is controversial. Some studies have suggested that *TERT* mutations in low-grade gliomas are associated with shorter progression-free survival.<sup>101</sup> Other researchers have found that *TERT* mutations are a predictor of a poorer response to temozolomide.<sup>102</sup> *TERT* mutations are associated with good outcome in gliomas with mutant *IDH*, but it is also related to poor outcome in gliomas with wild type *IDH*.<sup>97</sup> In gliomas with wildtype *IDH* or GBMs with hypomethylated *MGMT*, *TERT* mutations were found to predict poor prognosis.<sup>103</sup> Therefore, when using the *TERT* mutational status as a prognostic factor, other factors such as mutations in *IDH* and tumor grade should be considered.<sup>101</sup> Primer sequences for *TERT* mutation is summarized in Table 5.

### *C11orf95-RELA* fusion

More than two-thirds of supratentorial ependymomas contain oncogenic fusions between *RELA* (the principle effector of canonical nuclear factor  $\kappa$ B [NF- $\kappa$ B] signaling) and *C11orf95* (an uncharacterized gene) (Table 2).<sup>32,34</sup> Ependymomas carrying the *C11orf95-RELA* fusion are characterized by a nuclear accumulation of p65RelA (NF $\kappa$ B) indicating a pathological activation of the NF $\kappa$ B signaling pathway.<sup>34</sup> *C11orf95-RELA* fusions result from chromothripsis involving chromosome 11q13.1. Furthermore, the *C11orf95-RELA* fusion protein was found to spontaneously translocate to the nucleus to activate NF- $\kappa$ B target genes, and to rapidly transform neural stem cells, the cell of origin for ependymomas, to form these tumors in mice, which is a poor prognostic marker (Table 2).<sup>34</sup>

### *CTNNB1* mutations

Mutations in *CTNNB1* on chromosome 3p21, which encodes  $\beta$ -catenin, promote the stabilization and nuclear translocation of itself, therefore activating the WNT signaling pathway (Table 2). The nuclear translocation of  $\beta$ -catenin is present in medulloblastomas, solitary fibrous tumors/hemangiopericytomas, and adamantinomatous-type craniopharyngiomas. Nuclear expression of  $\beta$ -catenin is always focal. Overall, these mutations can act as future therapeutic targets in nuclear  $\beta$ -catenin-positive tumors.

### *MYC* and *MYCN* amplification

*MYC* is a regulator gene that encodes for transcription factors for c-myc, Mycn, and Mycl.<sup>77</sup> Nuclear myc protein has multiple functions such as cell cycle progression, apoptosis, and cellular transformation. *MYC/MYCN* amplification or overexpression is found not only in type-3 medulloblastomas, but also in other

aggressive subtypes of medulloblastomas, which account for approximately 10% of medulloblastomas.<sup>78,104</sup>

### *SMARCB1* and *SMARCA4* mutations

AT/RT are highly malignant CNS embryonal tumors with rhabdoid morphology, where biallelic inactivation of *SMARCB1* results in a loss of INI1 (BAF47) nuclear expression (Tables 2–4). The loss of BRG1 nuclear expression in AT/RT with mutations in *SMARCA4* is rarely reported.<sup>105</sup> The tumor suppressors *SMARCB1* and *SMARCA4* are located on 22q11.23 and 19p13.2, respectively.

The biallelic loss of *SMARCB1* and *SMARCA4* can be recognized by nuclear negativity of the INI1 and BRG1 immunostaining. However, FISH and DNA sequencing can also be used to detect these genetic alterations.

WES and RNA sequencing of AT/RT revealed few somatic mutations and several deregulated signaling pathways related to the *SMARCB1* deficiency.<sup>106</sup>

### *C19MC* amplification

Chromosomal 19 micro-ribosomal clusters (*C19MC*), localized at 19q13.42, are produced by chromothripsis, a phenomenon of chromosomal breakage and inaccurate recombination, resulting in the rearrangement of thousands of clustered chromosomes in a single event to a localized and restricted genomic region on one or more chromosomes.<sup>107</sup> *C19MC* amplification is a genetic feature of embryonal tumors with multilayer rosettes (ETMR), supratentorial ependymomas, and medulloepitheliomas (Table 2).<sup>108</sup> This abnormality can be detected by FISH.

### *MGMT* promoter hypermethylation

One of the most clinically important DNA methylation markers in GBMs is the promoter of *MGMT*, a DNA repair enzyme that can abrogate the effects of alkylating chemotherapy such as temozolomide. More than 50% of oligodendrogliomas and 30%–40% of adult high-grade gliomas (approximately 40% of IDH-wildtype GBMs) reveal *MGMT* methylation. *MGMT* promoter hypermethylation induces gene silencing and susceptibility to combined temozolomide and radiation therapy. In cases of oligodendroglioma with promoter methylation of the *MGMT* gene, whether or not PCV chemotherapy is advantageous remains controversial.<sup>59</sup> However, it is still considered to be the most accurate predictive factor for survival during PCV chemotherapy.<sup>60</sup>

## METHODS OF MOLECULAR TESTING

The molecular testing methods commonly used in pathology laboratories include immunohistochemical staining, direct sequencing, FISH, chromosomal genomic hybridization, and NGS.

### Immunohistochemical studies

Some of the genetic changes can be detected by immunohistochemical studies. *IDH* R132H, H3 K27M, *BRAF* V600E, and *EGFRvIII* can be diagnosed using mutation-specific monoclonal antibodies (mAbs). IDH1 (H09), K27M, and BRAF VE1 antibodies have 100% sensitivity and specificity to detect gene mutations.<sup>36</sup> The INI-1 (*SMARCB1*), BRG1 (*SMARCA4*), p16 (*CDKN2A*), *CIC*, and *FUBP1* mutations and *MGMT* methylation can be detected by the loss of expression. *TP53* mutations are detected by the complete loss of expression or overexpression via the stabilization of the mutant protein. In addition, *STAT6* (*NAB2-STAT6* fusion), *LICAM* (protein marker for *RELA-c9ORF95* fusion), and the amplifications of *EGFR*, *MET*, and *PDGFR* can be analyzed by overexpression assays (Table 4).<sup>21,24,36,55</sup> Mutations in several genes give rise to the overexpression or loss of proteins, depending on whether the mutation is a gain of function or a loss of function mutation, respectively. For example, p53 nuclear overexpression reflects a *TP53* mutation, and p16 nuclear and cytoplasmic losses are associated with a *CDKN2A* homozygous deletion. Furthermore, the nuclear loss of *ATRX* is associated with an *ATRX* mutation, and *MLH1*, *MSH2*, and *PMS* nuclear losses are associated with methylation of these genes. Among these, all but *TP53* have high correlations between immunohistochemical results and molecular genetic studies. The correlation rate of p53 between immunohistochemistry and mutation studies is low. This is because p53 immunoreactivity may have resulted from the prolongation of half-life either due to p53 mutations or the accumulation of wild type protein brought about by mechanisms other than those caused by mutations, such as a complex formation with *MDM2* overexpression products,<sup>109</sup> whereas p53 negativity can be observed by the methylation of the *TP53* promoter. Therefore, overexpression of p53 protein is not always associated with mutations in conserved exons of the p53 gene.

### Direct sequencing

The rapidly growing number of prognostic and predictive genetic markers in neuro-oncology has led to an increasing need for a more thorough molecular analysis of brain tumor specimens in a modern pathology setting. Although several diagnos-

tically important mutations can be detected by immunohistochemistry, this is not the case for the full spectrum of alterations now known to be of relevance. Therefore, the mutations of *IDH* 1/2, *BRAF*, *CTNNB1*, *H3F3A* (K27M, G34), *TP53*, *ATRX*, and *TERTp* are usually detected by direct sequencing. The sequencing conditions, primer sequences, and PCR product sizes that are currently being used for brain tumor diagnosis are summarized in Table 5.

In order to detect mutations in *CIC* (missense mutations or small in-frame deletions) and *FUBP1* (indel, splicing alteration, and nonsense mutations) in the functional regions such as the HMG box and CI motif, NGS is required because the mutation sites of these two genes are widely distributed along the coding regions.<sup>88</sup>

Sanger sequencing is a method of DNA sequencing based on the selective incorporation of chain-terminating dideoxynucleotides by DNA polymerase during DNA replication *in vitro*, which was developed by Frederick Sanger and colleagues in 1977.<sup>91</sup>

Recently, one-step Sanger sequencing (combining the amplification and sequencing steps) methods such as Ampliseq and SeqSharp have been developed that allows for rapid sequencing of target genes without cloning or prior amplification.

However, covering all potentially clinically relevant genes in a routine diagnostic setting by these methods has become virtually impossible. Reliable high-throughput methods allowing for parallel analysis of multiple targets emerged as an attractive alternative for comprehensive diagnostic neuropathology. NGS provides opportunities to evaluate many genomic targets with high accuracy and sensitivity due to high sequencing coverage. However, the Sanger method is widely used for small-scale projects, and validation of NGS results, especially long serial DNA sequence reads that are greater than 500 nucleotides.

### Pyrosequencing

Pyrosequencing is a method of DNA sequencing based on the “sequencing by synthesis” principle.<sup>110</sup> It differs from Sanger sequencing in that it relies on the detection of pyrophosphates that are released upon nucleotide incorporation rather than chain termination with dideoxynucleotides. Various gene alterations can be detected by pyrosequencing, including *IDH1/IDH2* mutations, *TERTp* mutation and *MGMT* methylation.<sup>92,111-113</sup>

### NGS

More recently, high volume Sanger sequencing has been sup-

planted by NGS methods, especially for large-scale, automated genome analyses. NGS is a high-capacity parallel sequencing process that handles hundreds to millions of DNA fragments simultaneously.<sup>114,115</sup> Currently, there are second- and third-generation sequencing technologies that continue to reduce the cost of DNA sequencing and improve accuracy. The ability to multiplex several samples also leads to increased throughput and reduced cost. Soon, NGS will enter clinical practices but it is still uncertain whether it can replace the established techniques. Depending on the type of NGS panel, it can only detect single nucleotide variations and indels or embrace CNV and translocations. The performance of the NGS panel requires rigorous validations and strict quality control for its sensitivity, specificity, and accuracy. There are several NGS panels for brain tumor companion diagnosis.<sup>78,79,95,116</sup> Current practice and guidelines for the clinical use of a NGS-based oncology test are described in Strom's 2016 paper.<sup>117</sup> A comparison of different NGS-based diagnostic tools is summarized in Lapin *et al.* paper (2016).<sup>118</sup>

### FISH

FISH studies can be easily used to identify chromosomal aberrations, such as a 1p/19q codeletion, *EGFR* amplification or high polysomy, *PTEN* and *CDKN2A* homozygous or hemizygous deletions, *C-MYC* and *N-MYC* amplifications, *BRAF* fusions or copy gains, *C11orf95-RELA* fusions, *C11orf95-YAP1* fusions, *YAP1-MAMLD1* fusions, and *MYB-QKI* fusions. The probes and reading criteria of currently used FISH for the diagnosis and prognosis of brain tumors are summarized in Table 6.

The presence or absence of the 1p/19q codeletion can be determined by FISH, comparative genomic hybridization (CGH), or microsatellite analyses for a loss of heterozygosity (LOH) on chromosomes 1p and 19q.<sup>119,120</sup>

When the amount of DNA is insufficient to carry out the single nucleotide polymorphism or CGH array, microsatellite analysis is performed to evaluate via PCR to determine whether there is a LOH of chromosome 1p and 19q.<sup>121</sup> In cases of 1p/19q codeletion, the evaluation and interpretation of FISH results are based on International Society of Pediatric Oncology

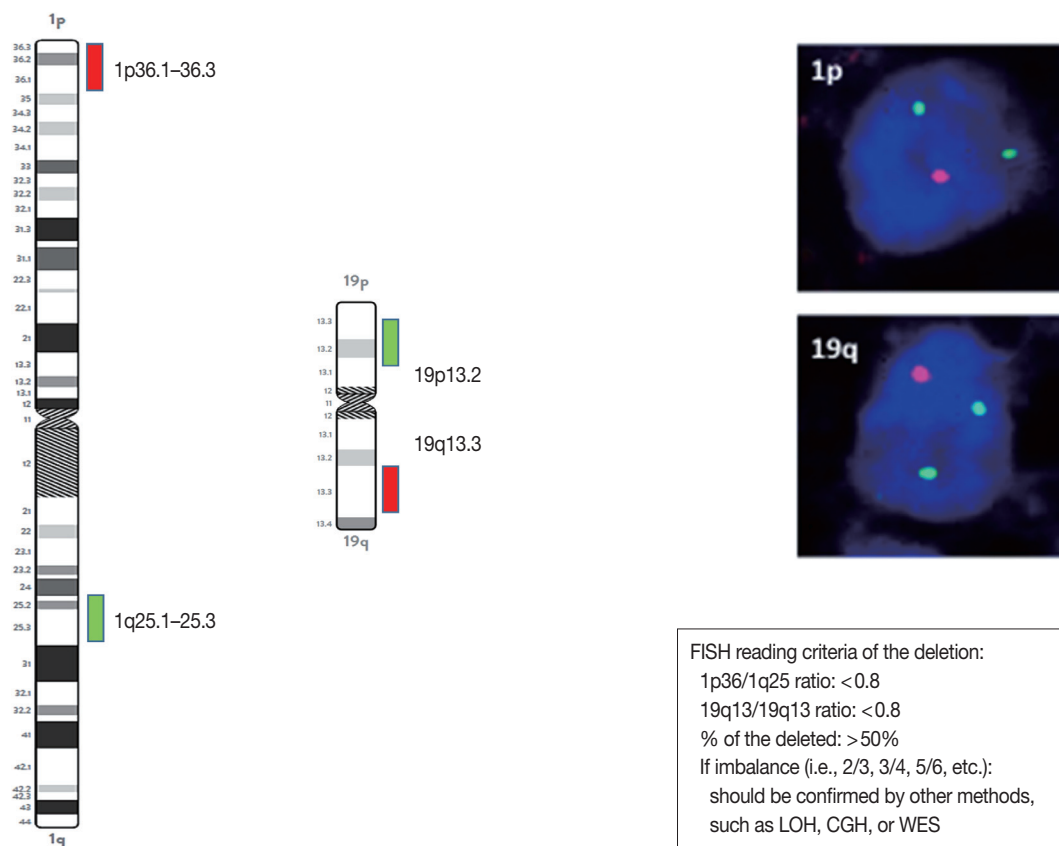


**Fig. 3.** Schematic view, photographs, and reading criteria of the FISH probes for detecting 1p and 19q deletion. The FISH probes are long enough to find out the whole arm deletion. 1p/19q deleted cases show one orange signal and two green signals. The diagnostic cut-off of 1p and 10q deletion is written in the box. FISH, fluorescent *in situ* hybridization; LOH, loss of heterozygosity; CGH, comparative genomic hybridization; WES, whole exome sequencing.

(SIOP) guidelines for neuroblastoma study.<sup>80</sup> For each hybridization, the number of green and orange signals is assessed for a minimum of 100 nonoverlapping nuclei. An interpretation of a deletion was made when > 50% of nuclei harbored less than a single orange signal (0/2, 1/2, 0/3, 1/3, etc). Such deletions most likely correspond to a LOH (Fig. 3). However, with increasing grades of malignancy, genomic polyploidies may be encountered. These chromosomal polysomies may be balanced (e.g., 3/3, 4/4, 5/5, etc.) or imbalanced (e.g., 3/2, 4/2, 3/5, 4/5, etc.), indicating relative gains or losses. Whether an imbalance situation with relative loss of the target 1p or 19q corresponds to a hemizygous deletion in the presence of reduplication cannot be solved by FISH. In such cases, secondary assays such as PCR-based LOH or CGH studies should be used for better specificity.<sup>80</sup>

#### Methylation specific PCR (O6 methyl guanine methyl transferase)

Methylation can be detected by methylation specific PCR (MSP), pyrosequencing, multiplex ligation-dependent probe assay, or BeadChip microarray.<sup>57,113,122</sup> In the Seoul National University Hospital, MSP is conducted using an EZ DNA methylation Kit (catalog No. D5005, Zymo Research, Irvine, CA, USA) to determine the methylation status of the *MGMT* promoter. The primer set is described in Table 5. The primer sequences for *MGMT* were as follows: methylated forward, 5'-TTT CGA CGT TCG TAG GTT TTC GC-3'; methylated reverse, 5'-GCA CTC TTC CGA AAA CGA AACG 3'; unmethylated forward, 5'-TTT GTG TTT TGA TGT TTG TAG GTT TTT GT-3'; and unmethylated reverse, 5'-AAC TCC ACA CTC TTC CAA AAA CAA AAC A-3'.

## DISCUSSION

Among primary adult and pediatric CNS tumors, diffuse gliomas are the largest and most diverse group. They usually arise in the cerebral hemispheres and are defined by their widely infiltrative properties and tendency for biological progression. According to the 2016 WHO criteria, gliomas can be classified using combined histological and molecular markers as diffuse astrocytic and oligodendroglial tumors, other astrocytic tumors, ependymal tumors, or other gliomas. The most aggressive astrocytic tumors with a dismal prognosis are the GBMs with wild type IDH and DMG, histone-mutant (H3 K27, G34, and K36). Less infiltrative gliomas in children and young adults include WHO grade I pilocytic astrocytomas, WHO grade II/III

pleomorphic xanthoastrocytomas, and WHO grade I subependymal giant cell astrocytomas. Other major classes of CNS tumors include neuronal and mixed glioneuronal tumors as well as embryonal tumors such as cerebellar medulloblastomas, and AT/RT, and extra-axial meningiomas.

The diagnosis of CNS tumors is historically primarily based on histopathological features. However, studies have shown that patients with morphologically identical tumors have different clinical outcomes and treatment responses due to the different molecular genetic characteristics of the tumor. Therefore, many molecular markers became deeply integrated into the diagnosis of CNS tumors and are now used to guide prognosis and treatment of patients. If molecular genetic testing is not possible, a diagnosis is made with the nonspecific term “glioma, not otherwise specified (NOS).” In this case, because the grade and the exact diagnosis of the tumor as well as the biological markers are covered, the precision diagnosis and the appropriate treatments are no longer possible. These “NOS diagnostics” must be reclassified using molecular genetic diagnostic tools.

#### Diffuse astrocytic and oligodendroglial tumors

Molecular genetic testing can classify diffuse astrocytic and oligodendroglial tumors (WHO grades II–III) and differentiate IDH-mutant GBMs from IDH-wildtype GBMs based on molecular signature of astrocytic and oligodendroglial tumors. Diffuse astrocytic tumors and IDH-mutant GBMs are characterized by mutations in *IDH1/2*, *TP53*, and *ATRX*, whereas oligodendrogliomas are characterized by mutations in *IDH1/2*, *CIC*, *FUBP1*, and *TERT*, and a codeletion in 1p/19q (whole chromosomal arm deletion) (Fig. 1). IDH-wildtype GBMs can be identified by demonstrating a dysregulation of several critical signaling pathways and a lack of the above-mentioned genetic alterations except *TERT* mutations, which are common in IDH-wildtype GBM. The main signaling pathways involved in IDH-wildtype GBMs are RTK/RAS/PI3K pathways (via amplification and mutations in *EGFR* [*EGFRvIII*], *PIK3CA*, *RAS*, *NF1*, and *MET*) and *TP53* and *RB1* suppressor pathways (via mutations in or loss of *TP53*, *CDKN2A*, and *RB1* genes) (Fig. 1).<sup>94</sup>

Mutations in *IDH1/2* should be studied in diffuse gliomas for the WHO classification of CNS tumors. They are favorable prognostic markers and are genomic abnormalities initially present in both astrocytic and oligodendroglial tumors. Therefore, from the revised version of 2016 fourth edition of the CNS Tumor Classification, these two tumor categories have been combined as diffuse astrocytic and oligodendroglial tumors.<sup>7</sup> *P53* and *ATRX* mutations are now the hallmark of WHO

grade II and grade III astrocytic tumors. *TERT* mutations, such as C228T and C250T, are found in more than 90% of oligodendroglial tumors and in more than 80% of GBMs as well as about 30%–40% of lower grade gliomas. Mutations in *TERT* were associated with poor survival and resistance to radiotherapy in GBMs and in lower grade gliomas (grade II and III) without *IDH* mutation; however, *TERT* mutations were associated with a favorable prognosis in lower grade gliomas with *IDH* mutations.<sup>63,123</sup>

### High- and low-grade pediatric gliomas

Pediatric high-grade gliomas are unique, featuring mutations in *H3F3A*, *ATRX*, and *DAXX*, whereas PLGGs contain mutations or rearrangements in *BRAF*, *FGFR1*, or *MYB*. Furthermore, mutations in *IDH* are rare unless the patient is an adolescent (Fig. 2).<sup>22,64,65</sup> The circumscribed low-grade gliomas such as pilocytic astrocytoma, pilomyxoid astrocytoma, ganglioglioma, and PXA often harbor the *BRAF* V600E or *FGFR1* mutation, or gene fusions involving *BRAF* with *KIAA1549* or *FAM131B*.<sup>35,62,65</sup> Histone H3 K27M, K36, and G34 mutations should be studied in pediatric glioma arising in the midline of CNS, i.e., the thalamus, pons, and spinal cord.<sup>124</sup> However, the histone G34 mutation can be present in cerebral high-grade diffuse gliomas of the adult (about 5%) and the histone K36 mutation is rarely found in pediatric midline gliomas.<sup>84</sup>

Finally, the *BRAF* V600E mutation can be studied in low-grade glioneuronal tumors, such as PXA (about 60%), ganglioglioma (about 25%), pilocytic astrocytoma (about 15%), epithelioid GBM (about 50%), and papillary type of craniopharyngioma (about 100%).<sup>35,66</sup>

### Medulloblastomas and other embryonic tumors

Medulloblastomas have been recently divided into several subtypes based on specific driver mutations including *WNT*, *SHH*, group 3, and group 4.<sup>125–127</sup> Mutations in *CTNNB1*, *DDX3X* or monosomy 6 in the Wnt pathway of medulloblastomas tend to lead to a much better prognosis. In contrast, *MYC* or *MYCN/CDK6* amplification is characteristic of group 3 and 4 medulloblastomas, which are far more likely to metastasize and have a poor prognosis even with intensive therapy. Tumors with *PTCH* and *SMO* belong to the *SHH* class, and have a relatively intermediate prognosis between *Wnt* and group 3/4 tumors. *CTNNB1* mutations can be present in classical-type medulloblastomas and adamantinomatous-type craniopharyngiomas.<sup>61,125,128</sup>

*SMARCB1 (INI1)* or *SMARCA4 (BRG1)* gene mutations or deletions are essential for the diagnosis of AT/RT, which show

dismal prognosis.<sup>44–46</sup> The molecular genetic hallmark of ETMR is chromosome 19 miRNA cluster (*C19MC*) amplification.<sup>129</sup> If certain tumors are morphologically similar to these tumors, i.e., rhabdoid feature, but molecular studies do not reveal these genetic abnormalities or molecular studies cannot be done, CNS embryonal tumor with rhabdoid feature or ETMR, NOS can be made as a pathological diagnosis.<sup>7,129</sup> Therefore, the molecular characterization of medulloblastomas and embryonal tumors have lasting clinical value.

### Meningioma and meningeal solitary fibrous tumor/hemangiopericytoma

Meningiomas often have mutations in the *NF2*, *AKT1*, *SMO*, and *KLF4* genes. Furthermore, meningiomas with mutant *NF2* are far more likely to exhibit atypical grade II features than the other subtypes.<sup>50–52</sup> Recurrent mutations in *KLF4*, *AKT1*, and *SMO* genes are often present in *NF2*-negative sporadic meningiomas.<sup>50</sup> Clinical trials involving *SMO/AKT/NF2* inhibitors are open for patients with progressive meningiomas with *SMO/AKT/NF2* mutations.<sup>50,81</sup>

Meningeal hemangiopericytomas and solitary fibrous tumors have the same genetic modification as *NAB2-STAT6* gene fusion and are considered as the same tumor.<sup>48</sup> This gene fusion study is essential for the differential diagnosis of histologically similar tumors.

### Genetic alterations as prognostic and predictive markers and therapeutic targets

Overall, the analysis of multiple molecular markers not only aids in establishing a correct morphological diagnosis, but also highlights the biological differences between morphologically similar tumors. It can also help with the clinical management of patients. For example, patients with *IDH1/TERTp/CIC/FUBP1* positive lower grade gliomas (WHO grades II–III) have a significantly longer median overall survival than those with *IDH1/TP53/ATRX* mutations.<sup>86,130</sup>

In addition, several molecular biomarkers showed promise in predicting responses to targeted therapies.<sup>94,131</sup> For example, clinical trials are now open for GBMs with *EGFRvIII* mutations, vemurafenib is being evaluated in *BRAF* V600E mutant gliomas, and clinical response has already been observed in *FGFR3-TACC3*-positive patients treated with an *FGFR* inhibitor.<sup>78</sup> NGS-based high-throughput molecular testing may provide potential new targets for precision medicine.

## CONCLUSION

We are now in the era of precision medicine, and have slowly caught up with the rapid development of precision medicine. High-throughput assays that can test multiple genes at once are essential for pathological diagnosis in daily practice, and NGS technology has made this possible. Current practices and guidelines for the clinical use of NGS-based oncology tests are well documented in Strom's paper.<sup>117</sup> However, the medical insurance system has not kept up with the speed of technical development, the advances in diagnostic modalities, and newly developed treatment options. These are obstacles that prevents the doctors from implementing the precision medicine. In order to introduce the advanced knowledge and technologies into the daily practice of pathological diagnosis and clinical fields and reduce the costs, the medical insurance system should be formulated accordingly.

### Conflicts of Interest

No potential conflict of interest relevant to this article was reported.

### Acknowledgments

This work was supported by Grant from Korean Society of Pathologist (2016).

## REFERENCES

1. Lee CH, Jung KW, Yoo H, Park S, Lee SH. Epidemiology of primary brain and central nervous system tumors in Korea. *J Korean Neurosurg Soc* 2010; 48: 145-52.
2. Jung KW, Ha J, Lee SH, Won YJ, Yoo H. An updated nationwide epidemiology of primary brain tumors in republic of Korea. *Brain Tumor Res Treat* 2013; 1: 16-23.
3. Cancer Genome Atlas Research Network, Brat DJ, Verhaak RG, *et al.* Comprehensive, integrative genomic analysis of diffuse lower-grade gliomas. *N Engl J Med* 2015; 372: 2481-98.
4. Brennan CW, Verhaak RG, McKenna A, *et al.* The somatic genomic landscape of glioblastoma. *Cell* 2013; 155: 462-77.
5. Phillips HS, Kharbanda S, Chen R, *et al.* Molecular subclasses of high-grade glioma predict prognosis, delineate a pattern of disease progression, and resemble stages in neurogenesis. *Cancer Cell* 2006; 9: 157-73.
6. Parsons DW, Jones S, Zhang X, *et al.* An integrated genomic analysis of human glioblastoma multiforme. *Science* 2008; 321: 1807-12.
7. Louis DN, Perry A, Reifenberger G, *et al.* The 2016 World Health Organization classification of tumors of the central nervous system: a summary. *Acta Neuropathol* 2016; 131: 803-20.
8. Weller M, Weber RG, Willscher E, *et al.* Molecular classification of diffuse cerebral WHO grade II/III gliomas using genome- and transcriptome-wide profiling improves stratification of prognostically distinct patient groups. *Acta Neuropathol* 2015; 129: 679-93.
9. Rajmohan KS, Sugur HS, Shwetha SD, *et al.* Prognostic significance of histomolecular subgroups of adult anaplastic (WHO Grade III) gliomas: applying the 'integrated' diagnosis approach. *J Clin Pathol* 2016; 69: 686-94.
10. Malzkorn B, Reifenberger G. Practical implications of integrated glioma classification according to the World Health Organization classification of tumors of the central nervous system 2016. *Curr Opin Oncol* 2016; 28: 494-501.
11. Clark K, Voronovich Z, Horbinski C. How molecular testing can help (and hurt) in the workup of gliomas. *Am J Clin Pathol* 2013; 139: 275-88.
12. Reuss DE, Sahm F, Schrimpf D, *et al.* ATRX and IDH1-R132H immunohistochemistry with subsequent copy number analysis and IDH sequencing as a basis for an "integrated" diagnostic approach for adult astrocytoma, oligodendroglioma and glioblastoma. *Acta Neuropathol* 2015; 129: 133-46.
13. Aldape K, Zadeh G, Mansouri S, Reifenberger G, von Deimling A. Glioblastoma: pathology, molecular mechanisms and markers. *Acta Neuropathol* 2015; 129: 829-48.
14. Bush NA, Chang SM, Berger MS. Current and future strategies for treatment of glioma. *Neurosurg Rev* 2017; 40: 1-14.
15. Chan AK, Pang JC, Chung NY, *et al.* Loss of CIC and FUBP1 expressions are potential markers of shorter time to recurrence in oligodendrogial tumors. *Mod Pathol* 2014; 27: 332-42.
16. Kreth S, Thon N, Kreth FW. Epigenetics in human gliomas. *Cancer Lett* 2014; 342: 185-92.
17. Ostrom QT, Gittleman H, Stetson L, Virk SM, Barnholtz-Sloan JS. Epidemiology of gliomas. *Cancer Treat Res* 2015; 163: 1-14.
18. Reis GF, Pekmezci M, Hansen HM, *et al.* CDKN2A loss is associated with shortened overall survival in lower-grade (World Health Organization Grades II-III) astrocytomas. *J Neuropathol Exp Neurol* 2015; 74: 442-52.
19. Simeonova I, Huillard E. *In vivo* models of brain tumors: roles of genetically engineered mouse models in understanding tumor biology and use in preclinical studies. *Cell Mol Life Sci* 2014; 71: 4007-26.
20. Cachia D, Kamiya-Matsuoka C, Mandel JJ, *et al.* Primary and secondary gliosarcomas: clinical, molecular and survival characteristics. *J Neurooncol* 2015; 125: 401-10.

21. Louis DN, Perry A, Burger P, et al. International Society of Neuro-pathology: Haarlem consensus guidelines for nervous system tumor classification and grading. *Brain Pathol* 2014; 24: 429-35.
22. Schwartzenuber J, Korshunov A, Liu XY, et al. Driver mutations in histone H3.3 and chromatin remodelling genes in paediatric glioblastoma. *Nature* 2012; 482: 226-31.
23. Khuong-Quang DA, Buczkowicz P, Rakopoulos P, et al. K27M mutation in histone H3.3 defines clinically and biologically distinct subgroups of pediatric diffuse intrinsic pontine gliomas. *Acta Neuropathol* 2012; 124: 439-47.
24. Solomon DA, Wood MD, Tihan T, et al. Diffuse midline gliomas with histone H3-K27M mutation: a series of 47 cases assessing the spectrum of morphologic variation and associated genetic alterations. *Brain Pathol* 2016; 26: 569-80.
25. Zhang R, Han J, Daniels D, Huang H, Zhang Z. Detecting the *H3F3A* mutant allele found in high-grade pediatric glioma by real-time PCR. *J Neurooncol* 2016; 126: 27-36.
26. Nambirajan A, Malgulwar PB, Sharma MC, et al. *C11orf95-RELA* fusion present in a primary intracranial extra-axial ependymoma: report of a case with literature review. *Neuropathology* 2016; 36: 490-5.
27. Wu J, Armstrong TS, Gilbert MR. Biology and management of ependymomas. *Neuro Oncol* 2016; 18: 902-13.
28. Figarella-Branger D, Lechapt-Zalcman E, Tabouret E, et al. Supratentorial clear cell ependymomas with branching capillaries demonstrate characteristic clinicopathological features and pathological activation of nuclear factor-kappaB signaling. *Neuro Oncol* 2016; 18: 919-27.
29. Nobusawa S, Hirato J, Sugai T, et al. Atypical teratoid/rhabdoid tumor (AT/RT) arising from ependymoma: a type of AT/RT secondarily developing from other primary central nervous system tumors. *J Neuropathol Exp Neurol* 2016; 75: 167-74.
30. Olar A, Sulman EP. Molecular markers in low-grade glioma-toward tumor reclassification. *Semin Radiat Oncol* 2015; 25: 155-63.
31. Capper D, Reifenberger G. Classification of gliomas: current progress and perspectives. *Nervenarzt* 2015; 86: 672-83.
32. Cachia D, Wani K, Penas-Prado M, et al. *C11orf95-RELA* fusion present in a primary supratentorial ependymoma and recurrent sarcoma. *Brain Tumor Pathol* 2015; 32: 105-11.
33. Nobusawa S, Hirato J, Yokoo H. Molecular genetics of ependymomas and pediatric diffuse gliomas: a short review. *Brain Tumor Pathol* 2014; 31: 229-33.
34. Parker M, Mohankumar KM, Punchihewa C, et al. *C11orf95-RELA* fusions drive oncogenic NF-kappaB signalling in ependymoma. *Nature* 2014; 506: 451-5.
35. Schindler G, Capper D, Meyer J, et al. Analysis of *BRAF* V600E mutation in 1,320 nervous system tumors reveals high mutation frequencies in pleomorphic xanthoastrocytoma, ganglioglioma and extra-cerebellar pilocytic astrocytoma. *Acta Neuropathol* 2011; 121: 397-405.
36. Tanboon J, Williams EA, Louis DN. The diagnostic use of immunohistochemical surrogates for signature molecular genetic alterations in gliomas. *J Neuropathol Exp Neurol* 2016; 75: 4-18.
37. Thomas L, Di Stefano AL, Ducray F. Predictive biomarkers in adult gliomas: the present and the future. *Curr Opin Oncol* 2013; 25: 689-94.
38. Zhang J, Wu G, Miller CP, et al. Whole-genome sequencing identifies genetic alterations in pediatric low-grade gliomas. *Nat Genet* 2013; 45: 602-12.
39. Korshunov A, Meyer J, Capper D, et al. Combined molecular analysis of *BRAF* and *IDH1* distinguishes pilocytic astrocytoma from diffuse astrocytoma. *Acta Neuropathol* 2009; 118: 401-5.
40. Tian Y, Rich BE, Vena N, et al. Detection of *KIAA1549-BRAF* fusion transcripts in formalin-fixed paraffin-embedded pediatric low-grade gliomas. *J Mol Diagn* 2011; 13: 669-77.
41. Cin H, Meyer C, Herr R, et al. Oncogenic *FAM131B-BRAF* fusion resulting from 7q34 deletion comprises an alternative mechanism of MAPK pathway activation in pilocytic astrocytoma. *Acta Neuropathol* 2011; 121: 763-74.
42. Collins VP, Jones DT, Giannini C. Pilocytic astrocytoma: pathology, molecular mechanisms and markers. *Acta Neuropathol* 2015; 129: 775-88.
43. Roth JJ, Fierst TM, Waanders AJ, Yimei L, Biegel JA, Santi M. Whole chromosome 7 gain predicts higher risk of recurrence in pediatric pilocytic astrocytomas independently from *KIAA1549-BRAF* fusion status. *J Neuropathol Exp Neurol* 2016; 75: 306-15.
44. Sredni ST, Tomita T. Rhabdoid tumor predisposition syndrome. *Pediatr Dev Pathol* 2015; 18: 49-58.
45. Hasselblatt M, Gesk S, Oyen F, et al. Nonsense mutation and inactivation of *SMARCA4 (BRG1)* in an atypical teratoid/rhabdoid tumor showing retained *SMARCB1 (INI1)* expression. *Am J Surg Pathol* 2011; 35: 933-5.
46. Fruhwald MC, Biegel JA, Bourdeaut F, Roberts CW, Chi SN. Atypical teratoid/rhabdoid tumors-current concepts, advances in biology, and potential future therapies. *Neuro Oncol* 2016; 18: 764-78.
47. Diamandis P, Ferrer-Luna R, Huang RY, et al. Case report: next generation sequencing identifies a *NAB2-STAT6* fusion in glioblastoma. *Diagn Pathol* 2016; 11: 13.
48. Han N, Kim H, Min SK, et al. Meningeal solitary fibrous tumors with delayed extracranial metastasis. *J Pathol Transl Med* 2016; 50: 113-21.
49. Maekawa A, Kohashi K, Yamada Y, et al. A case of intracranial soli-

- tary fibrous tumor/hemangiopericytoma with dedifferentiated component. *Neuropathology* 2015; 35: 260-5.
50. Brastianos PK, Horowitz PM, Santagata S, *et al.* Genomic sequencing of meningiomas identifies oncogenic *SMO* and *AKT1* mutations. *Nat Genet* 2013; 45: 285-9.
  51. Clark VE, Erson-Omay EZ, Serin A, *et al.* Genomic analysis of non-NF2 meningiomas reveals mutations in *TRAF7*, *KLF4*, *AKT1*, and *SMO*. *Science* 2013; 339: 1077-80.
  52. Reuss DE, Piro RM, Jones DT, *et al.* Secretory meningiomas are defined by combined *KLF4* K409Q and *TRAF7* mutations. *Acta Neuropathol* 2013; 125: 351-8.
  53. Yuzawa S, Nishihara H, Tanaka S. Genetic landscape of meningioma. *Brain Tumor Pathol* 2016; 33: 237-47.
  54. Mehes G, Irsai G, Bedekovics J, *et al.* Activating *BRAF* V600E mutation in aggressive pediatric Langerhans cell histiocytosis: demonstration by allele-specific PCR/direct sequencing and immunohistochemistry. *Am J Surg Pathol* 2014; 38: 1644-8.
  55. Rodriguez FJ, Vizcaino MA, Lin MT. Recent advances on the molecular pathology of glial neoplasms in children and adults. *J Mol Diagn* 2016; 18: 620-34.
  56. Maire CL, Ligon KL. Molecular pathologic diagnosis of epidermal growth factor receptor. *Neuro Oncol* 2014; 16 Suppl 8: viii1-6.
  57. Masui K, Mischel PS, Reifenberger G. Molecular classification of gliomas. *Handb Clin Neurol* 2016; 134: 97-120.
  58. Jones DT, Kocialkowski S, Liu L, *et al.* Tandem duplication producing a novel oncogenic *BRAF* fusion gene defines the majority of pilocytic astrocytomas. *Cancer Res* 2008; 68: 8673-7.
  59. van den Bent MJ, Dubbink HJ, Sanson M, *et al.* *MGMT* promoter methylation is prognostic but not predictive for outcome to adjuvant PCV chemotherapy in anaplastic oligodendroglial tumors: a report from EORTC Brain Tumor Group Study 26951. *J Clin Oncol* 2009; 27: 5881-6.
  60. Dubbink HJ, Atmodimedjo PN, Kros JM, *et al.* Molecular classification of anaplastic oligodendroglioma using next-generation sequencing: a report of the prospective randomized EORTC Brain Tumor Group 26951 phase III trial. *Neuro Oncol* 2016; 18: 388-400.
  61. Ramaswamy V, Remke M, Bouffet E, *et al.* Risk stratification of childhood medulloblastoma in the molecular era: the current consensus. *Acta Neuropathol* 2016; 131: 821-31.
  62. Roth JJ, Santi M, Pollock AN, *et al.* Chromosome band 7q34 deletions resulting in *KIAA1549-BRAF* and *FAM131B-BRAF* fusions in pediatric low-grade gliomas. *Brain Pathol* 2015; 25: 182-92.
  63. Zhang ZY, Chan AK, Ding XJ, *et al.* *TERT* promoter mutations contribute to *IDH* mutations in predicting differential responses to adjuvant therapies in WHO grade II and III diffuse gliomas. *Oncotarget* 2015; 6: 24871-83.
  64. Bandopadhyay P, Ramkissoon LA, Jain P, *et al.* *MYB-QKI* rearrangements in angiocentric glioma drive tumorigenicity through a tripartite mechanism. *Nat Genet* 2016; 48: 273-82.
  65. Qaddoumi I, Orisme W, Wen J, *et al.* Genetic alterations in uncommon low-grade neuroepithelial tumors: *BRAF*, *FGFR1*, and *MYB* mutations occur at high frequency and align with morphology. *Acta Neuropathol* 2016; 131: 833-45.
  66. Behling F, Barrantes-Freer A, Skardelly M, *et al.* Frequency of *BRAF* V600E mutations in 969 central nervous system neoplasms. *Diagn Pathol* 2016; 11: 55.
  67. Appin CL, Brat DJ. Molecular pathways in gliomagenesis and their relevance to neuropathologic diagnosis. *Adv Anat Pathol* 2015; 22: 50-8.
  68. Dang L, White DW, Gross S, *et al.* Cancer-associated *IDH1* mutations produce 2-hydroxyglutarate. *Nature* 2010; 465: 966.
  69. Dang L, White DW, Gross S, *et al.* Cancer-associated *IDH1* mutations produce 2-hydroxyglutarate. *Nature* 2009; 462: 739-44.
  70. Yang H, Ye D, Guan KL, Xiong Y. *IDH1* and *IDH2* mutations in tumorigenesis: mechanistic insights and clinical perspectives. *Clin Cancer Res* 2012; 18: 5562-71.
  71. Dimitrov L, Hong CS, Yang C, Zhuang Z, Heiss JD. New developments in the pathogenesis and therapeutic targeting of the *IDH1* mutation in glioma. *Int J Med Sci* 2015; 12: 201-13.
  72. Noushmehr H, Weisenberger DJ, Diefes K, *et al.* Identification of a CpG island methylator phenotype that defines a distinct subgroup of glioma. *Cancer Cell* 2010; 17: 510-22.
  73. Appin CL, Brat DJ. Biomarker-driven diagnosis of diffuse gliomas. *Mol Aspects Med* 2015; 45: 87-96.
  74. Claus EB, Walsh KM, Wiencke JK, *et al.* Survival and low-grade glioma: the emergence of genetic information. *Neurosurg Focus* 2015; 38: E6.
  75. Cohen AL, Colman H. Glioma biology and molecular markers. *Cancer Treat Res* 2015; 163: 15-30.
  76. Jha P, Pia Patric IR, Shukla S, *et al.* Genome-wide methylation profiling identifies an essential role of reactive oxygen species in pediatric glioblastoma multiforme and validates a methylome specific for H3 histone family 3A with absence of G-CIMP/isocitrate dehydrogenase 1 mutation. *Neuro Oncol* 2014; 16: 1607-17.
  77. Swartling FJ. Myc proteins in brain tumor development and maintenance. *Ups J Med Sci* 2012; 117: 122-31.
  78. Northcott PA, Pfister SM, Jones DT. Next-generation (epi)genetic drivers of childhood brain tumours and the outlook for targeted therapies. *Lancet Oncol* 2015; 16: e293-302.
  79. Blumenthal DT, Dvir A, Lossos A, *et al.* Clinical utility and treatment outcome of comprehensive genomic profiling in high grade glioma patients. *J Neurooncol* 2016; 130: 211-9.

80. Ambros PF, Ambros IM; SIOP Europe Neuroblastoma Pathology, Biology, and Bone Marrow Group. Pathology and biology guidelines for resectable and unresectable neuroblastic tumors and bone marrow examination guidelines. *Med Pediatr Oncol* 2001; 37: 492-504.
81. Abedalthagafi M, Bi WL, Aizer AA, et al. Oncogenic *PI3K* mutations are as common as *AKT1* and *SMO* mutations in meningioma. *Neuro Oncol* 2016; 18: 649-55.
82. Clynes D, Higgs DR, Gibbons RJ. The chromatin remodeller *ATRX*: a repeat offender in human disease. *Trends Biochem Sci* 2013; 38: 461-6.
83. Gibbons RJ, McDowell TL, Raman S, et al. Mutations in *ATRX*, encoding a SWI/SNF-like protein, cause diverse changes in the pattern of DNA methylation. *Nat Genet* 2000; 24: 368-71.
84. Chan KM, Fang D, Gan H, et al. The histone H3.3K27M mutation in pediatric glioma reprograms H3K27 methylation and gene expression. *Genes Dev* 2013; 27: 985-90.
85. Chen P, Zhao J, Wang Y, et al. H3.3 actively marks enhancers and primes gene transcription via opening higher-ordered chromatin. *Genes Dev* 2013; 27: 2109-24.
86. Jiao Y, Killela PJ, Reitman ZJ, et al. Frequent *ATRX*, *CIC*, *FUBP1* and *IDH1* mutations refine the classification of malignant gliomas. *Oncotarget* 2012; 3: 709-22.
87. Bettegowda C, Agrawal N, Jiao Y, et al. Mutations in *CIC* and *FUBP1* contribute to human oligodendroglioma. *Science* 2011; 333: 1453-5.
88. Sahm F, Koelsche C, Meyer J, et al. *CIC* and *FUBP1* mutations in oligodendrogliomas, oligoastrocytomas and astrocytomas. *Acta Neuropathol* 2012; 123: 853-60.
89. Jiménez G, Shvartsman SY, Paroush Z. The Capicua repressor: a general sensor of RTK signaling in development and disease. *J Cell Sci* 2012; 125(Pt 6): 1383-91.
90. Chittaranjan S, Chan S, Yang C, et al. Mutations in *CIC* and *IDH1* cooperatively regulate 2-hydroxyglutarate levels and cell clonogenicity. *Oncotarget* 2014; 5: 7960-79.
91. Sanger F, Nicklen S, Coulson AR. DNA sequencing with chain-terminating inhibitors. *Proc Natl Acad Sci U S A* 1977; 74: 5463-7.
92. Switzeny OJ, Christmann M, Renovanz M, Giese A, Sommer C, Kaina B. *MGMT* promoter methylation determined by HRM in comparison to MSP and pyrosequencing for predicting high-grade glioma response. *Clin Epigenetics* 2016; 8: 49.
93. Tritz R, Habita C, Robbins JM, Gomez GG, Kruse CA. Catalytic nucleic acid enzymes for the study and development of therapies in the central nervous system: review article. *Gene Ther Mol Biol* 2005; 9A: 89-106.
94. Venkatesan S, Lamfers ML, Dirven CM, Leenstra S. Genetic biomarkers of drug response for small-molecule therapeutics targeting the RTK/Ras/PI3K, p53 or Rb pathway in glioblastoma. *CNS Oncol* 2016; 5: 77-90.
95. Nikiforova MN, Wald AI, Melan MA, et al. Targeted next-generation sequencing panel (GliSeq) provides comprehensive genetic profiling of central nervous system tumors. *Neuro Oncol* 2016; 18: 379-87.
96. Mistry M, Zhukova N, Merico D, et al. *BRAF* mutation and *CDKN2A* deletion define a clinically distinct subgroup of childhood secondary high-grade glioma. *J Clin Oncol* 2015; 33: 1015-22.
97. Yang P, Cai J, Yan W, et al. Classification based on mutations of *TERT* promoter and *IDH* characterizes subtypes in grade II/III gliomas. *Neuro Oncol* 2016; 18: 1099-108.
98. Chan AK, Yao Y, Zhang Z, et al. Combination genetic signature stratifies lower-grade gliomas better than histological grade. *Oncotarget* 2015; 6: 20885-901.
99. Arita H, Narita Y, Takami H, et al. *TERT* promoter mutations rather than methylation are the main mechanism for *TERT* upregulation in adult gliomas. *Acta Neuropathol* 2013; 126: 939-41.
100. Arita H, Narita Y, Fukushima S, et al. Upregulating mutations in the *TERT* promoter commonly occur in adult malignant gliomas and are strongly associated with total 1p19q loss. *Acta Neuropathol* 2013; 126: 267-76.
101. Heidenreich B, Rachakonda PS, Hosen I, et al. *TERT* promoter mutations and telomere length in adult malignant gliomas and recurrences. *Oncotarget* 2015; 6: 10617-33.
102. Chen C, Han S, Meng L, Li Z, Zhang X, Wu A. *TERT* promoter mutations lead to high transcriptional activity under hypoxia and temozolomide treatment and predict poor prognosis in gliomas. *PLoS One* 2014; 9: e100297.
103. Arita H, Yamasaki K, Matsushita Y, et al. A combination of *TERT* promoter mutation and *MGMT* methylation status predicts clinically relevant subgroups of newly diagnosed glioblastomas. *Acta Neuropathol Commun* 2016; 4: 79.
104. Morrissy AS, Garzia L, Shih DJ, et al. Divergent clonal selection dominates medulloblastoma at recurrence. *Nature* 2016; 529: 351-7.
105. Masliah-Planchon J, Machet MC, Fréneaux P, et al. *SMARCA4*-mutated atypical teratoid/rhabdoid tumor with retained *BRG1* expression. *Pediatr Blood Cancer* 2016; 63: 568-9.
106. Sandgren J, Holm S, Marino AM, et al. Whole exome- and mRNA-sequencing of an AT/RT case reveals few somatic mutations and several deregulated signalling pathways in the context of *SMARCB1* deficiency. *Biomed Res Int* 2015; 2015: 862039.
107. Rode A, Maass KK, Willmund KV, Lichter P, Ernst A. Chromothripsis in cancer cells: an update. *Int J Cancer* 2016; 138: 2322-33.
108. Gajjar A, Pfister SM, Taylor MD, Gilbertson RJ. Molecular insights

- into pediatric brain tumors have the potential to transform therapy. *Clin Cancer Res* 2014; 20: 5630-40.
109. Das A, Tan WL, Teo J, Smith DR. Glioblastoma multiforme in an Asian population: evidence for a distinct genetic pathway. *J Neurooncol* 2002; 60: 117-25.
  110. Zascavage RR, Shewale SJ, Planz JV. Deep-sequencing technologies and potential applications in forensic DNA testing. *Forensic Sci Rev* 2013; 25: 79-105.
  111. Cykowski MD, Allen RA, Fung KM, Harmon MA, Dunn ST. Pyrosequencing of *IDH1* and *IDH2* mutations in brain tumors and non-neoplastic conditions. *Diagn Mol Pathol* 2012; 21: 214-20.
  112. Quillien V, Lavenu A, Ducray F, *et al.* Validation of the high-performance of pyrosequencing for clinical MGMT testing on a cohort of glioblastoma patients from a prospective dedicated multicentric trial. *Oncotarget* 2016; 7: 61916-29.
  113. Havik AB, Brandal P, Honne H, *et al.* MGMT promoter methylation in gliomas-assessment by pyrosequencing and quantitative methylation-specific PCR. *J Transl Med* 2012; 10: 36.
  114. Worst BC, van Tilburg CM, Balasubramanian GP, *et al.* Next-generation personalised medicine for high-risk paediatric cancer patients: The INFORM pilot study. *Eur J Cancer* 2016; 65: 91-101.
  115. Sahm F, Schrimpf D, Jones DT, *et al.* Next-generation sequencing in routine brain tumor diagnostics enables an integrated diagnosis and identifies actionable targets. *Acta Neuropathol* 2016; 131: 903-10.
  116. Zacher A, Kaulich K, Stepanow S, *et al.* Molecular diagnostics of gliomas using next generation sequencing of a glioma-tailored gene panel. *Brain Pathol* 2017; 27: 146-59.
  117. Strom SP. Current practices and guidelines for clinical next-generation sequencing oncology testing. *Cancer Biol Med* 2016; 13: 3-11.
  118. Lapin V, Mighion LC, da Silva CP, Cuperus Y, Bean LJ, Hegde MR. Regulating whole exome sequencing as a diagnostic test. *Hum Genet* 2016; 135: 655-73.
  119. Woehrer A, Sander P, Haberler C, *et al.* FISH-based detection of 1p 19q codeletion in oligodendroglial tumors: procedures and protocols for neuropathological practice: a publication under the auspices of the Research Committee of the European Confederation of Neuropathological Societies (Euro-CNS). *Clin Neuropathol* 2011; 30: 47-55.
  120. Jha P, Sarkar C, Pathak P, *et al.* Detection of allelic status of 1p and 19q by microsatellite-based PCR versus FISH: limitations and advantages in application to patient management. *Diagn Mol Pathol* 2011; 20: 40-7.
  121. Idbaih A, Ducray F, Dehais C, *et al.* SNP array analysis reveals novel genomic abnormalities including copy neutral loss of heterozygosity in anaplastic oligodendrogliomas. *PLoS One* 2012; 7: e45950.
  122. Wiestler B, Capper D, Hovestadt V, *et al.* Assessing CpG island methylator phenotype, 1p/19q codeletion, and MGMT promoter methylation from epigenome-wide data in the biomarker cohort of the NOA-04 trial. *Neuro Oncol* 2014; 16: 1630-8.
  123. Gao K, Li G, Qu Y, *et al.* *TERT* promoter mutations and long telomere length predict poor survival and radiotherapy resistance in gliomas. *Oncotarget* 2016; 7: 8712-25.
  124. Gessi M, Gielen GH, Dreschmann V, Waha A, Pietsch T. High frequency of *H3F3A* (K27M) mutations characterizes pediatric and adult high-grade gliomas of the spinal cord. *Acta Neuropathol* 2015; 130: 435-7.
  125. Ellison DW, Dalton J, Kocak M, *et al.* Medulloblastoma: clinicopathological correlates of SHH, WNT, and non-SHH/WNT molecular subgroups. *Acta Neuropathol* 2011; 121: 381-96.
  126. Kool M, Korshunov A, Remke M, *et al.* Molecular subgroups of medulloblastoma: an international meta-analysis of transcriptome, genetic aberrations, and clinical data of WNT, SHH, Group 3, and Group 4 medulloblastomas. *Acta Neuropathol* 2012; 123: 473-84.
  127. Taylor MD, Northcott PA, Korshunov A, *et al.* Molecular subgroups of medulloblastoma: the current consensus. *Acta Neuropathol* 2012; 123: 465-72.
  128. Sekine S, Shibata T, Kokubu A, *et al.* Craniopharyngiomas of adamantinomatous type harbor beta-catenin gene mutations. *Am J Pathol* 2002; 161: 1997-2001.
  129. Jakobiec FA, Kool M, Stagner AM, *et al.* Intraocular medulloepitheliomas and embryonal tumors with multilayered rosettes of the brain: comparative roles of LIN28A and C19MC. *Am J Ophthalmol* 2015; 159: 1065-74.
  130. Cahill DP, Louis DN, Cairncross JG. Molecular background of oligodendroglioma: 1p/19q, *IDH*, *TERT*, *CIC* and *FUBP1*. *CNS Oncol* 2015; 4: 287-94.
  131. Jue TR, McDonald KL. The challenges associated with molecular targeted therapies for glioblastoma. *J Neurooncol* 2016; 127: 427-34.

## Molecular Testing of Lymphoproliferative Disorders: Current Status and Perspectives

Yoon Kyung Jeon · Sun Och Yoon<sup>1</sup>  
Jin Ho Paik<sup>2</sup> · Young A Kim<sup>3</sup>  
Bong Kyung Shin<sup>4</sup> · Hyun-Jung Kim<sup>5</sup>  
Hee Jeong Cha<sup>6</sup> · Ji Eun Kim<sup>3</sup>  
Jooryung Huh<sup>7</sup> · Young-Hyeh Ko<sup>8</sup>  
The Hematopathology Study Group  
of the Korean Society of  
Pathologists · The Molecular  
Pathology Study Group of Korean  
Society of Pathologists

Department of Pathology, Seoul National University Hospital, Seoul National University College of Medicine, Seoul; <sup>1</sup>Department of Pathology, Yonsei University College of Medicine, Seoul; <sup>2</sup>Department of Pathology, Seoul National University Bundang Hospital, Seoul National University College of Medicine, Seongnam; <sup>3</sup>Department of Pathology, SMG-SNU Boramae Medical Center, Seoul National University College of Medicine, Seoul; <sup>4</sup>Department of Pathology, Korea University Guro Hospital, Korea University School of Medicine, Seoul; <sup>5</sup>Department of Pathology, Inje University Sanggye Paik Hospital, Seoul; <sup>6</sup>Department of Pathology, Ulsan University Hospital, University of Ulsan College of Medicine, Ulsan; <sup>7</sup>Department of Pathology, Asan Medical Center, University of Ulsan College of Medicine, Seoul; <sup>8</sup>Department of Pathology, Samsung Medical Center, Sungkyunkwan University School of Medicine, Seoul, Korea

Received: March 17, 2017

Accepted: April 9, 2017

### Corresponding Author

Yoon Kyung Jeon, MD, PhD  
Department of Pathology, Seoul National University Hospital, Seoul National University College of Medicine, 101 Daehak-ro, Jongno-gu, Seoul 03080, Korea  
Tel: +82-2-2072-1347  
Fax: +82-2-743-5530  
E-mail: ykjeon@snu.ac.kr

Young-Hyeh Ko, MD, PhD  
Department of Pathology, Samsung Medical Center, Sungkyunkwan University School of Medicine, 81 Inwon-ro, Gangnam-gu, Seoul 06351, Korea  
Tel: +82-2-3410-2762  
Fax: +82-2-3410-0025  
E-mail: yhko310@skku.edu

Molecular pathologic testing plays an important role for the diagnosis, prognostication and decision of treatment strategy in lymphoproliferative disease. Here, we briefly review the molecular tests currently used for lymphoproliferative disease and those which will be implicated in clinical practice in the near future. Specifically, this guideline addresses the clonality test for B- and T-cell proliferative lesions, molecular cytogenetic tests for malignant lymphoma, determination of cell-of-origin in diffuse large B-cell lymphoma, and molecular genetic alterations incorporated in the 2016 revision of the World Health Organization classification of lymphoid neoplasms. Finally, a new perspective on the next-generation sequencing for diagnostic, prognostic, and therapeutic purpose in malignant lymphoma will be summarized.

**Key Words:** Lymphoproliferative disorders; Malignant lymphoma; Pathology, molecular; Molecular diagnostics; Clonality test; Gene translocation; In situ hybridization, fluorescence; Next-generation sequencing

Molecular pathologic testing plays an important role for the diagnosis, prognostication and decision of treatment in lymphoproliferative disease. Classification of malignant lymphomas has been evolved to define unique clinicopathological entities for optimizing management of patients and thereby improving the clinical outcome. Advances in radiological and diagnostic techniques in medicine have made it possible to detect diseases earlier and with smaller sized tissues. Thus, pathologists are facing challenges in the diagnosis of lymphoproliferative disease. In addition, gene expression profile has clinical implication for the prognosis and patient management as exemplified by diffuse large B-cell lymphoma (DLBCL). Moreover, various molecular genetic alterations have been reported in lymphoma, which are likely candidates for target therapy in the era of precision medicine. Therefore, pathologic diagnosis of malignant lymphoma currently demands multimodal approach including morphology, immunophenotype, viral status, and genetic alterations. In addition, introduction of next-generation sequencing (NGS) techniques to the pathologic diagnosis of lymphoma is around the corner. This review is intended to give a brief overview and guideline for molecular tests for lymphoproliferative disease with a focus on malignant lymphoma, including the B- and T-cell clonality test, molecular cytogenetic test, determination of cell-of-origin (COO) in DLBCL, and molecular genetic tests incorporated in the 2016 revision of World Health Organization (WHO) classification of lymphoid neoplasm. A perspective on NGS tests in lymphoma will also be addressed.

## B- AND T-CELL CLONALITY TEST

### Background: Ig and T-cell receptor gene rearrangements

B and T cells are the only cells undergoing physiological gene rearrangement of their genomic DNA to produce unique Ig and T-cell receptor (TCR) molecules, respectively. The Ig and TCR genes contain many different variable (V), diversity (D), and joining (J) gene segments, which undergoes random gene rearrangement during early lymphoid development.<sup>1,2</sup> Ig heavy chain (*IGH*), TCR beta (*TCRB*), and TCR delta (*TCRD*) genes have V, D, and J gene segments, and Ig kappa (*IGK*), Ig lambda (*IGL*), TCR alpha (*TCRA*), and TCR gamma (*TCRG*) genes have V and J gene segments.<sup>3</sup> To further create diversity of Ig and TCR molecules, variable numbers of nucleotides are lost and inserted at the joining lesion (i.e., the V-D, V-J, or D-J junction) through the action of terminal deoxynucleotidyl transferase (TdT).<sup>4</sup> Consequently, these processes produce an incredibly large repertoire of Ig and TCR molecules due to both the com-

binatorial diversity and the junctional diversity.<sup>5</sup> The normal blood B-cell receptor (BCR) and TCR repertoire is estimated to comprise more than  $10^{12}$  distinct sequences, and many of these are present at low frequency under physiologic condition.<sup>5</sup> Thus, the detection of a single predominant BCR or TCR population indicates the presence of a clonally expanded B- or T-cell population, respectively.

Ig and TCR gene rearrangements occur in a hierarchical order. During B-cell development, the *IGH* genes are first rearranged, followed by rearrangement of *IGK* genes potentially resulting in IgH/k expression. Alternatively, *IGH* gene rearrangement is followed by *IGK* deletion and *IGL* rearrangement, potentially resulting in IgH/k expression.<sup>5</sup> Thus, *IGH* gene is most widely utilized in the clonality test for B-cell proliferative disease, followed by *IGK* and *IGL*.<sup>3,6</sup> During T-cell development, *TCRD* gene rearrangement occurs first in early thymocytes, followed by *TCRG* gene rearrangement, potentially resulting in TCR $\gamma\delta$  expression in a small subset of thymocytes and differentiation to  $\gamma\delta$ T cells. However, in most thymocytes, *TCRG* and *TCRD* rearrangements are followed by *TCRB* rearrangement and subsequent *TCRA* rearrangement (this rearrangement leads to the deletion of the *TCRD* locus because *TCRD* gene is located within the *TCRA* gene), potentially followed by TCR $\alpha\beta$  expression and further differentiation into  $\alpha\beta$ T cells. Consistent with this hierarchical gene rearrangement, virtually all  $\alpha\beta$ T cells have rearranged *TCRG* as well as *TCRB* and *TCRA* genes; however, the  $\gamma\delta$ T cells harbor rearranged *TCRG* and only rarely contain rearranged *TCRB* genes.<sup>3,7,8</sup> This has important implications for T-cell clonality testing, because virtually all the  $\alpha\beta$ TCR expressing T-cell lymphomas as well as the  $\gamma\delta$ T cell neoplasms will have a rearranged *TCRG* gene. Thus, *TCRG* gene is most widely utilized, followed by *TCRB* and then *TCRA*, for T-cell clonality test.<sup>3,6,8</sup>

### Indication

Molecular clonality test is required for making a final diagnosis of lymphoproliferative disorder when the diagnosis is inconclusive despite of extensive morphologic and immunophenotypic analysis. Common indications are as follows: (1) all suspected T-cell proliferations, (2) any suspected B-cell proliferation when morphology and immunophenotyping are not conclusive, (3) when limited tissues are available (such as skin biopsy and needle biopsy), (4) to determine involvement of lymphoma in cytology material, especially in limited specimen such as cerebrospinal fluid and vitreous fluid, (5) to detect minimal residual disease, (6) when lymphoproliferations are noted in immunodeficient patients, including post-transplant patients, (7) to evalu-

ate the clonal relationship between two lymphoid malignancies in one patient or to differentiate a relapse from a second malignancy, (8) to further classify malignancy via Ig/TCR gene rearrangement patterns or particular chromosome aberrations, and (9) to stage lymphomas, occasionally.<sup>3</sup>

**Methodology**

B- and T-cell clonality can be either indirectly determined by detection of monotypic Ig and TCR molecules or directly by genetic tests. Because reactive polyclonal B cells have Igκ/Igλ ratio ranging from 0.7 to 2.8, Ig light chain expression with Igκ/Igλ ratios of >4.0 or <0.5 has been considered as an evidence suggestive of clonal B-cell proliferation. Ig light chain restriction can be detected by flow cytometry, *in situ* hybridization or immunohistochemistry.<sup>9</sup> The detection of monotypic TCR expression can be done using flow cytometry for TCR molecules. However, these indirect methods have limitations because flow cytometry is difficult to perform using tissue samples, antibodies against specific TCR molecules are limited and usage of TCR repertoire is often restricted even under non-neoplastic condition. In contrast, molecular techniques, including southern blot and polymerase chain reaction (PCR) analyses, are broadly applicable to the detection of clonally rearranged Ig and TCR genes.

Southern blot analysis has long been considered as a gold standard for molecular clonality studies. It detects rearranged DNA fragments after digestion with restriction enzymes. Large amount (10–20 mg) of high quality DNA from fresh tissue, well-chosen restriction enzymes, well-designed DNA probes and technical excellence are required for Southern blot analysis. In addition, because Southern blot analysis basically focuses on the combinational diversity of Ig and TCR gene segments, it is useful for the assessment of *IGH*, *IGK*, and *TCRB* genes, but is of limited value for highly complex *IGL* and *TCRA* genes or relatively simple *TCRG* and *TCRD* genes.<sup>3,8</sup> Thus, despite the high reliability of Southern blot, it has been replaced by PCR techniques in clinical laboratories.

PCR techniques to detect rearranged Ig and TCR genes have considerable merits; it can be performed using a small amount of DNA and a variety of clinical samples including formalin fixed paraffin-embedded (FFPE) tissue, fresh tissue, and cytology samples, the turnaround time is short, and the PCR-based assay is relatively easy to perform and standardize. In PCR-based clonality test, as mentioned above, *IGH* genes are most widely used for B-cell clonality test followed by *IGK*, and *TCRG* genes are most widely utilized for T-cell clonality test followed by *TCRB*. PCR-based clonality test basically adopts multiplex-

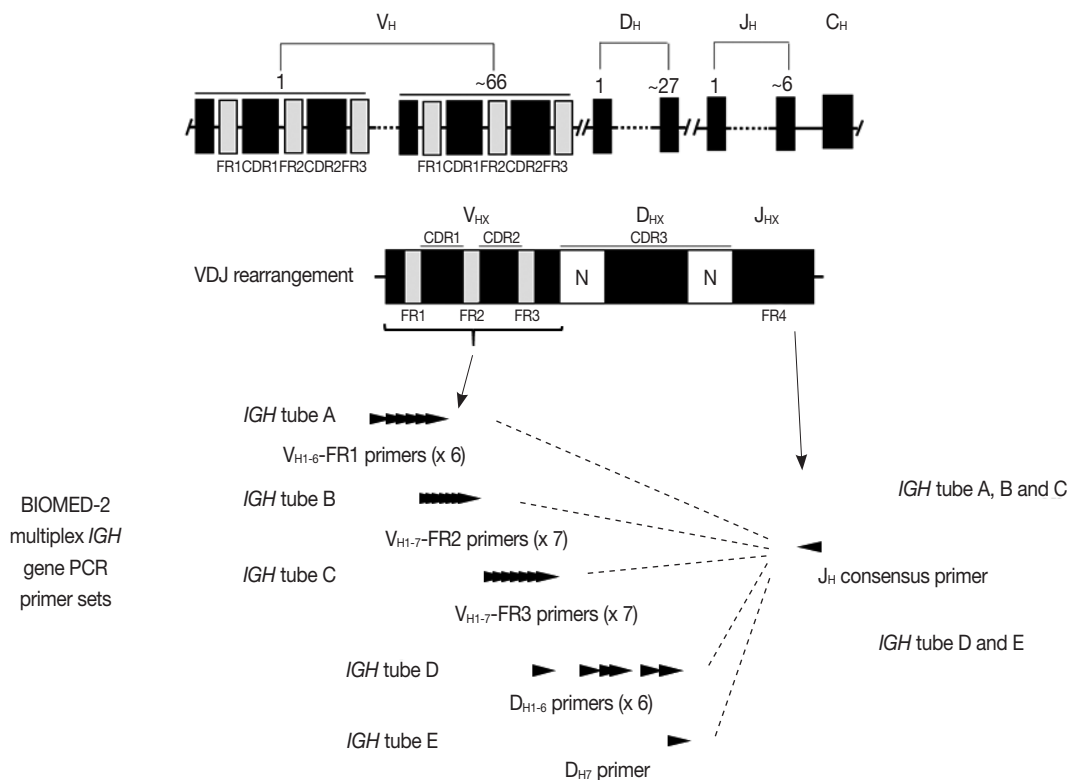


**Fig. 1.** Structure of *IGH* genes and the BIOMED-2 multiplex *IGH* gene polymerase chain reaction assay.

PCR techniques using multiple primers complementary to consensus or framework sequence of Ig and TCR gene families/segments. Due to the junctional diversity during gene rearrangement, polyclonal B and T cells produce PCR products having variable size and nucleotide composition. However, monoclonal B and T cells produce PCR products having identical size and nucleotide composition, which can be detected as an evidence of monoclonality.<sup>3,8</sup> Conventionally, a variety of primer sets have been developed and used among laboratories for PCR analysis of Ig and TCR gene rearrangement.<sup>10-13</sup> In recent years, laboratory-developed PCR tests to detect Ig and TCR gene rearrangement are being gradually replaced by BIOMED-2 (or EuroClonality) assay, which is now commercially available as IdentiClone clonality assay (Invivoscribe Technologies Inc., San Diego, CA, USA).<sup>3,6,14-17</sup> In brief, BIOMED-2 assays utilize 14 multiplex PCR tubes altogether, including three VH-JH, two DH-JH, two *IGK*, one *IGL*, three *TCRB*, two *TCRG*, and one *TCRD*, to detect B- and T-cell clonality (Figs. 1, 2). The primer sets and design of multiplex PCR for each Ig and TCR gene rearrangement were previously described in detail.<sup>3</sup> A set of BIOMED-2 assays can be selected and implemented in individual laboratory for clinical practice.<sup>6</sup>

### Interpretation and reporting: PCR-based clonality assay

Evaluation of PCR product for clonality test can be performed using gel-based assay or capillary electrophoresis (CE) by gene scanner (Fig. 3). Gel-based assays are represented by denaturing gradient gel electrophoresis (EP) and heteroduplex analysis followed by non-denaturing polyacrylamide gel electrophoresis (PAGE). While denaturing gel EP and CE analysis can discriminate PCR products based on the size difference, heteroduplex analysis with non-denaturing PAGE has a merit to discriminate PCR products on the basis of sequence differences as well as size differences.<sup>3</sup> Thus, heteroduplex analysis can be considered to prevent false positive results.

In principal, monoclonal B- or T-cell population exhibits prominent unequivocal one or two clonal peak(s) and band(s) when analyzed by CE and gel-EP, respectively.<sup>3,6,15,17</sup> A common definition of a prominent peak in CE is one that is greater than twice the size of the background polyclonal population.<sup>8</sup> Meanwhile, commercial kits for BIOMED-2 assay defines a positive peak as one that is at least three times the amplitude of the third largest peak in the same polyclonal background distribution or the closest polyclonal background distribution to the product. Otherwise, commercial kit for BIOMED-2 assay of *TCRG* provides automated interpretation for the significance of a peak

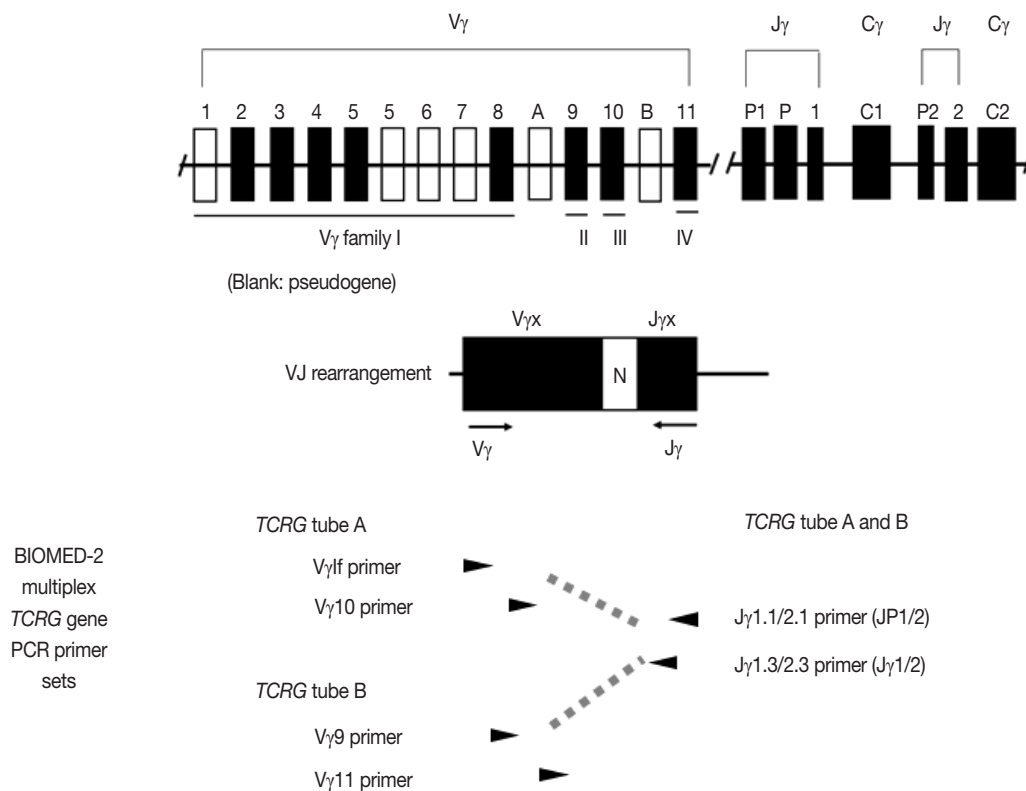
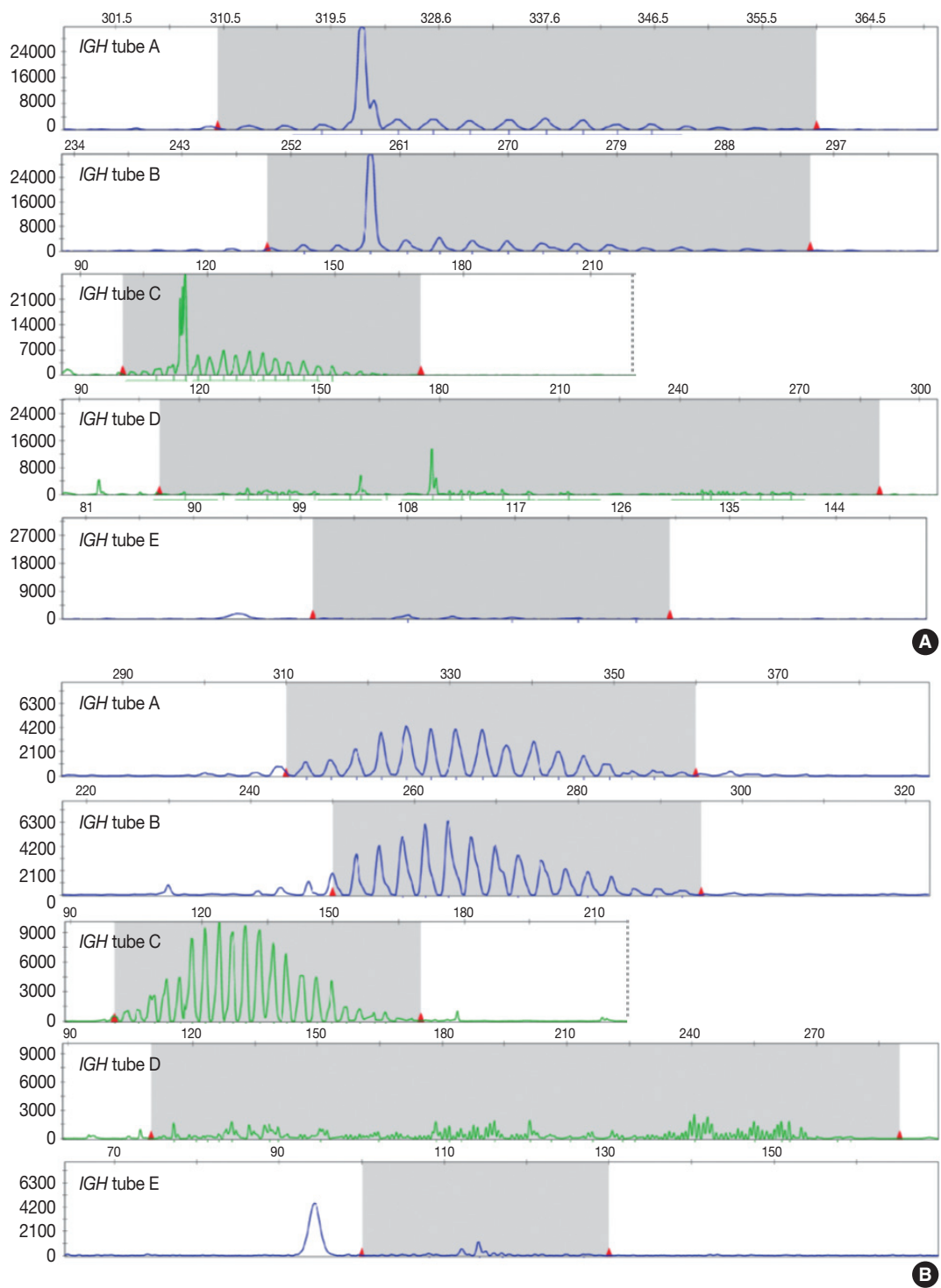


Fig. 2. Structure of *TCRG* genes and the BIOMED-2 multiplex *TCRG* gene polymerase chain reaction assay.

analyzed by CE through a mathematical algorithm. The presence of two predominant peaks rarely occurs, indicating biallelic rearrangements, usually at both TCR loci.<sup>17</sup> Polyclonal B- or T-cell populations typically exhibit a Gaussian distribution

when analyzed by CE and a smear when analyzed by gel-EP. However, in many clinical samples, a polyclonal background may not exhibit an expected distribution due to fewer number of reactive B or T cells, PCR efficiencies, and other factors.<sup>6</sup>



**Fig. 3.** Representative results and interpretation of BIOMED-2 multiplex IGH PCR analyzed by gene scanning. Clonal IGH gene rearrangement was detected in case (A), but not in case (B).

Moreover, it would be difficult to determine the presence of unequivocal clonality when weak peaks or bands are observed. Thus, interpretation of PCR-based clonality assay could be challenging.

Clonal peaks/bands observed in multiple multiplex-PCR reactions (i.e., tubes) and, moreover, reproducible in duplicate are highly convincing for the presence of monoclonal population. However, clear clonality would be detected in a single multiplex Ig/TCR PCR reaction (tube). The presence of an equivocal weak Ig/TCR band/peak within a polyclonal background can be regarded as low-level of clonality. Such equivocal products are often detected with either heteroduplex or Gene Scan. To avoid false-positivity of the clonality assay, duplicate test might be considered (see below), although not mandatory for the clonality test, particularly when using validated approved test.<sup>3,6</sup> General guidelines for interpretation and reporting of Ig/TCR clonality test are summarized in Table 1, on the condition that the test is appropriately validated.

#### Validation of test, quality assurance, and limitations and pitfalls

Utility and accuracy of molecular clonality test are affected by both biological and technical factors. For appropriate interpretation of results and quality assurance of clonality test, pathologists must be well-acquainted with the limitations and pitfalls.<sup>3</sup> Most importantly, pathologists and clinicians must understand that the results of clonality test should always be interpreted in the context of morphological, immunophenotypical, and clinical features of patients.

#### Validation of test and quality assurance

Each assay should be performed along with positive, negative, and no template controls. If the controls do not yield the expected results, the assay is not valid and the samples should not be interpreted. To ensure the quality and quantity of DNA and the absence of inhibitors of PCR reactions, specimen control size ladder, which amplifies multiple genes ranging the size of PCR product for Ig and TCR genes, is essential. If no bands are seen or smaller sized products are amplified only, the assay or sample should be re-evaluated unless the test result of specimen is positive.

#### Limited sensitivity and false-negative results

A sensitive PCR-based clonality test has detection limits of 1%–10%, depending on the applied techniques and the background of non-neoplastic B and T cells. In addition, false-negative results of PCR-based clonality test can be caused by improper primer annealing or difficulties in discrimination between monoclonal and polyclonal Ig/TCR gene rearrangements. Interpretation guideline of monoclonality and polyclonality is described above and in Table 1 and is also provided by manufacturer with commercial kit. However, this discrimination is occasionally not straightforward. In this case, analysis of multiple Ig and TCR genes and repeated examination might be helpful. Improper annealing of the PCR primers to the Ig and TCR genes can be mainly caused by two factors. First, family or consensus primers cannot precisely cover all different V, D, and J gene segments, particularly in Ig and TCR genes having many different gene segments. Second, mature B cells undergo somatic hypermutation in rearranged Ig genes and isotype class switching in germinal

**Table 1.** EuroClonality/BIOMED-2 guidelines for interpretation and reporting of Ig/TCR clonality testing

Type of profile per tube (in duplicate)	Technical description	Molecular interpretation/conclusion
No peaks/bands (but: poor DNA quality)	No (specific) product, poor DNA quality	Not evaluable, due to poor DNA quality
No peaks/bands (without background)	No (specific) product	No rearrangement in Ig/TCR targets detected
One or two reproducible clonal peaks/bands <sup>a</sup>	Clonal <sup>b</sup>	Clonality detected
One or two non-reproducible (clear) peaks/bands <sup>a</sup>	Pseudoclonal	No clonality detected, suggestive
Multiple (n ≥ 3) non-reproducible peaks/bands <sup>a</sup>	Pseudoclonal	of low template amount
Multiple (n ≥ 3) reproducible peaks/band <sup>a,c</sup>	Multiple products	Oligoclonality/multiple clones detected
Gaussian curve/smear <sup>d</sup> (with or without minor reproducible peaks/bands <sup>a</sup> )	Polyclonal (not clonal <sup>e</sup> )	Polyclonality detected (no clonality detected) Polyclonality detected plus minor clone of unknown significance <sup>e</sup>
Pattern that cannot be categorized as one of the above	Not evaluable <sup>f</sup>	Not evaluable

Reprinted by permission from Macmillan Publishers Ltd: [Leukemia] Langerak *et al.* 2012;26:2159-71,<sup>6</sup> copyright (2012). TCR, T-cell receptor.

<sup>a</sup>In heteroduplex analysis the number of bands does not necessarily reflect the number of different polymerase chain reaction products, as additional heteroduplexes can be formed between products; <sup>b</sup>Clonal peaks/bands are not necessarily seen for every Ig/TCR target analyzed to reach the molecular conclusion 'clonality detected'; <sup>c</sup>For *IGK* and *TCRB* loci up to four clonal products may be compatible with one clone; <sup>d</sup>In heteroduplex analysis a polyclonal smear may not always be smooth or clear, despite specific product in gel; hence this is scored as 'not clonal'; <sup>e</sup>For those cases in which minor reproducible peaks/bands are detected in the polyclonal background; <sup>f</sup>In <5% of polymerase chain reaction results the description per tube cannot be made.

centers for affinity maturation of the Ig molecules. This physiologic phenomenon can hamper the proper annealing of PCR primers. Thus, mature B-cell lymphomas of germinal center or post-germinal center origin with somatically mutated Ig genes are more likely to show false-negative results.<sup>15,18</sup>

#### *Pseudoclonality and false-positive results*

Pseudoclonality of a sensitive PCR assay refers to selective amplification of the Ig or TCR gene rearrangements from a few reactive B or T cells in the tissue samples, particularly in a small biopsy. Evaluating the reproducibility of clonal band/peak by performing duplicate or repeated PCR analyses will help to clarify whether the seemingly clonal PCR products are derived from different lymphocytes or not.<sup>6</sup> On the other hand, PCR analyses can produce false-positive results, especially when discriminating the monoclonal, oligoclonal, or polyclonal populations solely based on the size of PCR products using techniques with low resolution. To avoid serious false-positive PCR results, discrimination of PCR products can be achieved via Gene Scanning, which has higher resolution than gel-based assay or via single-strand conformation polymorphism analysis, denaturing gradient gel EP and heteroduplex analysis.<sup>19,20</sup> These latter techniques discriminate PCR products in terms of composition of nucleotides, in addition to the length of nucleotides, derived from junctional diversity during Ig/TCR gene rearrangements.

#### *Clonality is not equivalent to malignancy or lymphoma*

Some clinically benign lymphoproliferative diseases (i.e., monoclonal gammopathy of unknown significance, lymphomatoid papulosis) can exhibit clonality. In addition, non-neoplastic lymphoproliferations including viral infection (i.e., Epstein-Barr virus, cytomegalovirus), bacterial infection (i.e., *Helicobacter pylori gastritis*), autoimmune diseases, and immunodeficiency status can harbor predominance of several antigen-specific subclones or reduced diversity of B- or T-cell repertoire, thus displaying oligoclonality or even monoclonality.

#### *Ig and TCR gene rearrangements are not markers for lineage*

Crosslineage Ig/TCR gene rearrangements occur relatively frequently in immature T- or B-cell malignancies (i.e., acute lymphoblastic lymphomas), and even in acute myeloid leukemias.<sup>21-24</sup> Virtually all  $\alpha\beta$ T cell lymphomas have *TCRG* gene rearrangements and many  $\alpha\beta$ T cell lymphomas have *TCRB* gene rearrangements, implying that the detection of *TCRB* or *TCRG* rearrangements is not indicative of T cells of the  $\alpha\beta$  or  $\gamma\delta$  T-cell lineage, respectively, either.<sup>5,8,21,25,26</sup> Mature B- and T-

cell lymphomas might rarely contain TCR and Ig gene rearrangements, respectively.<sup>21,24</sup> Particularly, angioimmunoblastic T-cell lymphomas (AITL) frequently exhibit Ig gene rearrangements up to 20%–30% of cases.<sup>17</sup>

## CHROMOSOME AND GENE TRANSLOCATIONS

### Background and indications including changes in the 2016 revision of WHO classification

Structural alterations of chromosome and/or genes important for the diagnosis, prognostication and therapeutics in tumor include amplification, deletion and translocation (or rearrangement). B- and T-cell malignancies frequently undergo pathologic chromosome/gene rearrangement in addition to the physiologic rearrangement of Ig and TCR genes. Gene translocations in hematolymphoid malignancies result in the overexpression of oncogenes involving cell proliferation and apoptosis under the influence of Ig promoter or the production of fusion proteins having dysregulated expression or kinase activity. Gene translocations can be analyzed by multiple methods including conventional karyotyping, fluorescence *in situ* hybridization (FISH), Southern blotting, and reverse-transcription PCR. Otherwise, aberrant expression of proteins derived from gene translocation can be detected by immunohistochemistry.<sup>27</sup> Common chromosome/gene translocations with diagnostic and clinical implications in mature B and T-cell lymphomas and the detection method commonly used for clinical practice are summarized in Table 2.

Patients with DLBCL harboring *MYC* translocation (approximately in 5%–15% of DLBCL) or concurrent *MYC* and *BCL2* translocations (approximately in 5%–6% of DLBCL) had very poor prognosis.<sup>28-31</sup> Of note, the 2016 revision of WHO classification has newly introduced high-grade B-cell lymphomas with *MYC* and *BCL2* and/or *BCL6* translocations (other than follicular lymphoma and lymphoblastic lymphoma) as a category of “double-/triple-hit” lymphomas.<sup>32</sup> These lymphomas morphologically resemble DLBCL or B-cell lymphoma, unclassifiable, with features intermediate between DLBCL and Burkitt lymphoma which had been recognized in 2008 WHO classification.<sup>33</sup> The patients with “double-/triple-hit” lymphomas show a very aggressive clinical course and poor prognosis despite high-intensity chemotherapy. However, a consensus has not yet been reached for the guidelines to test FISH for *MYC*, *BCL2*, and *BCL6* rearrangements in high-grade B-cell lymphoma. In contrast, *MYC* protein expression is observed in 30%–50% of DLBCLs and concomitant expression of *MYC* and *BCL2* in

**Table 2.** Common chromosome/gene translocations having diagnostic and clinical implications in mature B- and T-cell lymphoma

Entity	Chromosome/Gene translocation	Frequency	Detection method	Implication
Mantle cell lymphoma	t(11;14)(q13;q32), <i>CCND1</i> and <i>IGH</i>	>90%	IHC, FISH	Diagnostic
Follicular lymphoma	t(14;18)(q32;q21), <i>BCL2</i> and <i>IGH</i> t(2;18)(p12;q21), <i>BCL2</i> and <i>IGK</i>	Grade 1, 2: 90% Grade 3a, 3b: <30%	IHC, FISH	Diagnostic
Burkitt lymphoma	t(8;14)(q24;q32), <i>MYC</i> and <i>IGH</i> t(2;8)(p12;q24), <i>MYC</i> and <i>IGK</i> t(8;22)(q24;q11), <i>MYC</i> and <i>IGL</i>	>95%	FISH	Diagnostic
Diffuse large B-cell lymphoma	t(8)(q24), <i>MYC</i>	~10%	FISH	Prognostic (poor)
High-grade B-cell lymphoma with <i>MYC</i> and <i>BCL2</i> and/or <i>BCL6</i> rearrangements (double-/triple-hit lymphoma) <sup>a</sup>	t(8)(q24), <i>MYC</i> t(14;18)(q32;q21), <i>BCL2</i> and <i>IGH</i> t(3)(q27), <i>BCL6</i>		FISH	Diagnostic Prognostic (poor)
MALT lymphoma	t(11;18)(q21;q21), <i>API2</i> and <i>MALT1</i>	5%–20% (stomach) 30%–50% (lung)	FISH RT-PCR	Therapeutic (resistance to <i>Helicobacter pylori</i> eradication)
Anaplastic large cell lymphoma, ALK-positive	t(2;5)(p23;q35), <i>NPM</i> and <i>ALK</i> Variants involving 2p23, <i>ALK</i>	t(2;5) 85% Variants 15%	IHC, FISH	Diagnostic Prognostic

IHC, immunohistochemistry; FISH, fluorescence *in situ* hybridization; MALT, mucosa-associated lymphoid tissue; RT-PCR, reverse transcription polymerase chain reaction; ALK, anaplastic lymphoma kinase.

<sup>a</sup>Included in the 2016 Revision of World Health Organization classification.

20%–35% of the cases; these “double-expressor lymphoma” cases are four to five times higher in incidence than those with *MYC* and *BCL2* double-hit (i.e., translocation).<sup>29–31,34</sup> Although a cutoff for *MYC* and *BCL2* expression for double-expressor has varied among studies, a cutoff of 30% or 40% for *MYC* and a cutoff of 50% or 70% for *BCL2* are usually used to define these cases.<sup>34</sup> Several studies demonstrated that the double-expressor lymphomas have a worse outcome than other DLBCL, even irrespective of COO.<sup>31</sup> Thus, the 2016 revision of WHO classification suggests that coexpression of *MYC* and *BCL2* should be considered new prognostic indicator in DLBCL, not otherwise specified (NOS).<sup>32</sup>

#### Method: FISH—procedures and probes

Interphase FISH is now widely used to detect chromosome/gene translocations using FFPE tissue, fresh tissue, and cytologic samples. FISH is a process by which fluorochrome-labeled specific DNA probe hybridizes to a complementary location on a chromosome. FISH test includes selection of appropriate probe, pretreatment, hybridization and interpretation.<sup>35,36</sup> When using validated probe, optimal pretreatment of tissue sections most affect the FISH test on FFPE tissue. Pretreatment refers to permeabilization of the cells to enable the probe to access the target DNA in the nucleus to hybridize. This procedure follows multiple steps including antigen retrieval procedure (i.e., citrate, EDTA), incubation with acid, detergent, and chaotropic agents (i.e., sodium thiocyanate [NaSCN]), and protease digestion, depending on the tissue condition. Hybridization procedures consist of co-denaturing target DNA and probe DNA at high

temperature in the presence of formamide into single strands and incubating the slide to allow the probe DNA to attach to the target DNA.<sup>35</sup>

For detection of the common gene translocations in lymphoma, various probe sets and protocols for hybridization are now commercially available. FISH test for gene translocations are usually performed by two types of FISH probe.<sup>35,36</sup> One is the dual-color “dual-fusion” probe (or two break points spanning probe), in which each translocation partner is identified by a probe of different color, usually red and green. The normal configuration is therefore two red signals and two green signals in each nucleus. When a translocation occurs between two genes, one of each signal is split and the different halves join together; these result in signal pattern of one red, one green, and two fused signals (Fig. 4A). This probe has a merit to assure the fusion partners exactly and is useful for the diagnosis of gene translocations involving specific genes as in follicular lymphoma, which mostly harbors *BCL2/IGH* fusion. However, it has limitations in applying to the gene translocations having multiple fusion partners and can show false positive signals due to nuclear or chromosome overlapping in tissue FISH. To detect a gene translocation that can involve multiple partners, a dual-color “break-apart” probe (or breakpoint flanking probe) can be more useful. With this type of probe, the normal configuration is two paired signals. If there is any translocation present involving this gene, the two colors will be split apart, resulting in one paired (normal) signal, one red, and one green (Fig. 4B). There could be a small gap or space between the two colors in some probe when the DNA is unwound. However, when the translocation occurs inter-chro-

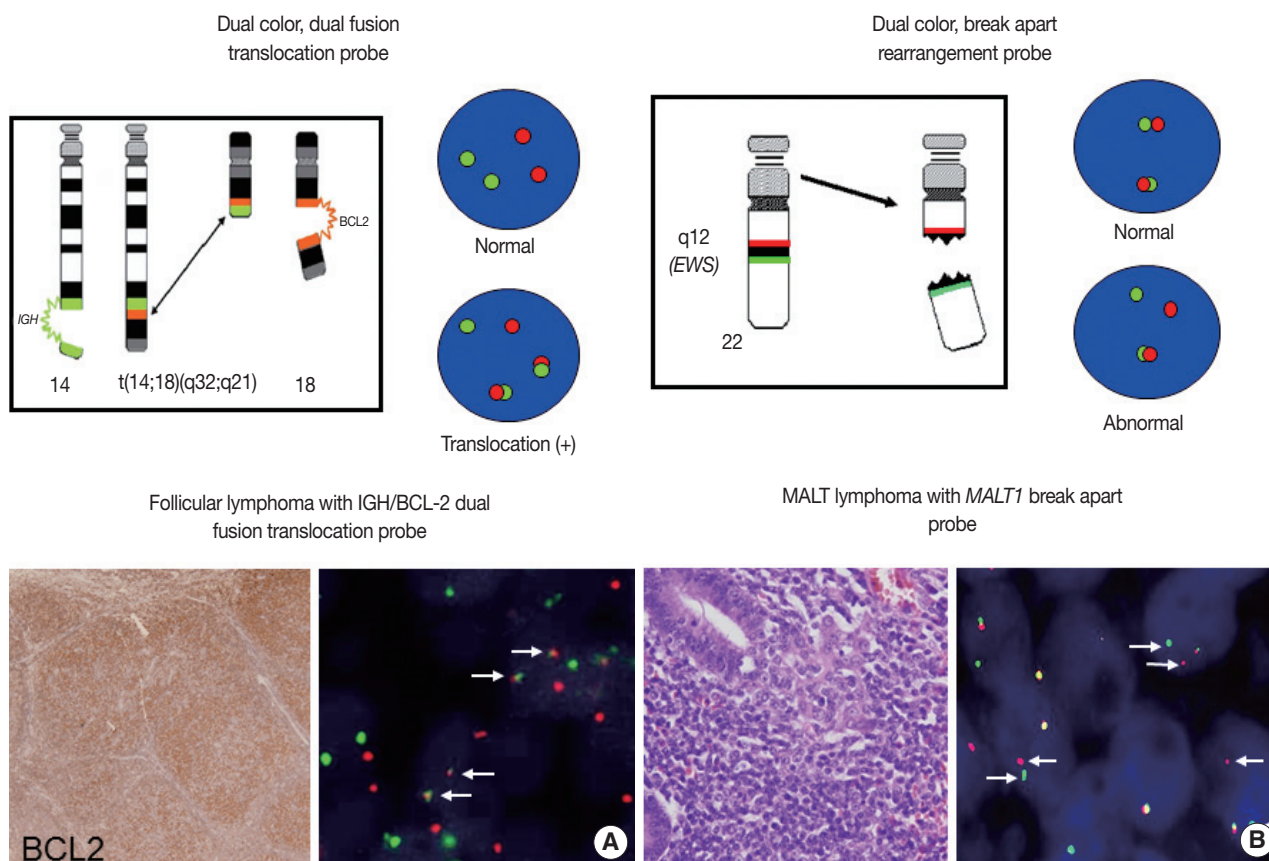


**Fig. 4.** Fluorescence *in situ* hybridization analysis to detect gene translocations using dual color, dual fusion probe (arrow, fused IGH and BCL2 genes) (A) and dual color, break apart probe (arrows, splitted *MALT1* genes) (B). MALT, mucosa-associated lymphoid tissue.

mosomally, the signals are usually separated with ample space and the rate of false-positivity is very low. Thus, this type of probe is useful for detecting gene translocation to make a diagnosis by integrating other pathological features. Selection of FISH probe depends on the disease entity and the purpose of the test.

### Reporting

In principle, FISH reporting follows a system for FISH nomenclature, the International System for Human Cytogenetic Nomenclature (ISCN) in both metaphase and interphase assay.<sup>27,35,37</sup>

If a 14;18 translocation resulting in fusion of the *IGH* and *BCL2* genes studied in interphase FISH using a dual-color, dual-fusion probe set, the ISCN nomenclature would be written as follows: nuc ish (*IGH* × 3), (*BCL2* × 3), (*IGH* con *BCL2* × 2), indicating that each of the probes has been split apart and juxtaposed by the translocation. However, the system may seem confusing to pathologists not familiar with conventional cytogenetics, particularly those who are generally dealing with interphase FISH for solid tumors. FISH reporting may be modified

according to the guideline provided by manufacturers of FISH probe and the purpose of the test in case of solid tumors. In principal, the report should also contain a statement as to the FISH results being normal or abnormal, and indicate the percentage of abnormal and normal cells. Specific names of the probes and the manufacturer and any specific limitations of the assay should be included in the report.<sup>36</sup> Interpretation of the report on the diagnostic and prognostic significance of the FISH findings, with the clinicopathological findings incorporated, and suggestion of any further tests could be recommended.

### Validation of the test and quality assurance

When a new FISH test is implemented in the laboratory, extensive validation is required, including validation of the probe itself (probe validation) and validation of the procedures using the probe (analytical validation) (American College of Medical Genetics and Genomics, Standards and Guidelines for Clinical Genetic Laboratories, Section E: Clinical Cytogenetics, <http://www.acmg.net>).<sup>36</sup> Commercial probes, which are supplied by various manufacturers including Abbott (Vysis), Cambio,

Cytocell, Dako, Kreotech, and Poseidon (Stretton), are generally easy to use and validated. However, because they can vary in terms of application, size (50 kb–1 Mb) and covered chromosome loci, users must read the datasheet and probe map very carefully and become familiar with the FISH pattern using the probe. Regarding the analytical validation in interphase FISH using FFPE tissue, normal reference ranges can be calculated by evaluating available tissues without the rearrangement being validated. To validate a FISH test, known normal and abnormal cases should be assessed to establish clearly defined scoring criteria for determining whether the assay is acceptable or not. For this, inter-laboratory cross-validation and participation in a proficiency testing program are recommended.<sup>36</sup>

## CELL-OF-ORIGIN OF DIFFUSE LARGE B-CELL LYMPHOMA

### Background and indications including changes in the 2016 revision of WHO classification

Gene expression profiling (GEP) studies classified DLBCL into clinically and biologically distinct subsets reflecting COO as follows: germinal center B-cell (GCB)-like DLBCL expresses genes related to normal GCBs, and activated B-cell (ABC)-like DLBCL lacks genes expressed in GCBs but expresses genes related to BCR activated B cells arrested during plasmacytic differentiation. Unclassifiable cases cannot be put into either category. Patients with ABC DLBCL have a worse clinical outcome than do patients with GCB DLBCL when treated with R-CHOP regimen.<sup>38-41</sup> Because GEP is hard to implement in a routine clinical test, many efforts have been made to classify COO of

DLBCL using immunohistochemistry (IHC) for several markers, despite issues on reproducibility and reliability of IHC algorithms.<sup>42-45</sup> The 2008 classification recognized GCB and ABC/non-GCB “molecular or immunohistochemical subgroups” of DLBCL based on GEP or IHC but considered this subclassification of DLBCL as optional.<sup>33</sup> Subsequent studies have demonstrated that the differences in genetic alterations and activation of signaling pathways as well as prognosis between GCB and ABC/non-GCB DLBCLs may affect the potential therapeutic targets and personalized therapy of patients with DLBCL as described previously.<sup>46</sup> Thus, the 2016 revision of WHO classification requires the identification of GCB versus ABC/non-GCB DLBCL using either GEP or IHC.<sup>32</sup>

### Methodology

GEP using microarray, including Lymphochip microarray and Affymetrix microarray, robustly classified the GCB versus ABC DLBCL with prognostic significance.<sup>38,39</sup> However, these assays need fresh tissue for a large amount of RNA of high-quality and have restrictions for clinical application. Thus, several immunohistochemical algorithms as surrogates have been developed, as represented by Hans and Choi algorithm (Fig. 5), which have shown reasonable correlations with GEP.<sup>42,43</sup> However, in the following studies, the concordance rate between the immunohistochemically defined and GEP-defined subgroups has been variable and the IHC algorithm has some limitations in terms of accuracy, reproducibility and prognostic utility.<sup>44,45</sup>

Recently, a 20-gene gene expression assay using FFPE tissues and NanoString-based digital gene expression technology has been proposed for the determination of COO subgroups of

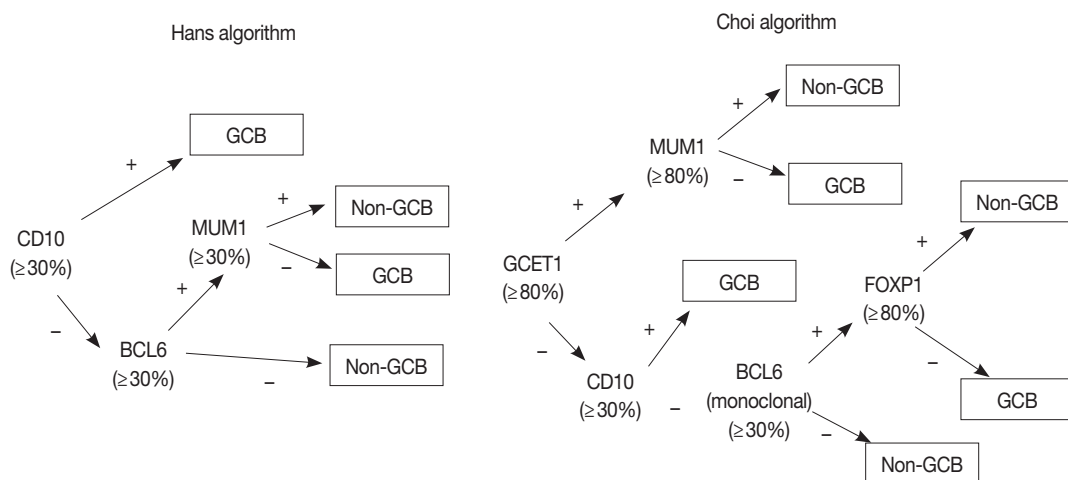


**Fig. 5.** Representative immunohistochemical algorithms for the subgrouping of diffuse large B-cell lymphoma.<sup>42,43</sup> GCB, germinal center B-cell.

DLBCL.<sup>47</sup> This assay (Lymph2CX) identified GCB versus ABC/non-GCB subgroups by quantifying the RNA transcripts extracted from FFPE tissue and produced reproducible accuracy and prognostic value.<sup>48</sup> Although these assays using nCounter system are not yet accessible to most laboratories, it may be a promising alternative to the IHC-based algorithms.

### MOLECULAR TESTING USING NEXT-GENERATION SEQUENCING: FUTURE NEXT-GENERATION SEQUENCING PANEL FOR DIAGNOSTIC, PROGNOSTIC AND PREDICTIVE PURPOSE

#### Background

Assays for single gene detection have been replaced by NGS which allows for the simultaneous evaluation of many genes. Targeted sequencing for gene sets is appropriate for clinical purpose and can acquire information for diagnosis, prognostication, and therapeutic targets. Currently, Korea Food and Drug Administration (KFDA) allows two levels of NGS test panel. Level 1 is composed of less than 50 genes including *TP53* and *MYD88*. Level II is composed of less than 200 genes including *NOTCH1* and *NOTCH2*. Although there is no general guideline for which gene sets should be included in molecular test using NGS, it is recommended that genes for pathologic diagnosis and prognostication according to the WHO classification and genes with implications for standard clinical management and current clinical trial be included in the level I gene set. Level II gene set may include potential therapeutic targets which are identified in high throughput sequencing of malignant lymphoma, but have no available drug yet. Recommended list of genes is depicted in Tables 3 and 4.

#### Genes incorporated in the 2016 revision of WHO classification as a diagnostic marker

Rearrangement of a specific gene is diagnostic for a certain type of malignant lymphoma. It includes *BCL2* for follicular lymphoma, *MYC* for Burkitt lymphoma, simultaneous rearrangement of *MYC* with *BCL2* and/or *BCL6* for high grade B-cell lymphoma, and *CCND1*, *CCND2*, and *CCND3* for mantle cell lymphoma (MCL).<sup>32,33</sup> The 2016 revision of WHO classification incorporated a few additional genes in the diagnostic criteria.<sup>32</sup> *BRAF* V600E mutations are found in almost all cases of hairy cell leukemia (HCL) but not in HCL-variant (HCL-v) or other small B-cell lymphoid neoplasms.<sup>49-52</sup> Mutations in *MAP2K1* which encodes MEK1 (which is downstream of *BRAF*)

**Table 3.** Level I gene list in NGS panel

Genes	Purpose of test		
	Diagnosis	Prognosis	Selection of drug
11q gain/loss	0	-	-
1P36 deletion	0	-	-
<i>AKT</i>	-	-	0
<i>ALK</i>	-	-	0
<i>BCL2</i> translocation	0	-	0
<i>BCL6</i> translocation	0	-	0
<i>BCOR</i>	-	-	0
<i>BIRC3</i>	-	0	-
<i>BRAF</i> V600E	0	-	-
<i>BTK</i>	-	-	0
Calcineurin	-	-	0
<i>CARD11</i>	-	-	0
<i>CCND1</i> rearrangement	0	-	-
<i>CD28</i>	-	-	0
<i>CD58</i>	-	0	-
<i>CD79A</i>	-	-	0
<i>CD79B</i>	-	-	0
<i>CDK4</i>	-	-	0
<i>CDK6</i>	-	-	0
<i>CHEK1</i>	-	-	0
<i>CTLA4</i>	-	-	0
<i>CXCR4</i>	-	0	0
<i>DDX3X</i>	-	0	-
<i>DUSP22</i> rearrangement	-	0	-
<i>EZH2</i>	-	-	0
<i>FYN</i>	-	-	0
<i>GATA3</i>	-	0	-
<i>IDH2</i>	-	0	0
<i>IRAK1</i>	-	-	0
<i>IRAK4</i>	-	-	0
<i>IRF4</i>	0	-	-
<i>JAK1</i>	-	-	0
<i>JAK2</i>	-	-	0
<i>MAP2K1</i>	-	-	-
<i>MAPK</i>	-	-	0
<i>MLL2</i>	-	-	0
<i>MTOR</i>	-	-	0
<i>MYC</i> rearrangement	0	-	0
<i>MYD88</i>	0	-	0
<i>PI3K</i>	-	-	0
<i>PI3KCD</i>	-	-	0
<i>PKCbeta</i>	-	-	0
<i>RHOA</i>	0	-	0
<i>STAT3</i>	-	-	0
<i>SYK</i>	-	-	0
<i>TBL1XR1</i>	-	-	0
<i>TP53</i>	-	0	-
<i>TP63</i> rearrangement	-	0	-
<i>VAV1</i>	-	-	0
<i>XPO1</i>	-	0	-

NGS, next-generation sequencing.

have been reported in almost half of HCL-v and in the majority of HCL that use IGHV4-34 and which, like HCL-v, lack *BRAF* V600E mutations.<sup>53,54</sup> *MYD88* mutation is important in the differential diagnosis between nodal marginal zone lymphoma and lymphoplasmacytic lymphoma (LPL).<sup>55-58</sup> Ninety percent of LPL or Waldenström macroglobulinemia have *MYD88* L265P mutations. This mutation is also found in a significant proportion of IgM, but not IgG or IgA, monoclonal gammopathy of undetermined significance cases, approximately

30% of non-GCB-type DLBCL, more than half of primary cutaneous DLBCL (leg type), and many DLBCL at immune-privileged sites, but not in plasma cell myeloma, even of IgM type. *IG/IRF4* fusions are associated with a distinct subgroup of germinal center B-cell lymphomas composed of follicular lymphoma (FL) grade 3 or (centroblastic) DLBCL characterized by coexpression of *MUM1* and *BCL6* in the absence of *PRDM1/BLIMP1*, a specific gene expression profile, and a disease onset predominantly in childhood or young adulthood.<sup>59</sup> A new provisional entity designated Burkitt-like lymphoma with 11q aberration has a chromosome 11q alteration characterized by proximal gains and telomeric losses, but without *MYC* rearrangement.<sup>60,61</sup>

**Table 4.** Level II gene list in NGS panel

<i>ACTB</i>	<i>ANKRD11</i>	<i>APC</i>	<i>AR1D1A</i>	<i>ATM</i>
<i>AURKA</i>	<i>AURKB</i>	<i>B2M</i>	<i>BAP1</i>	<i>BCL10</i>
<i>BCL11B</i>	<i>BCL2L2</i>	<i>BCL7A</i>	<i>BCORL1</i>	<i>BRCA1</i>
<i>BRCA2</i>	<i>BTG1</i>	<i>CCND2</i>	<i>CCND3</i>	<i>CCNE1</i>
<i>CCR4</i>	<i>CCT6B</i>	<i>CD22</i>	<i>CD274</i> ( <i>PDL1</i> )	<i>CDK12</i>
<i>CDK8</i>	<i>CDKN1B</i>	<i>CDKN2A</i>	<i>CDKN2B</i>	<i>CDKN2C</i>
<i>CHEK2</i>	<i>CIITA</i>	<i>DNMT3A</i>	<i>DUSP9</i>	<i>EGFR</i>
<i>EP300</i>	<i>ERG-1</i>	<i>ERK</i>	<i>ETS1</i>	<i>ETV1</i>
<i>ETV5</i>	<i>ETV6</i>	<i>FAK</i>	<i>FAS</i> ( <i>TNFRSF6</i> )	<i>FGFR1, 3</i>
<i>FOXO1</i>	<i>FOXO3</i>	<i>FOXP1</i>	<i>GNA13</i>	<i>HDAC1</i>
<i>HDAC4</i>	<i>HDAC7</i>	<i>HIST1H1C</i>	<i>HIST1H1D</i>	<i>HIST1H1E</i>
<i>HIST1H2AC</i>	<i>HIST1H2AG</i>	<i>HIST1H2AL</i>	<i>HIST1H2AM</i>	<i>HIST1H2BC</i>
<i>HIST1H2BJ</i>	<i>HIST1H2BK</i>	<i>HIST1H2BO</i>	<i>HIST1H3B</i>	<i>HRAS</i>
<i>ID3</i>	<i>IGH</i>	<i>IGK</i>	<i>IGL</i>	<i>IKBKE</i>
<i>IKKalpha</i>	<i>IKKbeta</i>	<i>IKKgamma</i>	<i>IL7R</i>	<i>IRF1</i>
<i>IRF8</i>	<i>JAK3</i>	<i>JUN</i>	<i>KLHL6</i>	<i>KMT2A (MLL)</i>
<i>KMT2B (MLL2)</i>	<i>KMT2C (MLL3)</i>	<i>KRAS</i>	<i>LEF1</i>	<i>LILRB1</i>
<i>LYN</i>	<i>MAF</i>	<i>MALT1</i>	<i>MAP2K2</i>	<i>MAP2K4</i>
<i>MAP3K1</i>	<i>MAP3K14</i>	<i>MAP3K6</i>	<i>MAP3K7</i>	<i>MAPK1</i>
<i>MCL1</i>	<i>MDM2</i>	<i>MDM4</i>	<i>MED12</i>	<i>MEF2B</i>
<i>MEF2C</i>	<i>MET</i>	<i>MUC2</i>	<i>MYCL</i> ( <i>MYCL1</i> )	<i>MYCN</i>
<i>NF1</i>	<i>NF2</i>	<i>NFAT</i>	<i>NFKBIA</i>	<i>NORE1</i>
<i>NOTCH 2</i>	<i>NOTCH1</i>	<i>NPM1</i>	<i>NRAS</i>	<i>NTRK2</i>
<i>NTRK3</i>	<i>P2RY8</i>	<i>PAX5</i>	<i>PCLO</i>	<i>PDCD1 (PD-1)</i>
<i>CD274 (PD-L1)</i>	<i>PDCD1LG2 (PD-L2)</i>	<i>PDGFRA</i>	<i>PDGFRB</i>	<i>PIK3CA</i>
<i>PIK3CG</i>	<i>PIK3R1</i>	<i>PIK3R2</i>	<i>PIM1</i>	<i>PLCgamma 1</i>
<i>PLCgamma2</i>	<i>POU2F2</i>	<i>PRDM1</i>	<i>PRKD2</i>	<i>PTEN</i>
<i>PTPN1</i>	<i>RAF</i>	<i>RASSF1</i>	<i>RB1</i>	<i>RET</i>
<i>RHOT2</i>	<i>RUNX1</i>	<i>SETBP1</i>	<i>SETD2</i>	<i>SF3B1</i>
<i>SF3B1</i>	<i>SFK</i>	<i>SGK1</i>	<i>SMAD2</i>	<i>SMAD4</i>
<i>SMARCA1</i>	<i>SMARCA4</i>	<i>SMARCA1</i>	<i>SMARCB1</i>	<i>SMARCD1</i>
<i>SOCS1</i>	<i>SOCS2</i>	<i>SOCS3</i>	<i>SOX10</i>	<i>SOX2</i>
<i>STAT1</i>	<i>STAT2</i>	<i>STAT4</i>	<i>STAT5A</i>	<i>STAT5B</i>
<i>STAT6</i>	<i>TCF3</i>	<i>TCL1A</i>	<i>TET1</i>	<i>TET2</i>
<i>TET3</i>	<i>TLL2</i>	<i>TNFAIP3</i>	<i>TNFRSF11A</i>	<i>TNFRSF14</i>
<i>TNFRSF17</i>	<i>TRAF2</i>	<i>TRAF3</i>	<i>TRAF5</i>	<i>TSC1</i>
<i>TSC2</i>	<i>TYK2</i>	<i>WIF1</i>	<i>WT1</i>	<i>XBP1</i>
<i>CTNNB1</i>	<i>GSK3B</i>	<i>PKD1</i>		

NGS, next-generation sequencing.

### Prognostic and predictive marker

*TP53*, *NOTCH1*, *SF3B1*, and *BIRC3*, are of clinical interest because of their adverse prognostic implications in chronic lymphocytic leukemia (CLL) and also because some are potential direct or indirect therapeutic targets.<sup>62,63</sup> *TP53* mutations are present in 10.6% of CLL, *ATM* mutations in 11.1%, *SF3B1* mutations in 12.6%, *NOTCH1* mutations in 21.8%, and *BIRC3* mutations in 4.2%. The *ATM*-p53 DNA damage response pathway plays a crucial role in chemoresistance in CLL, as indicated by the adverse prognostic impact of deletions of 17p (locus of *TP53*) and 11q (locus of *ATM*) detected by FISH analysis.<sup>64</sup> *BIRC3* is a negative regulator of noncanonical nuclear factor  $\kappa$ B (NF- $\kappa$ B) signaling. *BIRC3* disruption by inactivating mutations and/or gene deletions selectively affects fludarabine-refractory CLL cases.<sup>65</sup>

*MCL* is also characterized by having mutations affecting many different genes including *ATM* (40%–75%), *CCND1* (35%), and *TP53* (28%).<sup>20</sup> Mutations of *NOTCH1* and *NOTCH2* occur in less than 10% of cases and are identified in a subset of tumors with more adverse biological features including blastoid/pleomorphic morphology. *NOTCH1* and *NOTCH2* have prognostic impact and potential therapeutic importance in *MCL*.<sup>66</sup>

Mutations or copy number losses of *TP53* genes are independent unfavorable prognostic factors in different types of B-cell lymphomas.<sup>67</sup> *CD58* gene encodes a molecule involved in T and natural killer (NK)-cell-mediated responses. In addition to *TP53*, mutations or copy number losses of *CD58* in DLBCL are independent unfavorable prognostic factors.<sup>68</sup> Recurrent mutations of the exportin 1 gene (*XPO1*) have been observed in primary mediastinal B-cell lymphoma and Hodgkin lymphoma and they have prognostic implication.<sup>69,70</sup> *TET2* is a tumor suppressor gene and frequently mutated in a variety of T or NK-cell lymphoma. *TET2* mutation is associated with advanced-

stage disease, thrombocytopenia, high international prognostic index scores, and a shorter progression-free survival.<sup>71,72</sup>

### Therapeutic targets

Much has been learned about the mutational landscape of malignant lymphomas. Genes identified in NGS analysis are important in the development and progression of malignant lymphoma and are potential therapeutic targets although drugs are currently available for only some of these targets. Genes involved in BCR signaling which converges to mitogen-activated protein kinase pathway, NF- $\kappa$ B pathway, and phosphoinositide 3-kinase (PI3K) pathway are therapeutic targets of B-cell lymphomas (Fig. 6). These include CD79A/B, SYK, and SFK of BCR signaling pathway, BTK, PKC $\beta$ , CARD11, MALT1, BCL10, IKK $\alpha$ , IKK $\beta$ , and IKK $\gamma$  of NF- $\kappa$ B pathway, and PI3K, AKT, and mammalian target of rapamycin of PI3K pathway.<sup>73</sup> Most active clinical trials are targeting these genes. Mutations of chromatin regulator/modifier genes, such as *CREBBP*, *KMT2D* (MLL2), and *EZH2* are extremely common early events and may be potential therapeutic targets.<sup>74-77</sup> Chromosomal rearrangements of *DUSP22* and *TP63* were identified in 30% and 8% of anaplastic lymphoma kinase (ALK)-negative anaplastic large cell lymphoma (ALCL), respectively.<sup>78</sup> ALCLs with *DUSP22* rearrangements show significant differences from other ALK-negative ALCLs, typically showing sheets of hallmark cells with doughnut cells and a few large pleomorphic cells.<sup>78,79</sup> *DUSP22* functions as a tumor suppressor gene and potential therapeutic manipulation. T-cell lymphoma of follicular helper T-cell (TFH) phenotype including AITL is characterized by mutations of genes involved in the TCR signaling pathway including *RHOA* G17V mutation (70%), *CD28* mutation (11%), *CTLA4-CD28* fusion (58%), *PLCG1* (14.1%), *PI3K* elements (7%), *CTNBN1* (6%), and *GTF2I* (6%) (Fig. 7).<sup>80-85</sup> Although mutations of *RHOA*, *CD28*, and *CTLA4-CD28* fusion themselves have no prognostic impact, targeting of TCR-related events may hold promise for the treatment of TFH-derived lymphomas. *SYK-ITK* fusion is detected in peripheral T-cell lymphoma (PTCL)-NOS, or AITL. The fusion kinase *ITK-SYK* mimics a TCR signal and drives oncogenesis in conditional mouse models of PTCL.<sup>86,87</sup> *IDH2* mutation is frequently identified in AITL (19%–42%), but not in other types of T- or NK-cell lymphoma. These mutations alter IDH enzymatic function, resulting in the accumulation of D-2-hydroxyglutarate (D-2-HG) in cells and tissues. D-2-HG may act as an oncometabolite, driving tumor progression and affect hypoxia signaling (prolyl hydroxylases), histone methylation, and DNA methylation.<sup>88,89</sup> Genes involved

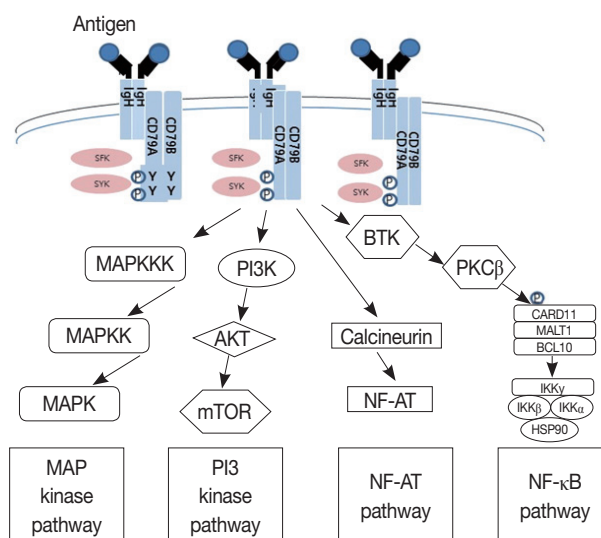


**Fig. 6.** Genes involved in B-cell receptor signaling which converges to mitogen-activated protein (MAP) kinase pathway, nuclear factor  $\kappa$ B (NF- $\kappa$ B) pathway, and phosphoinositide 3-kinase (PI3K) pathway are the therapeutic targets of B-cell lymphomas. MAPK, mitogen-activated protein kinase; MAPKK, mitogen-activated protein kinase kinase; MAPKKK, mitogen-activated protein kinase kinase kinase; mTOR, mammalian target of rapamycin. Modified from Young *et al.* *Semin Hematol* 2015;52:77-85, with permission of Elsevier.<sup>73</sup>

in JAK-STAT pathway are frequently mutated in extranodal NK/T-cell lymphoma, including STAT3 (most common), STAT5B, JAK3, and JAK1. Other commonly mutated genes include histone modification-related genes such as *BCOR* and *MLL2*, RNA helicase *DDX3*, and *P53*.<sup>90-92</sup> All these genes are important in the progression of NK/T-cell lymphoma and may be potential therapeutic targets. In addition to these genes, there are genes with inhibitors available, which are being tried in clinical trials.

### Samples for targeted sequencing

FFPE sample is available for targeted sequencing. Single nucleotide variants and copy number alteration can be detected using DNA extracted from FFPE tissue and the translocation can be identified by RNA sequencing using FFPE samples. In general, lymphoma is often highly cellular; therefore, DNA extracted from FFPE sample is sufficient to obtain sequencing data, although there is a variation in the minimum requirement of DNA amount according to the NGS platform. Before starting the test, development of optimum operating procedure in each laboratory is mandatory.

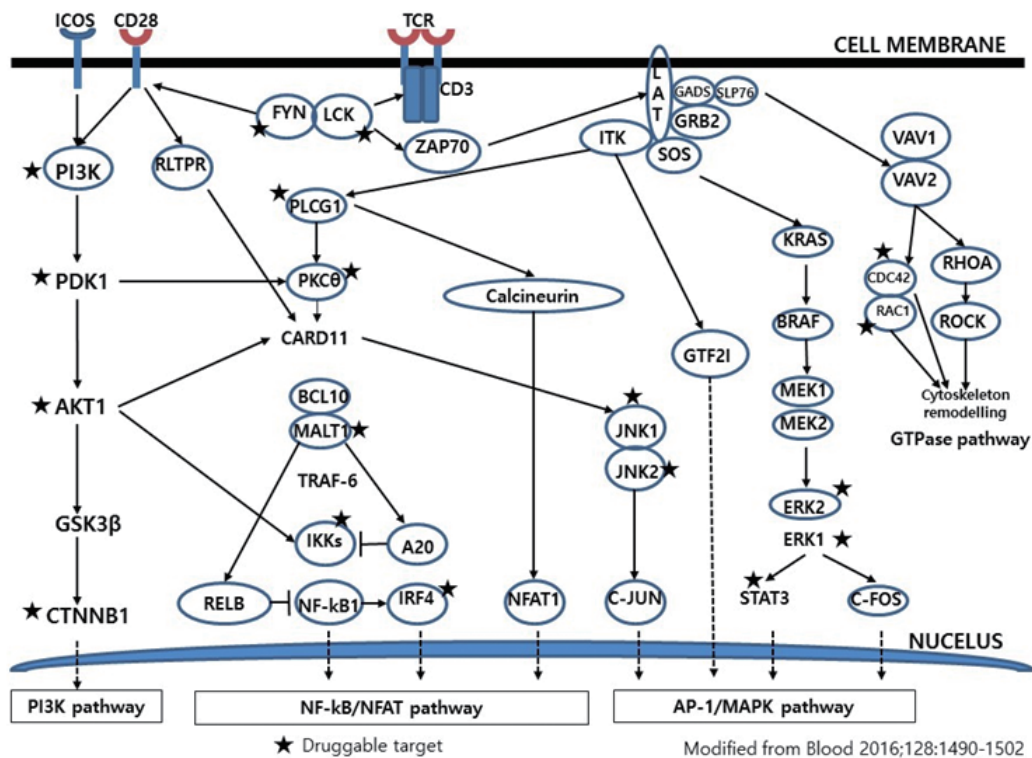


**Fig. 7.** T-cell receptor signaling-related genes in nodal lymphomas of follicular helper T-cell phenotype are therapeutic targets. PI3K, phosphoinositide 3-kinase; NF- $\kappa$ B, nuclear factor  $\kappa$ B; MAPK, mitogen-activated protein kinase. Modified from Vallois *et al.* Blood 2016;128:1490-502, with permission of American Society of Hematology.<sup>84</sup>

## CONCLUSION

Molecular diagnostics for B- and T-cell clonality test and cytogenetic test for malignant lymphoma have been much improved and introduced in routine clinical practice. In addition, determination of COO in DLBCL and NGS-based tests for genetic alterations in malignant lymphomas will open a pathway toward personalized medicine and targeted therapy in the near future.

### Conflicts of Interest

No potential conflict of interest relevant to this article was reported.

### Acknowledgments

The authors would like to thank all the executive officers of the Hematopathology Study Group of the Korean Society of Pathologists for careful review and discussion on this manuscript.

This research was supported by The Korean Society of Pathologists Grant (2016).

## REFERENCES

1. Tonegawa S. Somatic generation of antibody diversity. Nature 1983;302: 575-81.
2. Davis MM, Bjorkman PJ. T-cell antigen receptor genes and T-cell recognition. Nature 1988;334: 395-402.
3. van Dongen JJ, Langerak AW, Brüggemann M, *et al.* Design and standardization of PCR primers and protocols for detection of clonal immunoglobulin and T-cell receptor gene recombinations in suspect lymphoproliferations: report of the BIOMED-2 Concerted Action BMH4-CT98-3936. Leukemia 2003; 17: 2257-317.
4. Gilfillan S, Dierich A, Lemeur M, Benoist C, Mathis D. Mice lacking TdT: mature animals with an immature lymphocyte repertoire. Science 1993; 261: 1175-8.
5. van Dongen JJ, Szczepanski T, Adriaansens HJ. Immunobiology of leukemia. In: Henderson ES, Lister TA, Greaves MF, eds. 7th ed. Leukemia. Philadelphia: WB Saunders Company, 2002; 85-130.
6. Langerak AW, Groenen PJ, Brüggemann M, *et al.* EuroClonality/BIOMED-2 guidelines for interpretation and reporting of Ig/TCR clonality testing in suspected lymphoproliferations. Leukemia 2012; 26: 2159-71.
7. Sherwood AM, Desmarais C, Livingston RJ, *et al.* Deep sequencing

- of the human TCR $\gamma$  and TCR $\beta$  repertoires suggests that TCR $\beta$  rearranges after  $\alpha\beta$  and  $\gamma\delta$  T cell commitment. *Sci Transl Med* 2011; 3: 90ra61.
8. Bailey NG, Elenitoba-Johnson KS. Molecular diagnostics of T-cell lymphoproliferative disorders. *Cancer J* 2014; 20: 48-60.
  9. Schafernak KT, Variakojis D, Goolsby CL, et al. Clonality assessment of cutaneous B-cell lymphoid proliferations: a comparison of flow cytometry immunophenotyping, molecular studies, and immunohistochemistry/*in situ* hybridization and review of the literature. *Am J Dermatopathol* 2014; 36: 781-95.
  10. Födinger M, Winkler K, Mannhalter C, Chott A. Combined polymerase chain reaction approach for clonality detection in lymphoid neoplasms. *Diagn Mol Pathol* 1999; 8: 80-91.
  11. Thériault C, Galoin S, Valmary S, et al. PCR analysis of immunoglobulin heavy chain (IgH) and TcR- $\gamma$  chain gene rearrangements in the diagnosis of lymphoproliferative disorders: results of a study of 525 cases. *Mod Pathol* 2000; 13: 1269-79.
  12. Benhattar J, Delacretaz F, Martin P, Chaubert P, Costa J. Improved polymerase chain reaction detection of clonal T-cell lymphoid neoplasms. *Diagn Mol Pathol* 1995; 4: 108-12.
  13. Signoretti S, Murphy M, Cangi MG, Puddu P, Kadin ME, Loda M. Detection of clonal T-cell receptor  $\gamma$  gene rearrangements in paraffin-embedded tissue by polymerase chain reaction and nonradioactive single-strand conformational polymorphism analysis. *Am J Pathol* 1999; 154: 67-75.
  14. Patel KP, Pan Q, Wang Y, et al. Comparison of BIOMED-2 versus laboratory-developed polymerase chain reaction assays for detecting T-cell receptor- $\gamma$  gene rearrangements. *J Mol Diagn* 2010; 12: 226-37.
  15. van Krieken JH, Langerak AW, Macintyre EA, et al. Improved reliability of lymphoma diagnostics via PCR-based clonality testing: report of the BIOMED-2 Concerted Action BHM4-CT98-3936. *Leukemia* 2007; 21: 201-6.
  16. Langerak AW, Molina TJ, Lavender FL, et al. Polymerase chain reaction-based clonality testing in tissue samples with reactive lymphoproliferations: usefulness and pitfalls. A report of the BIOMED-2 Concerted Action BMH4-CT98-3936. *Leukemia* 2007; 21: 222-9.
  17. Brüggemann M, White H, Gaulard P, et al. Powerful strategy for polymerase chain reaction-based clonality assessment in T-cell malignancies Report of the BIOMED-2 Concerted Action BHM4-CT98-3936. *Leukemia* 2007; 21: 215-21.
  18. Kuppers R, Klein U, Hansmann ML, Rajewsky K. Cellular origin of human B-cell lymphomas. *N Engl J Med* 1999; 341: 1520-9.
  19. Davis TH, Yockey CE, Balk SP. Detection of clonal immunoglobulin gene rearrangements by polymerase chain reaction amplification and single-strand conformational polymorphism analysis. *Am J Pathol* 1993; 142: 1841-7.
  20. Bourguin A, Tung R, Galili N, Sklar J. Rapid, nonradioactive detection of clonal T-cell receptor gene rearrangements in lymphoid neoplasms. *Proc Natl Acad Sci U S A* 1990; 87: 8536-40.
  21. Medeiros LJ, Carr J. Overview of the role of molecular methods in the diagnosis of malignant lymphomas. *Arch Pathol Lab Med* 1999; 123: 1189-207.
  22. Boeckx N, Willemse MJ, Szczepanski T, et al. Fusion gene transcripts and Ig/TCR gene rearrangements are complementary but infrequent targets for PCR-based detection of minimal residual disease in acute myeloid leukemia. *Leukemia* 2002; 16: 368-75.
  23. Szczepański T, Beishuizen A, Pongers-Willemse MJ, et al. Cross-lineage T cell receptor gene rearrangements occur in more than ninety percent of childhood precursor-B acute lymphoblastic leukemias: alternative PCR targets for detection of minimal residual disease. *Leukemia* 1999; 13: 196-205.
  24. Szczepański T, Langerak AW, van Dongen JJ, van Krieken JH. Lymphoma with multi-gene rearrangement on the level of immunoglobulin heavy chain, light chain, and T-cell receptor  $\beta$  chain. *Am J Hematol* 1998; 59: 99-100.
  25. Moreau EJ, Langerak AW, van Gastel-Mol EJ, et al. Easy detection of all T cell receptor gamma (*TCRG*) gene rearrangements by Southern blot analysis: recommendations for optimal results. *Leukemia* 1999; 13: 1620-6.
  26. Langerak AW, Wolvers-Tettero IL, van Dongen JJ. Detection of T cell receptor beta (*TCRB*) gene rearrangement patterns in T cell malignancies by Southern blot analysis. *Leukemia* 1999; 13: 965-74.
  27. Kluin P, Schuurung E. Molecular cytogenetics of lymphoma: where do we stand in 2010? *Histopathology* 2011; 58: 128-44.
  28. Niitsu N, Okamoto M, Miura I, Hirano M. Clinical features and prognosis of de novo diffuse large B-cell lymphoma with t(14;18) and 8q24/c-MYC translocations. *Leukemia* 2009; 23: 777-83.
  29. Johnson NA, Slack GW, Savage KJ, et al. Concurrent expression of MYC and BCL2 in diffuse large B-cell lymphoma treated with rituximab plus cyclophosphamide, doxorubicin, vincristine, and prednisone. *J Clin Oncol* 2012; 30: 3452-9.
  30. Horn H, Ziepert M, Becher C, et al. MYC status in concert with BCL2 and BCL6 expression predicts outcome in diffuse large B-cell lymphoma. *Blood* 2013; 121: 2253-63.
  31. Hu S, Xu-Monette ZY, Tzankov A, et al. MYC/BCL2 protein coexpression contributes to the inferior survival of activated B-cell subtype of diffuse large B-cell lymphoma and demonstrates high-risk gene expression signatures: a report from The International DLBCL Rituximab-CHOP Consortium Program. *Blood* 2013; 121: 4021-31.
  32. Swerdlow SH, Campo E, Pileri SA, et al. The 2016 revision of the World Health Organization classification of lymphoid neoplasms.

- Blood 2016; 127: 2375-90.
33. Swerdlow SH, Campo E, Harris NL, *et al.* WHO classification of tumours of haematopoietic and lymphoid tissues. 4th ed. Lyon: IARC Press, 2008.
  34. Green TM, Young KH, Visco C, *et al.* Immunohistochemical double-hit score is a strong predictor of outcome in patients with diffuse large B-cell lymphoma treated with rituximab plus cyclophosphamide, doxorubicin, vincristine, and prednisone. *J Clin Oncol* 2012; 30: 3460-7.
  35. Campbell LJ. Cancer cytogenetics: methods and protocols. 2nd ed. New York: Humana Press, 2011.
  36. Wolff DJ, Bagg A, Cooley LD, *et al.* Guidance for fluorescence *in situ* hybridization testing in hematologic disorders. *J Mol Diagn* 2007; 9: 134-43.
  37. McGowan-Jordan J, Simons A, Schmid M. ISCN 2016: an international system for human cytogenomic nomenclature (2016). Basel: Karger, 2016.
  38. Alizadeh AA, Eisen MB, Davis RE, *et al.* Distinct types of diffuse large B-cell lymphoma identified by gene expression profiling. *Nature* 2000; 403: 503-11.
  39. Wright G, Tan B, Rosenwald A, Hurt EH, Wiestner A, Staudt LM. A gene expression-based method to diagnose clinically distinct subgroups of diffuse large B cell lymphoma. *Proc Natl Acad Sci U S A* 2003; 100: 9991-6.
  40. Testoni M, Zucca E, Young KH, Bertoni F. Genetic lesions in diffuse large B-cell lymphomas. *Ann Oncol* 2015; 26: 1069-80.
  41. Carbone A, Ghoghini A, Kwong YL, Younes A. Diffuse large B cell lymphoma: using pathologic and molecular biomarkers to define subgroups for novel therapy. *Ann Hematol* 2014; 93: 1263-77.
  42. Hans CP, Weisenburger DD, Greiner TC, *et al.* Confirmation of the molecular classification of diffuse large B-cell lymphoma by immunohistochemistry using a tissue microarray. *Blood* 2004; 103: 275-82.
  43. Choi WW, Weisenburger DD, Greiner TC, *et al.* A new immunostain algorithm classifies diffuse large B-cell lymphoma into molecular subtypes with high accuracy. *Clin Cancer Res* 2009; 15: 5494-502.
  44. Meyer PN, Fu K, Greiner TC, *et al.* Immunohistochemical methods for predicting cell of origin and survival in patients with diffuse large B-cell lymphoma treated with rituximab. *J Clin Oncol* 2011; 29: 200-7.
  45. Gutiérrez-García G, Cardesa-Salzmann T, Climent F, *et al.* Gene-expression profiling and not immunophenotypic algorithms predicts prognosis in patients with diffuse large B-cell lymphoma treated with immunochemotherapy. *Blood* 2011; 117: 4836-43.
  46. Intlekofer AM, Younes A. Precision therapy for lymphoma: current state and future directions. *Nat Rev Clin Oncol* 2014; 11: 585-96.
  47. Scott DW, Wright GW, Williams PM, *et al.* Determining cell-of-origin subtypes of diffuse large B-cell lymphoma using gene expression in formalin-fixed paraffin-embedded tissue. *Blood* 2014; 123: 1214-7.
  48. Scott DW, Mottok A, Ennishi D, *et al.* Prognostic significance of diffuse large B-cell lymphoma cell of origin determined by digital gene expression in formalin-fixed paraffin-embedded tissue biopsies. *J Clin Oncol* 2015; 33: 2848-56.
  49. Dietrich S, Pircher A, Endris V, *et al.* BRAF inhibition in hairy cell leukemia with low-dose vemurafenib. *Blood* 2016; 127: 2847-55.
  50. Raess PW, Mintzer D, Husson M, *et al.* BRAF V600E is also seen in unclassifiable splenic B-cell lymphoma/leukemia, a potential mimic of hairy cell leukemia. *Blood* 2013; 122: 3084-5.
  51. Blombery PA, Wong SQ, Hewitt CA, *et al.* Detection of BRAF mutations in patients with hairy cell leukemia and related lymphoproliferative disorders. *Haematologica* 2012; 97: 780-3.
  52. Arcaini L, Zibellini S, Boveri E, *et al.* The BRAF V600E mutation in hairy cell leukemia and other mature B-cell neoplasms. *Blood* 2012; 119: 188-91.
  53. Mason EF, Brown RD, Szeto DP, *et al.* Detection of activating MAP2K1 mutations in atypical hairy cell leukemia and hairy cell leukemia variant. *Leuk Lymphoma* 2017; 58: 233-6.
  54. Waterfall JJ, Arons E, Walker RL, *et al.* High prevalence of MAP2K1 mutations in variant and IGHV4-34-expressing hairy-cell leukemias. *Nat Genet* 2014; 46: 8-10.
  55. Kapoor P, Ansell SM, Fonseca R, *et al.* Diagnosis and management of waldenstrom macroglobulinemia: Mayo stratification of macroglobulinemia and risk-adapted therapy (mSMART) guidelines 2016. *JAMA Oncol* 2017 Jan 5 [Epub]. <https://doi.org/10.1001/jamaoncol.2016.5763>.
  56. Schmidt J, Federmann B, Schindler N, *et al.* MYD88 L265P and CXCR4 mutations in lymphoplasmacytic lymphoma identify cases with high disease activity. *Br J Haematol* 2015; 169: 795-803.
  57. Martinez-Lopez A, Curiel-Olmo S, Mollejo M, *et al.* MYD88 (L265P) somatic mutation in marginal zone B-cell lymphoma. *Am J Surg Pathol* 2015; 39: 644-51.
  58. Hamadeh F, MacNamara SP, Aguilera NS, Swerdlow SH, Cook JR. MYD88 L265P mutation analysis helps define nodal lymphoplasmacytic lymphoma. *Mod Pathol* 2015; 28: 564-74.
  59. Salaverria I, Philipp C, Oschlies I, *et al.* Translocations activating IRF4 identify a subtype of germinal center-derived B-cell lymphoma affecting predominantly children and young adults. *Blood* 2011; 118: 139-47.
  60. Salaverria I, Martin-Guerrero I, Wagener R, *et al.* A recurrent 11q aberration pattern characterizes a subset of MYC-negative high-grade B-cell lymphomas resembling Burkitt lymphoma. *Blood*

- 2014; 123: 1187-98.
61. Ferreiro JF, Morscio J, Dierickx D, et al. Post-transplant molecularly defined Burkitt lymphomas are frequently MYC-negative and characterized by the 11q-gain/loss pattern. *Haematologica* 2015; 100: e275-9.
  62. Stilgenbauer S, Schnaiter A, Paschka P, et al. Gene mutations and treatment outcome in chronic lymphocytic leukemia: results from the CLL8 trial. *Blood* 2014; 123: 3247-54.
  63. Nadeu F, Delgado J, Royo C, et al. Clinical impact of clonal and subclonal *TP53*, *SF3B1*, *BIRC3*, *NOTCH1*, and *ATM* mutations in chronic lymphocytic leukemia. *Blood* 2016; 127: 2122-30.
  64. te Raa GD, Malcikova J, Pospisilova S, et al. Overview of available p53 function tests in relation to *TP53* and *ATM* gene alterations and chemoresistance in chronic lymphocytic leukemia. *Leuk Lymphoma* 2013; 54: 1849-53.
  65. Rossi D, Fangazio M, Rasi S, et al. Disruption of *BIRC3* associates with fludarabine chemorefractoriness in *TP53* wild-type chronic lymphocytic leukemia. *Blood* 2012; 119: 2854-62.
  66. Beà S, Valdés-Mas R, Navarro A, et al. Landscape of somatic mutations and clonal evolution in mantle cell lymphoma. *Proc Natl Acad Sci U S A* 2013; 110: 18250-5.
  67. Xu-Monette ZY, Wu L, Visco C, et al. Mutational profile and prognostic significance of *TP53* in diffuse large B-cell lymphoma patients treated with R-CHOP: report from an International DLBCL Rituximab-CHOP Consortium Program Study. *Blood* 2012; 120: 3986-96.
  68. Cao Y, Zhu T, Zhang P, et al. Mutations or copy number losses of *CD58* and *TP53* genes in diffuse large B cell lymphoma are independent unfavorable prognostic factors. *Oncotarget* 2016; 7: 83294-307.
  69. Jardin F, Pujals A, Pelletier L, et al. Recurrent mutations of the exportin 1 gene (*XPO1*) and their impact on selective inhibitor of nuclear export compounds sensitivity in primary mediastinal B-cell lymphoma. *Am J Hematol* 2016; 91: 923-30.
  70. Camus V, Stamatoullas A, Mareschal S, et al. Detection and prognostic value of recurrent exportin 1 mutations in tumor and cell-free circulating DNA of patients with classical Hodgkin lymphoma. *Haematologica* 2016; 101: 1094-101.
  71. Nakajima H, Kunimoto H. *TET2* as an epigenetic master regulator for normal and malignant hematopoiesis. *Cancer Sci* 2014; 105: 1093-9.
  72. Lemonnier F, Couronné L, Parrens M, et al. Recurrent *TET2* mutations in peripheral T-cell lymphomas correlate with TFH-like features and adverse clinical parameters. *Blood* 2012; 120: 1466-9.
  73. Young RM, Shaffer AL 3rd, Phelan JD, Staudt LM. B-cell receptor signaling in diffuse large B-cell lymphoma. *Semin Hematol* 2015; 52: 77-85.
  74. Okosun J, Bödör C, Wang J, et al. Integrated genomic analysis identifies recurrent mutations and evolution patterns driving the initiation and progression of follicular lymphoma. *Nat Genet* 2014; 46: 176-81.
  75. Bouska A, Zhang W, Gong Q, et al. Combined copy number and mutation analysis identifies oncogenic pathways associated with transformation of follicular lymphoma. *Leukemia* 2017; 31: 83-91.
  76. Younes A. Promising novel agents for aggressive B-cell lymphoma. *Hematol Oncol Clin North Am* 2016; 30: 1229-37.
  77. Kurmasheva RT, Sammons M, Favours E, et al. Initial testing (stage 1) of tazemetostat (EPZ-6438), a novel EZH2 inhibitor, by the pediatric preclinical testing program. *Pediatr Blood Cancer* 2017; 64: e26218.
  78. Parrilla Castellar ER, Jaffe ES, Said JW, et al. ALK-negative anaplastic large cell lymphoma is a genetically heterogeneous disease with widely disparate clinical outcomes. *Blood* 2014; 124: 1473-80.
  79. King RL, Dao LN, McPhail ED, et al. Morphologic features of ALK-negative anaplastic large cell lymphomas with *DUSP22* rearrangements. *Am J Surg Pathol* 2016; 40: 36-43.
  80. Manso R, Sánchez-Beato M, Monsalvo S, et al. The *RHOA* G17V gene mutation occurs frequently in peripheral T-cell lymphoma and is associated with a characteristic molecular signature. *Blood* 2014; 123: 2893-4.
  81. Yoo HY, Sung MK, Lee SH, et al. A recurrent inactivating mutation in *RHOA* GTPase in angioimmunoblastic T cell lymphoma. *Nat Genet* 2014; 46: 371-5.
  82. Sakata-Yanagimoto M, Enami T, Yoshida K, et al. Somatic *RHOA* mutation in angioimmunoblastic T cell lymphoma. *Nat Genet* 2014; 46: 171-5.
  83. Palomero T, Couronné L, Khiabani H, et al. Recurrent mutations in epigenetic regulators, *RHOA* and *FYN* kinase in peripheral T cell lymphomas. *Nat Genet* 2014; 46: 166-70.
  84. Vallois D, Dobay MP, Morin RD, et al. Activating mutations in genes related to TCR signaling in angioimmunoblastic and other follicular helper T-cell-derived lymphomas. *Blood* 2016; 128: 1490-502.
  85. Rohr J, Guo S, Huo J, et al. Recurrent activating mutations of *CD28* in peripheral T-cell lymphomas. *Leukemia* 2016; 30: 1062-70.
  86. Streubel B, Vinatzer U, Willheim M, Raderer M, Chott A. Novel t(5;9)(q33;q22) fuses *ITK* to *SYK* in unspecified peripheral T-cell lymphoma. *Leukemia* 2006; 20: 313-8.
  87. Pechloff K, Holch J, Ferch U, et al. The fusion kinase *ITK-SYK* mimics a T cell receptor signal and drives oncogenesis in conditional mouse models of peripheral T cell lymphoma. *J Exp Med* 2010; 207: 1031-44.
  88. Wang C, McKeithan TW, Gong Q, et al. *IDH2R172* mutations

- define a unique subgroup of patients with angioimmunoblastic T-cell lymphoma. *Blood* 2015; 126: 1741-52.
89. Cairns RA, Iqbal J, Lemonnier F, *et al.* *IDH2* mutations are frequent in angioimmunoblastic T-cell lymphoma. *Blood* 2012; 119: 1901-3.
90. Jiang L, Gu ZH, Yan ZX, *et al.* Exome sequencing identifies somatic mutations of *DDX3X* in natural killer/T-cell lymphoma. *Nat Genet* 2015; 47: 1061-6.
91. Lee S, Park HY, Kang SY, *et al.* Genetic alterations of JAK/STAT cascade and histone modification in extranodal NK/T-cell lymphoma nasal type. *Oncotarget* 2015; 6: 17764-76.
92. Dobashi A, Tsuyama N, Asaka R, *et al.* Frequent *BCOR* aberrations in extranodal NK/T-cell lymphoma, nasal type. *Genes Chromosomes Cancer* 2016; 55: 460-71.

## Molecular Testing of Lung Cancers

Hyo Sup Shim · Yoon-La Choi<sup>1</sup>  
Lucia Kim<sup>2</sup> · Sunhee Chang<sup>3</sup>  
Wan-Seop Kim<sup>4</sup> · Mee Sook Roh<sup>5</sup>  
Tae-Jung Kim<sup>6</sup> · Seung Yeon Ha<sup>7</sup>  
Jin-Haeng Chung<sup>8</sup> · Se Jin Jang<sup>9</sup>  
Geon Kook Lee<sup>10</sup> · The Korean  
Cardiopulmonary Pathology Study  
Group · The Korean Molecular  
Pathology Study Group

Department of Pathology, Yonsei University College of Medicine, Seoul; <sup>1</sup>Department of Pathology and Translational Genomics, Samsung Medical Center, Sungkyunkwan University School of Medicine, Seoul; <sup>2</sup>Department of Pathology, Inha University School of Medicine, Incheon; <sup>3</sup>Department of Pathology, Inje University Ilsan Paik Hospital, Inje University, Goyang; <sup>4</sup>Department of Pathology, Konkuk University School of Medicine, Seoul; <sup>5</sup>Department of Pathology, Dong-A University College of Medicine, Busan; <sup>6</sup>Department of Pathology, College of Medicine, The Catholic University of Korea, Seoul; <sup>7</sup>Department of Pathology, Gachon University Gil Medical Center, Incheon; <sup>8</sup>Department of Pathology, Seoul National University Bundang Hospital, Seongnam; <sup>9</sup>Department of Pathology, Asan Medical Center, University of Ulsan College of Medicine, Seoul; <sup>10</sup>Department of Pathology, National Cancer Center, Goyang, Korea

Received: April 3, 2017

Accepted: April 9, 2017

### Corresponding Author

Geon Kook Lee, MD  
Department of Pathology, National Cancer Center,  
323 Ilsan-ro, Ilsandong-gu, Goyang 10408, Korea  
Tel: +82-31-920-1746  
Fax: +82-31-920-1369  
E-mail: gklee@ncc.re.kr

Targeted therapies guided by molecular diagnostics have become a standard treatment of lung cancer. Epidermal growth factor receptor (*EGFR*) mutations and anaplastic lymphoma kinase (*ALK*) rearrangements are currently used as the best predictive biomarkers for *EGFR* tyrosine kinase inhibitors and *ALK* inhibitors, respectively. Besides *EGFR* and *ALK*, the list of druggable genetic alterations has been growing, including *ROS1* rearrangements, *RET* rearrangements, and *MET* alterations. In this situation, pathologists should carefully manage clinical samples for molecular testing and should do their best to quickly and accurately identify patients who will benefit from precision therapeutics. Here, we grouped molecular biomarkers of lung cancers into three categories—mutations, gene rearrangements, and amplifications—and propose expanded guidelines on molecular testing of lung cancers.

**Key Words:** Lung neoplasms; Molecular testing; Guideline; Precision medicine

Molecular diagnostics-guided targeted therapies have become a standard treatment for patients with lung cancer.<sup>1</sup> Driver genetic alterations such as epidermal growth factor receptor (*EGFR*) mutations and anaplastic lymphoma kinase (*ALK*) rearrangements are currently used as predictive biomarkers for

*EGFR* tyrosine kinase inhibitors (TKIs) and *ALK* inhibitors, respectively.<sup>1</sup> Since Korean guideline recommendations for *EGFR* and *ALK* molecular testing were published,<sup>2,3</sup> the list of druggable genetic alterations has been growing as tremendous amounts of information on the cancer genome are becoming

**Table 1.** Targetable genetic alterations in lung cancer

Gene	Representative subtypes or variants	Frequency	Targeted agents
<b>Mutations</b>			
<i>EGFR</i>	Exon 19 deletion, Exon 21 L858R, Exon 20 T790M	40%–50% in ADCs <sup>a</sup> 10%–20% in ADCs <sup>b</sup>	Gefitinib, erlotinib, afatinib, osimertinib
<i>KRAS</i>	G12X, G13X, G61X	5%–10% in ADCs <sup>a</sup> 20%–30% in ADCs <sup>b</sup>	MEK inhibitors
<i>BRAF</i>	V600E	1%–4% in ADCs	Vemurafenib, dabrafenib,
<i>HER2</i>	p.A775 G776insYVMA in exon 20	1%–2% in ADCs	Trastuzumab, afatinib
<i>MET</i>	Splice site mutations around or in exon 14	3%–4% in ADCs	Crizotinib, cabozantinib
<b>Gene fusions</b>			
<i>ALK</i>	<i>EML4-ALK</i> , <i>TGF-ALK</i> , <i>KIF5B-ALK</i>	5% in ADCs	Crizotinib, ceritinib, alectinib
<i>ROS1</i>	<i>CD74-ROS1</i> , <i>EZR-ROS1</i> , <i>SLC34A2-ROS1</i> , <i>SDC4-ROS1</i>	1% in ADCs	Crizotinib, ceritinib
<i>RET</i>	<i>KIF5B-RET</i> , <i>CCDC6-RET</i>	1% in ADCs	Cabozantinib, vandetanib, alectinib
<i>NTRK1</i>	<i>MPRIP-NTRK1</i> and <i>CD74-NTRK1</i> , <i>TPM3-NTRK1</i>	< 1% in ADCs	Entrectinib
<i>FGFR1/3</i>	<i>FGFR3-TACC3</i> , <i>BAG4-FGFR1</i>	1% in NSCLCs	FGFR inhibitor
<i>NRG1</i>	<i>CD74-NRG1</i> , <i>SLC3A2-NRG1</i> , <i>VAMP2-NRG1</i>	7% in mucinous ADCs	NA
<b>Amplifications</b>			
<i>FGFR1</i>	Gene amplification	13%–22% in SQCs	FGFR inhibitor
<i>EGFR</i>	Gene amplification	8%–9% in SQCs,	EGFR inhibitor
<i>MET</i>	Gene amplification	2%–4% in ADCs	Crizotinib
<i>HER2</i>	Gene amplification	1%–2% in ADCs	Trastuzumab, afatinib

ADC, adenocarcinoma; NSCLC, non-small cell lung carcinoma; FGFR, fibroblast growth factor receptor; NA, not available; SQC, squamous cell carcinoma; EGFR, epidermal growth factor receptor.

<sup>a</sup>Asian populations; <sup>b</sup>Western populations.

available (Table 1).<sup>4-6</sup> Molecular analyses of various biomarkers in tumor tissue or cytology specimens have become standard laboratory tests for the clinical management of lung cancers. In this context, an updated and more comprehensive set of guidelines is necessary.

In this article, we propose expanded guidelines for molecular testing of lung cancers including recently updated genetic alterations and well-known biomarkers. Here, we grouped molecular biomarkers into three categories—mutations, gene rearrangements, and amplifications (Fig. 1)—and reviewed the background, indications, methods, reporting, test validations, and quality assurance for each category.

## MOLECULAR TESTING

### Mutations including *EGFR*, *KRAS*, *BRAF*, *HER2*, and *MET*

#### Background

Activating somatic mutations including point substitution, small insertion, and in-frame deletion are major oncogenic drivers in lung cancer. The discovery of activating *EGFR* mutations and their close relation with the response to EGFR TKIs opened the new era of precision medicine. Since then, clinical trials have confirmed that *EGFR* mutations are the best predictive factor of EGFR TKI efficacy.<sup>7,8</sup> *EGFR* mutations have been

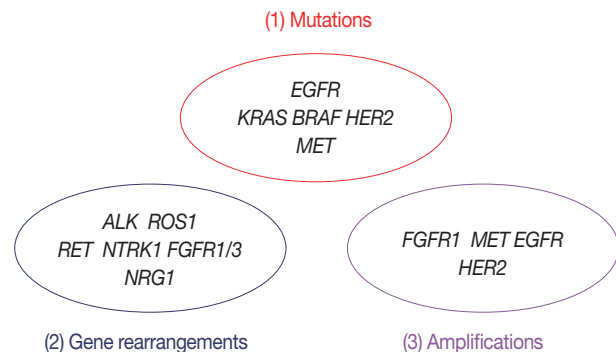


**Fig. 1.** Three categories of molecular biomarkers used in these guidelines. EGFR, epidermal growth factor receptor; ALK, anaplastic lymphoma kinase; FGFR, fibroblast growth factor receptor.

more frequently found in lung adenocarcinomas in Asian populations than Western populations.<sup>9</sup> The overall *EGFR* mutation rate is approximately up to 46% among Korean patients with adenocarcinoma.<sup>10,11</sup> More than 90% of sensitizing *EGFR* mutations are composed of an in-frame deletion in exon 19 and a point mutation (L858R) in exon 21. Nonetheless, most patients experience disease progression usually after 12 months of treatment.<sup>12,13</sup> A variety of mechanisms are involved in acquired resistance to EGFR TKIs.<sup>12-14</sup> Among these, the most common resistance mechanism is the T790M mutation in *EGFR*, constituting 50%–60% of cases.<sup>12,13,15</sup> Recently, osimertinib was approved for the treatment of T790M-positive lung cancers in

Korea.<sup>16</sup> The acquired *EGFR* C797S mutation has been reported to mediate resistance to osimertinib in a subset of *EGFR* T790M–positive non-small cell lung carcinomas (NSCLCs).<sup>17,18</sup> Thus, *EGFR* mutation testing covering sensitizing as well as nonsensitizing mutations has become the most important step in treatment decision-making for lung cancer patients because of the high frequency of *EGFR* mutations and the availability of targeted therapeutic agents.

The frequency of *KRAS* mutations has been reported to be 8%–15% in lung adenocarcinoma among Korean patients.<sup>19,20</sup> Unfortunately, targeted therapies thus far have been unsuccessful.<sup>21</sup> *KRAS* mutations are known as negative predictive markers of a poor response to *EGFR* TKIs. In addition, a *KRAS* mutation has been reported to be a poor prognostic factor. This also appears to be dependent both on the specific *KRAS* codon mutation and disease stage at the time of diagnosis.<sup>21</sup> Invasive mucinous adenocarcinomas show a high incidence of *KRAS* mutations.<sup>22</sup>

Besides *EGFR* mutations, other targetable mutations have been found although their frequency is low. A *BRAF* mutation has been found in 3%–4% of lung adenocarcinomas in Western patients.<sup>23,24</sup> Among never-smoker Korean women with lung cancer, the frequency of tumor *BRAF* mutation is 1%.<sup>25</sup> The V600E mutation constitutes only 50% of *BRAF* mutations in contrast to other cancers (such as melanoma and papillary thyroid carcinoma).<sup>23,24</sup> Vemurafenib and dabrafenib show clinical activity in *BRAF* V600E-mutant NSCLC.<sup>26–28</sup> *HER2* mutations are present in approximately 1%–2% of lung adenocarcinomas.<sup>29</sup> The most common mutation is an in-frame insertion within exon 20.<sup>29</sup> The exon 20 insertion results in increased *HER2* kinase activity. The clinical response to *HER2*-targeting agents, such as trastuzumab and afatinib, is observed in patients with lung cancer harboring a *HER2* mutation.<sup>29</sup>

Recently, *MET* splice site mutations have emerged as targetable oncogenic drivers. Oncogenic mutations in the *MET* exon 14 splice sites (these mutations cause exon 14 skipping) occur in 3%–4% of lung adenocarcinomas.<sup>30,31</sup> Patients with lung cancer harboring *MET* exon 14 skipping show a clinical response to *MET* inhibitors including crizotinib.<sup>30,31</sup>

### Indications

The important reason for molecular testing of lung cancers is to select patients who may benefit from targeted therapies. In addition, patients with lung cancer can get benefits from molecular testing of their tumors regardless of stage. For example, molecular testing can provide accurate information on staging (in case of multiple tumors), prognostic stratification, and prompt

treatment in case of recurrence. Because of the high frequency of *EGFR* mutations in Asian populations as mentioned above, *EGFR* mutation testing is especially important for the treatment of Korean lung cancer patients. The Korean Food and Drug Administration (FDA) approved only *EGFR* molecular testing from among five genes important for decision-making with respect to first-line chemotherapy during standard treatment. Other mutations can also be approved and used as predictive markers in the near future. Each mutation is significantly associated with some clinical factors or histological subtypes. Nevertheless, clinical findings alone cannot completely predict specific mutation status.<sup>32,33</sup> In most of the guidelines published so far, histological types have been recommended as the most important factor in determining whether to perform molecular tests.<sup>34–36</sup> In particular, for patients who have a diagnosis of NSCLC with an adenocarcinoma component or nonsquamous cell type, molecular testing is routinely recommended.<sup>35</sup> Thus, pathologists should try to further classify NSCLCs into more specific subtypes, such as adenocarcinoma or squamous cell carcinoma (SQC).<sup>2</sup> In addition, a minimum immunohistochemical panel, such as one adenocarcinoma marker and one SQC marker, is recommended to preserve as much tissue as possible for molecular testing in small tissue samples.<sup>35,37</sup> Besides histological analysis, in cases of young age, female gender, never-smokers, small biopsies, or patients with a combined tumor type, molecular testing can be done.

### Methodology

#### Methods

A variety of methods can be used for detecting mutations including direct sequencing, real-time polymerase chain reaction (PCR), and commercial kits (Table 2).<sup>38,39</sup> Pathologists should consider the available approaches and the advantages and disadvantages of each method, including analytical sensitivity and turnaround time. In addition, new technologies for molecular testing must be approved by the Korean government before incorporation into clinical practice.

Direct sequencing is considered the gold standard for mutation analysis. On the other hand, direct DNA sequencing requires a high ratio of tumor tissue to normal tissue (more than 50% tumor content) for reliable results. In contrast, PCR-based methods show high sensitivity, requiring mutant DNA content of only 1%.<sup>38</sup> Nevertheless, these PCR-based methods can detect only previously known mutations or targeted sites. PCR-based methods including the peptide nucleic acid–mediated PCR

**Table 2.** Representative methods categorized by mechanisms of oncogene activation and by targeted molecules

Category	Mutation	Gene rearrangement	Amplification
DNA	Direct sequencing	FISH	FISH
	PCR-based methods	NGS	qPCR
	NGS		NGS
RNA		RT-PCR (fusion transcript) NGS	Real-time PCR (mRNA overexpression)
Protein	IHC (mutation-specific antibody)	IHC (protein expression)	IHC (protein overexpression)

PCR, polymerase chain reaction; NGS, next-generation sequencing; FISH, fluorescence *in situ* hybridization; qPCR, quantitative polymerase chain reaction; RT-PCR, reverse transcriptase polymerase chain reaction; IHC, immunohistochemistry.

clamping method and allele-specific PCR method have been approved in Korea. Among the targetable mutations, *EGFR* mutations have been the most studied in the field of lung cancer. In studies comparing two representative methods, clinical outcomes are not significantly different among groups harboring *EGFR* mutations detected by direct sequencing or by PCR-based methods.<sup>40,41</sup> Highly sensitive methods may also be useful for the detection of *EGFR* mutations associated with acquired resistance, e.g., T790M.<sup>15</sup> As with the *EGFR* mutation, direct sequencing or real-time PCR can be used for the detection of *KRAS*, *BRAF*, and *HER2* mutations, which include a point mutation or small indel. In the case of *MET* exon 14 alterations, most alterations are a point mutation or indel, affecting the splice acceptor site, splice donor site, or the approximately 25-base pair (bp) intronic noncoding region. In rare cases, however, whole-exon deletions of *MET* exon 14 have been reported.<sup>42</sup> A DNA-based method including direct sequencing is possible, but the mRNA-based method including real-time PCR is better at detecting *MET* exon 14 skipping.

As targetable genetic alterations are increasingly discovered, individual genotyping may become relatively inefficient and costly. Thus, next-generation sequencing (NGS) technology with DNA or RNA is reported to be useful for multiplexed and deep genomic sequencing.<sup>43,44</sup> Especially, targeted deep sequencing of selected gene sets (a so-called cancer panel) is approaching integration into daily clinical practice. Nonetheless, due to the methodological complexity of NGS, analytical validation and quality control are crucial for implementation in routine practice. Furthermore, to become a companion diagnostic assay, an NGS-based method should be comparatively validated with previous companion diagnostics.

#### Sample types

As previously described in our proposed guideline, small biopsy and cytology samples are used for mutation testing.<sup>2</sup> In particular, all samples obtained from a variety of methods are acceptable, including transbronchial lung biopsy, endobronchial ultrasound-

guided transbronchial needle aspiration, bronchial brushing or washing, computed tomography-guided gun biopsy or needle aspiration, and pleural fluid sampling.<sup>34,45,46</sup> The results using cytology samples are highly concordant with those of the corresponding tissue samples, especially with more sensitive methods.<sup>45,47</sup>

Since most driver mutations develop in early steps of carcinogenesis, tumor samples from either primary masses or metastatic lesions are equally suitable for mutation testing.<sup>48</sup> In the case of multiple primary lung cancers, each tumor may be tested.<sup>49</sup>

Formalin-fixed, paraffin-embedded (FFPE) tissues are most frequently used in molecular testing. Routinely prepared FFPE tissues are the most practical resource for molecular analysis, in spite of fixation-related artifacts.<sup>50</sup> The optimal fixative for preparing FFPE samples is generally 10% neutral-buffered formalin.<sup>34</sup> The optimal fixation time ranges from 6 to 72 hours to avoid underfixation or overfixation, respectively.<sup>34,50</sup> Routinely prepared cytology samples such as alcohol-fixed smears or Thin Prep slides<sup>45,47</sup> and cell block samples<sup>51</sup> are also suitable for mutation testing.

Because obtaining a tissue sample from bronchoscopy or a transthoracic needle biopsy is difficult and nonrepeatable, a liquid biopsy, which contains circulating tumor DNA, circulating tumor cells, or exosomes using plasma or body fluids, has recently been attracting attention as a new source for identification of somatic mutations.<sup>52,53</sup> Nonetheless, due to the high rate of false negative results at present, negative results require a tissue biopsy to determine exact mutation status.<sup>53</sup>

#### Sample requirements

Pathologists must confirm the presence of tumor cells in a sample before mutation analysis. The percentage and quality of tumor cells are crucial for proper mutation testing. For example, direct sequencing requires at least 20% tumor cells in the sample for reliable testing result. Thus, evaluation of the percentage of tumor cells (tumor purity) in a given sample is highly recommended, especially for less sensitive methods. Tumor dissection may be used to increase the tumor content if required. Thus, as

noted, the minimum number or percentage of cancer cells required for adequate testing depends on the analytic sensitivity of the testing method.

### Reporting

Mutation testing reports should contain identification of the patient (pathology number, hospital unit number, age, and gender), requesting physician with department, receipt day, report day, sample used for the testing (site or organ, sample type, and tumor purity), methodology used, exons tested, test results, comments on results, and names of the testing technician and corresponding pathologist.<sup>2</sup>

### Validation of a test

Analytical and clinical validation should be done when the testing is implemented in the laboratory. One of the references is indexes of evaluation from the Korean Institute of Genomic Testing Evaluation.

Repeat examination can be considered in cases of poor sequencing data, results not matching previously well-defined clinical features or a unique histological subtype, or concurrent detection of mutually exclusive driver mutations. Other types of methods may be useful in equivocal cases.

### Quality assurance

For optimal mutation testing, the quality of a sample and validation status of the testing method are crucial. Laboratories must incorporate mutation testing methods into their overall laboratory quality improvement program, by establishing appropriate quality improvement monitors as needed to ensure consistent performance at all steps of the testing and reporting processes. In particular, laboratories should participate in a formal proficiency testing program, if available, or an alternative proficiency assurance activity. There is an external quality control program for mutation testing from the Korean Institute of Genomic Testing Evaluation and the Korean Society of Pathologists. To improve the reliability of assays in terms of detection of mutations, a regular quality control program should be implemented, such as examination of reference materials or comparison of the results between different diagnostic assays.

## Gene rearrangements including *ALK*, *ROS1*, *RET*, *NTRK1*, *NRG1*, and *FGFR*

### Background

Since the discovery of a transforming fusion gene between

echinoderm microtubule-associated protein-like 4 (*EML4*) and *ALK* in 2007, the list of targetable gene fusions in lung cancer has been growing.<sup>54,55</sup> Although the prevalence of each gene fusion is low (approximately 1%–5%), molecularly tailored treatments have resulted in dramatic clinical responses. The presence of an *ALK* rearrangement and *ROS1* proto-oncogene receptor tyrosine kinase (*ROS1*) rearrangement in lung cancer has become the best predictor of response to crizotinib.<sup>56,57</sup> Subsequently, *RET* proto-oncogene (*RET*) fusions were found comprising 1% of lung adenocarcinomas.<sup>58,59</sup> Cabozantinib or vandetanib showed clinical activity against lung cancer harboring *RET* fusions.<sup>60,61</sup> Besides *ALK*, *ROS1*, and *RET* fusions, *NTRK1* and fibroblast growth factor receptor (*FGFR*) 1/3 fusions were reported in lung cancer, which are expected to give a therapeutic opportunity to patients with no known driver alterations.<sup>62,63</sup> Of note, *NRG1* fusions were predominantly found in invasive mucinous adenocarcinoma, which is a unique variant of lung adenocarcinoma.<sup>22,64</sup>

### Indications

Clinical characteristics associated with gene fusions such as *ALK*, *ROS1*, *RET*, and *NTRK1* are adenocarcinoma histological features, never- or light-smoking history, and younger age. Nevertheless, not all gene fusions have these characteristics. *FGFR* fusions are associated with smoking history.<sup>65</sup> Therefore, clinical characteristics alone cannot determine gene rearrangement testing.

Histological type is an important factor in determining whether to perform genetic analysis or which genes to test.<sup>36</sup> Most targetable gene fusions are discovered in NSCLCs. Because *ALK*, *ROS1*, and *RET* fusions are predominantly found in adenocarcinomas or NSCLCs with an adenocarcinoma component, pathologists should try to further classify NSCLCs into more specific subtypes. On the other hand, *FGFR* fusions can be found in adenocarcinomas and SQCs.<sup>63,65</sup>

### Methodology

#### Methods

Several methods are currently available for assessing gene rearrangement, including fluorescence *in situ* hybridization (FISH), immunohistochemistry (IHC), reverse-transcriptase polymerase chain reaction (RT-PCR), and NGS (Table 2).

Break apart FISH is the currently standard method for the detection of gene rearrangements. Although the FISH assay requires technical expertise and experience for interpretation, this assay is reasonably sensitive and specific for the detection of

gene rearrangements regardless of fusion partners. The pathologist should recognize the probe design, especially which sides are labeled with a red and green signal and the positive criteria. Crizotinib, a first generation ALK inhibitor, was approved by the United States FDA in conjunction with a companion diagnostic FISH test (ALK Break Apart FISH Probe Kit, Abbott Molecular Inc.). Positive criteria for the Abbott FISH probe kit are as follows. Positive signals are defined as separate signals or a single red signal. Initially, 50 tumor cells are counted. A sample is considered positive if > 25 cells out of 50 (> 25/50 or > 50%) test positive. A sample is considered equivocal if 5 to 25 cells (10 to 50%) test positive. If the sample is equivocal, a second reader should evaluate the slide. The first and second cell count readings are added up, and a percentage is calculated out of 100 cells. If the percentage of positive cells is  $\geq 15\%$  ( $\geq 15/100$ ), the sample is considered positive. The Korean FDA also approved the ALK FISH as a selection test for crizotinib treatment in lung cancer patients.

Because protein expression can serve as a surrogate marker of gene rearrangements, IHC is useful for screening of gene rearrangements when it is appropriately validated.<sup>3,66-68</sup> In particular, ALK IHC was extensively studied and validated.<sup>3</sup> Among ALK IHC antibodies, 5A4 and D5F3 appear to be superior to the ALK1 antibody for detecting *ALK*-rearranged lung cancer.<sup>69,70</sup> IHC can effectively predict *ALK* fusion status because lung adenocarcinoma in general does not express the ALK protein without genetic alterations. The VENTANA ALK (D5F3) CDx Assay was approved by the U.S. FDA for identification of patients eligible for treatment with crizotinib. Other antibodies are not validated as companion diagnostics; therefore, their use should be limited to a screening step within controlled settings.

Besides *ALK*, there are no approved companion diagnostics for other gene rearrangements. Break apart FISH is generally used to detect gene arrangements in clinical samples, and IHC can serve as a screening method.

In terms of mRNA expression, the RT-PCR assay is used to find fusion transcripts with unique sequences. RT-PCR methods are generally known to be sensitive.<sup>71</sup> Nonetheless, RT-PCR has some limitations in clinical practice. Primer design requires information about fusion partners and breakpoints. Thus, only known fusion variants can be detected. In addition, most materials for molecular testing are FFPE samples, where RNAs can be severely degraded compared to fresh frozen tissue. Nevertheless, RT-PCR can be useful when only cytology samples are available.<sup>71</sup>

The NGS technology has emerged as an alternative to the

detection of gene rearrangements. It can simultaneously detect a variety of gene fusions using targeted DNA sequencing or RNA sequencing.<sup>43,44</sup> The sensitivity and specificity for calling a gene fusion mainly depend on the detection algorithm. The NGS-based gene rearrangement method should be vigorously validated before implementation in routine practice. Furthermore, to become a companion diagnostic test, an NGS-based method should be comparatively validated with previous companion diagnostics.

#### Sample type

A variety of biopsy specimens can be used for gene rearrangement testing as described above in the section on mutation testing. Previous studies have shown that cytology samples are suitable for gene rearrangement analysis, especially as validated in *ALK* fusion testing.<sup>72</sup> The cell block is usually first used if there are enough tumor cells in the block. Smear slides can also be used for the detection of gene rearrangement.<sup>72</sup> Thus, both tissue and cytology samples are acceptable for gene rearrangement testing, if appropriately validated. Details were described in the previous guideline.<sup>3</sup>

#### Sample requirements

For adequate evaluation of break apart FISH, a minimum of 50 to 100 well-preserved tumor cells are required. Tumor purity is not as critical for FISH tests, however, it is necessary to choose areas of a slide in which the viable tumor cells are most abundant. Because a dark-field fluorescence microscope does not provide perfect visualization of tumor morphology, the pathologist should determine whether the selected area contains a sufficient number of tumor cells and should interpret the result carefully by distinguishing between cancer cells and intimately mixed non-neoplastic cells.

As for RT-PCR and NGS technologies, the tumor percentage can be critical in gene rearrangement testing as described in mutation testing. The pathologist should verify the quality of the sample and the presence of tumor cells. Tumor dissection may be used to increase the tumor content if required.

#### Reporting

Reports on gene rearrangement testing should contain identification of the patient (pathology number, hospital unit number, age, and gender), requesting physician with department, receipt day, report day, sample used for the testing (site or organ, sample type, and tumor purity), methodology used, detectable fusion variants, test results (negativity or positivity for the gene

rearrangement), comments on results, and names of the testing technician and corresponding pathologist. We recommend reporting the additional details in the case of a FISH test: information on probe design, total number of counted nuclei, and percentage of the tumor nuclei showing positive signals (split signal or isolated signal containing a kinase domain).<sup>5</sup>

#### Validation of the test

General principles are similar to those of mutation testing. Technical and clinical validation procedures should be carried out when the testing is set up in the laboratory. One of the references is indexes of the evaluation from the Korean Institute of Genomic Testing Evaluation.

Pathologists should recognize the limitations of each methodology. With respect to the break apart FISH test, repeat examination can be considered in cases of poor signals, atypical signal patterns (including predominantly isolated 5' signals), a borderline range that approached the 15% cutoff line, results not matching well-validated IHC, or concurrent detection of driver mutations. Other types of methods may be useful in equivocal cases.

#### Quality assurance

There is an external quality control program for *ALK* fusion testing from the Korean Institute of Genomic Testing Evaluation and the Korean Society of Pathologists. To improve the reliability of assays for detecting gene rearrangements, a regular quality control program should be performed, and the results of molecular testing can be confirmed by different diagnostic assays, such as validated IHC.

### Amplifications including *FGFR1*, *EGFR*, *MET*, and *HER2*

#### Background

Gene amplification is an important mechanism for oncogene activation. *HER2*-targeting therapy has been implemented in breast and gastric cancer on the basis of molecular testing for *HER2*. Amplifications of several genes have been studied in lung cancer.

*FGFR1* is one of the most commonly amplified genes in human cancers. Amplified *FGFR1* has been described in 13%–22% of lung SQCs.<sup>73,74</sup> It is expected to become a promising targetable alteration in lung SQCs because there are no known targeted therapeutic agents for SQCs.<sup>73</sup> *In vivo* studies have revealed that inhibition of the *FGFR1* pathway with *FGFR* inhibitors leads to significant tumor shrinkage, suggesting that *FGFR* inhibitors might be an effective therapeutic option in

SQCs with *FGFR1* amplification.<sup>75</sup> Nevertheless, clinical trials of *FGFR* inhibitors were not impressive.<sup>76</sup> Additional biomarkers should be studied to predict the drug response to *FGFR* inhibitors.<sup>77</sup> A study showed that homogeneous high-level amplification was associated more strongly with a clinical response to *FGFR* inhibition.<sup>78</sup> Thus, *FGFR1* amplification can still be a promising candidate for targeted therapy.

*EGFR* amplifications were found in adenocarcinomas and SQCs. Initially, *EGFR* amplification was regarded as a predictive biomarker of *EGFR* TKI treatment.<sup>79</sup> Subsequent studies revealed that *EGFR* amplification was closely related to *EGFR* mutation, and *EGFR* mutation was the strongest predictive marker of the response to *EGFR* TKIs.<sup>7,80</sup> Among SQCs, *EGFR* high copy number gains/amplifications were present in 8%–9% of cases.<sup>4,81</sup> Patients with lung SQC harboring an *EGFR* high copy number gains or amplifications showed a higher response rate to *EGFR* TKI.<sup>81</sup>

*De novo MET* amplification was present in 2%–4% of lung adenocarcinomas.<sup>5,82</sup> NSCLC patients with *de novo MET* amplification showed a rapid and durable response to crizotinib.<sup>83,84</sup> *MET* amplification was also identified as one of the acquired secondary resistance mechanisms in patients with *EGFR* mutations who progressed on *EGFR* TKIs.<sup>12,13</sup>

*De novo HER2* amplification was found to be present in 1%–2% of lung adenocarcinomas.<sup>5</sup> NSCLC patients with *de novo HER2* amplification can be treated with *HER2*-targeting agents.<sup>85</sup> *HER2* amplification was also identified as one of the acquired secondary resistance mechanisms in patients with *EGFR* mutations who progress on *EGFR* TKIs.<sup>18,86</sup>

#### Indications

Amplifications of receptor tyrosine kinase genes are present in lung cancers regardless of histological subtypes, while the frequencies are different. Thus, these gene amplifications can be examined in patients with lung cancer, especially previously targetable oncogene-negative cases. *FGFR1* amplification is especially meaningful for SQCs.

*EGFR* amplification can serve as a predictive marker of SQCs. *MET* and *HER2* amplification can be examined in the primary tumors or tumors with acquired resistance to TKIs.

#### Methodology

##### Method

Several methods can be used for detection of gene amplifications (Table 2). FISH using a locus-specific intensifier (LSI) gene

and a chromosome-specific centromere (CEP) probe is a standard method for the detection of gene amplifications. Although the FISH assay requires technical expertise and experience for interpretation, this method has the advantage of being able to evaluate gene amplification by selecting only cancer cells.

FISH-positive criteria have been used according to the corresponding genes. *FGFR1* high-level amplification is defined as copy number  $\geq 9$  or (1) an *FGFR1/CEP8* ratio of  $\geq 2.0$ , (2) the average number of *FGFR1* signals per tumor cell nucleus  $\geq 6$ , and (3) the percentage of tumor cells containing  $\geq 15$  *FGFR1* signals or large clusters  $\geq 10\%$ .<sup>74,87</sup> According to previously published criteria, the *EGFR* gene copy number was classified into six FISH strata: disomy (two or fewer copies in more than 90% of cells), low trisomy (two or fewer copies in 40% or more of the cells, three copies in 10%–40% of cells, and four or more copies in less than 10% of cells), high trisomy (two or fewer copies in  $\geq 40\%$  of cells, three copies in  $\geq 40\%$  of cells, and four or more copies in less than 10% of cells), low polysomy (four or more copies in 10%–40% of cells), high polysomy (four or more copies in 40% of the cells or more), and gene amplification (defined by the presence of tight *EGFR* clusters and a ratio of *EGFR* to the chromosome of  $\geq 2.0$ , or  $\geq 15$  copies of *EGFR* per cell in  $\geq 10\%$  of the cells analyzed).<sup>79</sup> Regarding *MET*, FISH-positive groups include (1) high-level amplification (presence of loose or tight clusters of *MET* signals too numerous to count) or a *MET/CEP7* ratio greater than 5.0 and (2) low-level amplification (tumors with the *MET/CEP7* ratio  $\geq 2.2$  and  $\leq 5.0$ ).<sup>83</sup> As for *HER2*, gene amplification can be defined as positive when the *HER2/CEP17* ratio is  $\geq 2.0$  or average *HER2* copy number is  $\geq 6.0$  signals/cell based on the American Society of Clinical Oncology/College of American Pathologists (ASCO/CAP) guidelines for dual-probe *in situ* hybridization.<sup>88</sup>

In clinical practice, for many years FISH has been the most widely used method for gene copy number assessment. Silver *in situ* hybridization (SISH) is a new technology with some clinical advantages over FISH. Examination can be made using conventional light microscopy with preserved tissue architecture. In addition, the slides are durable and can be reviewed several years after staining. Thus, the SISH technique can be more practically applied in routine diagnostic procedures.<sup>89</sup>

Quantitative real-time PCR can be used to detect gene amplification.<sup>90</sup> In this case, the optimal cutoff threshold of amplification should be determined considering clinical relevance and a response to targeted therapeutic agents.

The NGS technology can simultaneously detect a variety of genes with a copy number gain using DNA sequencing.<sup>45</sup> None-

theless, currently, the NGS algorithm for determination of a copy number gain in heterogeneous tumor tissue is not well established. The established guideline is based on a specific gene copy number, but the NGS technology cannot determine the specific gene number in given cancer cells. The reliability of testing results also depends on the tumor cell percentage and the degree of gene amplification. Before clinical implementation, thorough verification is required.

#### Sample type

Various biopsy samples can be used for amplification testing as in other molecular testing methods described above. Samples routinely consist of FFPE tissues. Tumor tissues from either primary tumors or metastatic lesions can be equally available for molecular testing especially regarding high-level homogeneous amplification.<sup>91</sup> Cytology samples can be used with quantitative real-time PCR or NGS.

#### Sample requirements

Regarding the *in situ* hybridization method, a minimum of 50 to 100 tumor cells are required. General principles are similar to those described above in the section on break apart FISH testing.

#### Reporting

Reports on gene amplification testing should contain identification of the patient (pathology number, hospital unit number, age, and gender), requesting physician with department, receipt day, report day, sample used for the testing (site or organ, sample type, and tumor purity), methodology used, test results (negativity or positivity for the gene amplification according to proposed criteria), comments on results, and names of the testing technician and corresponding pathologist. Additional information can be included in the case of *in situ* hybridization: the total number of counted nuclei, gene/CEP ratio, average copy number, or findings according to special diagnostic criteria.

#### Validation of a test

Analytical and clinical validation procedures should be conducted when the testing is set up in the laboratory. One of the references is indexes of evaluation from the Korean Institute of Genomic Testing Evaluation. General principles are similar to the ASCO/CAP guidelines for dual-probe *in situ* hybridization.<sup>88</sup>

#### Quality assurance

There is an external quality control program for FISH/SISH testing (for example, *HER2* amplification) from the Korean In-

**Table 3.** A summary of recommendations for molecular testing of lung cancer

	Recommendation
Indications	Mutations Do: adenocarcinoma, large cell carcinoma, NSCLC-NOS Consider: at a young age, never smokers or small biopsy samples or mixed histological features All types if clinically indicated
	Gene rearrangements Do: adenocarcinoma, large cell carcinoma, NSCLC-NOS for most gene fusions Consider: at a young age, never smokers or small biopsy samples or mixed histological features Squamous cell carcinoma for <i>FGFR</i> fusions All types if clinically indicated
	Amplifications All types if clinically indicated Squamous cell carcinoma for <i>FGFR1</i> amplification Adenocarcinoma, NSCLC-NOS for <i>MET</i> or <i>HER2</i> amplifications
Method	An appropriate method should be selected according to genetic alterations. The pathologist should consider the pros and cons of each method.
Type of specimen	Histological and cytological samples are both acceptable. Either a primary tumor or a metastatic lesion is equally suitable. In cases of multiple, synchronous primary lung adenocarcinomas, each tumor may be tested.
Specimen requirements	The presence of tumor cells must be verified by a pathologist. High percentage (ideally more than 50%) of tumor cells for direct sequencing Lower percentage acceptable for methods with higher sensitivity A minimum of 50–100 assessable tumor cells are required for a FISH assay.
Reporting	Patients and sample information, material used for analysis, type of method, results of the test, comments, names of the testing technician and corresponding pathologist
Validation of test	New methods must be approved by the Korean government. Analytical and clinical validation procedures should be conducted when the testing is set up in the laboratory. A combination of more than one method may be useful in equivocal cases.
Quality assurance	Quality assurance program (internal or external quality control) should be implemented.

NSCLC-NOS, non-small cell lung carcinoma not otherwise specified; FGFR, fibroblast growth factor receptor; FISH, fluorescence *in situ* hybridization.

stitute of Genomic Testing Evaluation and the Korean Society of Pathologists. To improve the reliability of assays for detection of gene amplification, a regular quality control program should be implemented, and the results of molecular testing can be confirmed by different diagnostic assays, such as validated IHC for protein overexpression.

## CONCLUSION

We proposed guideline recommendations for molecular testing according to three categories of genetic alterations in lung cancer (summarized in Table 3). Molecular diagnostics for targetable genetic alterations have become the standard of care in the management of lung cancer patients (Fig. 2). In addition, immunotherapy has emerged as a new therapeutic option for patients who do not have targetable alterations (Fig. 2). Both therapeutic approaches require pathological diagnosis based on molecular biomarker assessment. Therefore, pathologists should carefully manage clinical samples for molecular testing and should do their best to quickly and accurately identify patients who will benefit from precision therapeutics. Each pathology department should fully validate the detection methods and should also

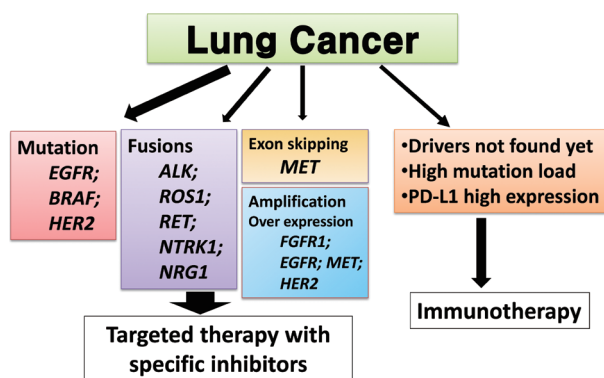


**Fig. 2.** The current therapeutic approach to patients with lung cancer. EGFR, epidermal growth factor receptor; ALK, anaplastic lymphoma kinase; FGFR1, fibroblast growth factor receptor 1; PD-L1, programmed death-ligand 1.

participate in a quality control and formal proficiency testing program.

## Conflicts of Interest

No potential conflict of interest relevant to this article was reported.

## Acknowledgments

This research was supported by The Korean Society of Pathologists Grant (2016).

## REFERENCES

- Li T, Kung HJ, Mack PC, Gandara DR. Genotyping and genomic profiling of non-small-cell lung cancer: implications for current and future therapies. *J Clin Oncol* 2013; 31: 1039-49.
- Shim HS, Chung JH, Kim L, *et al.* Guideline recommendations for *EGFR* mutation testing in lung cancer: proposal of the Korean Cardiopulmonary Pathology Study Group. *Korean J Pathol* 2013; 47: 100-6.
- Kim H, Shim HS, Kim L, *et al.* Guideline recommendations for testing of *ALK* gene rearrangement in lung cancer: a proposal of the Korean Cardiopulmonary Pathology Study Group. *Korean J Pathol* 2014; 48: 1-9.
- Cancer Genome Atlas Research Network. Comprehensive genomic characterization of squamous cell lung cancers. *Nature* 2012; 489: 519-25.
- Cancer Genome Atlas Research Network. Comprehensive molecular profiling of lung adenocarcinoma. *Nature* 2014; 511: 543-50.
- George J, Lim JS, Jang SJ, *et al.* Comprehensive genomic profiles of small cell lung cancer. *Nature* 2015; 524: 47-53.
- Mok TS, Wu YL, Thongprasert S, *et al.* Gefitinib or carboplatin-paclitaxel in pulmonary adenocarcinoma. *N Engl J Med* 2009; 361: 947-57.
- Maemondo M, Inoue A, Kobayashi K, *et al.* Gefitinib or chemotherapy for non-small-cell lung cancer with mutated *EGFR*. *N Engl J Med* 2010; 362: 2380-8.
- Yatabe Y, Kerr KM, Utomo A, *et al.* *EGFR* mutation testing practices within the Asia Pacific region: results of a multicenter diagnostic survey. *J Thorac Oncol* 2015; 10: 438-45.
- Lee SH, Kim WS, Choi YD, *et al.* Analysis of mutations in epidermal growth factor receptor gene in Korean patients with non-small cell lung cancer: summary of a nationwide survey. *J Pathol Transl Med* 2015; 49: 481-8.
- Lee B, Lee T, Lee SH, Choi YL, Han J. Clinicopathologic characteristics of *EGFR*, *KRAS*, and *ALK* alterations in 6,595 lung cancers. *Oncotarget* 2016; 7: 23874-84.
- Sequist LV, Waltman BA, Dias-Santagata D, *et al.* Genotypic and histological evolution of lung cancers acquiring resistance to *EGFR* inhibitors. *Sci Transl Med* 2011; 3: 75ra26.
- Yu HA, Arcila ME, Rekhtman N, *et al.* Analysis of tumor specimens at the time of acquired resistance to *EGFR*-TKI therapy in 155 patients with *EGFR*-mutant lung cancers. *Clin Cancer Res* 2013; 19: 2240-7.
- Camidge DR, Pao W, Sequist LV. Acquired resistance to TKIs in solid tumours: learning from lung cancer. *Nat Rev Clin Oncol* 2014; 11: 473-81.
- Arcila ME, Oxnard GR, Nafa K, *et al.* Rebiopsy of lung cancer patients with acquired resistance to *EGFR* inhibitors and enhanced detection of the T790M mutation using a locked nucleic acid-based assay. *Clin Cancer Res* 2011; 17: 1169-80.
- Jänne PA, Yang JC, Kim DW, *et al.* AZD9291 in *EGFR* inhibitor-resistant non-small-cell lung cancer. *N Engl J Med* 2015; 372: 1689-99.
- Thress KS, Paweletz CP, Felip E, *et al.* Acquired *EGFR* C797S mutation mediates resistance to AZD9291 in non-small cell lung cancer harboring *EGFR* T790M. *Nat Med* 2015; 21: 560-2.
- Planchard D, Loriot Y, André F, *et al.* *EGFR*-independent mechanisms of acquired resistance to AZD9291 in *EGFR* T790M-positive NSCLC patients. *Ann Oncol* 2015; 26: 2073-8.
- Lee B, Lee B, Han G, Kwon MJ, Han J, Choi YL. *KRAS* mutation detection in non-small cell lung cancer using a peptide nucleic acid-mediated polymerase chain reaction clamping method and comparative validation with next-generation sequencing. *Korean J Pathol* 2014; 48: 100-7.
- Kim HR, Ahn JR, Lee JG, *et al.* The impact of cigarette smoking on the frequency of and qualitative differences in *KRAS* mutations in Korean patients with lung adenocarcinoma. *Yonsei Med J* 2013; 54: 865-74.
- Wood K, Hensing T, Malik R, Salgia R. Prognostic and predictive value in *KRAS* in non-small-cell lung cancer: a review. *JAMA Oncol* 2016; 2: 805-12.
- Shim HS, Kenudson M, Zheng Z, *et al.* Unique genetic and survival characteristics of invasive mucinous adenocarcinoma of the lung. *J Thorac Oncol* 2015; 10: 1156-62.
- Marchetti A, Felicioni L, Malatesta S, *et al.* Clinical features and outcome of patients with non-small-cell lung cancer harboring *BRAF* mutations. *J Clin Oncol* 2011; 29: 3574-9.
- Paik PK, Arcila ME, Fara M, *et al.* Clinical characteristics of patients with lung adenocarcinomas harboring *BRAF* mutations. *J Clin Oncol* 2011; 29: 2046-51.
- Ha SY, Choi SJ, Cho JH, *et al.* Lung cancer in never-smoker Asian females is driven by oncogenic mutations, most often involving *EGFR*. *Oncotarget* 2015; 6: 5465-74.
- Planchard D, Besse B, Groen HJ, *et al.* Dabrafenib plus trametinib in patients with previously treated *BRAF*(V600E)-mutant metastatic non-small cell lung cancer: an open-label, multicentre phase 2 trial. *Lancet Oncol* 2016; 17: 984-93.
- Planchard D, Kim TM, Mazieres J, *et al.* Dabrafenib in patients with *BRAF*(V600E)-positive advanced non-small-cell lung cancer: a sin-

- gle-arm, multicentre, open-label, phase 2 trial. *Lancet Oncol* 2016; 17: 642-50.
28. Hyman DM, Puzanov I, Subbiah V, *et al.* Vemurafenib in multiple nonmelanoma cancers with *BRAF* V600 mutations. *N Engl J Med* 2015; 373: 726-36.
  29. Mazieres J, Peters S, Lepage B, *et al.* Lung cancer that harbors an *HER2* mutation: epidemiologic characteristics and therapeutic perspectives. *J Clin Oncol* 2013; 31: 1997-2003.
  30. Paik PK, Drilon A, Fan PD, *et al.* Response to MET inhibitors in patients with stage IV lung adenocarcinomas harboring *MET* mutations causing exon 14 skipping. *Cancer Discov* 2015; 5: 842-9.
  31. Awad MM, Oxnard GR, Jackman DM, *et al.* *MET* exon 14 mutations in non-small-cell lung cancer are associated with advanced age and stage-dependent MET genomic amplification and c-Met overexpression. *J Clin Oncol* 2016; 34: 721-30.
  32. D'Angelo SP, Pietanza MC, Johnson ML, *et al.* Incidence of *EGFR* exon 19 deletions and L858R in tumor specimens from men and cigarette smokers with lung adenocarcinomas. *J Clin Oncol* 2011; 29: 2066-70.
  33. Sun PL, Seol H, Lee HJ, *et al.* High incidence of *EGFR* mutations in Korean men smokers with no intratumoral heterogeneity of lung adenocarcinomas: correlation with histologic subtypes, *EGFR*/*TTF-1* expressions, and clinical features. *J Thorac Oncol* 2012; 7: 323-30.
  34. Pirker R, Herth FJ, Kerr KM, *et al.* Consensus for *EGFR* mutation testing in non-small cell lung cancer: results from a European workshop. *J Thorac Oncol* 2010; 5: 1706-13.
  35. Travis WD, Brambilla E, Noguchi M, *et al.* International Association for the Study of Lung Cancer/American Thoracic Society/European Respiratory Society international multidisciplinary classification of lung adenocarcinoma. *J Thorac Oncol* 2011; 6: 244-85.
  36. Lindeman NI, Cagle PT, Beasley MB, *et al.* Molecular testing guideline for selection of lung cancer patients for *EGFR* and *ALK* tyrosine kinase inhibitors: guideline from the College of American Pathologists, International Association for the Study of Lung Cancer, and Association for Molecular Pathology. *J Thorac Oncol* 2013; 8: 823-59.
  37. Noh S, Shim H. Optimal combination of immunohistochemical markers for subclassification of non-small cell lung carcinomas: a tissue microarray study of poorly differentiated areas. *Lung Cancer* 2012; 76: 51-5.
  38. Pao W, Ladanyi M. Epidermal growth factor receptor mutation testing in lung cancer: searching for the ideal method. *Clin Cancer Res* 2007; 13: 4954-5.
  39. Lee HJ, Xu X, Kim H, *et al.* Comparison of direct sequencing, PNA clamping-real time polymerase chain reaction, and pyrosequencing methods for the detection of *EGFR* mutations in non-small cell lung carcinoma and the correlation with clinical responses to *EGFR* tyrosine kinase inhibitor treatment. *Korean J Pathol* 2013; 47: 52-60.
  40. Kim HJ, Lee KY, Kim YC, *et al.* Detection and comparison of peptide nucleic acid-mediated real-time polymerase chain reaction clamping and direct gene sequencing for epidermal growth factor receptor mutations in patients with non-small cell lung cancer. *Lung Cancer* 2012; 75: 321-5.
  41. Han HS, Lim SN, An JY, *et al.* Detection of *EGFR* mutation status in lung adenocarcinoma specimens with different proportions of tumor cells using two methods of differential sensitivity. *J Thorac Oncol* 2012; 7: 355-64.
  42. Frampton GM, Ali SM, Rosenzweig M, *et al.* Activation of *MET* via diverse exon 14 splicing alterations occurs in multiple tumor types and confers clinical sensitivity to *MET* inhibitors. *Cancer Discov* 2015; 5: 850-9.
  43. Frampton GM, Fichtenholtz A, Otto GA, *et al.* Development and validation of a clinical cancer genomic profiling test based on massively parallel DNA sequencing. *Nat Biotechnol* 2013; 31: 1023-31.
  44. Zheng Z, Liebers M, Zhelyazkova B, *et al.* Anchored multiplex PCR for targeted next-generation sequencing. *Nat Med* 2014; 20: 1479-84.
  45. Rekhtman N, Brandt SM, Sigel CS, *et al.* Suitability of thoracic cytology for new therapeutic paradigms in non-small cell lung carcinoma: high accuracy of tumor subtyping and feasibility of *EGFR* and *KRAS* molecular testing. *J Thorac Oncol* 2011; 6: 451-8.
  46. Navani N, Brown JM, Nankivell M, *et al.* Suitability of endobronchial ultrasound-guided transbronchial needle aspiration specimens for subtyping and genotyping of non-small cell lung cancer: a multicenter study of 774 patients. *Am J Respir Crit Care Med* 2012; 185: 1316-22.
  47. Sun PL, Jin Y, Kim H, Lee CT, Jheon S, Chung JH. High concordance of *EGFR* mutation status between histologic and corresponding cytologic specimens of lung adenocarcinomas. *Cancer Cytopathol* 2013; 121: 311-9.
  48. Yatabe Y, Matsuo K, Mitsudomi T. Heterogeneous distribution of *EGFR* mutations is extremely rare in lung adenocarcinoma. *J Clin Oncol* 2011; 29: 2972-7.
  49. Chung JH, Choe G, Jheon S, *et al.* Epidermal growth factor receptor mutation and pathologic-radiologic correlation between multiple lung nodules with ground-glass opacity differentiates multicentric origin from intrapulmonary spread. *J Thorac Oncol* 2009; 4: 1490-5.
  50. Eberhard DA, Giaccone G, Johnson BE; Non-Small-Cell Lung Cancer Working Group. Biomarkers of response to epidermal growth factor receptor inhibitors in Non-Small-Cell Lung Cancer Working Group: standardization for use in the clinical trial setting. *J Clin Oncol* 2008; 26: 983-94.
  51. Nicholson AG, Gonzalez D, Shah P, *et al.* Refining the diagnosis

- and EGFR status of non-small cell lung carcinoma in biopsy and cytologic material, using a panel of mucin staining, TTF-1, cytokeratin 5/6, and P63, and EGFR mutation analysis. *J Thorac Oncol* 2010; 5: 436-41.
52. Sacher AG, Paweletz C, Dahlberg SE, *et al.* Prospective validation of rapid plasma genotyping for the detection of *EGFR* and *KRAS* mutations in advanced lung cancer. *JAMA Oncol* 2016; 2: 1014-22.
  53. Oxnard GR, Thress KS, Alden RS, *et al.* Association between plasma genotyping and outcomes of treatment with osimertinib (AZD9291) in advanced non-small-cell lung cancer. *J Clin Oncol* 2016; 34: 3375-82.
  54. Shaw AT, Hsu PP, Awad MM, Engelman JA. Tyrosine kinase gene rearrangements in epithelial malignancies. *Nat Rev Cancer* 2013; 13: 772-87.
  55. Stransky N, Cerami E, Schalm S, Kim JL, Lengauer C. The landscape of kinase fusions in cancer. *Nat Commun* 2014; 5: 4846.
  56. Solomon BJ, Mok T, Kim DW, *et al.* First-line crizotinib versus chemotherapy in ALK-positive lung cancer. *N Engl J Med* 2014; 371: 2167-77.
  57. Shaw AT, Ou SH, Bang YJ, *et al.* Crizotinib in *ROS1*-rearranged non-small-cell lung cancer. *N Engl J Med* 2014; 371: 1963-71.
  58. Kohno T, Ichikawa H, Totoki Y, *et al.* *KIF5B-RET* fusions in lung adenocarcinoma. *Nat Med* 2012; 18: 375-7.
  59. Wang R, Hu H, Pan Y, *et al.* *RET* fusions define a unique molecular and clinicopathologic subtype of non-small-cell lung cancer. *J Clin Oncol* 2012; 30: 4352-9.
  60. Drilon A, Wang L, Hasanovic A, *et al.* Response to cabozantinib in patients with *RET* fusion-positive lung adenocarcinomas. *Cancer Discov* 2013; 3: 630-5.
  61. Yoh K, Seto T, Satouchi M, *et al.* Vandetanib in patients with previously treated *RET*-rearranged advanced non-small-cell lung cancer (LURET): an open-label, multicentre phase 2 trial. *Lancet Respir Med* 2017; 5: 42-50.
  62. Vaishnavi A, Capelletti M, Le AT, *et al.* Oncogenic and drug-sensitive *NTRK1* rearrangements in lung cancer. *Nat Med* 2013; 19: 1469-72.
  63. Wang R, Wang L, Li Y, *et al.* *FGFR1/3* tyrosine kinase fusions define a unique molecular subtype of non-small cell lung cancer. *Clin Cancer Res* 2014; 20: 4107-14.
  64. Nakaoku T, Tsuta K, Ichikawa H, *et al.* Druggable oncogene fusions in invasive mucinous lung adenocarcinoma. *Clin Cancer Res* 2014; 20: 3087-93.
  65. Wu YM, Su F, Kalyana-Sundaram S, *et al.* Identification of targetable *FGFR* gene fusions in diverse cancers. *Cancer Discov* 2013; 3: 636-47.
  66. Paik JH, Choe G, Kim H, *et al.* Screening of anaplastic lymphoma kinase rearrangement by immunohistochemistry in non-small cell lung cancer: correlation with fluorescence *in situ* hybridization. *J Thorac Oncol* 2011; 6: 466-72.
  67. Cha YJ, Lee JS, Kim HR, *et al.* Screening of *ROS1* rearrangements in lung adenocarcinoma by immunohistochemistry and comparison with *ALK* rearrangements. *PLoS One* 2014; 9: e103333.
  68. Lee SE, Lee B, Hong M, *et al.* Comprehensive analysis of *RET* and *ROS1* rearrangement in lung adenocarcinoma. *Mod Pathol* 2015; 28: 468-79.
  69. Mino-Kenudson M, Chirieac LR, Law K, *et al.* A novel, highly sensitive antibody allows for the routine detection of *ALK*-rearranged lung adenocarcinomas by standard immunohistochemistry. *Clin Cancer Res* 2010; 16: 1561-71.
  70. Conklin CM, Craddock KJ, Have C, Laskin J, Couture C, Ionescu DN. Immunohistochemistry is a reliable screening tool for identification of *ALK* rearrangement in non-small-cell lung carcinoma and is antibody dependent. *J Thorac Oncol* 2013; 8: 45-51.
  71. Soda M, Isoke K, Inoue A, *et al.* A prospective PCR-based screening for the *EML4-ALK* oncogene in non-small cell lung cancer. *Clin Cancer Res* 2012; 18: 5682-9.
  72. Betz BL, Dixon CA, Weigelin HC, Knoepp SM, Roh MH. The use of stained cytologic direct smears for *ALK* gene rearrangement analysis of lung adenocarcinoma. *Cancer Cytopathol* 2013; 121: 489-99.
  73. Weiss J, Sos ML, Seidel D, *et al.* Frequent and focal *FGFR1* amplification associates with therapeutically tractable *FGFR1* dependency in squamous cell lung cancer. *Sci Transl Med* 2010; 2: 62ra93.
  74. Kim HR, Kim DJ, Kang DR, *et al.* Fibroblast growth factor receptor 1 gene amplification is associated with poor survival and cigarette smoking dosage in patients with resected squamous cell lung cancer. *J Clin Oncol* 2013; 31: 731-7.
  75. Dutt A, Ramos AH, Hammerman PS, *et al.* Inhibitor-sensitive *FGFR1* amplification in human non-small cell lung cancer. *PLoS One* 2011; 6: e20351.
  76. Lim SH, Sun JM, Choi YL, *et al.* Efficacy and safety of dovitinib in pretreated patients with advanced squamous non-small cell lung cancer with *FGFR1* amplification: a single-arm, phase 2 study. *Cancer* 2016; 122: 3024-31.
  77. Wynes MW, Hinz TK, Gao D, *et al.* *FGFR1* mRNA and protein expression, not gene copy number, predict *FGFR* TKI sensitivity across all lung cancer histologies. *Clin Cancer Res* 2014; 20: 3299-309.
  78. Pearson A, Smyth E, Babina IS, *et al.* High-level clonal *FGFR* amplification and response to *FGFR* inhibition in a translational clinical trial. *Cancer Discov* 2016; 6: 838-51.
  79. Cappuzzo F, Hirsch FR, Rossi E, *et al.* Epidermal growth factor receptor gene and protein and gefitinib sensitivity in non-small-cell lung cancer. *J Natl Cancer Inst* 2005; 97: 643-55.
  80. Soh J, Okumura N, Lockwood WW, *et al.* Oncogene mutations, copy number gains and mutant allele specific imbalance (MASI)

- frequently occur together in tumor cells. *PLoS One* 2009; 4: e7464.
81. Lee Y, Shim HS, Park MS, *et al.* High *EGFR* gene copy number and skin rash as predictive markers for *EGFR* tyrosine kinase inhibitors in patients with advanced squamous cell lung carcinoma. *Clin Cancer Res* 2012; 18: 1760-8.
  82. Schildhaus HU, Schultheis AM, Rüschoff J, *et al.* *MET* amplification status in therapy-naive adeno- and squamous cell carcinomas of the lung. *Clin Cancer Res* 2015; 21: 907-15.
  83. Ou SH, Kwak EL, Siwak-Tapp C, *et al.* Activity of crizotinib (PF02341066), a dual mesenchymal-epithelial transition (*MET*) and anaplastic lymphoma kinase (*ALK*) inhibitor, in a non-small cell lung cancer patient with *de novo MET* amplification. *J Thorac Oncol* 2011; 6: 942-6.
  84. Zhang Y, Wang W, Wang Y, *et al.* Response to crizotinib observed in lung adenocarcinoma with *MET* copy number gain but without a high-level *MET/CEP7* ratio, *MET* overexpression, orexon 14 splicing mutations. *J Thorac Oncol* 2016; 11: e59-62.
  85. Mar N, Vredenburg JJ, Wasser JS. Targeting *HER2* in the treatment of non-small cell lung cancer. *Lung Cancer* 2015; 87: 220-5.
  86. Takezawa K, Pirazzoli V, Arcila ME, *et al.* *HER2* amplification: a potential mechanism of acquired resistance to *EGFR* inhibition in *EGFR*-mutant lung cancers that lack the second-site *EGFR*T790M mutation. *Cancer Discov* 2012; 2: 922-33.
  87. Schildhaus HU, Heukamp LC, Merkelbach-Bruse S, *et al.* Definition of a fluorescence *in-situ* hybridization score identifies high- and low-level *FGFR1* amplification types in squamous cell lung cancer. *Mod Pathol* 2012; 25: 1473-80.
  88. Wolff AC, Hammond ME, Hicks DG, *et al.* Recommendations for human epidermal growth factor receptor 2 testing in breast cancer: American Society of Clinical Oncology/College of American Pathologists clinical practice guideline update. *J Clin Oncol* 2013; 31: 3997-4013.
  89. Dziadziuszko R, Wynes MW, Singh S, *et al.* Correlation between *MET* gene copy number by silver *in situ* hybridization and protein expression by immunohistochemistry in non-small cell lung cancer. *J Thorac Oncol* 2012; 7: 340-7.
  90. Gadgeel SM, Chen W, Cote ML, *et al.* Fibroblast growth factor receptor 1 amplification in non-small cell lung cancer by quantitative real-time PCR. *PLoS One* 2013; 8: e79820.
  91. Goke F, Franzen A, Menon R, *et al.* Rationale for treatment of metastatic squamous cell carcinoma of the lung using fibroblast growth factor receptor inhibitors. *Chest* 2012; 142: 1020-6.

# Clinicopathological Study of 18 Cases of Inflammatory Myofibroblastic Tumors with Reference to ALK-1 Expression: 5-Year Experience in a Tertiary Care Center

Ramesh Babu Telugu  
Anne Jennifer Prabhu  
Nobin Babu Kalappurayil  
John Mathai<sup>1</sup>  
Birla Roy Gnanamuthu<sup>2</sup>  
Marie Therese Manipadam

Departments of General Pathology, <sup>1</sup>Paediatric Surgery, and <sup>2</sup>Thoracic Surgery, Christian Medical College and Hospital, Vellore, India

Received: September 5, 2016  
Revised: January 2, 2017  
Accepted: January 12, 2017

## Corresponding Author

Ramesh Babu Telugu, MD  
Department of General Pathology, Christian Medical College and Hospital, Vellore, Tamilnadu 632004, India  
Tel: +91-9566434081  
Fax: +91-416-2232054  
E-mail: dr.rameshtelugu@gmail.com

**Background:** Inflammatory myofibroblastic tumor is a histopathologically distinctive neoplasm of children and young adults. According to World Health Organization (WHO) classification, inflammatory myofibroblastic tumor is an intermediate-grade tumor, with potential for recurrence and rare metastasis. There are no definite histopathologic, molecular, or cytogenetic features to predict malignant transformation, recurrence, or metastasis. **Methods:** A 5-year retrospective study of histopathologically diagnosed inflammatory myofibroblastic tumors of various anatomic sites was conducted to correlate anaplastic lymphoma kinase-1 (ALK-1) expression with histological atypia, multicentric origin of tumor, recurrence, and metastasis. Clinical details of all the cases were noted from the clinical work station. Immunohistochemical stains for ALK-1 and other antibodies were performed. Statistical analysis was done using Fisher exact test. **Results:** A total of 18 cases of inflammatory myofibroblastic tumors were found during the study period, of which 14 were classical. The female-male ratio was 1:1 and the mean age was 23.8 years. Histologically atypical (four cases) and multifocal tumors (three cases, multicentric in origin) were noted. Recurrence was noted in 30% of ALK-1 positive and 37.5% of ALK-1 negative cases, whereas metastasis to the lung, liver, and pelvic bone was noted in the ALK-1 positive group only. **Conclusions:** Overall, ALK-1 protein was expressed in 55.6% of inflammatory myofibroblastic tumors. There was no statistically significant correlation between ALK-1 expression, tumor type, recurrence and metastasis. However, ALK-1 immunohistochemistry is a useful diagnostic aid in the appropriate clinical and histomorphologic context.

**Key Words:** ALK protein; Atypia; Prognostic marker; Recurrence; Neoplasms

Inflammatory myofibroblastic tumor is a histopathologically distinctive neoplasm that has been described in various anatomic sites of children and young adults. It is composed of myofibroblastic spindle cells admixed with infiltrates of plasma cells, lymphocytes and eosinophils.<sup>1</sup> Most common site is the lung followed by other sites. In 1954, Umiker and Iverson<sup>2</sup> first described it in the lung. According to World Health Organization (WHO) classification, inflammatory myofibroblastic tumor is an intermediate tumor (rarely metastasizing), with potential for recurrence. These tumors were initially considered as reactive in nature, however, the neoplastic nature was revealed by molecular analysis that showed clonal rearrangement of the anaplastic lymphoma kinase (*ALK*) gene on the short arm of chromosome 2 at 2p23 with fusion of the 3' kinase region of the *ALK* gene with various partners including TPM3, TPM4, CLTC, and rans-binding protein 2 (*RANBP2*) in 50%–70% of inflammatory

myofibroblastic tumors.<sup>3</sup>

A few cases of inflammatory myofibroblastic tumors undergo malignant transformation displaying large polygonal cells and higher mitotic rate including atypical mitosis.<sup>4</sup> Marino-Enriquez *et al.*<sup>4</sup> in 2011 first described the term epithelioid inflammatory myofibroblastic sarcoma because of the malignant nature of these tumours. Inflammatory myofibroblastic tumors expressing *RANBP2* and *ALK* rearrangement (*RANBP2-ALK*) fusion usually display high grade epithelioid/round cell morphology with nuclear membrane staining pattern and predict poor prognosis.<sup>5</sup>

Expression of ALK fusion proteins in inflammatory myofibroblastic tumors can be detected by immunohistochemistry (IHC), the staining pattern of which is determined by the fusion partner: diffuse cytoplasmic staining when the partnering proteins are TPM3, TPM4, CARS, ATIC, and SEC31L122; granular cytoplasmic staining with CLTC; and nuclear membrane staining

with RANBP2.<sup>4</sup>

However, the biological nature may be aggressive even when the histologic appearance is bland.<sup>6</sup> There were no definite histopathologic, molecular, or cytogenetic features to predict the malignant transformation, recurrence, or metastasis.<sup>7</sup> Surgical resection is the preferred treatment for inflammatory myofibroblastic tumors. Nonsteroidal anti-inflammatory drugs (NSAIDs), steroids, chemotherapy, and radiotherapy have been used as adjuvant therapy when feasible.<sup>8</sup>

We undertook this retrospective study to correlate the histological atypia, multifocal appearance of tumor (multicentric in origin), recurrence, and metastasis with the immunohistochemical expression of ALK-1 in inflammatory myofibroblastic tumors, so as to objectively predict the biological behavior.

## MATERIALS AND METHODS

This was a retrospective study of 18 patients with inflammatory myofibroblastic tumors, diagnosed in the Department of General Pathology during the period of January 2011–December 2015. The study was approved by the institutional review board (IRB No. 10200). The clinical details and follow-up information of each patient were noted from the clinical work station. All the archived slides were taken out and reviewed. Wherever necessary, blocks were cut and fresh slides prepared. All classical tumors fulfilled the morphologic criteria described in the *WHO Classification of Tumours of Soft Tissue and Bone*.<sup>3</sup> Atypical cases were defined by increased cellularity, cellular atypia with large ganglion-like round to polygonal cells, multinucleated or anaplastic giant cells, atypical mitosis and necrosis.<sup>7</sup> The archival tissues obtained from institutional and consultation files were fixed in 10% buffered neutral formalin and paraffin-embedded tissue blocks were prepared. Hematoxylin and eosin (H&E) stained sections were made. IHC was done on representative paraffin block(s) from each tumor.

### IHC procedure

IHC slides and H&E slides prepared from formalin fixed, paraffin embedded tissue blocks were reviewed. Fresh sections were cut from archival blocks when necessary. IHCs had been done on Ventana Benchmark XT (Ventana Medical Systems, Tucson, AZ, USA). Details of primary antibodies used for IHC are shown in Table 1. Appropriate positive controls were used for each antibody throughout the study. The stain was considered to be positive if the tumor cells showed specific cytoplasmic and/or nuclear membrane staining for the particular antibody.

The immunohistochemical stains were evaluated semiquantitatively as follows: 0, negative; 1+, < 10% of cells positive; 2+, 10%–50% of cells positive; and 3+, > 50% of cells positive.<sup>7</sup>

Intra-abdominal tumors with epithelioid morphology, nuclear or perinuclear accentuation of ALK immunopositivity and aggressive clinical behavior were categorized as epithelioid inflammatory myofibroblastic sarcoma.<sup>4</sup>

### Statistical analysis

The statistical analysis done in this study was Fisher exact test. p-value of < .05 was considered to be statistically significant.

## RESULTS

A total of 18 cases of inflammatory myofibroblastic tumors were found during the study period. Of the 18 cases, 17 were institutional cases and one was a consultation case (case 2) from outside hospital. The clinicopathological features and outcome in the study group are depicted in Table 2. There were nine females and nine males with female to male ratio of 1:1 and the mean age was 23.8 years (range, 3 to 44 years). The most common locations were lung (six cases) and intra-abdominal region (six cases) followed by suprarenal, mastoid antrum, dorsum of nose, mediastinum, sphenoid wing, and breast (one case each). All the patients underwent surgical excision and a few patients had combination treatments: surgery plus chemotherapy or chemoradiotherapy. Limited follow-up information was available, ranging from 3 to 65 months (mean, 16.1 months). One patient

**Table 1.** Immunohistochemical panel with primary antibodies and dilutions

Antibody	Poly/Monoclonal	Source	Dilution
ALK-1	Monoclonal	Leica	Prediluted
SMA	1A4	Dako	Concentrated
MSA	HHF35	Dako	Concentrated
Vimentin	V9	Dako	Concentrated
Desmin	D33	Dako	Concentrated
EMA	E29	Dako	Concentrated
CK	AE1/AE3	Dako	Concentrated
Myogenin	F5D	Biosb	Concentrated
CD34	Q-bend 10	Dako	Concentrated
CD21	1F8	Dako	Concentrated
CD117	C-kit	Dako	Concentrated
H-Caldesmon	H/CD	Dako	Concentrated
TLE-1	M-101	Sigma	Concentrated
CD30	Ber H2	Dako	Concentrated
CD15	Carb-3	Dako	Concentrated

ALK-1, anaplastic lymphoma kinase-1; SMA, smooth muscle actin; MSA, muscle-specific actin; EMA, epithelial membrane antigen; CK, cytokeratin; TLE-1, transducin-like enhancer protein-1.

**Table 2.** Clinicopathological features and outcome in the study group

Case No.	Age (yr)	Sex	Anatomic site	Size (cm)	Treatment	Recurrence (mo)	Metastases	Follow-up status (mo)
1	3	F	Suprarenal	15	SE+CT	1	Liver and Lung	8 (DOD)
2	27	M	Colon	13	SE	NA	NA	NA
3	37	M	Lung	3.2	SE	No	No	4 (ANED)
4	26	F	Mastoid antrum	1	SE	No	No	38 (ANED)
5	29	F	Lung	4.2	SE+CT	No	No	11 (ANED)
6	25	F	Breast	6.5	SE	1	No	6 (ANED)
7	27	F	Colon	4.5	SE	No	No	3 (ANED)
8	25	M	Sphenoid wing	2	SE+CT+RT	24	No	51 (ANED)
9	18	M	Bronchus	5	SE	10	No	65 (ANED)
10	26	F	Lung	1	SE	6	No	16 (ANED)
11	10	M	Omentum	7	SE	No	No	14 (ANED)
12	37	F	Lung	6	SE	No	No	8 (ANED)
13	41	M	Jejunum, ileocaecum, mesentry, and omentum	8.5	SE+RT	6	No	9 (ANED)
14	24	M	Dorsum of nose	2	SE	No	No	8 (ANED)
15	13	M	Pelvic mass, omentum, and bladder	11	SE+CT	No	Pelvic bone	7 (ANED)
16	4	M	Mediastinum	2.5	SE	No	No	NA
17	44	F	Lung	7	SE	No	No	7 (ANED)
18	12	F	Distal CBD, cystic duct, and periportal lymph nodes	1	SE	No	No	3 (ANED)

F, female; SE, surgical excision; CT, chemotherapy; DOD, died of disease; M, male; NA, not available; ANED, alive with no evidence of disease; RT, radiotherapy; CBD, common bile duct.

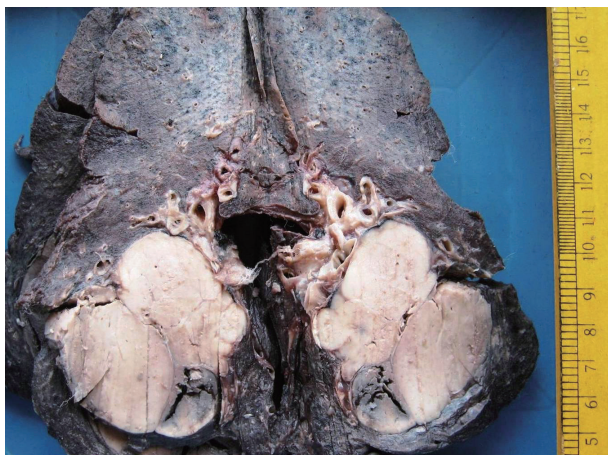


**Fig. 1.** Lobectomy specimen with a circumscribed nodular grey-white lesion with focal hemorrhage.

had died of disease. Two cases were lost for follow-up. Remaining patients were alive with no evidence of disease at last follow-up.

### Pathological findings

The tumor size ranged from 1 to 15 cm (mean, 5.6 cm). Grossly, the tumors were nodular circumscribed masses (Fig. 1) exhibiting soft to firm variegated appearance with grey white to tan fleshy and focal mucoid areas. One case showed variable hemorrhage and necrosis on the cut surface (case 1). Three cases (cases 13, 15, and 18) had multifocal appearance of tumor (multicentric

in origin) in various anatomic locations (Table 2). Histologically, among the 18 inflammatory myofibroblastic tumors (including recurrent and metastatic cases), 14 cases had classic histologic features (Fig. 2) and four cases had atypical histologic features, revealing diffuse and focal cytoplasmic IHC expression of ALK-1 (Fig. 3).

Classification of histological patterns was done for all the cases according to the dominant tumor area, which included cellular (77.8%), myxoid (11.1%), and fibrous (11.1%) types. All the classical inflammatory myofibroblastic tumors displayed a bland spindle cell proliferation admixed with an inflammatory infiltrate composed of lymphocytes, plasma cells, and eosinophils. The atypical histologic features included increased cellularity, cellular atypia with large ganglion-like round to polygonal cells, multinucleated or anaplastic giant cells, atypical mitosis, and necrosis.

Among the atypical cases, one case (case 1) showed dominant epithelioid morphology with focally ganglion like cells, hypercellularity, atypia, mitosis, and prominent nucleoli (Fig. 4); one case (case 13) showed dominant spindle cell morphology and focal epithelioid morphology (Fig. 5); remaining two cases (cases 2 and 6) showed atypical spindle cell morphology (Fig. 6).

Among the atypical cases, three cases had recurrence (cases 1, 6, and 13) and two cases had metastasis to the lung, liver (case 1), and pelvic bone (case 15).

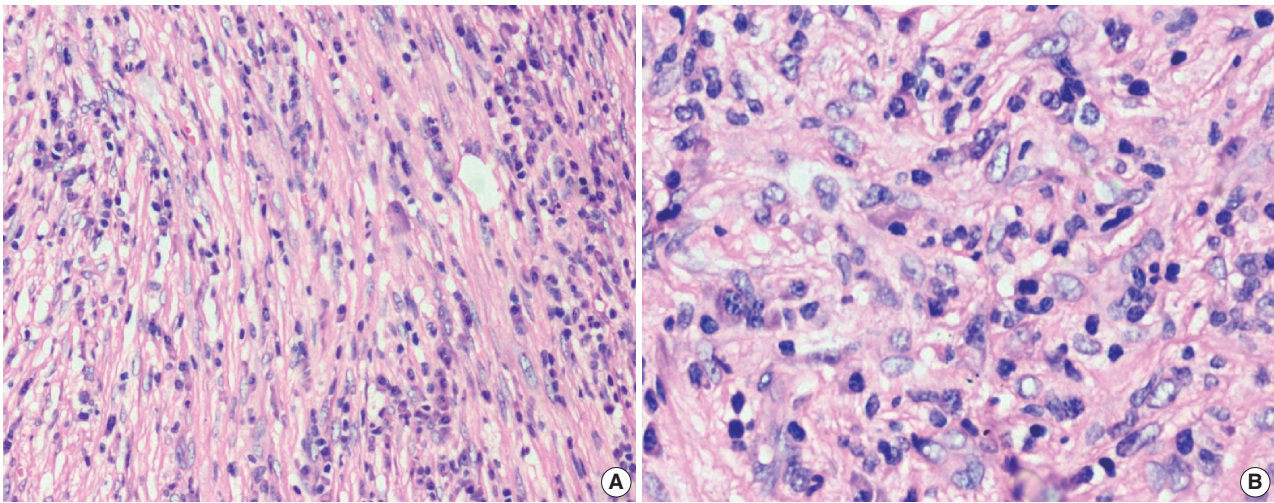


**Fig. 2.** (A, B) Classical inflammatory myofibroblastic tumor with bland spindle cell proliferation and pronounced inflammatory infiltrate.

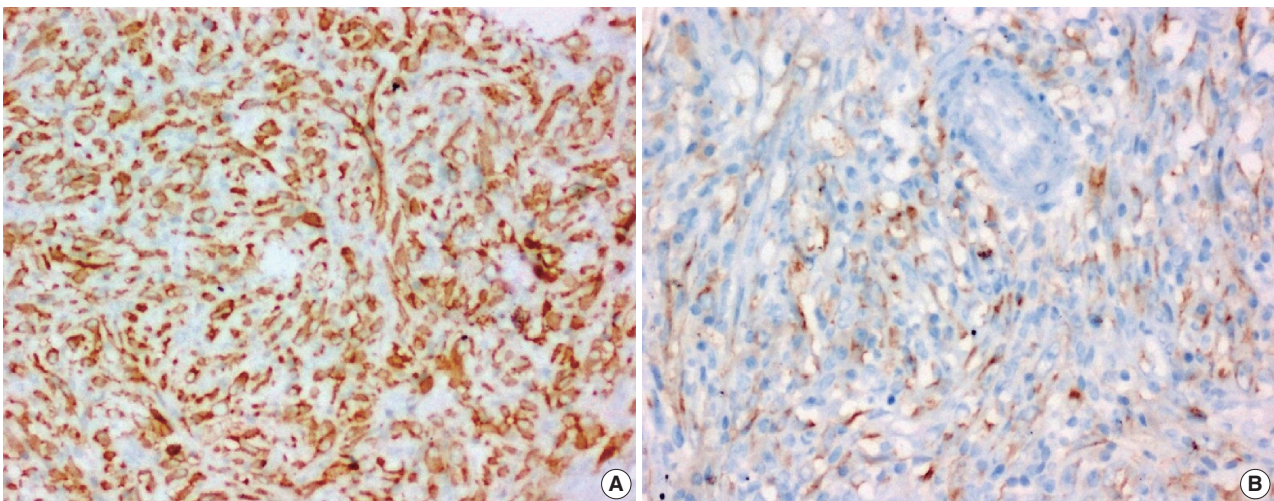


**Fig. 3.** Diffuse (A) and focal (B) cytoplasmic immunohistochemical stains of anaplastic lymphoma kinase-1.

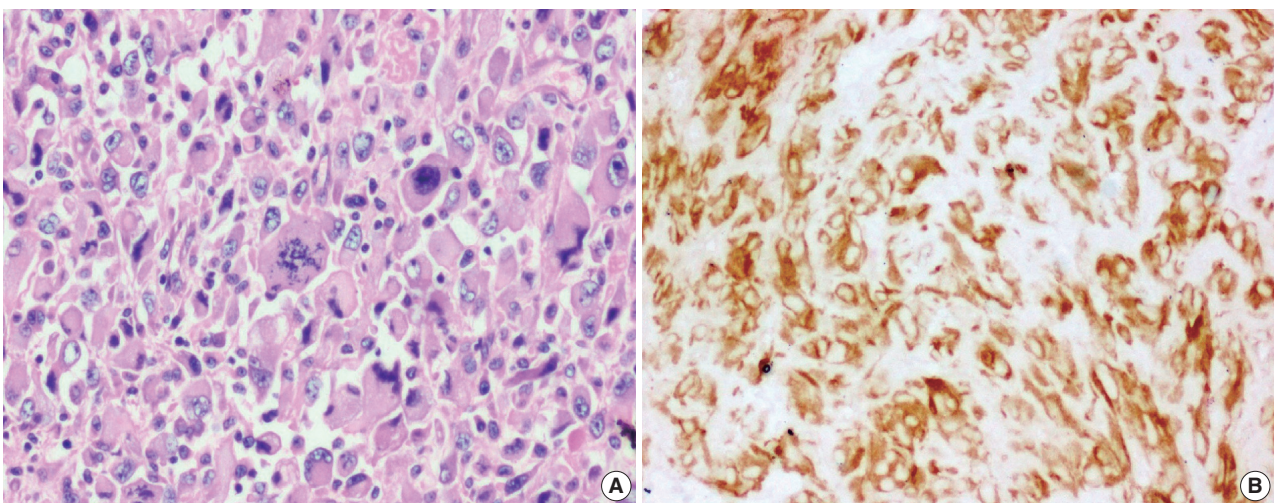


**Fig. 4.** Epithelioid inflammatory myofibroblastic sarcoma with increased cellularity, cellular atypia with large epithelioid like cells, multinucleated or anaplastic giant cells and atypical mitosis (A); perinuclear accentuation of anaplastic lymphoma kinase-1 expression (B).

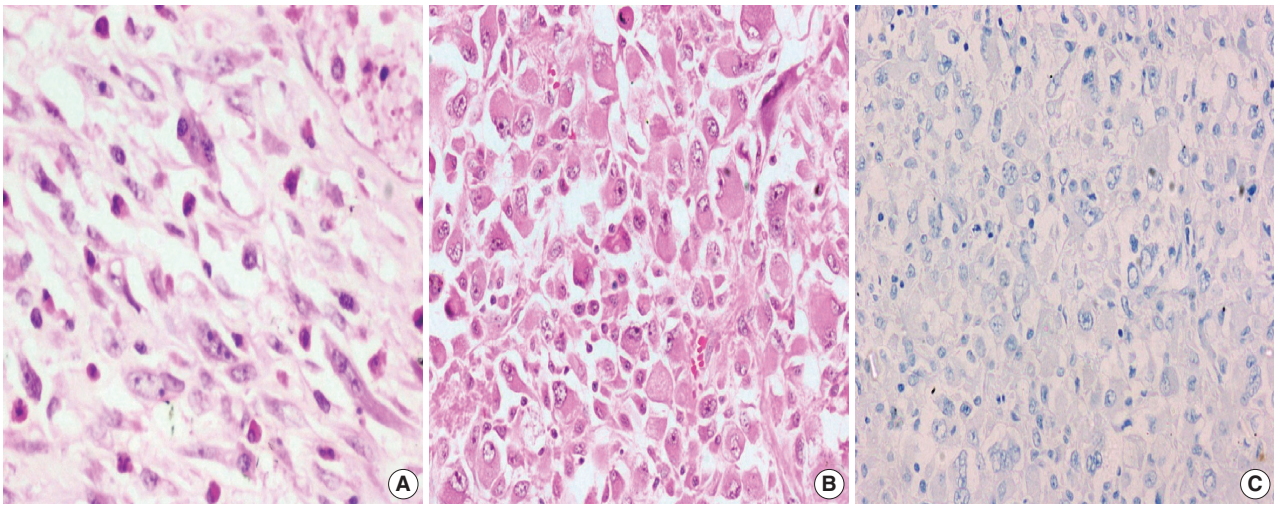


**Fig. 5.** Inflammatory myofibroblastic tumor with increased cellularity, cellular atypia with large atypical spindle shaped cells (A) and focal atypical epithelioid or ganglion-like cells with hyperchromasia (B); negative immunoreactivity of anaplastic lymphoma kinase-1 (C).

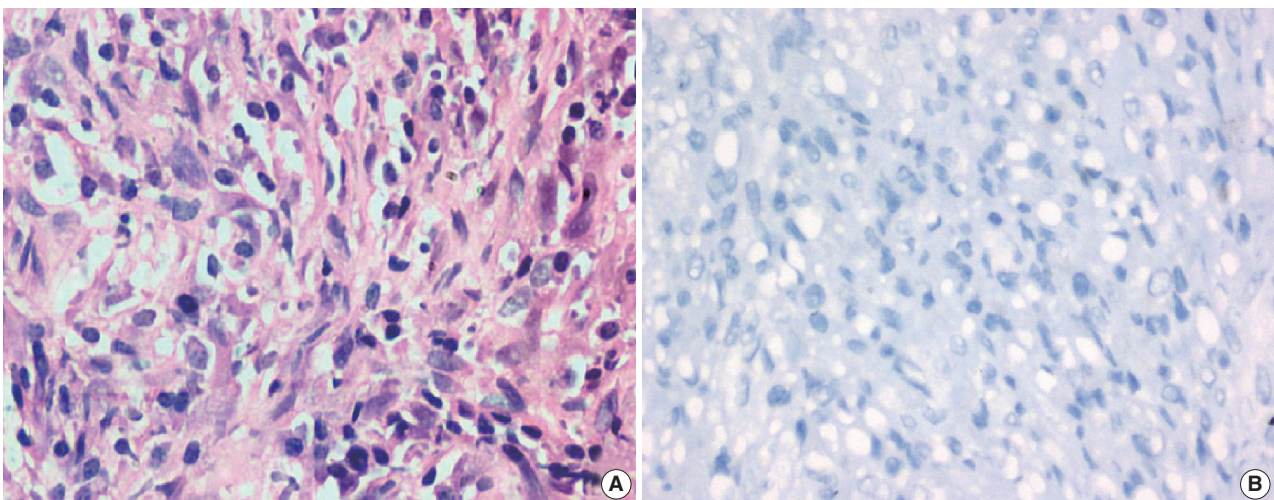


**Fig. 6.** Atypical inflammatory myofibroblastic tumor with increased cellularity, cellular atypia with large atypical spindle shaped cells and hyperchromasia (A); negative immunoreactivity of anaplastic lymphoma kinase-1 (B).

### Immunohistochemical findings

Spindled tumor cells of inflammatory myofibroblastic tumors showed cytoplasmic or membrane positivity for smooth muscle actin (12/16 cases), muscle-specific actin (3/6 cases), vimentin (8/8 cases), desmin (5/11 cases), and epithelial membrane antigen (2/4 cases). The spindled tumor cells were negative for cytokeratin, myogenin, CD34, CD21, CD117, h-caldesmon, TLE-1, CD30, and CD15 (Table 3).

Immunohistochemical stain for ALK-1 expression was available in all the 18 cases, demonstrating cytoplasmic reactivity of spindled or polygonal tumor cells for ALK-1 in 10 cases (55.6%) and no reactivity in eight cases (44.4%) (Tables 3, 4). Diffuse (3+) cytoplasmic staining was observed in six cases and focal (2+)

cytoplasmic staining in three cases.

An intra-abdominal inflammatory myofibroblastic tumor with dominant epithelioid morphology (case 1) revealed perinuclear accentuation of ALK-1 immunoreactivity, suggestive of epithelioid inflammatory myofibroblastic sarcoma (Fig. 4); the remaining atypical cases with spindle cell morphology (including case 13 with focal epithelioid morphology) were negative for ALK-1, suggestive of atypical inflammatory myofibroblastic tumors only (Figs. 5, 6).

ALK-1 positive tumors (55.6%) included five females and five males and the mean age was 23.8 years (range, 3 to 44 years), compared with the mean age of (four females and four males) 27.1 years (range, 18 to 41 years) for ALK-1 negative cases.

Recurrence was noted in 3/10 ALK-1 positive (30%) and 3/8 ALK-1 negative (37.5%) cases, whereas metastasis to the lung, liver and pelvic bone was noted in the ALK-1 positive group (Tables 4, 5).

### Statistical analysis

ALK-1 immunopositivity in neither of the classical ( $p = .275$ ), atypical ( $p = .275$ ) nor multifocal tumor ( $p > .99$ ) types was sta-

**Table 3.** Immunohistochemical stains performed in the study group

Marker (No. of tests)	Positive	Negative
ALK-1 (n=18)	10 (55.6)	8 (44.4)
SMA (n=16)	12 (75.0)	4 (25.0)
MSA (n=6)	3 (50.0)	3 (50.0)
Vimentin (n=8)	8 (100)	0
Desmin (n=11)	5 (45.5)	6 (54.5)
EMA (n=4)	2 (50.0)	2 (50.0)
CK (n=6)	0	6 (100)
Myogenin (n=3)	0	3 (100)
CD34 (n=7)	0	7 (100)
CD21 (n=3)	0	3 (100)
CD117 (n=2)	0	2 (100)
H Caldesmon (n=4)	0	4 (100)
TLE-1 (n=4)	0	4 (100)
CD30 (n=3)	0	3 (100)
CD15 (n=2)	0	2 (100)

Values are presented as number (%).

ALK-1, anaplastic lymphoma kinase-1; SMA, smooth muscle actin; MSA, muscle-specific actin; EMA, epithelial membrane antigen; CK, cytokeratin; TLE-1, transducin-like enhancer protein-1.

**Table 4.** Histological types with atypia, ALK-1 expression, recurrence, and metastasis

Case No.	Sex	Histological pattern	Atypia	ALK-1 expression	Recurrence (mo)	Metastases
1	F	C	Yes	3+	1	Liver and lung
2	M	C	Yes	0	NA	NA
3	F	C	No	2+	No	No
4	F	Fi	No	0	No	No
5	F	My	No	0	No	No
6	F	C	Yes	0	1	No
7	F	C	No	2+	No	No
8	M	C	No	3+	24	No
9	M	My	No	0	10	No
10	F	C	No	2+	6	No
11	M	C	No	3+	No	No
12	F	C	No	0	No	No
13	M	C	Yes	0	6	No
14	M	C	No	0	No	No
15	M	Fi	No	3+	No	Pelvic bone
16	M	C	No	3+	No	No
17	F	C	No	3+	No	No
18	F	C	No	2+	No	No

ALK-1, anaplastic lymphoma kinase-1; F, female; C, cellular histological pattern; NA, not available; M, male; Fi, fibrous histological pattern; My, myxoid histological pattern; 0, negative; 1+, <10% positive cells; 2+, 10-50% positive cells; 3+, >50% of cells positive.

tistically significant at 5% level of significance with Fisher exact test. There was no statistically significant correlation between ALK-1 expression and either of the recurrence ( $p > .99$ ) or metastasis ( $p = .485$ ) of inflammatory myofibroblastic tumors.

## DISCUSSION

Inflammatory myofibroblastic tumors formerly described as inflammatory pseudotumor, with an unpredictable behavior ranging from benign to low-grade malignant, are classified as intermediate grade tumors, with potential for recurrence and rare metastasis, in the current *WHO Classification of Tumours of Soft tissue and Bone*.<sup>3</sup> These tumors are described in children and young adults in various anatomic sites with a tendency towards local recurrence in about 25% of abdominopelvic lesions and rare metastasis (< 5%).<sup>3,7</sup> A few cases of inflammatory myofibroblastic tumors may appear morphologically benign but the biological nature may be aggressive even when the histologic appearance is bland. There were no definite predictors of the histologic transformation, recurrence, or metastasis. These tumors were considered as a neoplasm after the discovery of clonal rearrangement of the *ALK* gene on the short arm of chromosome 2 at 2p23 in 50%–75% of extrapulmonary inflammatory myofibroblastic tumors.<sup>7</sup>

In a study by Wang *et al.*,<sup>9</sup> the most common site of inflammatory myofibroblastic tumors was abdominopelvic region (73.9%) followed by other locations. The present study included

**Table 5.** Correlation of ALK-1 positive and ALK-1 negative inflammatory myofibroblastic tumors

Variable	ALK-1 positive (n=10)	ALK-1 negative (n=8)	p-value
Male:Female	1:1	1:1	-
Age (yr)			
Range	3–44	18–41	-
Mean	23.8	27.1	
Tumor type			
Classical	9	5	.275
Atypical	1	3	.275
Multifocal (multicentric in origin)	2	1	>.99
Biological behavior			
Recurrence	3	3	>.99
Metastasis	2	0	.485

ALK-1, anaplastic lymphoma kinase-1.

33.3% each of intrapulmonary and intra-abdominal locations followed by other locations. There was slight male predominance in the literature,<sup>10,11</sup> however, there was an equal incidence in each gender in the present study.

Hussong *et al.*<sup>12</sup> in 1999 stated that the combination of cellular atypia, presence of ganglionlike cells, p53 expression and DNA aneuploidy are all possible predictors to identify the malignant change and aggressive behavior of inflammatory myofibroblastic tumors. In a study by Coffin *et al.*,<sup>7</sup> 27.1% were classical and 72.9% were atypical inflammatory myofibroblastic tumors. The atypical features in his study were increased cellularity, cellular and nuclear pleomorphism, distinct fascicular and focal herringbone pattern, cellular atypia with large ganglion-like round to polygonal cells, multinucleated or anaplastic giant cells, atypical mitosis, and necrosis. ALK immunopositivity was noted in 78% atypical, 54% recurrent and 60% classical inflammatory myofibroblastic tumors. Metastatic inflammatory myofibroblastic tumors (10.1%) were negative for ALK expression.

In another study,<sup>13</sup> there were 60% classical and 40% atypical inflammatory myofibroblastic tumors. Twenty-six point seven percent cases showed ALK expression. Twenty-five percent of ALK-positive and 63.6% of ALK-negative inflammatory myofibroblastic tumors revealed recurrence. Metastasis was restricted to the ALK-negative group. Statistically significant correlation was found between atypia, recurrence and metastasis. There was a significant correlation between ALK expression and recurrence. The present study revealed 77.8% classical and 22.2% atypical inflammatory myofibroblastic tumors. Overall ALK-1 immunopositivity was noted in 55.6% and negativity in 44.4% of inflammatory myofibroblastic tumors. Metastatic inflammatory myofibroblastic tumors were ALK-1 positive in the present

study. There was no statistically significant correlation between ALK-1 expression, atypia, recurrence and metastasis in the present study compared to the other studies, probably due to a small sample size and limited follow up data; a larger study may be taken up in the future to evaluate the statistical significance.

Marino-Enriquez *et al.*<sup>4</sup> proposed a term epithelioid inflammatory myofibroblastic sarcoma for epithelioid variant of intra-abdominal inflammatory myofibroblastic tumors with a nuclear membrane or perinuclear pattern of ALK expression and aggressive clinical behavior. In the present study, one patient with an intra abdominal mass, which was categorized as inflammatory myofibroblastic sarcoma, with epithelioid morphology and perinuclear accentuation of ALK-1 expression, developed liver and lung metastasis and expired within 8 months. *ALK* gene rearrangement was demonstrated in all the tested cases of epithelioid variant of inflammatory myofibroblastic tumors by fluorescence *in situ* hybridization (FISH).<sup>4</sup> Janik *et al.*<sup>14</sup> studied pulmonary and extrapulmonary pseudotumors with overall recurrence rate of 14%. Multifocality of pulmonary and extrapulmonary pseudotumors had a high chance of recurrence compared with tumors confined to a single organ. Intraabdominal pseudotumors were associated with >75% of the recurrences when compared to other extrapulmonary pseudotumors. In the present study, extrapulmonary multifocal inflammatory myofibroblastic tumors were associated with recurrence and metastasis. Study by Chaudhary<sup>15</sup> pointed out that *ALK* gene rearrangements were often seen in inflammatory myofibroblastic tumors of children and young adults compared to adults over 40 years of age. The search for *ALK* gene rearrangement by FISH is a useful tool for the diagnosis of inflammatory myofibroblastic tumors.

Ramotar *et al.*<sup>16</sup> reported a case of inflammatory pseudotumor of the head and neck mimicking a metastatic disease in a human immunodeficiency virus-positive 49-year-old female. In immunocompromised patients, the likelihood of inflammatory pseudotumor should also be considered in the differential diagnosis. ALK protein immunopositivity was detected in various other tumors including lipomatous tumors, rhabdomyosarcomas, Ewing's sarcoma/primitive neuroectodermal tumors, malignant fibrous histiocytomas, and leiomyosarcomas. Except inflammatory myofibroblastic tumors, almost all other tumors displayed low level of ALK expression.<sup>17</sup>

The differential diagnosis of these tumors includes both benign and malignant spindle or epithelioid cell tumors. The spindle cell tumors include fibroblastic/myofibroblastic tumors, fibrous histiocytoma, and solitary fibrous tumor.<sup>6</sup> The tumors with epithelioid or round cell morphology include anaplastic large cell

lymphoma, epithelioid leiomyosarcoma, rhabdomyosarcoma, undifferentiated sarcoma, myxoid/round cell liposarcoma, myxofibrosarcoma, dedifferentiated liposarcoma, poorly differentiated carcinoma, malignant melanoma, and epithelioid gastrointestinal stromal tumor.<sup>4,5</sup>

Anaplastic large cell lymphoma can be differentiated from epithelioid variant of inflammatory myofibroblastic sarcoma by immunoreactivity for CD30, CD3, and CD43, diffuse membranous or cytoplasmic staining of ALK-1 and absence of *RANBP2-ALK* rearrangement. High-grade leiomyosarcoma usually reveals fascicles of spindle and epithelioid cells with increased cellularity, cellular atypia, pleomorphism, cigar-shaped nuclei and abundant brightly eosinophilic cytoplasm. The tumor cells are positive for h-caldesmon and negative for ALK staining. Alveolar rhabdomyosarcoma shows uniform round cells with scant cytoplasm and usually lacks myxoid background and inflammatory infiltrates. Immunohistochemical stain for myogenin reveals nuclear positivity. Dedifferentiated liposarcoma can have features of inflammatory myofibroblastic tumor, but with expression of MDM2 and absence of ALK-1. Epithelioid malignant peripheral nerve sheath tumor will be strongly and diffusely positive for S100 and negative for ALK-1 and also SMARCB1. Malignant melanoma shows polygonal cells with prominent nucleoli and the cells are positive for S100 and human melanoma black 45. Epithelioid gastrointestinal stromal tumors reveal immunorepression of CD117, discovered on GIST-1 (DOG1) and negative for ALK-1.<sup>3,5</sup>

Surgical resection is the preferred treatment for inflammatory myofibroblastic tumors. NSAIDs, steroids, chemotherapy, and radiotherapy have been used as adjuvant therapy when feasible.<sup>8</sup>

In a study by Jacob *et al.*,<sup>18</sup> systemic (liver and lumbar spine) involvement of inflammatory myofibroblastic tumor in a 45-year-old female, expressing *ALK* gene rearrangement, responded very well to ALK inhibitor (Crizotinib). In a series of cases by Butrynski *et al.*,<sup>19</sup> multifocal intra-abdominal inflammatory myofibroblastic tumors which expressed *ALK* gene rearrangement, were treated successfully by ALK inhibitor (Crizotinib). Fragoso *et al.*<sup>11</sup> in 2011 stated that, although surgical resection is the preferred treatment for inflammatory myofibroblastic tumors, cases which are not amenable to surgical excision may be treated conservatively.

In conclusion, this study demonstrates that inflammatory myofibroblastic tumors exhibit a wide age group distribution with an equal incidence in males and females. Most of the tumors with histological atypia were associated with recurrence, irrespective of ALK-1 expression. Epithelioid inflammatory myofi-

broblastic sarcoma with perinuclear accentuation of ALK-1 showed aggressive clinical course with metastasis and mortality. Few cases which were benign in histology also exhibited recurrence irrespective of ALK-1 expression. Metastasis was seen in ALK-1 positive tumors. However, there was no statistically significant correlation between ALK-1 expression, tumor type, recurrence, and metastasis. Overall, ALK-1 IHC is a useful diagnostic aid in the appropriate histomorphologic context, especially in identifying epithelioid inflammatory myofibroblastic sarcomas. There were no definite histopathologic criteria to predict malignant transformation, recurrence, or metastasis. However, this study is limited by the very small number of cases, limited follow-up data and also the lack of identification of *ALK* gene rearrangement by FISH. A search for newer molecular tools by larger studies needs to be performed to identify prognostic features to guide treatment and predict the outcome.

### Conflicts of Interest

No potential conflict of interest relevant to this article was reported.

### Acknowledgments

The authors thank the staff Mrs. Annie Rebecca and Mr. S. Daniel Dilip in the Immunohistochemical laboratory in the Department of Pathology at Christian Medical College, Vellore for their technical help and Mr. Prakash Ramasami, senior demonstrator, biostatistics, CMC, Vellore for the statistical analysis performed.

### REFERENCES

1. Ufuk F, Herek D, Karabulut N. Inflammatory myofibroblastic tumor of the lung: unusual imaging findings of three cases. *Pol J Radiol* 2015; 80: 479-82.
2. Umiker WO, Iverson L. Postinflammatory tumors of the lung: report of four cases simulating xanthoma, fibroma or plasma cell tumor. *J Thorac Surg* 1954; 28: 55-63.
3. Fletcher CD, Bridge JA, Hogendoorn P, Mertens F. WHO classification of tumours of soft tissue and bone. 4th ed. Lyon: IARC Press, 2013; 83-4.
4. Marino-Enriquez A, Wang WL, Roy A, *et al.* Epithelioid inflammatory myofibroblastic sarcoma: an aggressive intra-abdominal variant of inflammatory myofibroblastic tumor with nuclear membrane or perinuclear ALK. *Am J Surg Pathol* 2011; 35: 135-44.
5. Li J, Yin WH, Takeuchi K, Guan H, Huang YH, Chan JK. Inflam-

- matory myofibroblastic tumor with *RANBP2* and *ALK* gene rearrangement: a report of two cases and literature review. *Diagn Pathol* 2013; 8: 147.
6. Savvidou OD, Sakellariou VI, Papakonstantinou O, Skarpidi E, Papanagelopoulos PJ. Inflammatory myofibroblastic tumor of the thigh: presentation of a rare case and review of the literature. *Case Rep Orthop* 2015; 2015: 814241.
  7. Coffin CM, Hornick JL, Fletcher CD. Inflammatory myofibroblastic tumor: comparison of clinicopathologic, histologic, and immunohistochemical features including ALK expression in atypical and aggressive cases. *Am J Surg Pathol* 2007; 31: 509-20.
  8. Tao YL, Wang ZJ, Han JG, Wei P. Inflammatory myofibroblastic tumor successfully treated with chemotherapy and nonsteroidals: a case report. *World J Gastroenterol* 2012; 18: 7100-3.
  9. Wang Z, Zhao X, Li K, *et al.* Analysis of clinical features and outcomes for inflammatory myofibroblastic tumors in China: 11 years of experience at a single center. *Pediatr Surg Int* 2016; 32: 239-43.
  10. Karnak I, Senocak ME, Ciftci AO, *et al.* Inflammatory myofibroblastic tumor in children: diagnosis and treatment. *J Pediatr Surg* 2001; 36: 908-12.
  11. Fragoso AC, Eloy C, Estevão-Costa J, Campos M, Farinha N, Lopes JM. Abdominal inflammatory myofibroblastic tumor a clinicopathologic study with reappraisal of biologic behavior. *J Pediatr Surg* 2011; 46: 2076-82.
  12. Hussong JW, Brown M, Perkins SL, Dehner LP, Coffin CM. Comparison of DNA ploidy, histologic, and immunohistochemical findings with clinical outcome in inflammatory myofibroblastic tumors. *Mod Pathol* 1999; 12: 279-86.
  13. Jiang YH, Cheng B, Ge MH, Cheng Y, Zhang G. Comparison of the clinical and immunohistochemical features, including anaplastic lymphoma kinase (ALK) and p53, in inflammatory myofibroblastic tumours. *J Int Med Res* 2009; 37: 867-77.
  14. Janik JS, Janik JP, Lovell MA, Hendrickson RJ, Bensard DD, Greffe BS. Recurrent inflammatory pseudotumors in children. *J Pediatr Surg* 2003; 38: 1491-5.
  15. Chaudhary P. Mesenteric inflammatory myofibroblastic tumors. *Ann Gastroenterol* 2015; 28: 49-54.
  16. Ramotar H, Cheung L, Pitkin L. The great mimicker: a rare case of head and neck inflammatory pseudotumour in the presence of human immunodeficiency virus. *J Laryngol Otol* 2016; 130: 107-10.
  17. Li XQ, Hisaoka M, Shi DR, Zhu XZ, Hashimoto H. Expression of anaplastic lymphoma kinase in soft tissue tumors: an immunohistochemical and molecular study of 249 cases. *Hum Pathol* 2004; 35: 711-21.
  18. Jacob SV, Reith JD, Kojima AY, Williams WD, Liu C, Vila Duckworth L. An unusual case of systemic inflammatory myofibroblastic tumor with successful treatment with ALK-inhibitor. *Case Rep Pathol* 2014; 2014: 470340.
  19. Butrynski JE, D'Adamo DR, Hornick JL, *et al.* Crizotinib in ALK-rearranged inflammatory myofibroblastic tumor. *N Engl J Med* 2010; 363: 1727-33.

# Characteristic Changes in Decidual Gene Expression Signature in Spontaneous Term Parturition

Haidy El-Azzamy<sup>1,\*</sup> · Andrea Balogh<sup>1,2,\*</sup>  
Roberto Romero<sup>1,3,4,5</sup> · Yi Xu<sup>1</sup>  
Christopher LaJeunesse<sup>1</sup> · Olesya Plazyo<sup>1</sup>  
Zhonghui Xu<sup>1</sup> · Theodore G. Price<sup>1</sup>  
Zhong Dong<sup>1</sup> · Adi L. Tarca<sup>1,6</sup>  
Zoltan Papp<sup>7</sup> · Sonia S. Hassan<sup>1,6</sup>  
Tinnakorn Chaiworapongsa<sup>1,6</sup>  
Chong Jai Kim<sup>1,8,9</sup>  
Nardhy Gomez-Lopez<sup>1,6</sup>  
Nandor Gabor Than<sup>1,6,7,10,11</sup>

<sup>1</sup>Perinatology Research Branch, NICHD/NIH/DHHS, Bethesda, MD, and Detroit, MI, USA; <sup>2</sup>Department of Immunology, Eotvos Lorand University, Budapest, Hungary; <sup>3</sup>Department of Obstetrics and Gynecology, University of Michigan, Ann Arbor, MI; <sup>4</sup>Department of Epidemiology and Biostatistics, Michigan State University, East Lansing, MI; <sup>5</sup>Center for Molecular Medicine and Genetics, Wayne State University, Detroit, MI; <sup>6</sup>Department of Obstetrics and Gynecology, Wayne State University, School of Medicine, Detroit, MI, USA; <sup>7</sup>Maternity Private Department, Kertvolgyi Clinical Block, Semmelweis University, Budapest, Hungary; <sup>8</sup>Department of Pathology, Wayne State University, School of Medicine, Detroit, MI, USA; <sup>9</sup>Department of Pathology, Asan Medical Center, University of Ulsan College of Medicine, Seoul, Korea; <sup>10</sup>Systems Biology of Reproduction Lendulet Research Group, Institute of Enzymology, Research Centre for Natural Sciences, Hungarian Academy of Sciences, Budapest; <sup>11</sup>First Department of Pathology and Experimental Cancer Research, Semmelweis University, Budapest, Hungary

Received: October 2, 2016

Revised: December 3, 2016

Accepted: December 20, 2016

## Corresponding Author

Nandor Gabor Than, MD, PhD  
Systems Biology of Reproduction Lendulet Research Group, Institute of Enzymology, Research Centre for Natural Sciences, Hungarian Academy of Sciences, 2 Magyar Tudosok korutja, H-1117 Budapest, Hungary  
Tel: +36-1-382-6788  
E-mail: than.gabor@ttk.mta.hu

Roberto Romero, MD, DMedSci  
Perinatology Research Branch, NICHD/NIH/DHHS, Hutzel Women's Hospital, 3990 John R Street, 4 Brush, Detroit, MI 48201, USA  
Tel: +1-313-993-2700  
Fax: +1-313-993-2694  
E-mail: prbchiefstaff@med.wayne.edu

\*Haidy El-Azzamy and Andrea Balogh contributed equally to this work.

**Background:** The decidua has been implicated in the “terminal pathway” of human term parturition, which is characterized by the activation of pro-inflammatory pathways in gestational tissues. However, the transcriptomic changes in the decidua leading to terminal pathway activation have not been systematically explored. This study aimed to compare the decidual expression of developmental signaling and inflammation-related genes before and after spontaneous term labor in order to reveal their involvement in this process. **Methods:** Chorionic membranes were obtained from normal pregnant women who delivered at term with spontaneous labor (TIL, n = 14) or without labor (TNL, n = 15). Decidual cells were isolated from snap-frozen chorionic membranes with laser microdissection. The expression of 46 genes involved in decidual development, sex steroid and prostaglandin signaling, as well as pro- and anti-inflammatory pathways, was analyzed using high-throughput quantitative real-time polymerase chain reaction (qRT-PCR). Chorionic membrane sections were immunostained and then semi-quantified for five proteins, and immunoassays for three chemokines were performed on maternal plasma samples. **Results:** The genes with the highest expression in the decidua at term gestation included insulin-like growth factor-binding protein 1 (*IGFBP1*), galectin-1 (*LGALS1*), and progesterone-associated endometrial protein (*PAEP*); the expression of estrogen receptor 1 (*ESR1*), homeobox A11 (*HOXA11*), interleukin 1 $\beta$  (*IL1B*), IL8, progesterone receptor membrane component 2 (*PGRMC2*), and prostaglandin E synthase (*PTGES*) was higher in TIL than in TNL cases; the expression of chemokine C-C motif ligand 2 (*CCL2*), *CCL5*, *LGALS1*, *LGALS3*, and *PAEP* was lower in TIL than in TNL cases; immunostaining confirmed qRT-PCR data for IL-8, *CCL2*, galectin-1, galectin-3, and *PAEP*; and no correlations between the decidual gene expression and the maternal plasma protein concentrations of *CCL2*, *CCL5*, and IL-8 were found. **Conclusions:** Our data suggests that with the initiation of parturition, the decidual expression of anti-inflammatory mediators decreases, while the expression of pro-inflammatory mediators and steroid receptors increases. This shift may affect downstream signaling pathways that can lead to parturition.

**Key Words:** Chemokines; Cytokines; Estrogens; Galectins; Leukocytes; Progesterone

Parturition is a complex process tightly regulated by the cooperation of the neuroendocrine and immune systems.<sup>1,2</sup> Among the numerous hormonal factors implicated in the regulation of uterine quiescence and parturition (e.g., corticotropin-releasing hormone, cortisol, oxytocin), the changes in the bioavailability of estrogen and progesterone seem to be key in parturition.<sup>2,3</sup> While estrogen promotes labor by stimulating biochemical and physiological changes in myometrial cells that augment uterine contractility and excitability,<sup>4</sup> the actions of progesterone support pregnancy maintenance and prevent parturition by promoting myometrial quiescence.<sup>5,6</sup> In humans, the changes in the relative expression of various progesterone receptors (elevation in the progesterone receptor A [PR-A]/PR-B ratio) in uterine tissues and fetal membranes are responsible for decreasing progesterone actions (functional progesterone withdrawal).<sup>7-9</sup> A strong positive association between the PR-A/PR-B ratio and estrogen receptor  $\alpha$  (ER $\alpha$ ) expression in the myometrium of term pregnant women has been demonstrated,<sup>7</sup> suggesting that functional progesterone withdrawal generates “functional estrogen activation.”<sup>3</sup> All of these changes can then lead to the stimulation of pro-inflammatory pathways in the cervix, decidua, and fetal membranes.<sup>10-12</sup>

The pro-inflammatory microenvironment in various gestational tissues,<sup>10,13,14</sup> generated by the influx and local activation of maternal leukocytes<sup>15,16</sup> and the increased production of soluble immune mediators, is essential for the onset of labor.<sup>17,18</sup> The selective influx of leukocytes into gestational tissues<sup>19-21</sup> and various layers of the fetal membranes<sup>22,23</sup> is driven by chemokines,<sup>24,25</sup> a subset of cytokines with chemotactic properties.<sup>26</sup> The infiltrating monocytes and differentiated macrophages, neutrophils, and T cells as well as decidual stromal cells<sup>27,28</sup> are rich sources of pro-inflammatory cytokines, including interleukin 1 (IL-1), IL-6, and tumor necrosis factor  $\alpha$  (TNF $\alpha$ ).<sup>29-32</sup> These cytokines have been shown to regulate inflammatory processes leading to labor<sup>33</sup> by promoting myometrial contractility, cervical ripening, and membrane rupture.<sup>34,35</sup> For example, pro-inflammatory cytokines induce the expression of prostaglandin-endoperoxide synthase 2 (PTGS2) in the chorioamniotic membranes and decidua, leading to the increase in local and amniotic fluid concentrations of prostaglandins<sup>36-40</sup> that contribute to the transition from myometrial quiescence to labor initiation.<sup>41</sup> These data suggest that cytokines and chemokines orchestrate the activation of decidual tissue during labor.<sup>20</sup>

To promote labor-associated inflammation, the actions of anti-inflammatory mechanisms, at least in part, need to be attenuated in gestational tissues.<sup>5</sup> Among anti-inflammatory molecules, soluble tumor necrosis factor receptors (TNF-R), IL-1 receptor

antagonist (IL-1RA), IL-4, and IL-10 have been previously examined in the amniotic fluid in relation to labor. The concentrations of soluble TNF-R1 and TNF-R2<sup>42</sup> were lower in the amniotic fluid of women in spontaneous labor at term than in women who were not in labor at term, while there was no difference in amniotic fluid IL-1RA<sup>43,44</sup> concentrations regardless of the labor status, either at term or preterm. Data on amniotic fluid IL-10 and IL-4 concentrations were inconsistent,<sup>45</sup> since IL-10<sup>46,47</sup> or IL-4<sup>47</sup> concentrations were not different or even higher (IL-10<sup>48</sup> and IL-4<sup>49</sup>) in term or preterm labor than in gestational age-matched groups of non-laboring women. The expression of these anti-inflammatory molecules in decidual cells during term parturition has not been widely investigated. In this context, it is of importance that some other anti-inflammatory mediators (e.g., cytokines, galectins,<sup>50-52</sup> and progesterone-associated endometrial protein [PAEP]<sup>53</sup>) have their strongest expression in the decidua within the uterus<sup>53,54</sup> and may be involved in the regulation of local inflammatory pathways.

The decidua is localized between the chorioamnion and the myometrium and, thus, may play a key role in the cross-talk between the maternal and fetal compartments and in the regulation of labor. Maternal leukocyte populations in the decidua and their interaction with fetal trophoblasts as well as the network of soluble factors produced by the decidua involved in the regulation of implantation are increasingly characterized.<sup>55-60</sup> However, the complex and multifaceted roles of the decidua in the mechanisms leading to the onset of labor have been relatively understudied,<sup>61-63</sup> in spite of that, the activation of the decidual layer of the chorioamniotic membranes is one of the earliest events in spontaneous term parturition. This is supported by a recent concept stating that there is a “decidual clock,”<sup>64</sup> one of the multiple gestational clocks that regulates the timing of birth.<sup>65</sup> This suggests that advancing gestational age is associated with the withdrawal of active suppression and/or an enhanced sensitivity of the decidua to signals capable of inducing inflammation, which then promotes the release of a variety of biologically active inflammatory mediators, such as prostaglandins, cytokines, and chemokines, leading to the onset of labor.<sup>64</sup>

In relation to the “decidual clock” concept, it is tempting to hypothesize that the entire decidual developmental program may also play a role in the regulation of the local micro-environmental balance, controlling the maintenance of pregnancy and then the activation of labor. This developmental program may involve the key action of homeobox (HOX) gene expression in the uterus.<sup>66</sup> So far, it has been demonstrated that steroids regulate the expression of HOX genes in a tissue-specific manner,<sup>67</sup> and the changing

steroid responsiveness of the decidua during the perilabor period may also influence their expression. Although several publications outline the importance of HOX genes in uterine development, the menstrual cycle, and implantation,<sup>68-73</sup> their involvement in the labor process is poorly understood.

Taken together, these data show that the importance of uncovering molecular events in the decidua seems pivotal to our better understanding of the regulation of term labor. To date, most of the studies that focus on gene, protein, hormonal, or other molecular changes in relation to labor utilize whole chorioamniotic membranes but fail to pinpoint the involvement of the decidua in these changes. Therefore, the aim of this study was to compare decidual gene expression patterns in normal term delivery with or without labor. Based on the current state of knowledge about the cellular pathways involved in the activation of the decidua during labor, genes in the following categories were of interest to our study: (1) estrogen, progesterone, and prostaglandin signaling; (2) cytokines, chemokines, and chemokine receptors; (3) anti-inflammatory molecules with predominant decidual expression; (4) transcription factors involved in decidual development and immune cell differentiation; and (5) additional genes with predominant decidual expression.

## MATERIALS AND METHODS

### Ethics statement

Chorioamniotic membrane samples and maternal plasma specimens were retrieved from the Bank of Biological Specimens at Wayne State University, the Detroit Medical Center, and the Perinatology Research Branch of the Eunice Kennedy Shriver National Institute of Child Health and Human Development, National Institutes of Health, U.S. Department of Health and Human Services (NICHD/NIH/DHHS). Approval from the Institutional Review Boards of NICHD and Wayne State Univer-

sity for the collection and utilization of biological materials as well as written informed consent from all human subjects was obtained prior to the collection of samples.

### Human subjects, clinical specimens, and definitions

Women were included in the following gestational age-matched groups: (1) spontaneous term labor and delivery (TIL) (n = 14); and (2) elective Cesarean section at term without labor (TNL) (n = 15). There were no significant differences among the study groups regarding demographic and clinical characteristics (Table 1). Patients with multiple pregnancies or neonates having congenital or chromosomal abnormalities were excluded. No women had any medical or obstetrical complications or clinical or histological signs of chorioamnionitis, and they delivered neonates of appropriate birth weight for their gestational age, according to the national birth weight distribution curve.<sup>74</sup> Labor was defined by the presence of regular uterine contractions at a frequency of at least two contractions every 10 minutes and cervical changes that resulted in delivery.<sup>74</sup>

### Placental histopathological examinations

Five-micrometer-thick sections of formalin-fixed, paraffin-embedded chorioamniotic membrane specimens (n = 29) were cut and mounted on Superfrost slides (Erie Scientific LLC, Portsmouth, NH, USA). After deparaffinization, the slides were rehydrated and stained with hematoxylin and eosin. Two pathologists, who were blinded to the clinical outcome, evaluated the slides according to published criteria.<sup>75,76</sup>

### Sample preparation

Fifteen-micrometer-thick sections of snap-frozen chorioamniotic membranes were embedded in Tissue-Tek O.C.T. Compound (Tissue-Tek 4538, Sakura Finetek USA, Inc., Torrance, CA, USA), sectioned with a Leica CM3050S Cryostat (Leica Micro-

**Table 1.** Demographic and clinical characteristics of the study groups

Variable	Spontaneous term labor (n = 14)	Term no labor (n = 15)	p-value
Maternal age (yr)	25 (20–29)	27 (23–34)	.13
Race			.60
African American	12 (85.7)	11 (73.3)	-
Caucasian	1 (7.1)	3 (20.0)	-
Other	1 (7.1)	1 (6.7)	-
Maternal weight (kg)	64 (62–85)	75 (68–82)	.13
Body mass index (kg/m <sup>2</sup> )	26.7 (24.6–32.9)	28.3 (27.4–30.9)	.49
Gravidity	3 (2.5–5)	3 (2–4)	.76
Gestational age at delivery (wk)	39.1 (38.7–39.3)	39.0 (38.9–39.1)	.31
Birth weight (g)	3,230 (3,083–3,602)	3,490 (3,185–3,560)	.66

Values are presented as median (interquartile range) or number (%).

systems, Wetzlar, Germany), and then mounted on polyethylene membrane glass slides (Leica) and stored at  $-80^{\circ}\text{C}$  until use. All further steps were carried out at room temperature. Slides were quickly treated with graded ethanol solutions (Val Tech Diagnostics, Inc., Pittsburgh, PA, USA), and then cleared by immersion in xylene (Dynamic Diagnostics Inc., Livonia, MI, USA). All steps were carried out under RNase-free conditions.

### Laser microdissection

Decidual cell populations were collected from snap-frozen chorioamniotic membranes ( $n = 29$ ,  $\sim 18 \text{ mm}^2/\text{sample}$ ) using laser microdissection with an LMD 6000 laser microdissection microscope (Leica Microsystems). To compare decidual and non-decidual gene expression, chorioamniotic cell populations were also collected for three cases. Dissections were completed within 60–90 minutes after the slides were thawed to ensure minimal RNA degradation. Cell populations were cut and collected in extraction buffer (Arcturus Picopure RNA Isolation Kit, Applied Biosystems, Life Technologies Corporation, Foster City, CA, USA), and then incubated at  $42^{\circ}\text{C}$  for 30 minutes. Cell extracts were vortexed, centrifuged at  $800 \times g$ , and stored at  $-80^{\circ}\text{C}$  until use.

### Total RNA isolation

Total RNA was isolated from laser-microdissected and digested samples using the Arcturus Picopure RNA Isolation Kit (Applied Biosystems), according to the manufacturer's protocol. The Ambion DNA-free Kit (Life Technologies) was used to remove genomic DNA. Total RNA concentrations were measured using the NanoDrop ND-1000 Spectrophotometer (Thermo Scientific, Wilmington, DE, USA). The Bioanalyzer 2100 (Agilent Technologies, Santa Clara, CA, USA) was used to determine RNA integrity and quality. RNA samples were then stored at  $-80^{\circ}\text{C}$  until use.

### Complementary DNA preparation and quantitative real-time PCR

The SuperScript III First-Strand Kit (Life Technologies) was used to generate cDNA. TaqMan gene expression assays (Applied Biosystems) (Table 2), the Biomark System (Fluidigm, San Francisco, CA, USA), and Fluidigm's 96.96 Dynamic Array Chip were used for high-throughput quantitative real-time polymerase chain reaction (qRT-PCR). Pre-amplification procedures included combining cDNA with TaqMan PreAmp Master Mix (Applied Biosystems) and Pooled Assay Mix (Applied Biosystems), according to the manufacturer's instructions. The reaction was performed with a thermal cycler for one cycle at  $95^{\circ}\text{C}$  for 10 minutes fol-

lowed by another 14 cycles at  $95^{\circ}\text{C}$  for 15 seconds and at  $60^{\circ}\text{C}$  for 4 minutes. The Fluidigm 96.96 Dynamic Array Chip (Fluidigm) was used to perform the qRT-PCR assays. The 96.96 Array Chip was primed in an Integrated Fluidic Circuit Controller with control fluid. The TaqMan gene expression assays were mixed with  $2 \times$  assay loading reagent (Fluidigm) and loaded into the assay inlet on the chip after priming. The sample inlet was filled with a mixture of preamplified cDNA, TaqMan Universal PCR Master Mix (Applied Biosystems), and  $20 \times$  sample loading reagent (Fluidigm), and then the chip was loaded into the BioMark System. The cycle threshold (Ct) value of each reaction was obtained with the Fluidigm qRT-PCR analysis software.

### Immunohistochemistry

Five-micrometer-thick sections of formalin-fixed, paraffin-embedded chorioamniotic membrane specimens were cut and placed on salinized TruBond 380 adhesive microscope slides (Tru Scientific, Bellingham, WA, USA). Immunostainings were performed using the Leica Bond-Max (Leica Microsystems) and the Ventana Discovery (Ventana Medical Systems, Inc., Tucson, AZ, USA) autostainer systems, as detailed in Supplementary Table S1. The Bond Polymer Refine Detection Kit (Leica Microsystems) and DAB-MAP HRP Kit (Ventana Medical Systems) were used to detect the chromogenic reaction of horseradish peroxidase. Negative control immunostainings were performed by omitting primary antibodies and using either rabbit IgG or mouse IgG isotype control antibodies (Supplementary Fig. S1).

### Semi-quantitative immunoscore

Semi-quantitative immunoscore was carried out by scoring five random fields in each tissue section with an immunoreactive score modified from a previous publication.<sup>77</sup> The two examiners were blinded to the clinical information. Immunostaining intensity was graded as follows: 0, negative; 1, weak; 2, intermediate; and 3, strong.

### Immunoassays

Maternal plasma concentrations of CCL2 (chemokine C-C motif ligand-2), CCL5, and IL-8 were determined by sensitive and specific immunoassays (Meso Scale Discovery, Rockville, MD, USA), according to the manufacturer's protocol. Briefly, 1% (w/v) Blocker B Solution was dispensed into each well of the pre-coated plates and incubated with vigorous shaking for 1 hour at room temperature. Plates were then washed three times with phosphate buffered saline (PBS) and 0.05% Tween 20 (Sigma-Aldrich Corporation, St. Louis, MO, USA). Subsequently, samples

or calibrators were dispensed into separate wells and incubated for 2 hours with vigorous shaking at room temperature. Plates were then washed three times with PBS and 0.05% Tween-20,

followed by the addition of the 1 × Detection Antibody Solution (Meso Scale Discovery) into each well and incubation for 2 hours with vigorous shaking at room temperature. The plates were

**Table 2.** TaqMan assays used for qRT-PCR expression profiling

Group	Gene symbol	Gene name	Assay ID	
Chemokines	<i>CCL1</i>	Chemokine (C-C motif) ligand 1	Hs00171072_m1	
	<i>CCL2</i>	Chemokine (C-C motif) ligand 2	Hs00234140_m1	
	<i>CCL5</i>	Chemokine (C-C motif) ligand 5	Hs00174575_m1	
	<i>CCL7</i>	Chemokine (C-C motif) ligand 7	Hs00171147_m1	
	<i>CCL15</i>	Chemokine (C-C motif) ligand 15	Hs00361122_m1	
	<i>CXCL1</i>	Chemokine (C-X-C motif) ligand 1	Hs00236937_m1	
	<i>CXCL5</i>	Chemokine (C-X-C motif) ligand 5	Hs00171085_m1	
	<i>CXCL10</i>	Chemokine (C-X-C motif) ligand 10	Hs00171042_m1	
	<i>CXCL12</i>	Chemokine (C-X-C motif) ligand 12	Hs00171022_m1	
	<i>IL8</i>	Interleukin-8/Chemokine (C-X-C motif) ligand 8	Hs00174103_m1	
	Chemokine receptors	<i>CCR1</i>	Chemokine (C-C motif) receptor 1	Hs00174298_m1
		<i>CCR2</i>	Chemokine (C-C motif) receptor 2	Hs00356601_m1
<i>CCR5</i>		Chemokine (C-C motif) receptor 5	Hs00152917_m1	
<i>CCR8</i>		Chemokine (C-C motif) receptor 8	Hs00174764_m1	
<i>CXCR1</i>		Chemokine (C-X-C motif) receptor 1	Hs01921207_s1	
<i>CXCR2</i>		Chemokine (C-X-C motif) receptor 2	Hs01011557_m1	
<i>CXCR3</i>		Chemokine (C-X-C motif) receptor 3	Hs00171041_m1	
<i>CXCR4</i>		Chemokine (C-X-C motif) receptor 4	Hs00976734_m1	
Cytokines	<i>IL1A</i>	Interleukin 1, alpha	Hs99999028_m1	
	<i>IL1B</i>	Interleukin 1, beta	Hs00174097_m1	
	<i>IL4</i>	Interleukin 4	Hs00174122_m1	
	<i>IL10</i>	Interleukin 10	Hs00174086_m1	
	<i>IL17A</i>	Interleukin 17A	Hs00174383_m1	
	<i>IFNG</i>	Interferon, gamma	Hs99999041_m1	
	<i>TNF</i>	Tumor necrosis factor alpha	Hs00174128_m1	
Galectins	<i>LGALS1</i>	Lectin, galactoside-binding, soluble, 1	Hs00169327_m1	
	<i>LGALS3</i>	Lectin, galactoside-binding, soluble, 3	Hs00173587_m1	
	<i>LGALS8</i>	Lectin, galactoside-binding, soluble, 8	Hs00374634_m1	
	<i>LGALS9A</i>	Lectin, galactoside-binding, soluble, 9	Hs00371321_m1	
Endometrial proteins	<i>IGFBP1</i>	Insulin-like growth factor-binding protein 1	Hs00236877_m1	
	<i>PAEP</i>	Progesterone-associated endometrial protein	Hs01046125_m1	
HOX transcription factors	<i>HOXA9</i>	Homeobox A9	Hs00266821_m1	
	<i>HOXA10</i>	Homeobox A10	Hs00172012_m1	
	<i>HOXA11</i>	Homeobox A11	Hs00194149_m1	
Prostaglandin signaling molecules	<i>PTGER2</i>	Prostaglandin E receptor 2	Hs00168754_m1	
	<i>PTGES</i>	Prostaglandin E synthase	Hs00610420_m1	
	<i>PTGS2</i>	Prostaglandin-endoperoxide synthase 2	Hs01573471_m1	
Sex steroid receptors	<i>ESR1</i>	Estrogen receptor 1	Hs00174860_m1	
	<i>ESR2</i>	Estrogen receptor 2 (beta)	Hs01100356_m1	
	<i>PGRMC1</i>	Progesterone receptor membrane component 1	Hs00198499_m1	
	<i>PGRMC2</i>	Progesterone receptor membrane component 2	Hs01128672_m1	
	<i>PGR</i>	Progesterone receptor	Hs01556702_m1	
T-cell transcription factors	<i>FOXP3</i>	Forkhead box P3	Hs01085835_m1	
	<i>GATA3</i>	GATA binding protein 3	Hs00231122_m1	
	<i>RORC</i>	RAR-related orphan receptor gamma	Hs01076122_m1	
	<i>TBX21</i>	T-box 21	Hs00203436_m1	
Housekeeping genes	<i>GAPDH</i>	Glyceraldehyde 3-phosphate dehydrogenase	Hs99999905_m1	
	<i>RPLPO</i>	Ribosomal protein, large, P0	Hs99999902_m1	

qRT-PCR, quantitative real-time polymerase chain reaction; RAR, retinoic acid-receptor.

washed three times, and then  $2 \times$  Read Buffer T (Meso Scale Discovery) was added to each well; the signals were read by the SECTOR 2400 Imager (Meso Scale Discovery). Standard curves were generated and the assay values of the samples were interpolated from the curves. The sensitivity of the assays for CCL2, CCL5, and IL-8 was 0.769 pg/mL, 0.514 pg/mL, and 0.213 pg/mL, respectively.

### Statistical analysis

Demographic and clinical data were analyzed using SPSS ver. 19.0 (SPSS Inc., Chicago, IL, USA). All other data analysis was conducted within the R statistical environment.<sup>78</sup> When analyzing qRT-PCR data, group comparisons were evaluated via a gene-wise linear model where gene expression was treated as a response and explained by the group variable while adjusting for gestational age. The derived p-values were further adjusted for false discovery rate (FDR)<sup>79</sup> to account for simultaneous testing on multiple genes. An FDR-adjusted p-value (pFDR value) of .1 and a 1.5-fold change were used as thresholds for significance.

Immunoassay data were log-transformed, matched with the qRT-PCR data for samples from the TIL and TNL groups, and represented by a scatter plot. Pearson correlations and their p-values were computed to assess the linear associations of measurements between enzyme-linked immunosorbent assay and qRT-PCR. To account for heterogeneous sample groups, an ANOVA comparison between the linear models was also conducted.

Immunoreactive scores generated by two independent examiners were averaged to represent the quantity of a given protein in a given patient sample. The two patient groups were compared by using a t-test. A p-value of  $< .05$  was considered statistically significant.

## RESULTS

### Genes with the highest expression in the decidua at term gestation

Genes included in this expression profiling study (Table 2) were selected according to their biological plausibility and/or their implication in decidual physiology. As a good concordance with published evidence, insulin-like growth factor-binding protein 1 (*IGFBP1*) and galectin-1 (*LGALS1*), genes with predominant endometrial expression among all human tissues,<sup>80,81</sup> had their highest expression in the decidua at term gestation among the 46 tested genes (Fig. 1A). The expression of *IGFBP1* was 28-fold higher ( $p = .01$ ) in cells microdissected from the

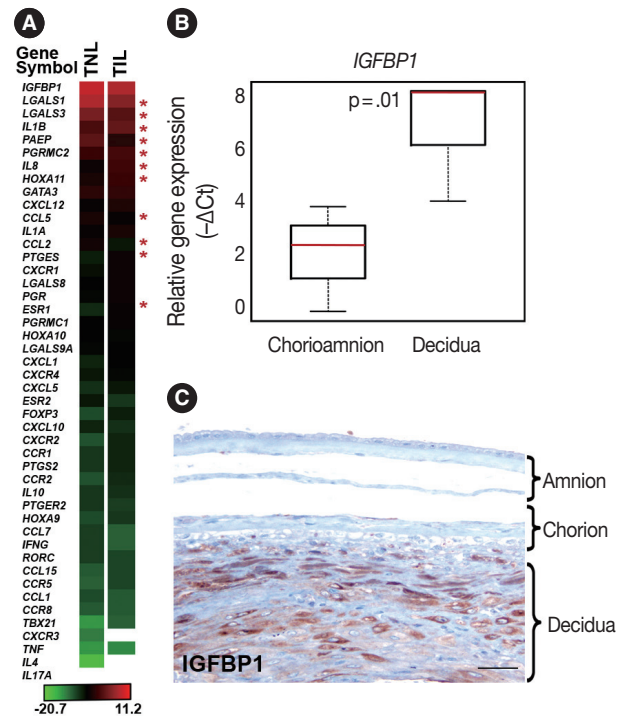


**Fig. 1.** Decidual gene expression in healthy term gestation. (A) The heatmap depicts the mean gene expression levels in the decidua of women with no labor at term (TNL,  $n = 15$ ) or those in term labor (TIL,  $n = 14$ ). Bar denotes color coding for gene expression levels ( $-\Delta Ct$ ). Out of all genes sorted by their expression levels, the expression of insulin-like growth factor-binding protein 1 (*IGFBP1*) was the highest and interleukin 17A (*IL17A*) expression could not be detected with our method. Stars depict the differentially expressed genes in the decidua between TIL and TNL cases. White areas represent non-detectable gene expression. (B) The relative expression of *IGFBP1* was 28-fold higher in the decidua compared to the chorioamnion as visualized in box-plots ( $p = .01$ ). (C) A representative micrograph shows that *IGFBP1* immunostaining was strong in the decidua, while it was weak in the chorion and amnion layers of the membrane.

decidua than in those collected from the chorioamnion as an internal control in our study (Fig. 1B). This is in accord with the strong *IGFBP-1* immunoreactivity in the decidual layer compared to the faint *IGFBP-1* immunostaining in other layers of the membranes (Fig. 1C), confirming the accurate isolation of decidual cell populations by laser microdissection.

### Genes with differential expression in the decidua in term labor

The expression of 11 genes was significantly different in TIL cases compared to TNL cases. These genes encode for sex steroid receptors, chemokines, cytokines, and galectins as well as an endometrial protein, a prostaglandin synthesis enzyme, and a transcription factor involved in uterine development.

**Genes involved in sex steroid signaling and decidual development**

Among the sex steroid receptor genes, estrogen receptor 1 (*ESR1*) and the progesterone receptor membrane component 2

(*PGRMC2*) had differential expression between the groups (Fig. 1A). *ESR1* had an 8.1-fold (pFDR = .032) while *PGRMC2* had a 1.7-fold (pFDR = .096) higher expression in TIL cases com-

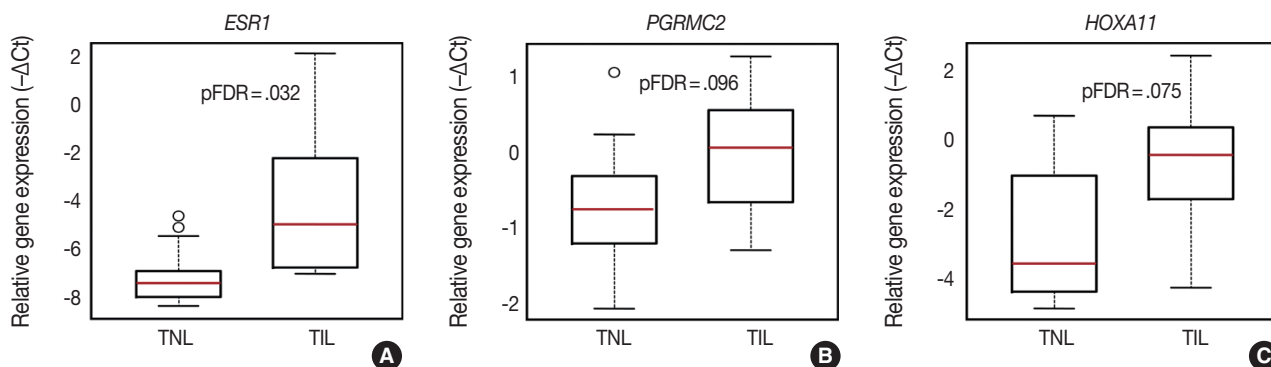


**Fig. 2.** Differential expression of genes involved in sex steroid signaling and decidual development. Box-plots represent gene expression levels ( $-\Delta Ct$ ) in the decidua of women with no labor at term (TNL,  $n = 15$ ) or those in term labor (TIL,  $n = 14$ ). Estrogen receptor 1 (*ESR1*) (A), progesterone receptor membrane component 2 (*PGRMC2*) (B), and homeobox A11 (*HOXA11*) (C) expression was higher in TIL cases compared to TNL cases (8.1-fold, false discovery rate-adjusted p-value [pFDR] = .032; 1.7-fold, pFDR = .096; 4-fold, pFDR = .032, respectively).

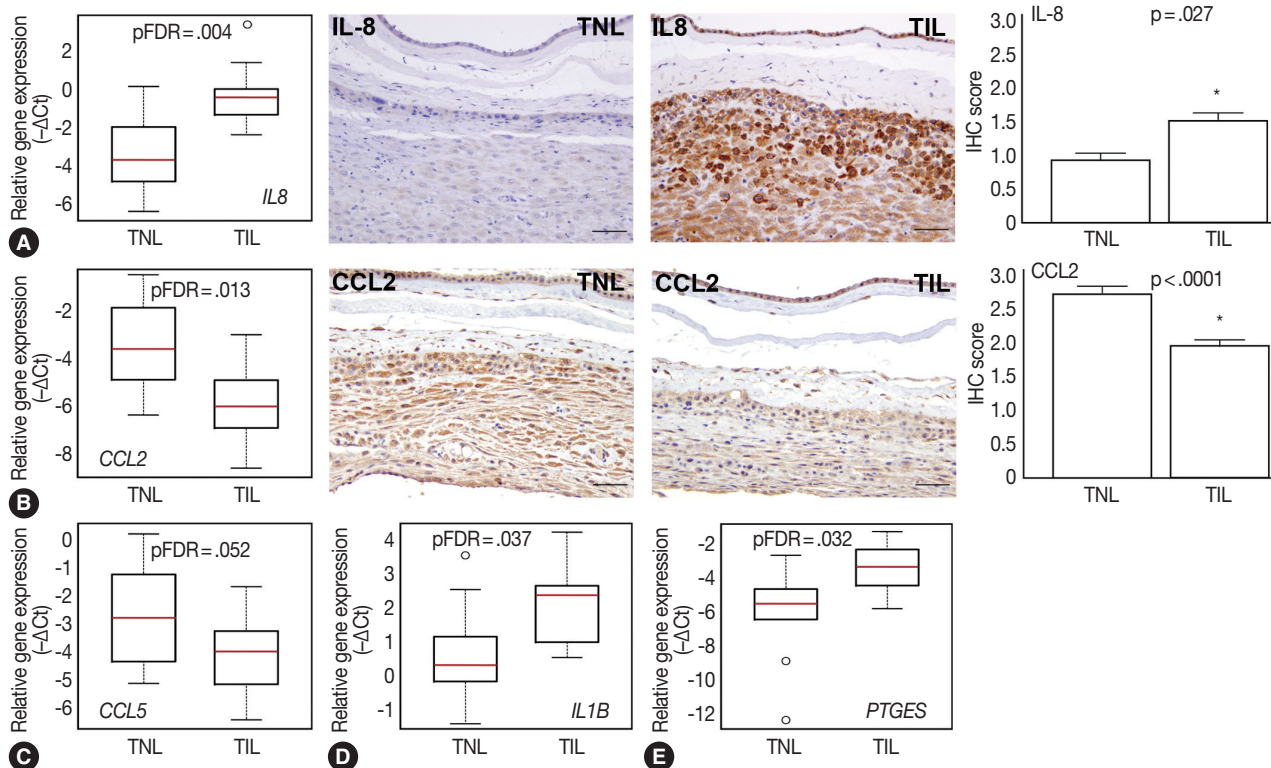


**Fig. 3.** Differential expression of chemokines, cytokines, and prostaglandin signaling genes. Box-plots represent gene expression levels ( $-\Delta Ct$ ), while immunohistochemical (IHC) staining and immunoscoring show protein abundance in the decidua of women with no labor at term (TNL,  $n = 15$ ) or those in term labor (TIL,  $n = 14$ ). (A) Relative mRNA expression of interleukin 8 (*IL8*) in the decidua was higher in TIL cases than in TNL cases (7.3-fold, false discovery rate-adjusted p-value [pFDR] = .004; left panel). IHC staining confirmed higher expression of IL-8 in TIL cases than in TNL cases (middle panels), also quantified by immunoscoring (right panel; TIL 1.5 vs TNL 0.9;  $p = .027$ ). (B, C) Relative mRNA expression of chemokine C-C motif ligand 2 (*CCL2*) and *CCL5* in the decidua was lower in TIL cases than in TNL cases (8.7-fold, pFDR = .013; 3.5-fold, pFDR = .052, respectively; left panel). IHC staining confirmed lower *CCL2* protein expression in TIL cases than in TNL cases (middle panels), also quantified by immunoscoring (right panel; TIL 1.9 vs TNL 2.7;  $p < .0001$ ). (D, E) Relative decidua mRNA expression of *IL1B* and *PTGES* was higher in TIL cases than in TNL cases (2.8-fold, pFDR = .037; 6.7-fold, pFDR = .032, respectively).

pared to TNL cases (Fig. 2A, B). Among the tested *HOX* genes involved in decidualization, *HOXA11* had the highest expression in the decidua (Fig. 1A), and it had higher expression in TIL cases compared to TNL cases (4-fold, pFDR = .075) (Fig. 2C).

#### Chemokine, cytokine, and prostaglandin signaling genes

Among the investigated chemokine genes, *IL8*, *CCL5*, and *CCL2* were the most abundantly expressed genes in the decidua (Fig. 1A). Two of these genes had differential expression between TIL cases and TNL cases (Fig. 3A–C). *IL8* expression was higher in TIL cases compared to TNL cases at the RNA (7.3-fold, pFDR = .004) and protein (immunohistochemistry [IHC] score, TIL 1.5 vs TNL 0.9;  $p = .027$ ) levels (Fig. 3A). In contrast, there were low expressions of *CCL2* in TIL cases compared to TNL cases at the mRNA (8.7-fold, pFDR = .013) and protein (IHC score, TIL 1.9 vs TNL 2.7;  $p < .0001$ ) levels (Fig. 3B). Decidual *CCL5* mRNA expression levels were lower in TIL cases compared to TNL cases (3.5-fold, pFDR = .052) (Fig. 3C).

Compared to the tested cytokine genes, *IL1B* had the strongest

expression in the decidua (Fig. 1A) and had an increased expression in TIL cases compared to TNL cases (2.8-fold, pFDR = .037) (Fig. 3D). Furthermore, among the prostaglandin signaling pathway genes, prostaglandin E synthase (*PTGES*) had higher expression levels in TIL cases compared to TNL cases (6.7-fold, pFDR = .032) (Fig. 3E).

#### Genes encoding anti-inflammatory proteins

Among the tested galectin genes, *LGALS1* and *LGALS3* had lower expression levels in TIL cases compared to TNL cases (*LGALS1*: 5.2-fold, pFDR = .039; *LGALS3*: 4.1-fold, pFDR = .075) (Fig. 4A, B). These findings were confirmed by immunostaining, as galectin-1 and galectin-3 proteins had decreased expression levels in TIL cases compared to TNL cases (galectin-1 IHC score, TIL 2.1 vs TNL 2.6,  $p = .016$ ; galectin-3 IHC score, TIL 1.4 vs TNL 2.0,  $p = .041$ ) (Fig. 4A, B).

Among the genes encoding for endometrial proteins, *PAEP*, one of the most abundantly expressed genes in the decidua,<sup>53</sup> had reduced expression levels in TIL cases compared to TNL cases

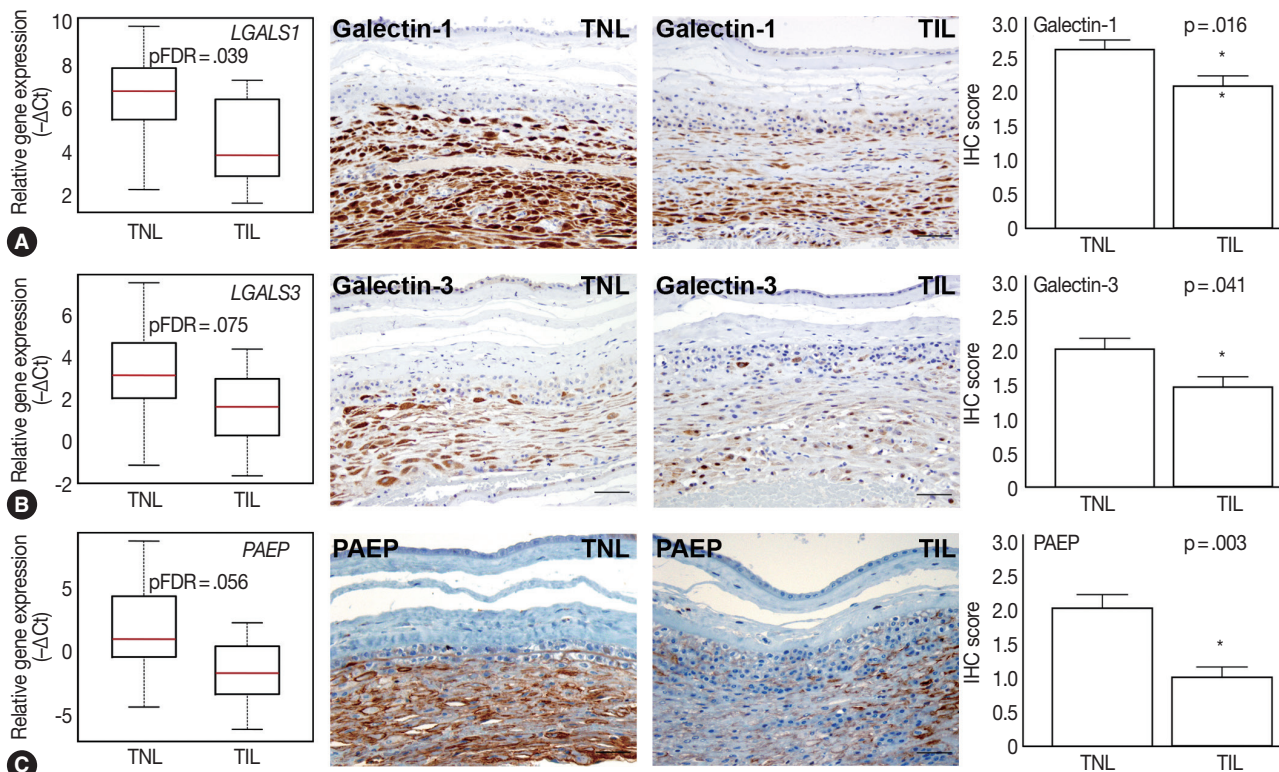


**Fig. 4.** Differential expression of anti-inflammatory mediators in the decidua. Box-plots represent gene expression levels ( $-\Delta Ct$ ), while immunohistochemical (IHC) staining and immunoscore show protein abundance in the decidua of women with no labor at term (TNL,  $n = 15$ ) or those in term labor (TIL,  $n = 14$ ). Galectin-1 (*LGALS1*) (A), galectin-3 (*LGALS3*) (B), and progesterone-associated endometrial protein (*PAEP*) (C) gene expression was lower in TIL cases than in TNL cases (5.2-fold, false discovery rate-adjusted p-value [pFDR] = .039; 4.1-fold, pFDR = .075; 12.6-fold, pFDR = .056, respectively). IHC staining confirmed lower galectin-1 (TIL 2.1 vs TNL 2.6,  $p = .016$ ) (A), galectin-3 (B) (TIL 1.4 vs TNL 2.0,  $p = .041$ ), and *PAEP* (C) (TIL 1.0 vs TNL 2.0,  $p = .003$ ) expression in TIL cases than in TNL cases.

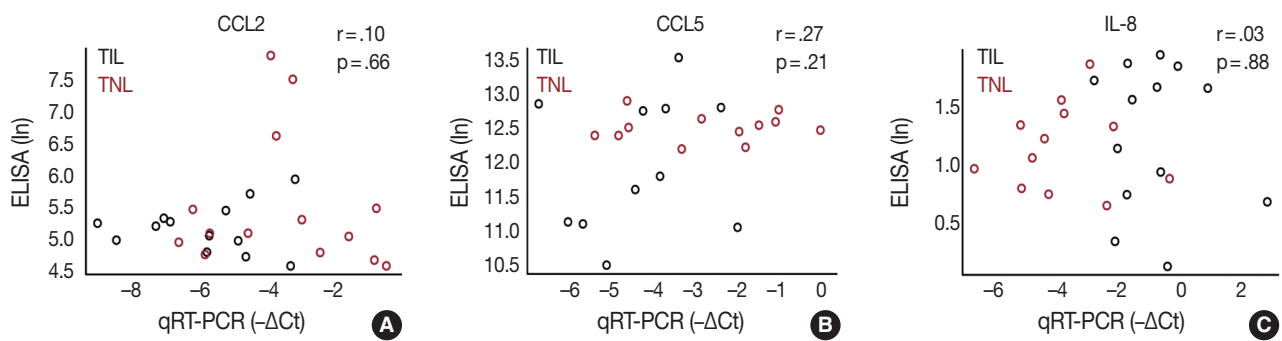


**Fig. 5.** Correlation analyses between decidual gene expression and maternal plasma concentrations of chemokines. (A–C) The scatterplots demonstrate the absence of correlation between the decidual gene expression and maternal plasma concentrations of secreted chemokines chemokine C-C motif ligand 2 (CCL2) ( $r = .10$ ,  $p = .66$ ), CCL5 ( $r = .27$ ,  $p = .21$ ), and interleukin 8 (IL-8) ( $r = .03$ ,  $p = .88$ ) in women with no labor at term (TNL,  $n = 15$ ) or those in term labor (TIL,  $n = 14$ ). ELISA, enzyme-linked immunosorbent assay; qRT-PCR, quantitative real-time polymerase chain reaction.

(12.6-fold,  $pFDR = .056$ ) (Fig. 4C). PAEP protein levels were also weaker in TIL cases compared to TNL cases (IHC score, TIL 1.0 vs TNL 2.0;  $p = .003$ ) (Fig. 4C).

#### Comparison of decidual gene expression and maternal plasma concentrations of chemokines

In order to determine whether the local, decidual differential expression of chemokines is also reflected by changes in their systemic concentrations, maternal plasma samples collected at the time of delivery were analyzed with immunoassays for CCL2, CCL5, and IL-8. There was no difference in the concentrations of these chemokines between patient groups, and there was no correlation between the mRNA expression of these chemokines in the decidua and their protein concentrations in maternal plasma samples obtained from the same patients (Fig. 5).

## DISCUSSION

### Principal findings of the study

(1) Transcriptomic analysis revealed differences in the expression of genes involved in developmental, signaling, and inflammatory pathways between decidual samples collected from women who delivered at TIL and TNL; (2) genes with the highest expression in the decidua at term included *IGFBP1*, *LGALS1*, and *PAEP*; (3) the expression of *ESR1*, *HOXA11*, *IL1B*, *IL8*, *PGRMC2*, and *PTGES* was higher in TIL cases compared to TNL cases; (4) the expression of *CCL2*, *CCL5*, *LGALS1*, *LGALS3*, and *PAEP* was lower in TIL cases compared to TNL cases; (5) immunostaining confirmed a high expression of IL-8 and a low expression of CCL2, galectin-1, and galectin-3 in TIL cases compared to TNL cases; and (6) no correlation between decidual gene expression and maternal plasma protein concentra-

tions of CCL2, CCL5, and IL-8 was found.

### Significance of differential gene expression in the decidua

Parturition is a result of pro-inflammatory processes in various gestational tissues, which interact with and orchestrate the terminal pathway of spontaneous labor.<sup>82</sup> This common pathway includes anatomical, physiological, biochemical, endocrinological, immunological, and clinical events that occur in the mother and her fetus. Based on targeted and high-dimensional studies, a growing body of evidence has shown that all uterine components of this terminal pathway—the increased myometrial contractility and cervical ripening as well as the activation of the decidua/fetal membranes—undergo pro-inflammatory changes during labor.<sup>82,83</sup> In spite of the similarities in gene expression signatures, the activation of certain biological pathways in various gestational tissues may be different. Unfortunately, the biological processes taking place in the decidua during spontaneous term parturition have been relatively underinvestigated. This is corroborated by a recent meta-analysis focusing on the transcriptomics of all human gestational tissues in the context of term and preterm birth.<sup>84</sup> This study found that the most commonly studied tissues are the placenta (61%), the fetal membranes (12%), and the myometrium (12%), while the decidua had been the focus of only less than 5% of all investigations.<sup>84</sup> Therefore, our study aimed to fill this gap in our understanding of the role of the decidua in the orchestration of pro-inflammatory pathways during spontaneous term parturition.

### Hormonal regulation of the decidua during labor

The appropriate hormonal regulation and development of the decidua are fundamental in the establishment and maintenance of pregnancy. Among hormones, estrogen and progesterone play

the most important roles in these processes mediated by estrogen and progesterone receptors,<sup>6</sup> while HOX genes are essential for endometrial development, growth, and differentiation under the regulation of estrogen and progesterone.<sup>85,86</sup> Therefore, we studied the most relevant estrogen and progesterone receptors as well as HOX genes to gain insights into their decidual expression changes during term parturition. Members of all of these gene groups were found to have transcriptional changes, since *ESR1*, *PGRMC2*, and *HOXA11* mRNA expression was increased in TIL cases compared to TNL cases.

ER $\alpha$  (*ESR1*) is an estrogen receptor predominantly expressed in the uterus, and its expression elevates in the human myometrium during labor.<sup>87,88</sup> Interestingly, the increased relative abundance of ER $\alpha$ , but not ER $\beta$  (*ESR2*) mRNA, is associated with increased PR-A expression and PR-A/PR-B expression ratios in the human myometrium, which, in turn, is responsible for the inhibition of progesterone's anti-inflammatory actions mediated by PR-B.<sup>7,8</sup> A similar increase in the PR-A/PR-B expression ratio was found in the decidua during term labor,<sup>8</sup> which, in conjunction with our finding on the increased decidual *ESR1* expression, may suggest that a similar regulatory process is effective in the decidua during term labor.

The decidualization of the human endometrium depends on the actions of progesterone<sup>89</sup> promoted by the expression of nuclear PR isoforms in decidual cells,<sup>90</sup> which are central to the genomic actions of progesterone. Moreover, the cellular responsiveness to this hormone also depends on the expression of the membrane progesterone receptors (mPR $\alpha$ , mPR $\beta$ , and mPR $\gamma$ ) and their adaptor proteins (PGRMC1 and PGRMC2), which act via a fast, "non-genomic pathway."<sup>91</sup> Several studies support the idea that membrane PRs actually suppress the actions of nuclear PRs and promote myometrial contractility<sup>92</sup> and that the PGRMC adaptor proteins are pivotal in enhancing the cell surface expression and receptor functions of membrane PRs.<sup>93</sup> A recent proteomics study on chorionic decidua revealed PGRMC2 to be up-regulated in samples from term and preterm labor samples compared to samples obtained from non-laboring women,<sup>94</sup> implicating this protein in the hormonal regulation of parturition. Our finding of the higher decidual expression of PGRMC2 in laboring women, compared to non-laboring women, corroborates these earlier results and may suggest that this "non-genomic pathway" may be involved in the functional progesterone withdrawal in the decidua.

Previous *in vitro* studies showed that estrogen and progesterone facilitated the expression of developmental HOX genes (*HOXA9*, *HOXA10*, and *HOXA11*) in human decidual cells at term,

among which *HOXA10* and *HOXA11* are expressed in the decidua from early pregnancy<sup>85,86</sup> throughout gestation.<sup>95,96</sup> Furthermore, it has been shown that the interactions of HOXA11 with CCAAT/enhancer binding protein beta (CEBPB) and forkhead box O1 (FOXO1) are especially necessary for the regulation of decidual gene expression during the decidualization of endometrial fibroblasts.<sup>97,98</sup> In this context, it is of interest that FOXO1 can promote IL-1 $\beta$ , IL-6, IL-8, and cyclooxygenase-2 expression and the release of prostaglandins as well as matrix metalloproteinase 9 (MMP-9) expression and MMP activity as detected in pregnant human myometrial cells.<sup>99</sup> It is possible that the increased *HOXA11* expression in the decidua of the TIL patients, compared to the TNL patients, who participated in our study may be related to the upstream regulatory events including *ESR1* up-regulation and estrogen-mediated actions as well as downstream pro-inflammatory pathways involving the cooperation of HOXA11 with FOXO1 in the TIL cases.

#### Chemokines, cytokines, and pro-inflammatory mediators in labor

Among the mediators of pro-inflammatory pathways, chemokines are essential for the recruitment and activation of various immune cell populations into distinct tissue compartments at the maternal-fetal interface.<sup>100-102</sup> These infiltrating immune cells are involved in the orchestration of local inflammation, partly by releasing cytokines that regulate prostaglandin production.<sup>45</sup> Members of these gene groups of chemokines, cytokines, and receptors (*CCL2*, *CCL5*, *IL8*, *IL1B*, and *PTGES*) that we studied had transcriptional changes in TIL cases compared to TNL cases.

*CCL2* and *CCL5* have been extensively studied in different gestational tissues as important inducers of immune cell infiltration. *CCL2*, a monocyte chemoattractant, has been studied in the context of pro-inflammatory changes and monocyte influx/activation in the myometrium, cervix, and fetal membranes during term and preterm parturition.<sup>103-105</sup> *CCL5*, another monocyte chemoattractant that has additional activity toward T cells, has been implicated in the regulation of inflammatory responses and in the recruitment of macrophages to the implantation site in early pregnancy.<sup>106-108</sup> The role of *CCL5* in the mechanisms of human parturition is demonstrated by the increased concentration of this chemokine in the amniotic fluid of women who undergo term labor compared to those who deliver at term without labor.<sup>109</sup> The concentration of *CCL5* is also higher in the amniotic fluid of women who undergo term or preterm labor with microbial invasion of the amniotic cavity than in those without this complication,<sup>107</sup> supporting the role for *CCL5* in the regula-

tion of the host response against intrauterine infection. Of note, monocytes/macrophages are the second most abundant leukocyte population in the human decidua that contributes to parturition by expressing pro-inflammatory mediators (e.g., IL-1 $\beta$ , IL-6, TNF $\alpha$ , and prostaglandins) and that plays a key role in tissue remodeling.<sup>15</sup> Our findings demonstrate higher *CCL2* and *CCL5* mRNA expression in the decidua prior to labor, compared to TIL cases, which was validated for *CCL2* expression at the protein level. These results are in agreement with rodent experiments showing pre-partum recruitment of macrophages into the uterine/decidual tissues in rats and mice<sup>110-113</sup> and with the increase in the proportion of human choriodecidual macrophages from preterm to term gestation.<sup>114</sup> Although the proportion of these macrophages among human choriodecidual leukocytes does not change before and after term labor,<sup>114</sup> it was recently demonstrated that macrophages undergo a pro-inflammatory M1-like polarization in the decidua during spontaneous term labor.<sup>115</sup> Therefore, it is likely that macrophages infiltrate the human decidua prior to term gestation, and they acquire an M1 phenotype prior to parturition.<sup>115</sup> Concentrations of *CCL2* and *CCL5* in the maternal blood of women who undergo term labor are similar to those in women who undergo term delivery without labor.<sup>116</sup> In accord with this earlier finding, there was no correlation between decidual mRNA abundance and concentrations of *CCL2* and *CCL5* in maternal plasma, which further confirms their importance in the local inflammatory process. Overall, these data suggest that monocyte recruitment into the decidua and macrophage-mediated decidual inflammatory processes are early events during parturition and precede the *CCL2*- and *CCL5*-mediated recruitment of monocytes into other uterine tissue compartments.

The local elevated expression of IL-8, a chief chemokine and activator of neutrophils,<sup>117,118</sup> fulfills multifaceted roles, both in humans and other examined mammals during term and preterm parturition,<sup>119,120</sup> and may determine the timing of neutrophil infiltration and activation in various compartments in the uterine cavity,<sup>121</sup> where these cells release cytokines and MMPs to contribute to labor and post-partum wound sealing and healing.<sup>122</sup> Accordingly, the expression of IL-8 by a variety of cells—including monocytes/macrophages, fibroblasts, decidual stromal cells, cervical epithelial cells, and amnion cells<sup>27,123</sup>—have been reported to be elevated in gestational tissues and amniotic fluid in term and preterm parturition.<sup>124-133</sup> Our findings of the higher expression of IL-8 mRNA and protein in the decidua in TIL cases compared to TNL cases support these previous reports. Interestingly, studies that focus on IL-8 concentrations in maternal blood

are controversial. One study found significantly higher IL-8 plasma concentrations in laboring women compared to non-laboring women who delivered at term or preterm,<sup>116</sup> while another study showed no difference between these groups.<sup>134</sup> Our study agrees with the latter, since we found no difference between the TNL and TIL groups and no correlation between decidual mRNA expression and maternal plasma concentrations of IL-8.

IL-1 $\beta$  and its receptor IL1R are widely expressed in human gestational tissues, where they are involved in the pro-inflammatory response during labor;<sup>135-137</sup> this is supported by the higher IL-1 $\beta$  concentrations in the amniotic, choriodecidual, and placental tissues<sup>31</sup> as well as in the amniotic fluid<sup>138</sup> of patients with spontaneous labor compared to those who delivered at term without labor. Our data suggests that the increased decidual *IL1B* expression in TIL cases compared to TNL cases is consistent with these earlier findings and further highlights the key role of IL-1 $\beta$  in parturition. As functional evidence, *in vitro* experiments with human decidual cells revealed that IL-1 $\beta$  treatment alters the expression of genes and microRNAs that function in pro-inflammatory signaling, including the induction of numerous cytokines and chemokines,<sup>139</sup> such as IL-8,<sup>140</sup> as well as prostaglandin production.<sup>141</sup>

Prostaglandins have central roles in the separate but integrated physiological events of parturition: fetal membrane rupture, cervical dilatation, myometrial contractility, placental separation, and uterine involution.<sup>142-144</sup> There is abundant evidence showing that the decidua, among other gestational tissues, is a major source of prostaglandins in parturition.<sup>144</sup> PGF<sub>2 $\alpha$</sub>  is the most abundant prostaglandin in the decidua, but decidual cells can also produce detectable amounts of prostaglandin E<sub>2</sub> (PGE<sub>2</sub>),<sup>145</sup> which was increased in decidual cells obtained during spontaneous vaginal delivery at term compared to those obtained before the onset of labor.<sup>146</sup>

Among the prostaglandin-synthesizing enzymes, PTGS2, the rate-limiting enzyme of the synthesis of prostaglandins, was found to be up-regulated in the human myometrium,<sup>102</sup> but not in the decidua,<sup>147</sup> for TIL cases compared to TNL cases. Among other key enzymes of prostaglandin synthesis, PTGES, involved in PGE<sub>2</sub> synthesis, was elevated in the amnion in TIL cases.<sup>148</sup> The same study found increased expression levels of AKR1C3 (aldo-keto reductase), involved in PGF<sub>2 $\alpha$</sub>  synthesis, in the choriodecidia in TIL cases.<sup>148</sup> The expression of CBR1 (carbonyl reductase), responsible for the conversion of PGE<sub>2</sub> to PGF<sub>2 $\alpha$</sub>  and thereby favoring PGF<sub>2 $\alpha$</sub>  elevation, was also detected in the decidua,<sup>148</sup> but no difference was found in its expression between

TIL and TNL cases. Our study only investigated *PTGES* from these three genes and found its increased expression in TIL cases compared to TNL cases. Since various pro-inflammatory cytokines<sup>149</sup> and estrogen can induce *PTGES* expression requiring nuclear factor  $\kappa$ B and estrogen receptor signaling pathways, respectively,<sup>150</sup> the elevated expression of *PTGES* during labor in the decidual inflammatory microenvironment is not surprising. All of these results may suggest that local inflammatory pathways induce *PTGES*, leading to heightened  $\text{PGE}_2$  production as well as increased production of  $\text{PGF}_{2\alpha}$  via enzymatic conversion.

### Transcription factors for T-cell polarization in labor

The proper balance between innate and adaptive immune cells in gestational tissues is required to sustain pregnancy, and an alteration of this balance may lead to labor at term or preterm gestation.<sup>121</sup> Most studies investigated the roles of macrophage and neutrophil infiltration into gestational tissues during labor; however, the importance of adaptive immune responses in parturition has only recently been recognized.<sup>114</sup> In human pregnancies, almost one-half of the leukocytes in the decidua basalis are  $\text{CD}3^+$  T cells in term cases compared to the low decidual percentage (6%–30%) of these immune cells observed in the first trimester.<sup>151</sup> It has been proposed that the high proportion of T cells concentrated in the choriondecidua is a result of the expansion of the total number of  $\text{CD}4^+$   $\text{CD}25^+$  regulatory T cells (Tregs)<sup>114</sup> induced by pregnancy.<sup>152,153</sup> It was suggested that these T cells are recruited during term gestation, particularly during parturition, to participate in the cascade of inflammatory mediators at the maternal-fetal interface.<sup>154</sup> Choriondecidual  $\text{CD}4^+$  T cells display a memory-like phenotype and express high levels of IL-1 $\beta$ , TNF $\alpha$ , and MMP-9 in spontaneous labor at term,<sup>114</sup> suggesting that these immune cells have an effector-memory phenotype.

The finding that different T helper (Th) lymphocyte populations (Th1, Th2, Treg, and Th17) could be identified in the early human decidua based on the expression of their lineage-specific differentiation transcription factors (TBX21, GATA3, FOXP3, and RORC)<sup>155</sup> gave us the idea to investigate various Th subsets in term decidua. The mRNAs for all of these transcription factors were found to be expressed, showing the presence of the four Th subsets in term decidua; however, no differences were found between the two groups. It is possible that certain differences could have been detected using phenotypic T-cell markers as previously reported<sup>156</sup> and also that the functional state of these cells may change during parturition.

### Anti-inflammatory molecules in labor

While we detected an increased decidual expression among key pro-inflammatory mediator genes, the mRNA and protein expression levels of some anti-inflammatory molecules (galectin-1, galectin-3, and PAEP) were lower in TIL cases compared to TNL cases.

Galectins are secreted proteins, multifunctional regulators of fundamental cellular processes. This is due to their high affinity for  $\beta$ -galactosides, which allow their binding to a broad range of glycosylated proteins critical for cell-cell and cell-extracellular matrix interactions<sup>157</sup> and the regulation of inflammation and immune responses.<sup>158</sup> Some galectins with strong expression at the maternal-fetal interface have been implicated in key functions of pregnancy maintenance in eutherian mammals.<sup>80,159,160</sup> Among these, galectin-1 and galectin-3 are expressed in the decidua under the regulation of sex steroids both in humans and mice<sup>54,80,161,162</sup> and are involved in decidual embryo implantation.<sup>163</sup> Of importance, decidual galectin-1 is one of the most potent mediators of maternal-fetal immune tolerance acting through multiple mechanisms, including the induction of tolerogenic dendritic cells, which, in turn, promote the expansion of IL-10-secreting regulatory T cells, as evidenced in mice.<sup>164</sup> Galectin-1 also has the ability to induce the apoptosis of Th1 cells, thereby causing a shift toward the Th2-type immune response, which is favorable during pregnancy.<sup>165</sup> Extracellular galectin-3 also has pro-apoptotic activity<sup>166</sup> and, thus, may have similar apoptotic functions compared to galectin-1 in the decidua. Our findings show decreased decidual *LGALS1* and *LGALS3* expression, which suggests that galectin-1 and galectin-3 may have important roles in the regulation of decidual immune cell populations and in the maintenance of a local microenvironment that favors progesterone production and pregnancy maintenance.

PAEP, also known as glycodeclin, placental protein 14, and progesteragen-dependent endometrial protein, is a glycoprotein that has several isoforms according to its glycosylation pattern.<sup>167,168</sup> The most abundant glycodeclin isoform, glycodeclin-A, is highly expressed in the decidua<sup>53</sup> and has major anti-inflammatory properties.<sup>169</sup> Decidual PAEP expression is regulated by progesterone,<sup>170</sup> and its immunoregulatory actions require estrogen priming.<sup>171</sup> This is in agreement with the role of PAEP as a potent regulator of predominant immune cell lineages at the maternal-fetal interface<sup>172</sup> and the capability of PAEP to induce the apoptosis of activated T cells,<sup>173</sup> the inhibition of monocyte chemotaxis,<sup>174</sup> and the induction of monocyte apoptosis.<sup>175</sup> Our results demonstrate decreased PAEP mRNA abundance and protein expression in TIL cases compared to TNL cases, which

may suggest that glycodelin-A, similar to galectins, is involved in the maintenance of a local immune balance in the decidua.

Our study also targeted the investigation of anti-inflammatory cytokines, but neither the decidual mRNA expression of *IL4* nor *IL10* changed with labor status at term. This may support other findings demonstrating no differences between IL-10 protein levels in decidual cells isolated from women who underwent labor compared to those who did not undergo labor at term.<sup>47</sup> However, the basal choriodecidual production rates of IL-10 have been found to be significantly decreased with labor,<sup>176</sup> which relates to our findings on PAEP and galectins. This suggests that changes may also occur in IL-10 mRNA/protein expression at certain time-points during term labor, and that IL-10 may also be a part of the local molecular mechanisms that main-

tain decidual quiescence during pregnancy.

### Strengths and limitations

The strengths of our study include the precise collection of decidual cells using laser microdissection, which allowed insights into decidual transcriptomic changes during spontaneous term parturition. High-throughput qRT-PCR enabled the parallel investigation of 46 genes involved in a large number of pathways. Immunostaining and semiquantitative immunoscore of tissue sections from the same chorioamniotic membranes supported the decidual investigation of differentially expressed genes at the protein level. The comparisons between local decidual and maternal systemic expression of certain genes and their protein products in the same patients provided an additional strength of our

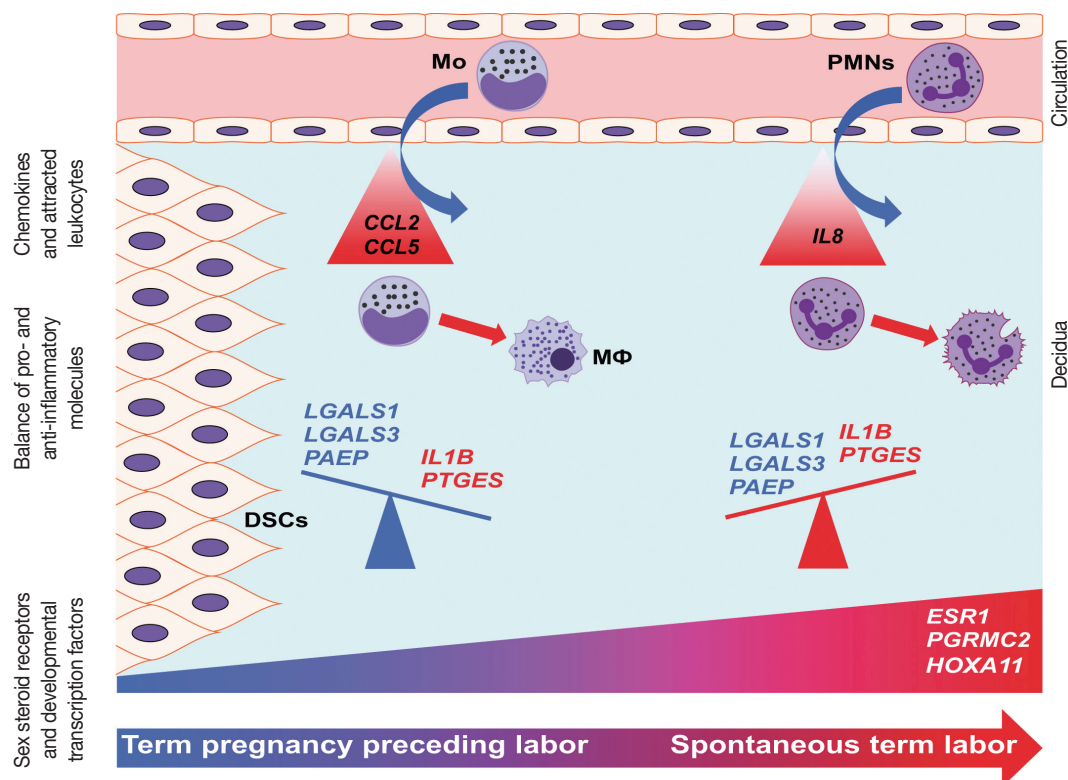


**Fig. 6.** Conceptual framework. The increased decidual expression of a signaling factor responsible for decidual maturation and development (*HOXA11*) is preceded by the increased expression of chemokines (*CCL2* and *CCL5*), which may stimulate the early recruitment of monocytes into the decidua as the onset of labor approaches. These immune cells will be activated by the local microenvironment and contribute to the orchestration of inflammation. With the initiation of parturition, the decidual expression of anti-inflammatory mediators (*LGALS1*, *LGALS3*, and *PAEP*) decreases, while the expression of pro-inflammatory mediators (*IL1B* and *PTGES*) and steroid receptors (*ESR1* and *PGRMC2*) increases, contributing to “functional progesterone withdrawal” and heightened inflammation, eventually leading to uterine contractions, cervical ripening, and membrane rupture. The relatively late increase of *IL8* expression will be followed by the recruitment of neutrophils, which plays a key role in tissue repair. These results strengthen earlier findings on the decidua being the earliest among gestational tissues that get primed during parturition. *CCL2*, chemokine C-C motif ligand 2; *CCL5*, chemokine C-C motif ligand 5; DSCs, decidual stromal cells; *ESR1*, estrogen receptor 1; *HOXA11*, homeobox A11; *IL1B*, interleukin-1 $\beta$ ; *IL8*, interleukin 8; *LGALS1*, galectin-1; *LGALS3*, galectin-3; Mo, monocytes; M $\Phi$ , macrophages; *PAEP*, progesterone-associated endometrial protein; *PGRMC2*, progesterone receptor membrane component 2; PMNs, neutrophil granulocytes; *PTGES*, prostaglandin E synthase.

study. This approach is unique since previous studies mainly focused on the investigation of the fetal membranes as a whole without illustrating which part of the membranes is responsible for the parturition-specific changes.

Limitations of our study included the relatively small sample sizes due to the technical limitations (low yield, high labor intensity, and slow workspace) of laser microdissection. Many parturition-related molecules as well as alternative splicing variants of the examined genes have not been investigated since the tiny amount of RNA samples, which could be obtained with our methodology, only allowed the study of a maximum of 48 genes in our high-throughput qRT-PCR system. That is why we selected several key parturition-related genes with well-characterized decidual expression in spontaneous term labor as positive controls for our study as well as many other genes not yet characterized in the context of term labor. Since we examined gene expression signatures at two time-points, it was not possible to analyze in detail the exact temporal changes in the cascade of decidual gene expression changes as term parturition progressed.

### Conclusions

Our data proposes that, with the initiation of parturition, the decidual expression of anti-inflammatory mediators decreases while the expression of pro-inflammatory mediators and steroid receptors increases, affecting downstream signaling pathways that lead to chorioamniotic membrane weakening and myometrial contractions (Fig. 6). Our results agree with earlier findings that suggest that the decidua is one of the earliest gestational tissues that becomes primed during parturition. Nevertheless, functional studies are required to further explore and establish a causal link between the pathways that were found in our descriptive study during term labor.

### Electronic Supplementary Material

Supplementary materials are available at the Journal of Pathology and Translational Medicine (<http://jpatholtm.org>).

### Conflicts of Interest

No potential conflict of interest relevant to this article was reported.

### Acknowledgments

The authors thank Lorraine Nikita, Newaj Abdullah, Ryan Cantarella, Ruowen Liu, Dayna Sheldon, and the nursing staff of the Perinatology Research Branch for their technical assistance, and Andrea Bernard, Maureen McGerty, and Sara Tipton

for their critical readings of the manuscript.

This research was supported, in part, by the Perinatology Research Branch, Division of Intramural Research, Eunice Kennedy Shriver National Institute of Child Health and Human Development, National Institutes of Health, U. S. Department of Health and Human Services (NICHD/NIH/DHHS); and, in part, by Federal funds from NICHD/NIH/DHHS under Contract No. HHSN275201300006C. Data analysis, interpretation, and manuscript writing were also supported by the Hungarian Academy of Sciences Momentum Grant “LP2014-7/2014” (to N.G.T.) and the OTKA-PD “104398” Grant (to A.B.). The funders had no role in the study design, data collection and analysis, decision to publish, or preparation of the manuscript.

### REFERENCES

1. Challis JR, Matthews SG, Gibb W, Lye SJ. Endocrine and paracrine regulation of birth at term and preterm. *Endocr Rev* 2000; 21: 514-50.
2. Iliodromiti Z, Antonakopoulos N, Sifakis S, *et al.* Endocrine, paracrine, and autocrine placental mediators in labor. *Hormones (Athens)* 2012; 11: 397-409.
3. Zakar T, Hertelendy F. Progesterone withdrawal: key to parturition. *Am J Obstet Gynecol* 2007; 196: 289-96.
4. Pepe GJ, Albrecht ED. Actions of placental and fetal adrenal steroid hormones in primate pregnancy. *Endocr Rev* 1995; 16: 608-48.
5. Tan H, Yi L, Rote NS, Hurd WW, Mesiano S. Progesterone receptor-A and -B have opposite effects on proinflammatory gene expression in human myometrial cells: implications for progesterone actions in human pregnancy and parturition. *J Clin Endocrinol Metab* 2012; 97: E719-30.
6. Csapo A. Progesterone block. *Am J Anat* 1956; 98: 273-91.
7. Mesiano S, Chan EC, Fitter JT, Kwek K, Yeo G, Smith R. Progesterone withdrawal and estrogen activation in human parturition are coordinated by progesterone receptor A expression in the myometrium. *J Clin Endocrinol Metab* 2002; 87: 2924-30.
8. Oh SY, Kim CJ, Park I, *et al.* Progesterone receptor isoform (A/B) ratio of human fetal membranes increases during term parturition. *Am J Obstet Gynecol* 2005; 193(3 Pt 2): 1156-60.
9. Mesiano S, Wang Y, Norwitz ER. Progesterone receptors in the human pregnancy uterus: do they hold the key to birth timing? *Reprod Sci* 2011; 18: 6-19.
10. Bollapragada S, Youssef R, Jordan F, Greer I, Norman J, Nelson S. Term labor is associated with a core inflammatory response in human fetal membranes, myometrium, and cervix. *Am J Obstet Gynecol* 2009; 200: 104.e1-11.
11. Hassan SS, Romero R, Haddad R, *et al.* The transcriptome of the

- uterine cervix before and after spontaneous term parturition. *Am J Obstet Gynecol* 2006; 195: 778-86.
12. Stephen GL, Lui S, Hamilton SA, *et al.* Transcriptomic profiling of human choriondecidua during term labor: inflammation as a key driver of labor. *Am J Reprod Immunol* 2015; 73: 36-55.
  13. Marvin KW, Keelan JA, Eykholt RL, Sato TA, Mitchell MD. Use of cDNA arrays to generate differential expression profiles for inflammatory genes in human gestational membranes delivered at term and preterm. *Mol Hum Reprod* 2002; 8: 399-408.
  14. Chaemsaihong P, Madan I, Romero R, *et al.* Characterization of the myometrial transcriptome in women with an arrest of dilatation during labor. *J Perinat Med* 2013; 41: 665-81.
  15. Thomson AJ, Telfer JF, Young A, *et al.* Leukocytes infiltrate the myometrium during human parturition: further evidence that labour is an inflammatory process. *Hum Reprod* 1999; 14: 229-36.
  16. Gomez-Lopez N, Tanaka S, Zaeem Z, Metz GA, Olson DM. Maternal circulating leukocytes display early chemotactic responsiveness during late gestation. *BMC Pregnancy Childbirth* 2013; 13 Suppl 1: S8.
  17. Sakamoto Y, Moran P, Bulmer JN, Searle RF, Robson SC. Macrophages and not granulocytes are involved in cervical ripening. *J Reprod Immunol* 2005; 66: 161-73.
  18. Haddad R, Tromp G, Kuivaniemi H, *et al.* Human spontaneous labor without histologic chorioamnionitis is characterized by an acute inflammation gene expression signature. *Am J Obstet Gynecol* 2006; 195: 394.e1-24.
  19. Gomez-Lopez N, Estrada-Gutierrez G, Jimenez-Zamudio L, Vega-Sanchez R, Vadillo-Ortega F. Fetal membranes exhibit selective leukocyte chemotactic activity during human labor. *J Reprod Immunol* 2009; 80: 122-31.
  20. Gomez-Lopez N, Laresgoiti-Servitje E, Olson DM, Estrada-Gutiérrez G, Vadillo-Ortega F. The role of chemokines in term and premature rupture of the fetal membranes: a review. *Biol Reprod* 2010; 82: 809-14.
  21. Gomez-Lopez N, Vadillo-Perez L, Nessim S, Olson DM, Vadillo-Ortega F. Choriondecidua and amnion exhibit selective leukocyte chemotaxis during term human labor. *Am J Obstet Gynecol* 2011; 204: 364.e9-16.
  22. Osman I, Young A, Jordan F, Greer IA, Norman JE. Leukocyte density and proinflammatory mediator expression in regional human fetal membranes and decidua before and during labor at term. *J Soc Gynecol Investig* 2006; 13: 97-103.
  23. Gomez-Lopez N, Vadillo-Perez L, Hernandez-Carbajal A, Godines-Enriquez M, Olson DM, Vadillo-Ortega F. Specific inflammatory microenvironments in the zones of the fetal membranes at term delivery. *Am J Obstet Gynecol* 2011; 205: 235.e15-24.
  24. Yellon SM, Mackler AM, Kirby MA. The role of leukocyte traffic and activation in parturition. *J Soc Gynecol Investig* 2003; 10: 323-38.
  25. Hua R, Pease JE, Sooranna SR, *et al.* Stretch and inflammatory cytokines drive myometrial chemokine expression via NF-kappaB activation. *Endocrinology* 2012; 153: 481-91.
  26. Kayisli UA, Mahutte NG, Arici A. Uterine chemokines in reproductive physiology and pathology. *Am J Reprod Immunol* 2002; 47: 213-21.
  27. Young A, Thomson AJ, Ledingham M, Jordan F, Greer IA, Norman JE. Immunolocalization of proinflammatory cytokines in myometrium, cervix, and fetal membranes during human parturition at term. *Biol Reprod* 2002; 66: 445-9.
  28. Montes MJ, Tortosa CG, Borja C, *et al.* Constitutive secretion of interleukin-6 by human decidual stromal cells in culture: regulatory effect of progesterone. *Am J Reprod Immunol* 1995; 34: 188-94.
  29. Romero R, Mazor M, Brandt F, *et al.* Interleukin-1 alpha and interleukin-1 beta in preterm and term human parturition. *Am J Reprod Immunol* 1992; 27: 117-23.
  30. Romero R, Mazor M, Sepulveda W, Avila C, Copeland D, Williams J. Tumor necrosis factor in preterm and term labor. *Am J Obstet Gynecol* 1992; 166: 1576-87.
  31. Keelan JA, Marvin KW, Sato TA, Coleman M, McCowan LM, Mitchell MD. Cytokine abundance in placental tissues: evidence of inflammatory activation in gestational membranes with term and preterm parturition. *Am J Obstet Gynecol* 1999; 181: 1530-6.
  32. Gomez-Lopez N, Hernandez-Santiago S, Lobb AP, Olson DM, Vadillo-Ortega F. Normal and premature rupture of fetal membranes at term delivery differ in regional chemotactic activity and related chemokine/cytokine production. *Reprod Sci* 2013; 20: 276-84.
  33. Christiaens I, Zaragoza DB, Guilbert L, Robertson SA, Mitchell BF, Olson DM. Inflammatory processes in preterm and term parturition. *J Reprod Immunol* 2008; 79: 50-7.
  34. Winkler M, Rath W. The role of cytokines in the induction of labor, cervical ripening and rupture of the fetal membranes. *Z Geburtshilfe Neonatol* 1996; 200 Suppl 1: 1-12.
  35. Bowen JM, Chamley L, Keelan JA, Mitchell MD. Cytokines of the placenta and extra-placental membranes: roles and regulation during human pregnancy and parturition. *Placenta* 2002; 23: 257-73.
  36. Mitchell MD, Dudley DJ, Edwin SS, Schiller SL. Interleukin-6 stimulates prostaglandin production by human amnion and decidual cells. *Eur J Pharmacol* 1991; 192: 189-91.
  37. Belt AR, Baldassare JJ, Molnár M, Romero R, Hertelendy F. The nuclear transcription factor NF-kappaB mediates interleukin-1beta-induced expression of cyclooxygenase-2 in human myometrial cells. *Am J Obstet Gynecol* 1999; 181: 359-66.
  38. Kniss DA, Rovin B, Fertel RH, Zimmerman PD. Blockade NF-kap-

- paB activation prohibits TNF-alpha-induced cyclooxygenase-2 gene expression in ED27 trophoblast-like cells. *Placenta* 2001; 22: 80-9.
39. Ackerman WE 4th, Summerfield TL, Vandre DD, Robinson JM, Kniss DA. Nuclear factor-kappa B regulates inducible prostaglandin E synthase expression in human amnion mesenchymal cells. *Biol Reprod* 2008; 78: 68-76.
  40. Li R, Ackerman WE 4th, Summerfield TL, *et al.* Inflammatory gene regulatory networks in amnion cells following cytokine stimulation: translational systems approach to modeling human parturition. *PLoS One* 2011; 6: e20560.
  41. Mitchell BF, Taggart MJ. Are animal models relevant to key aspects of human parturition? *Am J Physiol Regul Integr Comp Physiol* 2009; 297: R525-45.
  42. Maymon E, Ghezzi F, Edwin SS, *et al.* The tumor necrosis factor alpha and its soluble receptor profile in term and preterm parturition. *Am J Obstet Gynecol* 1999; 181(5 Pt 1): 1142-8.
  43. Romero R, Sepulveda W, Mazor M, *et al.* The natural interleukin-1 receptor antagonist in term and preterm parturition. *Am J Obstet Gynecol* 1992; 167(4 Pt 1): 863-72.
  44. Ammala M, Nyman T, Salmi A, Rutanen EM. The interleukin-1 system in gestational tissues at term: effect of labour. *Placenta* 1997; 18: 717-23.
  45. Keelan JA, Blumenstein M, Helliwell RJ, Sato TA, Marvin KW, Mitchell MD. Cytokines, prostaglandins and parturition: a review. *Placenta* 2003; 24 Suppl A: S33-46.
  46. Dudley DJ, Hunter C, Mitchell MD, Varner MW. Amniotic fluid interleukin-10 (IL-10) concentrations during pregnancy and with labor. *J Reprod Immunol* 1997; 33: 147-56.
  47. Jones CA, Finlay-Jones JJ, Hart PH. Type-1 and type-2 cytokines in human late-gestation decidual tissue. *Biol Reprod* 1997; 57: 303-11.
  48. Gotsch F, Romero R, Kusanovic JP, *et al.* The anti-inflammatory limb of the immune response in preterm labor, intra-amniotic infection/inflammation, and spontaneous parturition at term: a role for interleukin-10. *J Matern Fetal Neonatal Med* 2008; 21: 529-47.
  49. Dudley DJ, Hunter C, Varner MW, Mitchell MD. Elevation of amniotic fluid interleukin-4 concentrations in women with preterm labor and chorioamnionitis. *Am J Perinatol* 1996; 13: 443-7.
  50. Than NG, Romero R, Goodman M, *et al.* A primate subfamily of galectins expressed at the maternal-fetal interface that promote immune cell death. *Proc Natl Acad Sci U S A* 2009; 106: 9731-6.
  51. Barrientos G, Freitag N, Tirado-Gonzalez I, *et al.* Involvement of galectin-1 in reproduction: past, present and future. *Hum Reprod Update* 2014; 20: 175-93.
  52. Than NG, Romero R, Balogh A, *et al.* Galectins: Double-edged swords in the cross-roads of pregnancy complications and female reproductive tract inflammation and neoplasia. *J Pathol Transl Med* 2015; 49: 181-208.
  53. Julkunen M, Rutanen EM, Koskimies A, Ranta T, Bohn H, Seppala M. Distribution of placental protein 14 in tissues and body fluids during pregnancy. *Br J Obstet Gynaecol* 1985; 92: 1145-51.
  54. Phillips B, Knisley K, Weitlauf KD, Dorsett J, Lee V, Weitlauf H. Differential expression of two beta-galactoside-binding lectins in the reproductive tracts of pregnant mice. *Biol Reprod* 1996; 55: 548-58.
  55. Lockwood CJ, Paidas M, Krikun G, *et al.* Inflammatory cytokine and thrombin regulation of interleukin-8 and intercellular adhesion molecule-1 expression in first trimester human decidua. *J Clin Endocrinol Metab* 2005; 90: 4710-5.
  56. Huang SJ, Schatz F, Masch R, *et al.* Regulation of chemokine production in response to pro-inflammatory cytokines in first trimester decidual cells. *J Reprod Immunol* 2006; 72: 60-73.
  57. Sarno J, Schatz F, Huang SJ, Lockwood C, Taylor HS. Thrombin and interleukin-1beta decrease HOX gene expression in human first trimester decidual cells: implications for pregnancy loss. *Mol Hum Reprod* 2009; 15: 451-7.
  58. Segerer SE, Martignoni F, Bogdan A, *et al.* Thrombopoietin modulates the proliferation, migration and cytokine profile of decidual cell subsets during early gestation. *Mol Hum Reprod* 2013; 19: 361-8.
  59. Kim JS, Romero R, Cushenberry E, *et al.* Distribution of CD14+ and CD68+ macrophages in the placental bed and basal plate of women with preeclampsia and preterm labor. *Placenta* 2007; 28: 571-6.
  60. Kim SY, Romero R, Tarca AL, *et al.* Methylome of fetal and maternal monocytes and macrophages at the fetomaternal interface. *Am J Reprod Immunol* 2012; 68: 8-27.
  61. Paavola LG, Furth EE, Delgado V, *et al.* Striking changes in the structure and organization of rat fetal membranes precede parturition. *Biol Reprod* 1995; 53: 321-38.
  62. Norwitz ER, Robinson JN, Challis JR. The control of labor. *N Engl J Med* 1999; 341: 660-6.
  63. Mittal P, Romero R, Tarca AL, *et al.* A molecular signature of an arrest of descent in human parturition. *Am J Obstet Gynecol* 2011; 204: 177.e15-33.
  64. Norwitz ER, Bonney EA, Snegovskikh VV, *et al.* Molecular regulation of parturition: the role of the decidual clock. *Cold Spring Harb Perspect Med* 2015; 5: a023143.
  65. Menon R, Bonney EA, Condon J, Mesiano S, Taylor RN. Novel concepts on pregnancy clocks and alarms: redundancy and synergy in human parturition. *Hum Reprod Update* 2016; 22: 535-60.
  66. Daftary GS, Taylor HS. Implantation in the human: the role of HOX genes. *Semin Reprod Med* 2000; 18: 311-20.

67. Cermik D, Karaca M, Taylor HS. HOXA10 expression is repressed by progesterone in the myometrium: differential tissue-specific regulation of HOX gene expression in the reproductive tract. *J Clin Endocrinol Metab* 2001; 86: 3387-92.
68. Hsieh-Li HM, Witte DP, Weinstein M, *et al.* Hoxa 11 structure, extensive antisense transcription, and function in male and female fertility. *Development* 1995; 121: 1373-85.
69. Taylor HS. The role of HOX genes in the development and function of the female reproductive tract. *Semin Reprod Med* 2000; 18: 81-9.
70. Wong KH, Wintch HD, Capecchi MR. Hoxa11 regulates stromal cell death and proliferation during neonatal uterine development. *Mol Endocrinol* 2004; 18: 184-93.
71. Lu Z, Hardt J, Kim JJ. Global analysis of genes regulated by HOXA10 in decidualization reveals a role in cell proliferation. *Mol Hum Reprod* 2008; 14: 357-66.
72. Lynch VJ, Tanzer A, Wang Y, *et al.* Adaptive changes in the transcription factor HoxA-11 are essential for the evolution of pregnancy in mammals. *Proc Natl Acad Sci U S A* 2008; 105: 14928-33.
73. Xu B, Geerts D, Bu Z, *et al.* Regulation of endometrial receptivity by the highly expressed HOXA9, HOXA11 and HOXD10 HOX-class homeobox genes. *Hum Reprod* 2014; 29: 781-90.
74. Alexander GR, Himes JH, Kaufman RB, Mor J, Kogan M. A United States national reference for fetal growth. *Obstet Gynecol* 1996; 87: 163-8.
75. Redline RW. Placental pathology: a systematic approach with clinical correlations. *Placenta* 2008; 29 Suppl A: S86-91.
76. Kim CJ, Romero R, Kusanovic JP, *et al.* The frequency, clinical significance, and pathological features of chronic chorioamnionitis: a lesion associated with spontaneous preterm birth. *Mod Pathol* 2010; 23: 1000-11.
77. Than NG, Abdul Rahman O, Magenheimer R, *et al.* Placental protein 13 (galectin-13) has decreased placental expression but increased shedding and maternal serum concentrations in patients presenting with preterm pre-eclampsia and HELLP syndrome. *Virchows Arch* 2008; 453: 387-400.
78. R Development Core Team. R: a language and environment for statistical computing. Vienna: R Foundation for Statistical Computing, 2011.
79. Benjamini Y, Hochberg Y. Controlling the false discovery rate: a practical and powerful approach to multiple testing. *J R Stat Soc Series B Methodol* 1995; 57: 289-300.
80. Than NG, Romero R, Erez O, *et al.* Emergence of hormonal and redox regulation of galectin-1 in placental mammals: implication in maternal-fetal immune tolerance. *Proc Natl Acad Sci U S A* 2008; 105: 15819-24.
81. Han VK, Bassett N, Walton J, Challis JR. The expression of insulin-like growth factor (IGF) and IGF-binding protein (IGFBP) genes in the human placenta and membranes: evidence for IGF-IGFBP interactions at the fetomaternal interface. *J Clin Endocrinol Metab* 1996; 81: 2680-93.
82. Romero R, Espinoza J, Kusanovic JP, *et al.* The preterm parturition syndrome. *BJOG* 2006; 113 Suppl 3: 17-42.
83. Romero R, Espinoza J, Gotsch F, *et al.* The use of high-dimensional biology (genomics, transcriptomics, proteomics, and metabolomics) to understand the preterm parturition syndrome. *BJOG* 2006; 113 Suppl 3: 118-35.
84. Eidem HR, Ackerman WE 4th, McGary KL, Abbot P, Rokas A. Gestational tissue transcriptomics in term and preterm human pregnancies: a systematic review and meta-analysis. *BMC Med Genomics* 2015; 8: 27.
85. Taylor HS, Arici A, Olive D, Igarashi P. HOXA10 is expressed in response to sex steroids at the time of implantation in the human endometrium. *J Clin Invest* 1998; 101: 1379-84.
86. Taylor HS, Igarashi P, Olive DL, Arici A. Sex steroids mediate HOXA11 expression in the human peri-implantation endometrium. *J Clin Endocrinol Metab* 1999; 84: 1129-35.
87. Bisits AM, Smith R, Mesiano S, *et al.* Inflammatory aetiology of human myometrial activation tested using directed graphs. *PLoS Comput Biol* 2005; 1: 132-6.
88. Welsh T, Johnson M, Yi L, *et al.* Estrogen receptor (ER) expression and function in the pregnant human myometrium: estradiol via ERalpha activates ERK1/2 signaling in term myometrium. *J Endocrinol* 2012; 212: 227-38.
89. Brosens JJ, Hayashi N, White JO. Progesterone receptor regulates decidual prolactin expression in differentiating human endometrial stromal cells. *Endocrinology* 1999; 140: 4809-20.
90. Tan J, Paria BC, Dey SK, Das SK. Differential uterine expression of estrogen and progesterone receptors correlates with uterine preparation for implantation and decidualization in the mouse. *Endocrinology* 1999; 140: 5310-21.
91. Gellersen B, Fernandes MS, Brosens JJ. Non-genomic progesterone actions in female reproduction. *Hum Reprod Update* 2009; 15: 119-38.
92. Karteris E, Zervou S, Pang Y, *et al.* Progesterone signaling in human myometrium through two novel membrane G protein-coupled receptors: potential role in functional progesterone withdrawal at term. *Mol Endocrinol* 2006; 20: 1519-34.
93. Thomas P, Pang Y, Dong J. Enhancement of cell surface expression and receptor functions of membrane progesterone receptor alpha (mPRalpha) by progesterone receptor membrane component 1 (PGRMC1): evidence for a role of PGRMC1 as an adaptor protein for steroid receptors. *Endocrinology* 2014; 155: 1107-19.

94. Shankar R, Johnson MP, Williamson NA, *et al.* Molecular markers of preterm labor in the choriodecidual. *Reprod Sci* 2010; 17: 297-310.
95. Salih SM, Taylor HS. HOXA10 gene expression in human fallopian tube and ectopic pregnancy. *Am J Obstet Gynecol* 2004; 190: 1404-6.
96. Evans KN, Bulmer JN, Kilby MD, Hewison M. Vitamin D and placental-decidual function. *J Soc Gynecol Investig* 2004; 11: 263-71.
97. Lynch VJ, Brayer K, Gellersen B, Wagner GP. HoxA-11 and FOXO1A cooperate to regulate decidual prolactin expression: towards inferring the core transcriptional regulators of decidual genes. *PLoS One* 2009; 4: e6845.
98. Wagner GP, Kin K, Muglia L, Pavlicev M. Evolution of mammalian pregnancy and the origin of the decidual stromal cell. *Int J Dev Biol* 2014; 58: 117-26.
99. Lappas M. Forkhead box O1 (FOXO1) in pregnant human myometrial cells: a role as a pro-inflammatory mediator in human parturition. *J Reprod Immunol* 2013; 99: 24-32.
100. Dudley DJ, Edwin SS, Dangerfield A, Van Waggoner J, Mitchell MD. Regulation of cultured human chorion cell chemokine production by group B streptococci and purified bacterial products. *Am J Reprod Immunol* 1996; 36: 264-8.
101. Dudley DJ, Edwin SS, Van Wagoner J, Augustine NH, Hill HR, Mitchell MD. Regulation of decidual cell chemokine production by group B streptococci and purified bacterial cell wall components. *Am J Obstet Gynecol* 1997; 177: 666-72.
102. Mittal P, Romero R, Tarca AL, *et al.* Characterization of the myometrial transcriptome and biological pathways of spontaneous human labor at term. *J Perinat Med* 2010; 38: 617-43.
103. Tornblom SA, Klimaviciute A, Byström B, Chromek M, Brauner A, Ekman-Ordeberg G. Non-infected preterm parturition is related to increased concentrations of IL-6, IL-8 and MCP-1 in human cervix. *Reprod Biol Endocrinol* 2005; 3: 39.
104. Shynlova O, Tsui P, Dorogin A, Lye SJ. Monocyte chemoattractant protein-1 (CCL-2) integrates mechanical and endocrine signals that mediate term and preterm labor. *J Immunol* 2008; 181: 1470-9.
105. Esplin MS, Peltier MR, Hamblin S, *et al.* Monocyte chemotactic protein-1 expression is increased in human gestational tissues during term and preterm labor. *Placenta* 2005; 26: 661-71.
106. Jones RL, Hannan NJ, Kaitu'u TJ, Zhang J, Salamonsen LA. Identification of chemokines important for leukocyte recruitment to the human endometrium at the times of embryo implantation and menstruation. *J Clin Endocrinol Metab* 2004; 89: 6155-67.
107. Engert S, Rieger L, Kapp M, Becker JC, Dietl J, Kämmerer U. Profiling chemokines, cytokines and growth factors in human early pregnancy decidua by protein array. *Am J Reprod Immunol* 2007; 58: 129-37.
108. Li M, Wu ZM, Yang H, Huang SJ. NFkappaB and JNK/MAPK activation mediates the production of major macrophage- or dendritic cell-recruiting chemokine in human first trimester decidual cells in response to proinflammatory stimuli. *J Clin Endocrinol Metab* 2011; 96: 2502-11.
109. Athayde N, Romero R, Maymon E, *et al.* A role for the novel cytokine RANTES in pregnancy and parturition. *Am J Obstet Gynecol* 1999; 181: 989-94.
110. Mackler AM, Jezza G, Akin MR, McMillan P, Yellon SM. Macrophage trafficking in the uterus and cervix precedes parturition in the mouse. *Biol Reprod* 1999; 61: 879-83.
111. Shynlova O, Nedd-Roderique T, Li Y, Dorogin A, Nguyen T, Lye SJ. Infiltration of myeloid cells into decidua is a critical early event in the labour cascade and post-partum uterine remodelling. *J Cell Mol Med* 2013; 17: 311-24.
112. Hamilton S, Oomomian Y, Stephen G, *et al.* Macrophages infiltrate the human and rat decidua during term and preterm labor: evidence that decidual inflammation precedes labor. *Biol Reprod* 2012; 86: 39.
113. Srikhajon K, Shynlova O, Preechapornprasert A, Chanrachakul B, Lye S. A new role for monocytes in modulating myometrial inflammation during human labor. *Biol Reprod* 2014; 91: 10.
114. Gomez-Lopez N, Vega-Sanchez R, Castillo-Castrejon M, Romero R, Cubeiro-Arreola K, Vadillo-Ortega F. Evidence for a role for the adaptive immune response in human term parturition. *Am J Reprod Immunol* 2013; 69: 212-30.
115. Xu Y, Romero R, Miller D, *et al.* An M1-like macrophage polarization in decidual tissue during spontaneous preterm labor that is attenuated by rosiglitazone treatment. *J Immunol* 2016; 196: 2476-91.
116. Hamilton SA, Tower CL, Jones RL. Identification of chemokines associated with the recruitment of decidual leukocytes in human labour: potential novel targets for preterm labour. *PLoS One* 2013; 8: e56946.
117. Peveri P, Walz A, Dewald B, Baggiolini M. A novel neutrophil-activating factor produced by human mononuclear phagocytes. *J Exp Med* 1988; 167: 1547-59.
118. Kelly RW, Illingworth P, Baldie G, Leask R, Brouwer S, Calder AA. Progesterone control of interleukin-8 production in endometrium and chorio-decidual cells underlines the role of the neutrophil in menstruation and parturition. *Hum Reprod* 1994; 9: 253-8.
119. Gervasi MT, Chaiworapongsa T, Pacora P, *et al.* Phenotypic and metabolic characteristics of monocytes and granulocytes in pre-eclampsia. *Am J Obstet Gynecol* 2001; 185: 792-7.
120. Yuan M, Jordan F, McInnes IB, Harnett MM, Norman JE. Leukocytes are primed in peripheral blood for activation during term and preterm labour. *Mol Hum Reprod* 2009; 15: 713-24.

121. Gomez-Lopez N, StLouis D, Lehr MA, Sanchez-Rodriguez EN, Arenas-Hernandez M. Immune cells in term and preterm labor. *Cell Mol Immunol* 2014; 11: 571-81.
122. Giaglis S, Stoikou M, Grimolizzi F, *et al.* Neutrophil migration into the placenta: good, bad or deadly? *Cell Adh Migr* 2016; 10: 208-25.
123. Castillo-Castrejon M, Meraz-Cruz N, Gomez-Lopez N, *et al.* Chorionic cells from term human pregnancies show distinctive functional properties related to the induction of labor. *Am J Reprod Immunol* 2014; 71: 86-93.
124. Romero R, Ceska M, Avila C, Mazor M, Behnke E, Lindley I. Neutrophil attractant/activating peptide-1/interleukin-8 in term and preterm parturition. *Am J Obstet Gynecol* 1991; 165(4 Pt 1): 813-20.
125. Tashima LS, Millar LK, Bryant-Greenwood GD. Genes upregulated in human fetal membranes by infection or labor. *Obstet Gynecol* 1999; 94: 441-9.
126. Osman I, Young A, Ledingham MA, *et al.* Leukocyte density and pro-inflammatory cytokine expression in human fetal membranes, decidua, cervix and myometrium before and during labour at term. *Mol Hum Reprod* 2003; 9: 41-5.
127. Osmers RG, Bläser J, Kuhn W, Tschesche H. Interleukin-8 synthesis and the onset of labor. *Obstet Gynecol* 1995; 86: 223-9.
128. Sennström MK, Brauner A, Lu Y, Granström LM, Malmström AL, Ekman GE. Interleukin-8 is a mediator of the final cervical ripening in humans. *Eur J Obstet Gynecol Reprod Biol* 1997; 74: 89-92.
129. Sennström MB, Ekman G, Westergren-Thorsson G, *et al.* Human cervical ripening, an inflammatory process mediated by cytokines. *Mol Hum Reprod* 2000; 6: 375-81.
130. Charpigny G, Leroy MJ, Breuiller-Fouché M, *et al.* A functional genomic study to identify differential gene expression in the preterm and term human myometrium. *Biol Reprod* 2003; 68: 2289-96.
131. Bethin KE, Nagai Y, Sladek R, *et al.* Microarray analysis of uterine gene expression in mouse and human pregnancy. *Mol Endocrinol* 2003; 17: 1454-69.
132. Rehman KS, Yin S, Mayhew BA, Word RA, Rainey WE. Human myometrial adaptation to pregnancy: cDNA microarray gene expression profiling of myometrium from non-pregnant and pregnant women. *Mol Hum Reprod* 2003; 9: 681-700.
133. Axemo P, Brauner A, Pettersson M, Eriksson L, Rwamushajja E, Bergstrom S. Amniotic fluid interleukins in Swedish and Mozambican pregnant women. *Gynecol Obstet Invest* 1996; 41: 113-7.
134. Laham N, Rice GE, Bishop GJ, Ransome C, Brennecke SP. Interleukin 8 concentrations in amniotic fluid and peripheral venous plasma during human pregnancy and parturition. *Acta Endocrinol (Copenh)* 1993; 129: 220-4.
135. Romero R, Brody DT, Oyarzun E, *et al.* Infection and labor. III. Interleukin-1: a signal for the onset of parturition. *Am J Obstet Gynecol* 1989; 160(5 Pt 1): 1117-23.
136. Romero R, Wu YK, Brody DT, Oyarzun E, Duff GW, Durum SK. Human decidua: a source of interleukin-1. *Obstet Gynecol* 1989; 73: 31-4.
137. Steinborn A, Geisse M, Kaufmann M. Expression of cytokine receptors in the placenta in term and preterm labour. *Placenta* 1998; 19: 165-70.
138. Romero R, Parvizi ST, Oyarzun E, *et al.* Amniotic fluid interleukin-1 in spontaneous labor at term. *J Reprod Med* 1990; 35: 235-8.
139. Ibrahim SA, Ackerman WE 4th, Summerfield TL, Lockwood CJ, Schatz F, Kniss DA. Inflammatory gene networks in term human decidua define a potential signature for cytokine-mediated parturition. *Am J Obstet Gynecol* 2016; 214: 284.e1-47.
140. Dudley DJ, Trautman MS, Mitchell MD. Inflammatory mediators regulate interleukin-8 production by cultured gestational tissues: evidence for a cytokine network at the chorio-decidual interface. *J Clin Endocrinol Metab* 1993; 76: 404-10.
141. Alnaif B, Benzie RJ, Gibb W. Studies on the action of interleukin-1 on term human fetal membranes and decidua. *Can J Physiol Pharmacol* 1994; 72: 133-9.
142. Challis JR, Lye SJ. Parturition. *Oxf Rev Reprod Biol* 1986; 8: 61-129.
143. Challis JR, Lye SJ, Gibb W. Prostaglandins and parturition. *Ann N Y Acad Sci* 1997; 828: 254-67.
144. Olson DM. The role of prostaglandins in the initiation of parturition. *Best Pract Res Clin Obstet Gynaecol* 2003; 17: 717-30.
145. Mitchell MD, Edwin S, Romero RJ. Prostaglandin biosynthesis by human decidua: effects of inflammatory mediators. *Prostaglandins Leukot Essent Fatty Acids* 1990; 41: 35-8.
146. Skinner KA, Challis JR. Changes in the synthesis and metabolism of prostaglandins by human fetal membranes and decidua at labor. *Am J Obstet Gynecol* 1985; 151: 519-23.
147. Fuentes A, Spaziani EP, O'Brien WF. The expression of cyclooxygenase-2 (COX-2) in amnion and decidua following spontaneous labor. *Prostaglandins* 1996; 52: 261-7.
148. Phillips RJ, Fortier MA, López Bernal A. Prostaglandin pathway gene expression in human placenta, amnion and chorio-decidua is differentially affected by preterm and term labour and by uterine inflammation. *BMC Pregnancy Childbirth* 2014; 14: 241.
149. Phillips RJ, Al-Zamil H, Hunt LP, Fortier MA, López Bernal A. Genes for prostaglandin synthesis, transport and inactivation are differentially expressed in human uterine tissues, and the prostaglandin F synthase AKR1B1 is induced in myometrial cells by inflammatory cytokines. *Mol Hum Reprod* 2011; 17: 1-13.
150. Frasor J, Weaver AE, Pradhan M, Mehta K. Synergistic up-regulation of prostaglandin E synthase expression in breast cancer cells by 17beta-estradiol and proinflammatory cytokines. *Endocrinolo-*

- gy 2008; 149: 6272-9.
151. Vargas ML, Santos JL, Ruiz C, *et al.* Comparison of the proportions of leukocytes in early and term human decidua. *Am J Reprod Immunol* 1993; 29: 135-40.
  152. Aluvihare VR, Kallikourdis M, Betz AG. Regulatory T cells mediate maternal tolerance to the fetus. *Nat Immunol* 2004; 5: 266-71.
  153. Somerset DA, Zheng Y, Kilby MD, Sansom DM, Drayson MT. Normal human pregnancy is associated with an elevation in the immune suppressive CD25+ CD4+ regulatory T-cell subset. *Immunology* 2004; 112: 38-43.
  154. Gomez-Lopez N, Guilbert LJ, Olson DM. Invasion of the leukocytes into the fetal-maternal interface during pregnancy. *J Leukoc Biol* 2010; 88: 625-33.
  155. Mjösberg J, Berg G, Jenmalm MC, Ernerudh J. FOXP3+ regulatory T cells and T helper 1, T helper 2, and T helper 17 cells in human early pregnancy decidua. *Biol Reprod* 2010; 82: 698-705.
  156. Sindram-Trujillo AP, Scherjon SA, van Hulst-van Miert PP, Kanhai HH, Roelen DL, Claas FH. Comparison of decidual leukocytes following spontaneous vaginal delivery and elective cesarean section in uncomplicated human term pregnancy. *J Reprod Immunol* 2004; 62: 125-37.
  157. Hughes RC. Galectins as modulators of cell adhesion. *Biochimie* 2001; 83: 667-76.
  158. Rabinovich GA, Toscano MA. Turning 'sweet' on immunity: galectin-glycan interactions in immune tolerance and inflammation. *Nat Rev Immunol* 2009; 9: 338-52.
  159. Hirota Y, Burnum KE, Acar N, Rabinovich GA, Daikoku T, Dey SK. Galectin-1 markedly reduces the incidence of resorptions in mice missing immunophilin FKBP52. *Endocrinology* 2012; 153: 2486-93.
  160. Than NG, Romero R, Kim CJ, McGowen MR, Papp Z, Wildman DE. Galectins: guardians of eutherian pregnancy at the maternal-fetal interface. *Trends Endocrinol Metab* 2012; 23: 23-31.
  161. Szekeres-Bartho J, Halasz M, Palkovics T. Progesterone in pregnancy; receptor-ligand interaction and signaling pathways. *J Reprod Immunol* 2009; 83: 60-4.
  162. von Wolff M, Wang X, Gabius HJ, Strowitzki T. Galectin fingerprinting in human endometrium and decidua during the menstrual cycle and in early gestation. *Mol Hum Reprod* 2005; 11: 189-94.
  163. Tirado-González I, Freitag N, Barrientos G, *et al.* Galectin-1 influences trophoblast immune evasion and emerges as a predictive factor for the outcome of pregnancy. *Mol Hum Reprod* 2013; 19: 43-53.
  164. Blois SM, Ilarregui JM, Tometten M, *et al.* A pivotal role for galectin-1 in fetomaternal tolerance. *Nat Med* 2007; 13: 1450-7.
  165. Than NG, Kim SS, Abbas A, *et al.* Chorioamnionitis and increased galectin-1 expression in PPRM: an anti-inflammatory response in the fetal membranes? *Am J Reprod Immunol* 2008; 60: 298-311.
  166. Dumić J, Dabelić S, Flögel M. Galectin-3: an open-ended story. *Biochim Biophys Acta* 2006; 1760: 616-35.
  167. Seppälä M, Taylor RN, Koistinen H, Koistinen R, Milgrom E. Glycodelin: a major lipocalin protein of the reproductive axis with diverse actions in cell recognition and differentiation. *Endocr Rev* 2002; 23: 401-30.
  168. Than GN, Bohn H, Szabo DG. Advances in pregnancy-related protein research: functional and clinical applications. Boca Raton: CRC Press Inc., 1993.
  169. Alok A, Karande AA. The role of glycodelin as an immune-modulating agent at the feto-maternal interface. *J Reprod Immunol* 2009; 83: 124-7.
  170. Taylor RN, Savouret JF, Vaisse C, *et al.* Promegestone (R5020) and mifepristone (RU486) both function as progestational agonists of human glycodelin gene expression in isolated human epithelial cells. *J Clin Endocrinol Metab* 1998; 83: 4006-12.
  171. Li TC, Dalton C, Bolton AE, Ling E, Warren A, Cooke ID. An analysis of the variation of plasma concentrations of placental protein 14 in artificial cycles. *Fertil Steril* 1992; 57: 776-82.
  172. Bolton AE, Pockley AG, Clough KJ, *et al.* Identification of placental protein 14 as an immunosuppressive factor in human reproduction. *Lancet* 1987; 1: 593-5.
  173. Mukhopadhyay D, Sundereshan S, Rao C, Karande AA. Placental protein 14 induces apoptosis in T cells but not in monocytes. *J Biol Chem* 2001; 276: 28268-73.
  174. Vigne JL, Hornung D, Mueller MD, Taylor RN. Purification and characterization of an immunomodulatory endometrial protein, glycodelin. *J Biol Chem* 2001; 276: 17101-5.
  175. Alok A, Mukhopadhyay D, Karande AA. Glycodelin A, an immunomodulatory protein in the endometrium, inhibits proliferation and induces apoptosis in monocytic cells. *Int J Biochem Cell Biol* 2009; 41: 1138-47.
  176. Simpson KL, Keelan JA, Mitchell MD. Labor-associated changes in interleukin-10 production and its regulation by immunomodulators in human choriodecidua. *J Clin Endocrinol Metab* 1998; 83: 4332-7.

# A Small Case Series of Intravascular Large B-Cell Lymphoma with Unexpected Findings: Subset of Cases with Concomitant Extravascular Central Nervous System (CNS) Involvement Mimicking Primary CNS Lymphoma

Kate Poropatich · Dave Dittmann  
Yi-Hua Chen · Kirtee Raparia  
Kristy Wolniak · Juehua Gao

Department of Pathology, Northwestern University Feinberg School of Medicine, Chicago, IL, USA

Received: January 19, 2017  
Revised: February 13, 2017  
Accepted: February 15, 2017

## Corresponding Author

Kate Poropatich, MHS, MD  
Department of Pathology, Northwestern University Feinberg School of Medicine, Feinberg Pavilion 7-330, 251 E. Huron St., Chicago, IL 60611, USA  
Tel: +1-301-233-3533  
Fax: +1-312-503-0189  
E-mail: kate.poropatich@northwestern.edu

**Background:** Intravascular large B-cell lymphoma (IVLBCL) is a rare type of extranodal lymphoma with growth mainly in the lumina of vessels. We studied a small series of IVLBCL and focused on its central nervous system (CNS) involvement. **Methods:** Searching the medical records of Northwestern Memorial Hospital, we identified five cases of IVLBCL from January 2007 to January 2015. Clinical information, hematoxylin and eosin stained histologic slides and immunohistochemistry studies were reviewed for all cases. Polymerase chain reaction (PCR) analysis for the immunoglobulin (Ig) heavy and light chain gene rearrangement was performed on all five cases. **Results:** Three of the five cases of IVLBCL were autopsies. Patients' age ranged from 56 to 84. CNS involvement was present in two cases—in both patients, the CNS involvement showed an extravascular pattern with confluent sheet-like formation. PCR analysis confirmed that in one case the systemic intravascular and CNS extravascular components were clonally identical. **Conclusions:** In a small case series of IVLBCL, we observed that CNS involvement by IVLBCL often has an extravascular morphology, but is clonally identical to the intravascular counterpart by PCR analysis. As IVLBCL can have a rapidly progressing poor outcome, it should be kept in the differential diagnoses for patients presenting with lymphoma of the CNS. The presence of extravascular growth patterns in the CNS should not exclude IVLBCL as a diagnosis.

**Key Words:** Intravascular large B-cell lymphoma

Intravascular large B-cell lymphoma (IVLBCL) is a rare type of extranodal large B-cell lymphoma characterized by the selective growth of large lymphoma cells within smaller vessel lumina.<sup>1</sup> Classified as a “Mature B cell” neoplasm in the 2008 World Health Organization (WHO) classification,<sup>1</sup> IVLBCL is considered phenotypically and morphologically similar to diffuse large B cell lymphoma (DLBCL). However, with less than 500 reported cases, far less is understood about this non-Hodgkin's extranodal lymphoma. With vague clinical symptoms and the absence of lymphadenopathy characteristic of other lymphomas, this entity is thought to be widely underdiagnosed with clinical deterioration occurring rapidly and often resulting in the diagnosis being made at the time of autopsy.<sup>2-5</sup>

IVLBCL is divided into “Western” and “Eastern” variants, with the former showing a high frequency of central nervous system (CNS) and skin involvement and the latter frequently associated with bone marrow (BM) involvement and hemophago-

cytic syndrome.<sup>6</sup> When involving the BM, a predominantly sinusoidal pattern is seen.<sup>7</sup> The CNS is the most frequent site of involvement in IVLBCL, with over half of all cases presenting with neurologic symptoms and subsequent pathologic evidence of disease in the CNS.<sup>8-10</sup> It is important to recognize CNS involvement as early as possible in these patients as they have an overall worse clinical outcome and survival rate compared to other sites of involvement such as the skin.<sup>10</sup>

In a small subset of IVLBCL cases there is histomorphologic variability and perivascular involvement has been demonstrated in peripheral organs including the stomach, liver, adrenal glands, bladder, and testis.<sup>9,11-18</sup> However, little is known about the histologic heterogeneity of CNS IVLBCL. In particularly aggressive instances involving the CNS, concomitant minimal perivascular and extravascular tumor can be seen. To date, there have been over 10 documented cases of IVLBCL showing an extravascular growth pattern in the CNS, including some cases that presented

with mass-like lesions on magnetic resonance imaging (MRI).<sup>6,9,19-21</sup> Most striking about these cases is that they mimic patterns seen in primary CNS B-cell lymphoma based on angiocentric growth of large, atypical B cells that have a predilection for the leptomeninges.<sup>22</sup> It remains unclear what the incidence of this morphologic pattern is in the CNS of patients presenting with IVLBCL.

To further elucidate this question, we studied five cases of IVLBCL and observed two cases with CNS involvement that demonstrated an entirely perivascular and extravascular pattern without an intravascular component. For the first time, we used conventional polymerase chain reaction (PCR) to demonstrate that the extravascular CNS component has the same B-cell clone as the pure intravascular involvement seen in the rest of the organs.

## MATERIALS AND METHODS

### Sample characteristics

We searched medical records of Northwestern Memorial Hospital from January 2007 to January 2015, and identified five cases of IVLBCL that included three autopsies and two living patients. Clinical information was collected. Hematoxylin and eosin-stained diagnostic slides and immunohistochemical stains were reviewed. This study was approved by Northwestern University Institutional Review Board.

### Immunohistochemistry

Immunohistochemical staining was performed on formalin-fixed, paraffin-embedded tissue (FFPE). Antigen retrieval and immunohistochemical stains were performed on an automated immunostainer following the manufacturer's protocol (Ventana Medical Systems, Tuscon, AZ, USA). The following predilute antibodies were used: CD3 (Ventana Medical Systems), BCL2 (Cell Marque, Rocklin, CA, USA), BCL6 (Cell Marque), CD20 (Dako, Carpinteria, CA, USA), PAX5 (Cell Marque), CD10 (Leica, Buffalo Grove, IL, USA), and MUM1 (Leica). Determination for germinal center B cell (GCB) and non-GCB was based on expression patterns for CD10, BCL-6, and MUM1 per Hans *et al.* criteria.<sup>23</sup> A GCB phenotype was considered if a case was positive for CD10. A non-GCB phenotype was considered with any of the following expression patterns: CD10<sup>-</sup>BCL6<sup>+</sup>MUM1<sup>+</sup>, CD10<sup>-</sup>BCL6<sup>-</sup>MUM1<sup>+</sup>, and CD10<sup>-</sup>BCL6<sup>-</sup>MUM1<sup>-</sup>. Positive and negative controls were performed with all cases and showed appropriate staining pattern.

### Clonality assessment by PCR

Lymphoma cells were macrodissected from FFPE sections. DNA was quantified by spectrophotometry with NanoDrop 1000 (Thermo Scientific, Waltham, MA, USA). Isolated DNA was tested for gene rearrangements with multiplex PCR using universal primer sets (Invivoscribe Gene Clonality Assays, San Diego, CA, USA) for IgH V-J FR1, FR2, and FR3 primer sets as well as light-chain analysis with IgK V-J primer sets. IgK clonality testing utilized two master mixes, Tube A and Tube B, to target conserved regions within variable (Vk1-7) and joining regions (Jk1-5). The PCR products were detected by capillary gel electrophoresis on an ABI 3130XL genetic analyzer (Applied Biosystems, Foster City, CA, USA). Dominant peaks were considered to be monoclonal if they were at least three-times the height of the polyclonal background and indeterminate monoclonal cases applied to peaks that were between two-times and three-times the height of the background.

## RESULTS

### Clinical features

From our database search we obtained the records for five patient cases with a diagnosis of IVLBCL, including three autopsy patients and two living patients, both from outside hospitals, who sought a second-opinion diagnosis at our institution (Table 1). Three cases were female and two were male. The age range at the time of diagnosis was 56–84 years.

Among autopsy cases, case 1 was an 81-year-old male who suffered from rapidly progressive respiratory failure accompanied by coagulopathy. His laboratories were remarkable for splenomegaly, anemia and thrombocytopenia. He passed away abruptly prior to any further medical work-up and an autopsy was requested. Case 2 was a 76-year-old otherwise healthy female who presented with altered mental status, anemia, fever, hypotension, and renal failure with rapid neurological decompensation, ultimately resulting in death and a subsequent autopsy. Case 3 was an 84-year-old male who presented with three months of fevers and chills and idiopathic thrombocytopenia purpura that did not respond to treatment with intravenous immunoglobulin and steroids. Following his death, a limited 'abdomen-only' autopsy was performed.

Cases 4 and 5 were living patients at the time of diagnosis. Case 4 was a 61-year-old female who presented with a primary complaint of 6 months of a progressive skin rash and urticaria accompanied by weakness and intermittent fevers. Laboratory work-up was notable for mild pancytopenia. A skin biopsy was

**Table 1.** Summary of clinical and pathologic features of five cases of IVLBCL

Case	Age (yr)/ Sex	Clinical presentation	Sites of involvement	Cell of origin	Bone marrow involvement	Treatment and outcome
1	81/M	Respiratory failure	Lungs, heart, adrenal glands, kidneys, prostate, bladder, esophagus, stomach, pancreas, intestines	Non-GCB	No	None; deceased prior to diagnosis.
2	76/F	Encephalopathy	Brain, skin, breast, heart, lungs, liver, adrenal glands, stomach, pancreas, intestines	Non-GCB	Yes	None; deceased prior to diagnosis
3	84/M	Fever and chills	Adrenal glands, bladder, stomach, pancreas, intestines, appendix, liver	Non-GCB	No	IVIg, steroids, deceased shortly after diagnosis
4	61/F	Progressive skin rash; relapse 6 mo later presenting as loss of consciousness	Skin, brain	Initial: non-GCB Relapse: non-GCB	No	Status post R-CHOP, R-MPV, aSCT; disease-free at last follow-up (22 mo after CNS recurrence)
5	56/F	Skin rash	Skin	Non-GCB	No	N/A (outside consultation)

IVLBCL, intravascular large B-cell lymphoma; M, male; GCB, germinal center B cell; F, female; IVIg, intravenous immunoglobulin; R-CHOP, rituximab-cytoxan, doxorubicin, vincristine and prednisone; R-MPV, rituximab-methotrexate, procarbazine and vincristine; aSCT, autologous stem cell transplant; CNS, central nervous system; N/A, not available.

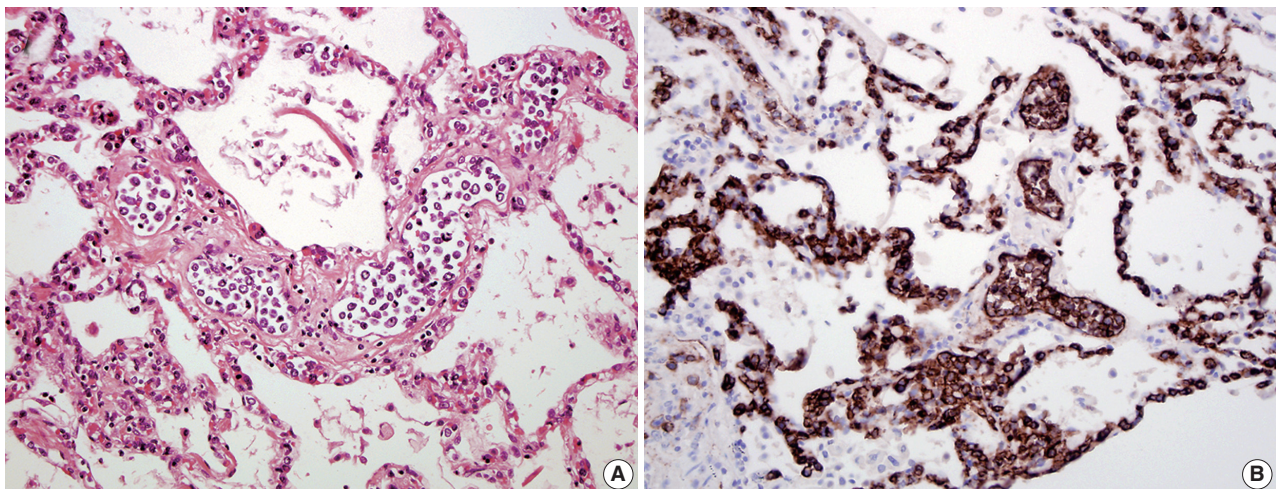


**Fig. 1.** An 81-year-old male presented with rapidly progressive respiratory failure (case 1). (A) Lung parenchyma showed extensive vascular distension and intravascular collection of large lymphoid cells. (B) A CD20 immunohistochemical stain confirmed many large B cells filling the lumina of the vessels.

performed, which revealed IVLBCL. A BM biopsy was negative for lymphoma. The patient underwent treatment with rituximab-cytoxan, doxorubicin, vincristine and prednisone (R-CHOP) and went into clinical remission. However, 6 months later, the patient presented with sudden loss of consciousness and laboratories remarkable for a markedly elevated lactate dehydrogenase. An MRI was ordered that revealed a 4.5 cm left frontal brain mass with cystic degeneration. A repeat biopsy of her BM was also performed and was negative for lymphomatous involvement. Following a diagnosis of CNS B-cell lymphoma, she was treated with a new chemotherapy regimen of rituximab-methotrexate, procarbazine and vincristine (R-MPV), intrathecal metho-

trexate and autologous stem cell transplantation. She responded positively to the treatment and follow-up MRI's showed resolution of the brain lesion. Case 5 was a 56-year-old female who presented with a history of abdominal skin rash clinically suggestive of acute panniculitis, prompting a skin biopsy of the lesion that was consistent with IVLBCL. A BM biopsy was performed at the time of diagnosis, which was negative for lymphoma.

#### Histologic, immunophenotypic, and molecular findings

In all three autopsy cases, intravascular lymphoma cells were present with extensive multi-system involvement as small vessels filled with large cells with scant cytoplasm, vesicular nuclei, and

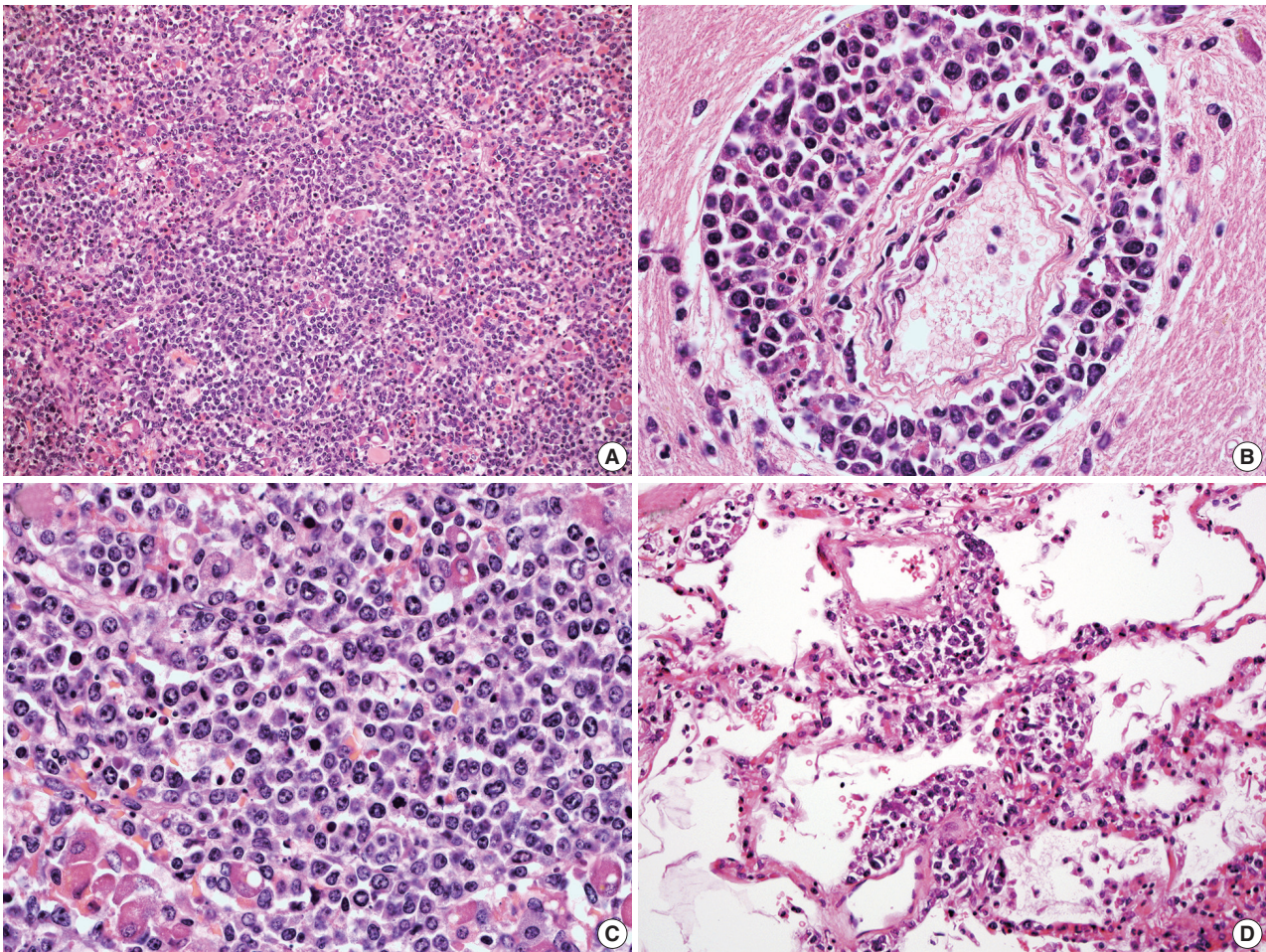


**Fig. 2.** A 76-year-old female presented with altered mental status and rapid neurologic decompensation (case 2). (A) Histology of the pituitary glands shows perivascular lymphoid infiltrates and areas of sheet-like architecture. (B) Perivascular lymphoid infiltrate cuffing the capillary vessels in the pons. (C) Higher magnification of the pituitary glands reveals sheet-like architecture and parenchymal effacement by abnormal large lymphoid cells with vesicular chromatin and prominent nucleoli. (D) The large lymphoma cells in the intravascular spaces of the lung interstitium from the same patient.

prominent nucleoli. In case 1, histology showed intravascular lymphomatous involvement of multiple organs including the lungs, heart, adrenal glands, esophagus, stomach, pancreas, intestines, kidneys, prostate, and bladder. The largest tumor burden was within the small vessels of the lung interstitium. A CD20 immunostain confirmed that the vessels were distended and filled with large B cells (Fig. 1). A brain dissection was not performed. In case 2, multiple organs were also involved, which included the brain, skin, breast, heart, lungs, liver, adrenal glands, stomach, pancreas, and intestines. The largest tumor burden was observed in the brain, including the cerebral hemispheres, meninges, midbrain, pons and basal ganglia, which demonstrated purely perivascular growth. The pituitary was also involved, and it showed near total effacement of the parenchyma with large, solid sheets of these cells in a sheet-like architecture

with an identical morphology to the perivascular component in the other locations in the brain as well as the intravascular component seen in other organs (Fig. 2). A BM biopsy showed intrasinusoidal infiltration of neoplastic B cells. Case 3 revealed predominantly intravascular involvement of large B cells in adrenal glands, bladder, stomach, pancreas, intestines, appendix, and liver. A brain dissection was not performed.

In cases 4 and 5, skin biopsies revealed large B cells with irregular nuclear contours and prominent nucleoli filling small vessels of the dermis. The patient in case 4 underwent a lumbar puncture after developing neurologic symptoms with a brain mass in the left frontal cortex on MRI, that showed rare atypical large B cells in the cerebrospinal fluid. A biopsy of the brain lesion revealed atypical B cells in the superficial subcortical brain parenchyma organized in sheets and with clustering around

small vascular spaces, without discernible intravascular involvement (Fig. 3).

For all cases, the cell of origin for the neoplastic large cells was consistent with the non-GCB phenotype according to the Hans *et al.* algorithm.<sup>23</sup> More specifically, the large B cells in cases 1–4

were CD10<sup>−</sup>BCL6<sup>−</sup>MUM1<sup>+</sup>; and the large B cells in case 5 showed CD10<sup>−</sup>BCL6<sup>+</sup>MUM1<sup>+</sup> staining pattern. In case 2, the neoplastic cells from the extravascular CNS involvement had the same non-GCB phenotype as the intravascular component.

Immunoglobulin gene rearrangement studies were performed

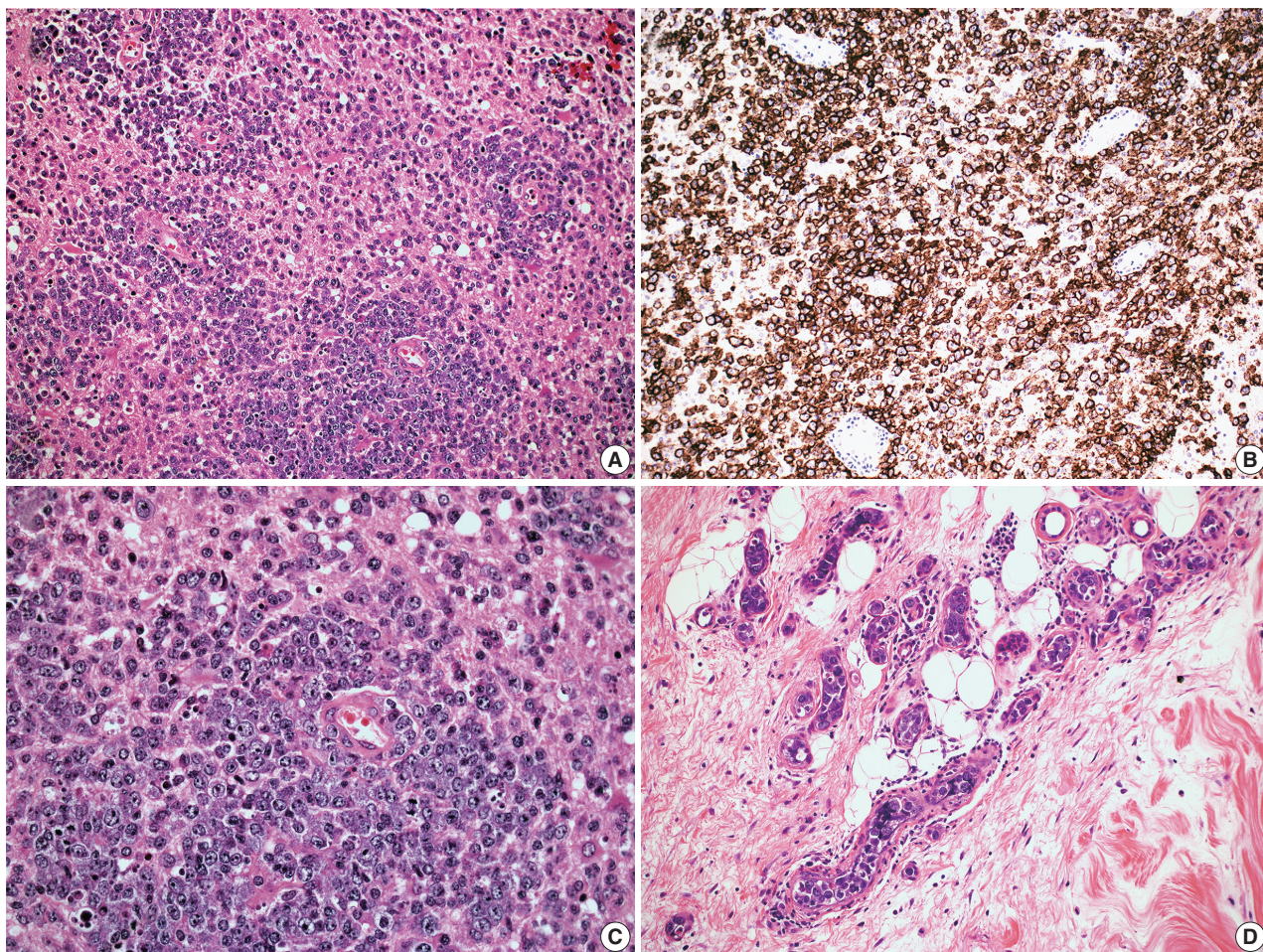


**Fig. 3.** A 61-year-old female with progressive skin rash and a diagnosis of intravascular large B-cell lymphoma who subsequently developed neurologic symptoms (case 4). (A) Brain biopsy (left frontal cortex) reveals lymphoid infiltrates in predominantly extravascular pattern. (B) CD20 highlights large B cells in the perivascular infiltrates. (C) Brain biopsy reveals sheets of large cells with vesicular chromatin and prominent nucleoli. (D) Diagnostic skin biopsy reveals large lymphoma cells filling the lumina of capillary vessels in the dermis in the same patient.

**Table 2.** Immunoglobulin heavy chain and light chain gene rearrangement analysis for five cases of IVLBCL

	Immunoglobulin gene rearrangement by PCR		
	IgH	IgK (tube A)	IgK (tube B)
Case 1	Negative	Positive (272 bp)	Positive (239 bp)
Case 2	Positive (319 bp, 254 bp)	Positive (149 bp, 201 bp)	Positive (275 bp)
CNS: meninges	Negative	Positive (149 bp, 201 bp)	Positive (275 bp)
CNS: pituitary	Positive (254 bp)	Negative	Negative
Case 3	Negative	Negative	Negative
Case 4	Negative	Negative	Negative
Case 5	Negative	Positive (149 bp)	Positive (237 bp)

IVLBCL, intravascular large B-cell lymphoma; PCR, polymerase chain reaction; CNS, central nervous system.

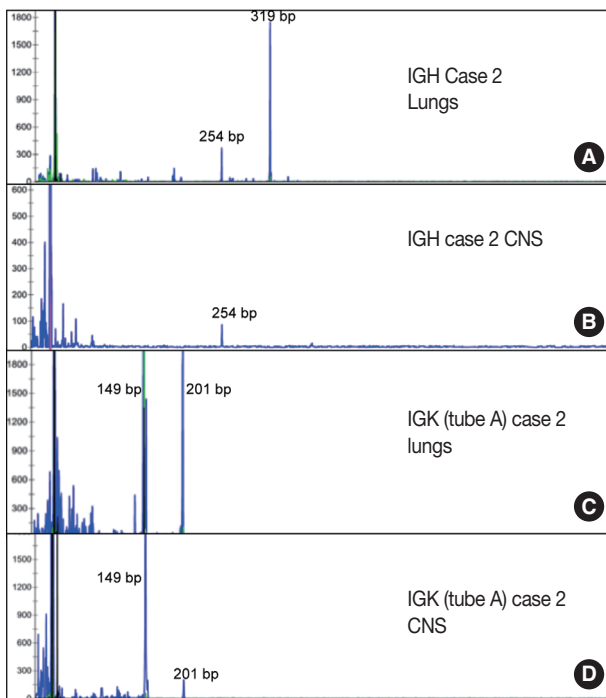


**Fig. 4.** Immunoglobulin heavy and light chain gene rearrangement performed on tumor cells with two distinct morphologic patterns (case 2). (A, B) Both the lung with intravascular pattern and central nervous system (CNS) pituitary with extravascular pattern show clonal heavy chain rearrangement with the same 254-bp clonal FR2 peak. (C, D) Both the lung with intravascular pattern and CNS meninges with extravascular pattern show clonal kappa light chain rearrangement with the same 149-bp and 201-bp clonal peaks.

in all five cases. Immunoglobulin heavy chain was clonally rearranged in one of the five cases (case 2). Kappa light chain gene rearrangement analysis provided evidence of clonality in two additional cases (cases 1 and 5) (Table 2). To confirm the clonal relationship between the extravascular and intravascular components, immunoglobulin heavy and light chain gene rearrangement studies were performed in case 2 from areas with two distinct morphologies. The pituitary gland, which showed sheet-like extravascular component, was positive for clonal heavy chain gene rearrangement with a 254-bp clonal FR2 peak, identical to one of the clonal peaks detected in the intravascular component from the lung parenchyma. Similarly, the perivascular lymphoid infiltrate from the meninges was positive for clonal kappa light chain rearrangement, with a clonal peak identical to those detected in the intravascular component from the lung parenchyma (Table 2, Fig. 4).

## DISCUSSION

In this study, we reported five cases of IVLBCL, comprised of

three autopsy cases and two living patient cases. In all three autopsy cases, the patients died before or shortly after the diagnosis was established. All cases demonstrated extensive organ involvement by the lymphoma cells. Not surprisingly, we observed that IVLBCL is a highly aggressive entity with non-specific clinical findings and where other differentials are more commonly exhausted, which delays the diagnosis and leads to unsalvageable clinical outcomes. In keeping with past findings,<sup>6,13,24</sup> our findings confirm that IVLBCL is predominantly non-germinal center B cell in origin as all five cases in this study showed this phenotype.

The CNS is the most common site to be involved by IVLBCL—up to two-thirds of all cases of IVLBCL—and is a frequent site of intra-organ recurrence.<sup>8-10</sup> Approximately one-half of all cases of IVLBCL involving the brain are diagnosed post-mortem.<sup>25</sup> Diagnosing IVLBCL premortem in the setting of CNS involvement is difficult because patients often present with non-specific encephalopathic symptoms, and less frequently stroke-like symptoms including extremity paralysis.<sup>10</sup> Among living patients diagnosed with CNS-IVLBCL, a subset of cases—approximately one-third—have been found to survive to 2 years following initial diagnosis.<sup>10</sup> In our small series of five IVLBCL, two patients developed neurologic symptoms. Both showed biopsy-proven CNS involvement of IVLBCL. Interestingly, in both cases, the CNS involvement was exclusively extravascular characterized by perivascular infiltrate of the abnormal large lymphocytes or confluent sheet like growth. It remains unknown how common the extravascular morphology is in the CNS of IVLBCL patients. In one study, two cases had CNS IVLBCL with a predominant angiocentric pattern,<sup>9</sup> accounting for one-third of the cases in that study. In a separate study of five cases of CNS IVLBCL, all five had predominantly extravascular parenchymal involvement.<sup>19</sup> Albeit these were small cohorts of cases, extravascular extension into the CNS parenchyma by IVLBCL is probably a more common phenomenon than currently appreciated.

When presenting with primarily CNS symptoms, IVLBCL can mimic CNS B-cell lymphoma and fail to tip off clinicians to look for a more systemic lymphomatous component. Primary CNS B-cell lymphoma, also a rare variant of DLBCL, has a proclivity to show angiocentric proliferation of neoplastic B cells.<sup>26</sup> In one instance, the perivascular growth pattern in the CNS in a patient with established IVLBCL resulted in an entirely separate diagnosis of primary CNS lymphoma being made, potentially creating unnecessary confusion.<sup>6</sup> Our findings raise the importance of keeping IVLBCL in the differential of primary CNS lymphomas and that the presence of perivascular growth

patterns should not exclude IVLBCL as a diagnosis. It is important to identify CNS involvement in patients with IVLBCL as they have a worse clinical outcome than those without CNS involvement and require closer clinical monitoring.<sup>10</sup>

In our series, both cases 4 and 5 presented with cutaneous involvement as their initial manifestation of IVLBCL, raising the possibility of a “cutaneous variant.” The “cutaneous variant” is thought to occur preferentially in females and make up a sizeable subset of all IVLBCL cases (up to 26% in one study of 38 patients), in which the only symptomatology is in the form of a skin rash or plaques, without other sites of involvement.<sup>27</sup> Up to one-third of patients with cutaneous presentation may go on to develop other sites of involvement, such as the CNS (as was the case for our case 4), but these cases do not fall under the ‘cutaneous variant’ subset. In keeping with findings in the literature that the patients with cutaneous involvement have improved survival, case 4 in our series was disease-free at 22 months following their CNS relapse. Case 5 received their clinical treatment outside of our institution and clinical follow-up could not be assessed.

Some challenge the notion of IVLBCL concomitantly involving the CNS extravascularly due to the fact that they are thought to have absent surface adhesion molecules CD29, CD54 (ICAM-1), and CD11a, preventing them from being able to cross small CNS vessels to form perivascular or extravascular infiltrates.<sup>28</sup> However, a biologic explanation for the predilection for IVLBCL to involve the CNS with an extravascular growth pattern could be due to the fact that as veno-occlusive events occur secondary to small vessel involvement by IVLBCL, the permeability of the blood-brain-barrier is altered<sup>29</sup> such that it allows for passive diffusion of neoplastic cells across vessels into the brain parenchyma to form extravascular infiltrates.

A diagnosis of IVLBCL is made based on the clinical features and histologic findings of selective intravascular growth of large B cells. Clonal rearrangement of immunoglobulin chains is not required for the diagnosis. In fact, the sensitivity of PCR-based clonality assays is not very high in large B-cell lymphomas. In our small series, only one case was positive for clonal heavy chain gene rearrangement. Using a combination of heavy and light chain approach, we were able to expand molecular evidence of clonality in three of the five cases.

Thus, in cases when two different histologies coexist in the same patient, molecular modalities are useful to determine the clonal relationship between distinct growth-patterns. Here, we used a molecular approach to confirm that CNS-involvement with extravascular morphology was clonally identical to the

intravascular component in the same patient. To our knowledge, this is the first study using conventional molecular diagnostic modalities to demonstrate that extravascular B cells in the CNS of a patient are clonally identical to systemic intravascular cells in the same patient with IVLBCL. Rare past efforts have failed, as indeed, it is difficult to work with such scant material for molecular studies.<sup>19</sup>

In summary, of the two of five cases in this study with CNS involvement, both show pure perivascular and extravascular growth, which in combination with other reported cases in the literature, raises the possibility that CNS involvement is more frequently extravascular in IVLBCL than currently appreciated. Therefore, it is the intent of this study to raise awareness that IVLBCL is not just a clinically heterogenous entity but is also a histologically heterogenous entity with potential proclivity to form extravascular foci in the CNS due to biologically unique properties of the blood brain barrier. Further analysis is needed, particularly in the form of large retrospective cohort studies of known IVLBCL patients, to pinpoint the frequency of extravascular morphology in the CNS in these patients.

---

### Conflicts of Interest

No potential conflict of interest relevant to this article was reported.

### REFERENCES

1. Campo E, Swerdlow SH, Harris NL, Pileri S, Stein H, Jaffe ES. The 2008 WHO classification of lymphoid neoplasms and beyond: evolving concepts and practical applications. *Blood* 2011; 117: 5019-32.
2. Murase T, Yamaguchi M, Suzuki R, *et al.* Intravascular large B-cell lymphoma (IVLBCL): a clinicopathologic study of 96 cases with special reference to the immunophenotypic heterogeneity of CD5. *Blood* 2007; 109: 478-85.
3. Fulling KH, Gersell DJ. Neoplastic angioendotheliomatosis: histologic, immunohistochemical, and ultrastructural findings in two cases. *Cancer* 1983; 51: 1107-18.
4. Ip M, Chan KW, Chan IK. Systemic inflammatory response syndrome in intravascular lymphomatosis. *Intensive Care Med* 1997; 23: 783-6.
5. Devlin T, Moll S, Hulette C, Morgenlander JC. Intravascular malignant lymphomatosis with neurologic presentation: factors facilitating antemortem diagnosis. *South Med J* 1998; 91: 672-6.
6. Ponzoni M, Ferreri AJ, Campo E, *et al.* Definition, diagnosis, and

- management of intravascular large B-cell lymphoma: proposals and perspectives from an international consensus meeting. *J Clin Oncol* 2007; 25: 3168-73.
7. Estalilla OC, Koo CH, Brynes RK, Medeiros LJ. Intravascular large B-cell lymphoma: a report of five cases initially diagnosed by bone marrow biopsy. *Am J Clin Pathol* 1999; 112: 248-55.
  8. Fonkem E, Lok E, Robison D, Gautam S, Wong ET. The natural history of intravascular lymphomatosis. *Cancer Med* 2014; 3: 1010-24.
  9. Glass J, Hochberg FH, Miller DC. Intravascular lymphomatosis: a systemic disease with neurologic manifestations. *Cancer* 1993; 71: 3156-64.
  10. Fonkem E, Dayawansa S, Stroberg E, *et al.* Neurological presentations of intravascular lymphoma (IVL): meta-analysis of 654 patients. *BMC Neurol* 2016; 16: 9.
  11. Wick MR, Mills SE, Scheithauer BW, Cooper PH, Davitz MA, Parkinson K. Reassessment of malignant "angioendotheliomatosis": evidence in favor of its reclassification as "intravascular lymphomatosis". *Am J Surg Pathol* 1986; 10: 112-23.
  12. Willemze R, Kerl H, Sterry W, *et al.* EORTC classification for primary cutaneous lymphomas: a proposal from the Cutaneous Lymphoma Study Group of the European Organization for Research and Treatment of Cancer. *Blood* 1997; 90: 354-71.
  13. Yegappan S, Coupland R, Arber DA, *et al.* Angiotropic lymphoma: an immunophenotypically and clinically heterogeneous lymphoma. *Mod Pathol* 2001; 14: 1147-56.
  14. Poddaturi V, Guileyardo JM, Soto LR, Krause JR. A case series of clinically undiagnosed hematopoietic neoplasms discovered at autopsy. *Am J Clin Pathol* 2015; 143: 854-60.
  15. Thomas CA, Guileyardo JM, Krause JR. An intravascular lymphoma with extravascular tendencies. *Proc (Bayl Univ Med Cent)* 2014; 27: 341-3.
  16. Demirer T, Dail DH, Abouafia DM. Four varied cases of intravascular lymphomatosis and a literature review. *Cancer* 1994; 73: 1738-45.
  17. Case records of the Massachusetts General Hospital. Weekly clinicopathological exercises. Case 39-1986. A 66-year-old woman with fever, fluctuating neurologic signs, and negative blood cultures. *N Engl J Med* 1986; 315: 874-85.
  18. Ferry JA, Harris NL, Picker LJ, *et al.* Intravascular lymphomatosis (malignant angioendotheliomatosis): a B-cell neoplasm expressing surface homing receptors. *Mod Pathol* 1988; 1: 444-52.
  19. Imai H, Kajimoto K, Taniwaki M, *et al.* Intravascular large B-cell lymphoma presenting with mass lesions in the central nervous system: a report of five cases. *Pathol Int* 2004; 54: 231-6.
  20. Takeuchi Y, Hashizume Y, Hoshiyama M, Hirose Y, Takahashi A. An autopsy case of intravascular malignant lymphomatosis with intracranial lymphomatous mass lesions. *Rinsho Shinkeigaku* 1995; 35: 158-63.
  21. Beal MF, Fisher CM. Neoplastic angioendotheliosis. *J Neurol Sci* 1982; 53: 359-75.
  22. Fonseca VR, Espada E, Galdes R, *et al.* Synchronous brain and intravascular B-cell lymphoma after remission of an adult hemophagocytic syndrome. *Clin Case Rep* 2016; 4: 327-30.
  23. Hans CP, Weisenburger DD, Greiner TC, *et al.* Confirmation of the molecular classification of diffuse large B-cell lymphoma by immunohistochemistry using a tissue microarray. *Blood* 2004; 103: 275-82.
  24. Murase T, Nakamura S, Kawauchi K, *et al.* An Asian variant of intravascular large B-cell lymphoma: clinical, pathological and cytogenetic approaches to diffuse large B-cell lymphoma associated with haemophagocytic syndrome. *Br J Haematol* 2000; 111: 826-34.
  25. Baehring JM, Longtine J, Hochberg FH. A new approach to the diagnosis and treatment of intravascular lymphoma. *J Neurooncol* 2003; 61: 237-48.
  26. Sugita Y, Muta H, Ohshima K, *et al.* Primary central nervous system lymphomas and related diseases: Pathological characteristics and discussion of the differential diagnosis. *Neuropathology* 2016; 36: 313-24.
  27. Ferreri AJ, Campo E, Seymour JF, *et al.* Intravascular lymphoma: clinical presentation, natural history, management and prognostic factors in a series of 38 cases, with special emphasis on the 'cutaneous variant'. *Br J Haematol* 2004; 127: 173-83.
  28. Kinoshita M, Izumoto S, Hashimoto N, *et al.* Immunohistochemical analysis of adhesion molecules and matrix metalloproteinases in malignant CNS lymphomas: a study comparing primary CNS malignant and CNS intravascular lymphomas. *Brain Tumor Pathol* 2008; 25: 73-8.
  29. Weiss N, Miller F, Cazaubon S, Couraud PO. The blood-brain barrier in brain homeostasis and neurological diseases. *Biochim Biophys Acta* 2009; 1788: 842-57.

## An Experimental Infarct Targeting the Internal Capsule: Histopathological and Ultrastructural Changes

Chang-Woo Han · Kyung-Hwa Lee  
Myung Giun Noh · Jin-Myung Kim  
Hyung-Seok Kim<sup>1</sup> · Hyung-Sun Kim<sup>2</sup>  
Ra Gyung Kim<sup>2</sup> · Jongwook Cho<sup>2</sup>  
Hyoung-Ihl Kim<sup>2</sup> · Min-Cheol Lee

Departments of Pathology and <sup>1</sup>Forensic Medicine, Chonnam National University Medical School and Research Institute of Medical Sciences, Gwangju; <sup>2</sup>Department of Medical System Engineering and School of Mechatronics, Gwangju Institute of Science and Technology, Gwangju, Korea

Received: September 24, 2016

Revised: February 3, 2017

Accepted: February 16, 2017

### Corresponding Author

Min-Cheol Lee, MD, PhD  
Department of Pathology, Chonnam National University Medical School and Research Institute of Medical Sciences, 160 Baekseo-ro, Dong-gu, Gwangju 61469, Korea  
Tel: +82-62-220-4303  
Fax: +82-62-220-5697  
E-mail: mclee@jnu.ac.kr

**Background:** Stroke involving the cerebral white matter (WM) has increased in prevalence, but most experimental studies have focused on ischemic injury of the gray matter. This study was performed to investigate the WM in a unique rat model of photothrombotic infarct targeting the posterior limb of internal capsule (PLIC), focusing on the identification of the most vulnerable structure in WM by ischemic injury, subsequent glial reaction to the injury, and the fundamental histopathologic feature causing different neurologic outcomes. **Methods:** Light microscopy with immunohistochemical stains and electron microscopic examinations of the lesion were performed between 3 hours and 21 days post-ischemic injury. **Results:** Initial pathological change develops in myelinated axon, concomitantly with reactive change of astrocytes. The first pathology to present is nodular loosening to separate the myelin sheath with axonal wrinkling. Subsequent pathologies include rupture of the myelin sheath with extrusion of axonal organelles, progressive necrosis, oligodendrocyte degeneration and death, and reactive gliosis. Increase of glial fibrillary acidic protein (GFAP) immunoreactivity is an early event in the ischemic lesion. WM pathologies result in motor dysfunction. Motor function recovery after the infarct was correlated to the extent of PLIC injury proper rather than the infarct volume. **Conclusions:** Pathologic changes indicate that the cerebral WM, independent of cortical neurons, is highly vulnerable to the effects of focal ischemia, among which myelin sheath is first damaged. Early increase of GFAP immunoreactivity indicates that astrocyte response initially begins with myelinated axonal injury, and supports the biologic role related to WM injury or plasticity. The reaction of astrocytes in the experimental model might be important for the study of pathogenesis and treatment of the WM stroke.

**Key Words:** Stroke; White matter; Models, animal; Pathology; Ultrastructure

As the human life span has continued to increase, stroke patterns have changed. Ischemic stroke, which constitute 80%–85% of stroke cases, comprise both the gray matter (GM) and white matter (WM) of the brain. The prevalence of WM injury causing motor and intellectual dysfunction has increased with the aging population.<sup>1</sup> Neuroimaging methods have shown rarefaction of the WM resulting from injury, which is termed leukoaraiosis.<sup>2</sup> Ischemic stroke confined to WM, called ischemic leukoencephalopathy, is a feature of leukoaraiosis that can be observed in humans through neuroimaging.<sup>3</sup> Currently, the most common etiology and pathogenesis of leukoaraiosis are undefined vascular or ischemic events.<sup>4,5</sup>

Up to 25% of WM strokes cause lacunar change, and the internal capsule (IC) is commonly affected in humans.<sup>6</sup> The posterior limb of the IC (PLIC) is the fundamental subcortical

motor pathway; it includes the major corticofugal tract that is directly related to motor function. Infarction of the PLIC results in a challenging clinical progress characterized by persistent motor disability; therefore, studies on pathophysiological alterations and therapeutics are essential.<sup>7</sup>

Animal models have been used to understand the pathophysiology of strokes and to guide the development of more effective therapeutic or rehabilitative interventions.<sup>8–11</sup> Few studies have investigated WM injury when compared with studies on the effect of ischemia in the GM. This limitation is partly due to the difficulty in generating animal models of WM stroke. While the weight of human brain is 1,300 to 1,500 g, that of the rat brain is 5.5 to 6.0 g. Moreover, the substantially lower WM/GM ratio in rodents (approximately 14%:86%) compared with primates (40%:60%) increases the difficulty in targeting the WM

structure.<sup>12</sup>

A literature search through publications spanning the last 10 years revealed several experimental methods used to develop WM stroke models, including occlusion of the common carotid artery, proximal middle cerebral artery<sup>13</sup> and anterior choroidal artery (AChA)<sup>14</sup> and administration of the vasoconstrictive agent endothelin-1 (ET-1) into the subcortical WM, IC, and striatum.<sup>15-19</sup> However, infarcts selectively targeting the IC and resulting in chronic motor impairment cannot be induced consistently. Long-term follow-up studies have failed to produce long-term, persistent motor deficits in the experimental models.<sup>19,20</sup> The lack of rat models of WM stroke has several possible neuroanatomical reasons, including the much smaller WM area of rats compared with primates, the irregularly elongated IC structure, and the absence of efficient tools selectively targeting the IC.<sup>6,12</sup> Therefore, accurately assessing and controlling the infarct location from the brain surface is difficult stereotactically.

To establish a WM infarct model producing long-term forelimb and hind limb motor deficits, selective ischemic injury of the pyramidal tract is critical. Previously, we created a highly reproducible rat model of IC-specific stroke using a photothrombotic technique, which involves selectively illuminating the PLIC after intravenous injection of Rose Bengal solution.<sup>21,22</sup> The infarct lesions occurred in the PLIC without any significant injury to surrounding structures including the putamen, optic nerve, and WM. Neurologic motor functions significantly decreased immediately after the ischemia and recovered variably. Through the investigation of the early and comprehensive histopathology and ultrastructural changes resulting from focal cerebral WM ischemia, the purpose of this study was to determine which structure of the WM is the first to be damaged, how glial response appears to the damage, and what is the most important factor causing different neurologic outcomes.

## MATERIALS AND METHODS

### Experimental animals

Male Sprague-Dawley rats, 8- to 9-week-old and weighing 200–240 g, were housed two per cage in a controlled husbandry unit with a 12/12 hour light/dark cycle and permitted *ad libitum* access to food and water. The temperature was maintained at  $21 \pm 1^\circ\text{C}$ . A total of 77 rats were used for the experimental study, and they were divided into three groups: 50 rats for light microscopic histological examination, 13 rats for electron microscopic examination, and 14 rats for measurement of infarct volume. The brain was harvested from 3 hours to 21 days after the photothrombotic ischemia and infarct volumes were measured at 14 days (Table 1). Animal experiments were performed according to the institutional guidelines of Chonnam National University Research Institute of Medical Science and Gwangju Institute of Science and Technology (GIST). All efforts were made to minimize animal suffering and to reduce the number of animals used. Institutional ethical committee approval was obtained prior to the experiments.

### Induction of IC infarction and behavioral evaluation

The photothrombotic capsular infarction model used in this study was described previously.<sup>21</sup> Experimental rats were divided into two groups: stroke lesion group (SLG) and sham-operated group (SOG). Briefly, experimental rats of SLG were anesthetized and fixed with a small animal stereotactic frame. A 28-gauge straight stainless steel needle implemented with a fine optical fiber transmitting laser light, a 125  $\mu\text{m}$  outer diameter, and a 62.5  $\mu\text{m}$  core diameter, was inserted through a midline scalp incision. The needle was stereotactically inserted into the PLIC target; 2.0 mm posterior, 3.1 mm lateral to midline, and 7.2 mm deep to bregma, as shown in Fig. 1. The coordinate used in this experiment was deeper than those previously suggested.<sup>16</sup> Rose Bengal dye was injected through the tail vein, followed by 1.5 minutes of laser irradiation with an intensity of 2.5 mW at the fiber tip. After the scalp wound was secured, the

**Table 1.** Experimental design of time interval and number of rats in photothrombotic capsular infarct

	Time of post-ischemia							
	3 hr	6 hr	12 hr	1 day	4 days	7 days	14 days	21 days
Light microscopy								
Stroke lesion group	2	2	2	4	4	4	8 <sup>a</sup>	8 <sup>a</sup>
Sham operation group	2	2	2	2	2	2	2	2
Electron microscopy	1	1	1	2	2	2	2	2
Infarct volume	-	-	-	-	-	-	14 <sup>b</sup>	-

<sup>a</sup>Four rats each for the moderate recovery group (MRG) and poor recovery group (PRG); <sup>b</sup>Seven rats each MRG and PRG for measurement of lesion volume.

rat was transferred to a recovery chamber. The experimental rats of SOG underwent an identical lesion-making procedure except for receiving an injection of saline solution (0.2 mL/100 g) instead of Rose Bengal dye.

The behavioral tests employed were described in the previous study,<sup>21</sup> and single pellet reaching tasks (SPRTs) were used to measure motor performance in this study. Briefly, an experimental apparatus was made of clear Plexiglas with a 1-cm wide slit in the middle of the front wall for the food shelf. Once rats began to show a forelimb preference to obtain a sucrose pellet (Bio-Serve, Frenchtown, NJ, USA) through the slit, a pellet was obliquely placed contralateral to the preferred paw to prevent the use of the nonpreferred paw. Animals were subsequently administered 20 pellets per session for 21 days. Successful reach was defined as a reach in which an animal grasped a food pellet, brought it into the cage, and consumed it without dropping. Reaching performance was scored and the success rate was calculated as the formula, number of successful reaches  $\times$  100/20 scores before the operation were averaged to represent preoperative reaching performance. After the photothrombotic infarct, the experimental rats were subdivided as follows from the SPRT score: early recovery group (ERG) characterized by  $>$  50% recovery in 7 days; moderate recovery group (MRG) characterized by  $>$  50% recovery of the prelesion status in 14 days; and poor recovery group (PRG) which had reaching performance at  $<$  50% of the prelesion status. Subjects in the ERG were excluded from the study. Persistent motor impairment, characteristic of both MRG and PRG subjects, developed effectively in 71% of rats. SOG rats did not show a significant decrease in SPRT performance within the observation period.

#### Measurement of infarct size

To measure the infarct size in both MRG and PRG rats, seven

fresh brains were perfused at 14 days after the ischemia. Coronal brain sections of 2.5-mm thickness were obtained from the center of the needle insertion sites using a metallic tissue plate covered with optimal cutting temperature (OCT) compound and immediately frozen at  $-25^{\circ}\text{C}$  in a frozen tissue microtome. Serial tissue slices from the frozen brains (20- $\mu\text{m}$  thick sections at 200- $\mu\text{m}$  intervals) were prepared and stained with hematoxylin and eosin (H&E) and cresyl violet. Histologic images were scanned with a ScanScope virtual microscope (Aperio Technologies, Vista, CA, USA). Images from five to six sections were assessed for infarct lesions with Image J software (NIH, Bethesda, MD, USA). The total volume of brain injury was determined by summing the area of damaged tissue recorded from all sections and multiplying by the distance between sections.<sup>23</sup> The completeness of the IC destruction was determined by three of the authors, all of whom were blinded to the motor recovery group.

#### Histopathology and immunohistochemistry

Experimental time-points after PLIC ischemia were as follows. To assess early changes of PLIC infarct,  $n = 2$  each at 3, 6, and 12 hours, and  $n = 4$  each at 1, 4 and 7 days. To assess late changes between MRG and PRG infarcts,  $n = 8$  each at 14 and 21 days. For SOG,  $n = 2$  for each postlesion time-points. After the behavioral evaluation, rats were anesthetized with intraperitoneal sodium pentobarbital (70 mg/kg) and killed by intra-aortic perfusion of 1% paraformaldehyde in phosphate buffer solution (PBS; 0.12 M, pH 7.4) delivered by a perfusion pump (36 mL/min) for 5 minutes followed by 4% paraformaldehyde in PBS for 15 minutes at the same flow rate. The brains were then removed and coronally sectioned into 4-mm-thick slices surrounding the center of the needle insertion site. For light microscopy examinations, the brains were removed from the skull, postfixed in 4% paraformaldehyde for 2 days at room temperature, and subse-

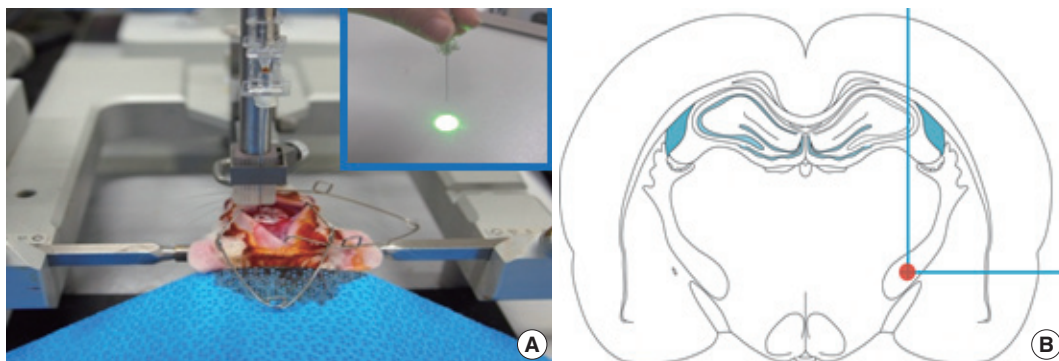


**Fig. 1.** A 28-gauge needle with an optical fiber (A, inset) inserted stereotactically into the posterior limb of the internal capsule (B), 2.0 mm posterior, 3.1 mm lateral to midline, and 7.2 mm deep from bregma, to produce the infarction.

quently kept in processed paraffin-embedded tissue blocks. Routine H&E, luxol fast blue–periodic acid-Schiff (LBPAS), and immunohistochemical stainings were performed on tissue sections (6- $\mu$ m-thick) on probed-glass slides. Immunohistochemical staining with anti–glial fibrillary acidic protein (GFAP; 1:400, polyclonal, Zymed, South San Francisco, CA, USA) and anti–neurofilament protein (NFP; 1:600, clone 2F11, Dako Cytomation, Carpinteria, CA, USA) was done using the avidin-biotin peroxidase method<sup>24</sup> with the ABC kit (Vector Laboratories, Burlingame, CA, USA). Antigen retrieval was conducted by heating the tissue sections at 60°C for 5 minutes in sodium citrate buffer, after which the sections were incubated in a mixture of 3% hydrogen peroxide and 10% methanol for 20 minutes, followed by 10% goat serum for 1 hour at room temperature. The sections were incubated with each primary antibody for 2 hours, biotinylated secondary antibody for 20 minutes, and streptavidin-horseradish peroxidase (Dako Cytomation) for 20 minutes. They were then developed with a chromogenic solution of diaminobenzidine and counterstained with hematoxylin to visualize cell nuclei. Known positive and negative tissues were used as controls.

### Electron microscopy

One rat each at 3, 6, and 12 hours, and two rats each at 1, 4, 7, 14, and 21 days after the ischemia (n = 13) and one SOG rat were studied by transthoracic cardiac perfusion.<sup>25</sup> Rats were perfused with 1% paraformaldehyde/0.1% glutaraldehyde in cold phosphate buffer (PB) delivered by a perfusion pump (36 mL/min) for 5 minutes, followed by 2% paraformaldehyde/2% glutaraldehyde in cold PB at the same flow rate for 5 minutes. Brains were removed and coronally cut into 2-mm-thick slices. After the lesion was evaluated macroscopically in the brain slices, tissues were trimmed to approximately 2 × 2 × 1 mm, placed in 4% glutaraldehyde in PB for 24 hours at 4°C, postfixed in 2% osmium tetroxide for 2 hours at room temperature, rinsed in 0.1 mol/L cacodylate buffer, dehydrated in graded concentrations of ethanol followed by propylene oxide, incubated in a mixture of epon/propylene oxide (50/50, then 80/20 for 4 hours), and embedded in epon at 60°C in an oven for 2 days. Semi-thin sections (1- $\mu$ m-thick) were stained with 1% toluidine blue and screened by light microscopy to select thin section areas from multiple blocks at each lesion time-point for electron microscopy. Selected thin sections (800-Å thick) were cut with a diamond knife on an ultramicrotome (LKB-Produkter, Bromma, Sweden), mounted on copper grids, contrasted with uranyl acetate and lead citrate, and viewed on a JEOL 120S electron micro-

scope (Nihon Denshi, Tokyo, Japan). The investigators were initially blinded to the treatment conditions. Axon and myelin thicknesses were quantified from 3 hours to 21 days after ischemia. Two random fields per grid from two grids were analyzed per experimental brain. Four random images within each field were collected at × 5,000 magnification and analyzed with ImagePro Plus (MediaCybernetics, Rockville, MD, USA). The axon and myelin sheath diameters were determined for every myelinated axon from a minimum of 30 axons for each experimental group. The myelin thickness was calculated by subtracting the axon diameter from the total fiber diameter. The g-ratio of each myelinated axon was calculated by dividing the average axon diameter by the average total fiber diameter.<sup>26</sup>

### Statistical analysis

Data were analyzed with SPSS ver. 10.0 statistical analysis software (SPSS Inc., Chicago, IL, USA). SPRTs for skilled reaching performances were analyzed with a repeated measure analysis of variances for group and time. Electron microscopy data (g-ratio, axon caliber, and myelin thickness) were tested with a one-way ANOVA. Data are presented as the mean ± standard error of mean, with  $p < .05$  considered significant.

## RESULTS

### Infarct volumes

A series of frozen tissue slices stained with cresyl violet to measure infarct volume is illustrated in Fig. 2A. Infarct volume included the area of necrosis and surrounding demyelination and astrogliosis. At 14 days after ischemia, the infarct volume was  $0.6 \pm 0.2$  mm<sup>3</sup> in the PRG and  $0.5 \pm 0.2$  mm<sup>3</sup> in the MRG (Fig. 2B). Infarcts in the PRG were slightly larger than those in the MRG; however, there was no significant relationship between infarct volume and the degree of motor recovery in each group.

### Light microscopy findings

Myelinated axons in the PLIC were well defined by LBPAS and NFP immunohistochemical staining. The presence of reactive astrocytes was clearly indicated by GFAP immunohistochemical staining. At 3 hours post-ischemia, a pale focal lesion was observed on H&E stained preparation (Fig. 3A). The lesion boundary was not clear and gradually merged with the neighboring normal WM. The lesion was highlighted by light brown positivity on GFAP staining (Fig. 3B). Focal lesions of myelin pallor showed separated, swollen myelinated axons in edematous PLIC by LB-

PAS staining. Nuclear pyknosis of oligodendrocytes was identified in the lesion. Edematous change was noted in the upper portion of the optic tract and was limited to the vicinity of PLIC.

At 6 hours to 1 day poststroke, the focal lesion of PLIC was more clearly identifiable with time through low magnification microscopy. A focal infarct manifested as a well-demarcated, pale, whitish lesion due to the lack of staining with H&E and

LBPAS (Fig. 3C, D). Immunohistochemical staining revealed increased positivity for GFAP (Fig. 3E) and decreased positivity for NFP (Fig. 3F). Immunopositivity for GFAP in the infarct lesion indicated the reactive change of astrocytes. No inflammatory cell infiltration in the infarct lesion was noted.

At 4 days post-ischemia, myelinated axons in the PLIC were completely lost by LBPAS staining (Fig. 3G). The lesion had a

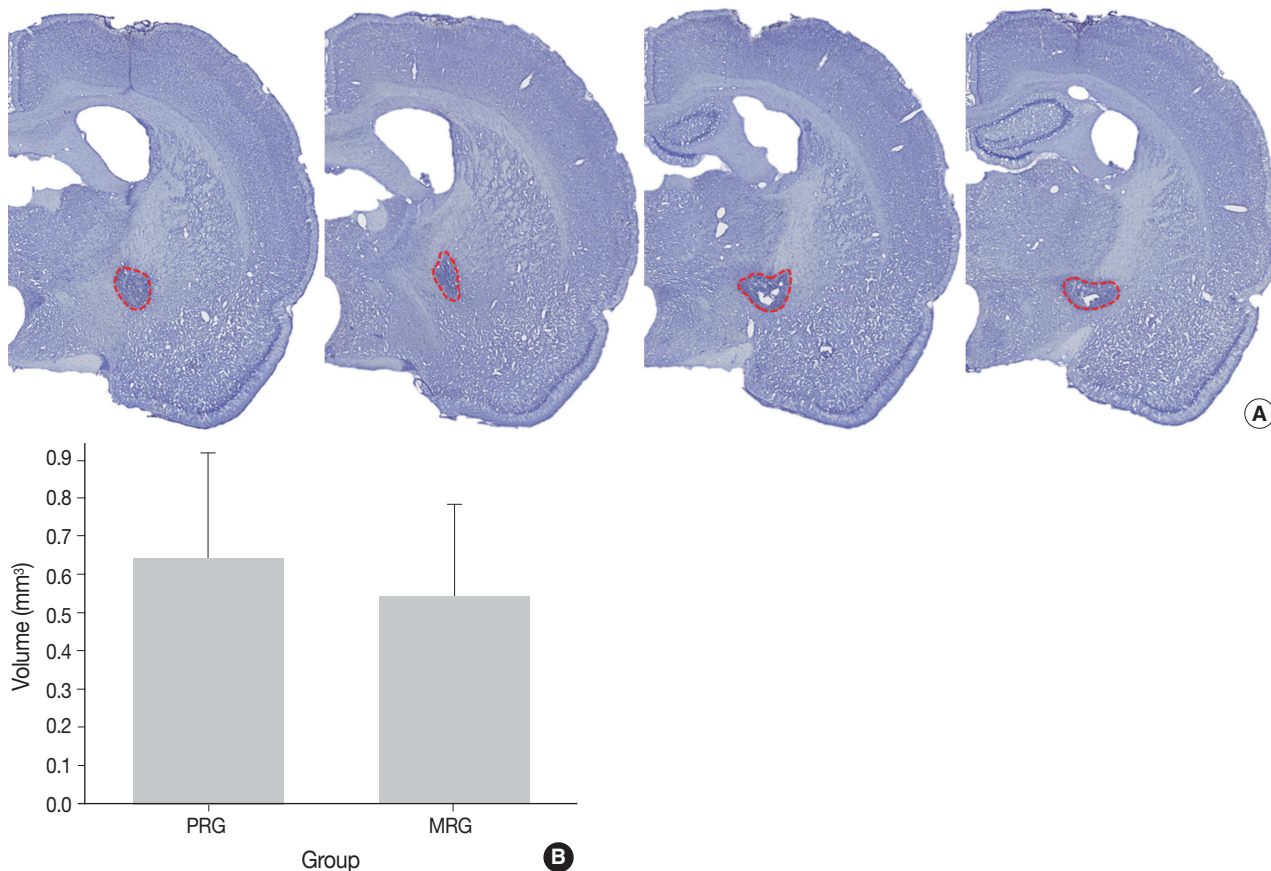


**Fig. 2.** A series of frozen sections with Nissl staining to measure infarct volume, marked with red dotted line, are present (A). Graphic presentation of the volumes reveals no significant difference between the moderate recovery group (MRG) and poor recovery group (PRG) (B).

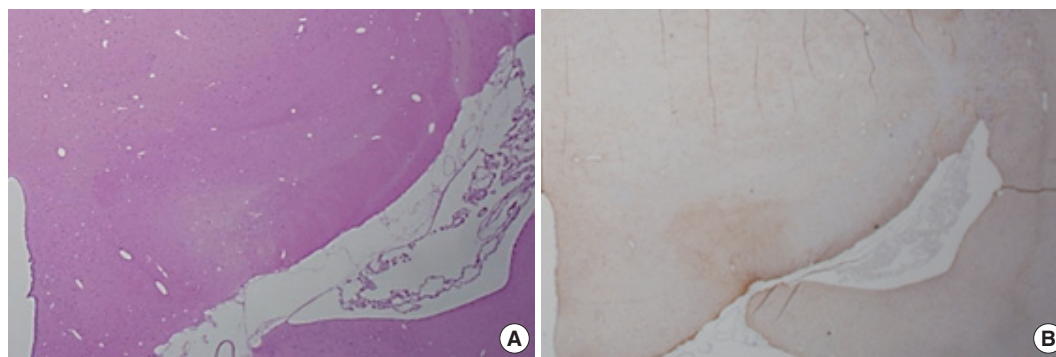


**Fig. 3.** Light microscopy findings of stroke involving the poster limb of the internal capsule (PLIC). Coronal sectioning reveals a poorly defined focal lesion characterized by loss of hematoxylin and eosin (H&E) staining (A) and increased glial fibrillary acidic protein (GFAP) staining (B) at 3 hours post-ischemia. (Continued to the next page)

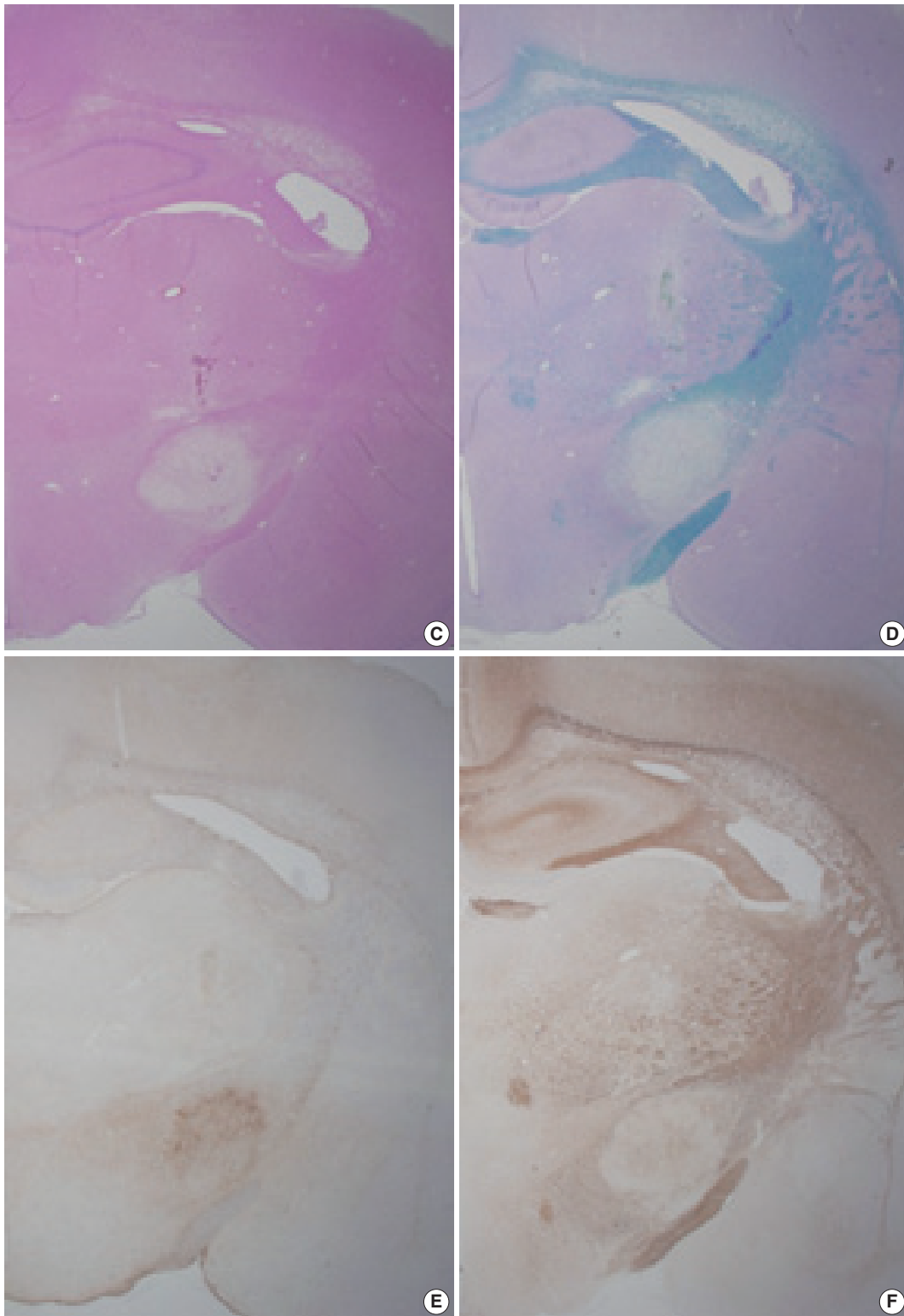


**Fig. 3.** (Continued from the previous page) A well-demarcated, pale, whitish lesion is identified by low magnification microscopy via H&E and luxol fast blue–periodic acid-Schiff (LBPAS) staining (C, D), and GFAP and neurofilament protein immunostaining (E, F) at 12 hours to 1 day post-ischemia. (Continued to the next page)

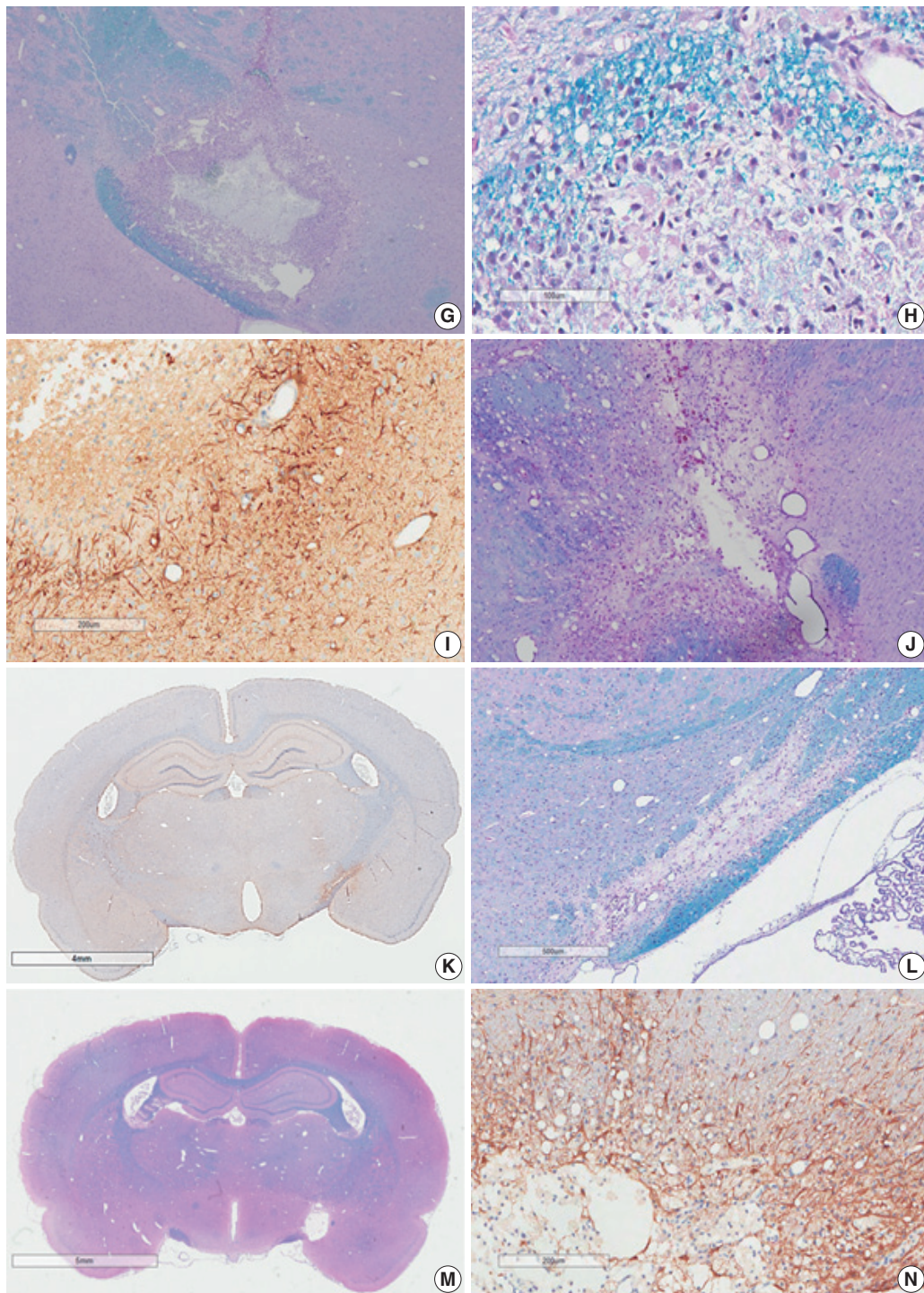


**Fig. 3.** (Continued from the previous page) The focal lesion shows central necrosis surrounded by macrophages (G) phagocytized with myelinated axon debris (H) by LBPAS staining, and GFAP-positive hypertrophic astrocytes along the lesion periphery (I) at 4 days post-ischemia. The necrotic center is gradually reduced in volume, and infiltrating macrophages decrease in number at 7 days post-ischemia. However, macrophages persist, and phagocytize periodic acid-Schiff-positive myelin debris as shown through LBPAS staining (J). At 14 to 21 days post-ischemia, the infarct lesion presents as a pseudocystic cavity consisting of reactive astrocytes, macrophages, and newly formed capillaries. The motor recovery at 14 to 21 days post-ischemia is related to the completeness of axonal injury in the PLIC. In the moderate recovery group, LBPAS staining in the PLIC revealed a pseudocystic lesion surrounded by GFAP-positive reactive astrocytes (K), and partially preserved myelinated axons passing in the PLIC periphery (L). In the poor recovery group, myelinated axons in the PLIC were completely disrupted as shown by LBPAS staining (M) and were replaced by a cystic cavity surrounded by GFAP-positive reactive astrocytes (N).

central geographic necrosis surrounded by a wall of macrophages, in which each macrophage had a central nucleus with prominent nucleoli and abundant cytoplasm phagocytized with light-blue or reddish granular debris (Fig. 3H). Loss of NFP staining in the PLIC also indicated lesion developed. Neutrophil did not infiltrate in the lesion. Strong GFAP staining highlighted presence of hypertrophic astrocytes along the periphery of the infarct lesion and neighboring WM (Fig. 3I).

At 7 days post-ischemia, the necrotic center showed a decreased volume, and was surrounded by infiltrating macrophages, reactive hypertrophic astrocytes, and newly formed capillaries. Infiltrating macrophages actively phagocytized reddish granular debris throughout the infarct lesion, clearly shown by LBPAS staining (Fig. 3J). At 14 to 21 days post-ischemia, central necrosis was distinctly resolved and the lesion was a pseudocystic with loosely arranged cellular elements. The lesion consisted of a mixture of foamy macrophages, hypertrophic astrocytes with elongated processes, and newly formed capillaries. Critical histopathological features related to motor dysfunction differences between the MRG and PRG were investigated. A portion of myelinated axon bundles passing the PLIC was preserved, as illustrated by immunohistochemical stains for GFAP and NFP and LBPAS staining (Fig. 3K, L). However, the fiber tract of myelinated axons forming the PLIC was severely disrupted and

formed pseudocysts in the PRG group, which was clearly identified by LBPAS staining at low magnification (Fig. 3M). In the interpretation of PLIC injury by light microscopy, careful examination of serial tissue sections is important. At 21 days post-ischemia, the focal infarct lesion persisted as a pseudocystic cavity. A few macrophages were still observed along the inner side of the angiolytic cavity (Fig. 3N). Microscopic examinations confirmed the presence of PLIC lesions (Table 2). The optic tract adjacent to the IC was partially injured in a few rats. However, the adjacent striatum and anterior limb of the IC were intact. The SOG did not show any damage within the underlying IC.

### Ultrastructural findings

Histopathological alterations resulting from early ischemic injury were further studied by electron microscopy (Table 2). In SOG, normal myelinated axons presented as a unit of a compact lamellar sheath closely encompassing an axon, and oligodendrocytes were surrounded by myelinated axons (Fig. 4A). Size measurement revealed two types of myelinated axons: large ( $0.85 \pm 0.18 \mu\text{m}$  diameter) and small ( $0.41 \pm 0.13 \mu\text{m}$ ). Even large axons presented in groups or singular aligned intimately with small axons. Each axon was filled with organized intermediate filament structures; called neurofilaments, and mitochondria were

**Table 2.** Histopathologic features of photothrombotic capsular infarct through the time

Time (post-ischemia)	Light microscopy	Electron microscopy
3–12 hr	Focal lesion with blurred margin Myelin pallor by H&E and LBPAS stain Increased GFAP and decreased NFP immunoreactivity from lesion center	Nodular swelling and loosening of compact myelin sheath Submyelin edema, interstitial Mild wrinkling of axons, but intact neurofilaments and mitochondria Reactive astrocytes with hypertrophic processes
1 day	Focal lesion on PLIC with well-defined margin Increased GFAP immunopositivity in the lesion and surrounding white matter Loss of NFP immunopositivity and LBPAS stainability No inflammatory cell infiltration	Fibrin thrombosis and capillary luminal obstruction Axonal swelling and flooding of organelles, extracellular edema Rupture of myelin sheath with subsequent demyelination Reactive astrocytes with hypertrophic processes Degeneration and apoptosis of oligodendrocytes
4 days	Focal infarct with central necrotic cavity surrounded by macrophages engulfing myelin debris Loss of myelinated axons of PLIC GFAP immunopositive hypertrophic astrocytes along the border of infarct and its vicinity	Markedly swollen axons with demyelination forming inflated ball or cystic appearance Marked extracellular edema with exudation Necrosis of cellular elements Macrophages phagocytized with myelin debris and dense bodies
7 days	Focal infarct with necrotic cavity surrounded by macrophages engulfing myelin debris, newly formed capillaries, and reactive astrogliosis	Reduced exudative change Degeneration and loss of myelin sheath, demyelinated axons Macrophages phagocytized with myelin debris and dense bodies
14 days	Focal infarct with necrotic cavity containing macrophages, hypertrophic astrocytes and newly formed capillaris Macrophages, progressively reduced in number	Demyelinated axons Astrogliosis Macrophages, markedly reduced phagocytic debris
21 days	Focal infarct with reduced necrotic cavity containing few macrophages and angiogliosis	Demyelinated axons Astrogliosis Macrophages with phagocytic debris still present

H&E, hematoxylin and eosin; LBPAS, luxol fast blue–periodic acid-Schiff; GFAP, glial fibrillary acidic protein; NFP, neurofilament protein; PLIC, posterior limb of internal capsule.

occasionally identified within axons. Progressive structural abnormalities in myelinated axons were observed within the ischemic lesion.

At 3 hours post-ischemia, platelets aggregated in the capillary lumen and exudative changes were present in interstitial spaces among myelinated axons. Nodular swelling with loosening of the myelin sheath and irregular wrinkling of axons was observed in both large and small myelinated fibers (Fig. 4B). Nodular loosening of the myelin sheath led to the formation of lamellar knob. With nodular loosening of myelin, a clear space devel-

oped in the submyelin area and contacted wrinkled axons with polygonal outlines. However, axonal integrity consisting of filamentous structures and mitochondria was relatively well preserved. Oligodendrocytes had relatively intact nuclei, rough endoplasmic reticulum (ER), and mitochondria. Myelin pallor observed by light microscopy in the early stage of the ischemic injury matched the ultrastructural edematous change in the myelin sheath, submyelin space, and wrinkled axons.

At 6 hours post-ischemia, whorled myelinated axons were formed by progressive loosening of the compact myelin lamellae

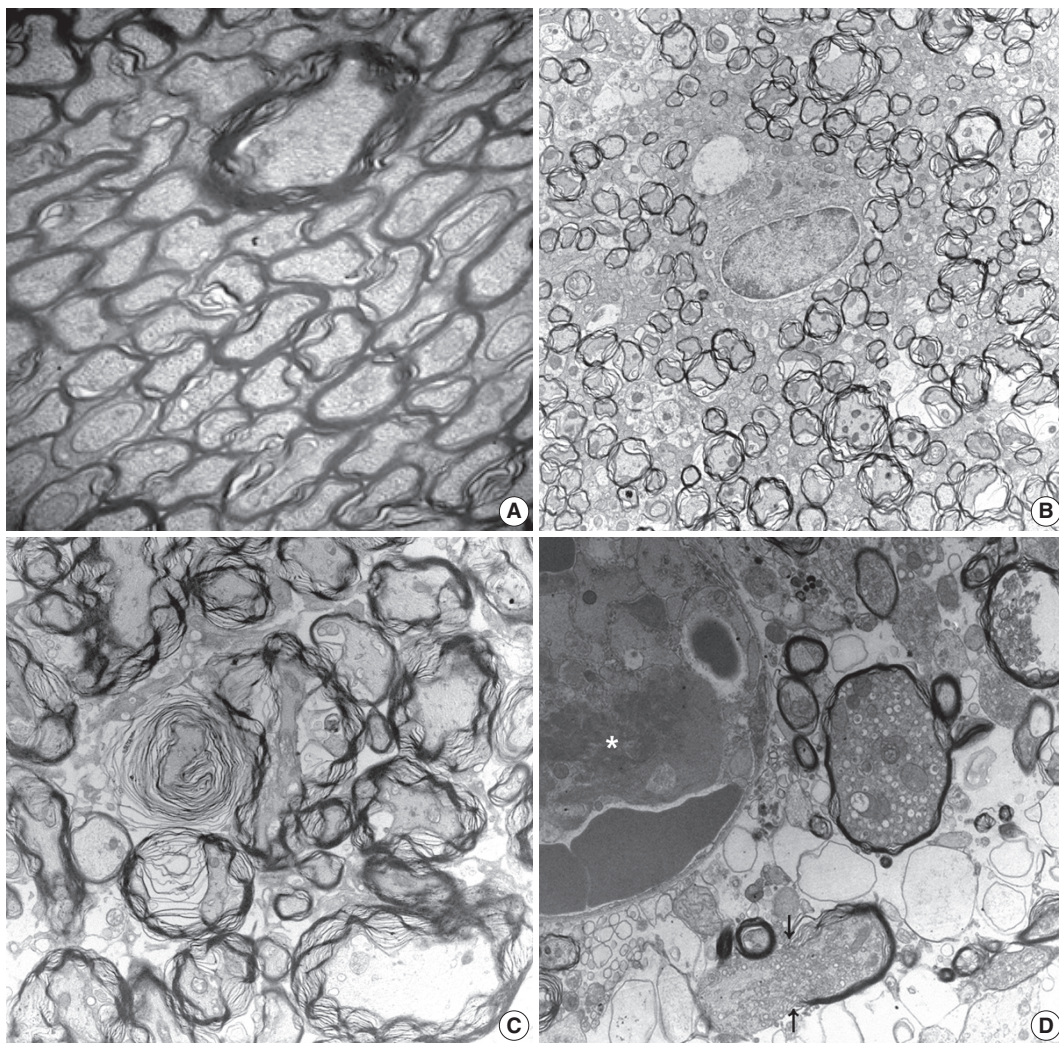


**Fig. 4.** Ultrastructural findings during the early stage of stroke involving the poster limb of internal capsule (PLIC). In the control group, a myelinated axon unit in PLIC had a compact lamellar sheath closely encompassing an axon (A,  $\times 6,000$ ). Each axon was filled with intermediate filament structures, called neurofilaments, and mitochondria. The lesion group presents early pathologic changes; nodular swelling and loosening of the myelin sheath, empty cystic change of submyelin space, polygonal wrinkling of axons, and accentuated cleft along the nuclear membrane of an oligodendrocyte (B,  $\times 3,000$ ) at 3 hours post-ischemia. Progressive loosening of the myelin sheath covers crinkled axons developing characteristic laminating whorled appearance (C,  $\times 10,000$ ) at 6 hours post-ischemia. Axonal swelling with a reactive change of the glial cells presented at 12 hours to 1 day post-ischemia (D-G). Swollen axons full of mitochondria, vesicles, and granules surrounded by a compact myelin sheath appeared. Fibrin thrombosis in capillary lumen (asterisk), a ruptured myelin sheath with extrusion of axonal organelles (arrows), and cystic vacuoles in the vicinity of swollen axons presented (D,  $\times 12,000$ ). (Continued to the next page)

covered with wrinkled axons (Fig. 4C). Large and small axons identified in SOG rats did not distinct significantly in MRG and PRG groups due to irregular loosening of the myelin sheath and markedly swollen axons. Small hydropic vacuoles developed, and intermediate filaments dissolved in wrinkled axons. At 12 hours to 1 day post-ischemia, the capillary lumen was obliterated by fibrin thrombosis. Nodular loosening of the myelin sheath decreased markedly, and wrinkled axons changed to plump, swollen axons. Swollen axons were filled with many mitochondria, vesicles, and granules, and showed mildly increased electron density (Fig. 4D). With rupture of the myelin sheath,

axonal organelles (mitochondria, neurofilaments, and vesicles) extruded. Large vacuoles formed by demyelination with axonal flooding were common. Expansion of the extracellular space containing edema fluid presented. Reactive astrocytes were identified by clubbed hypertrophic processes containing abundant intermediate filaments that intimately connected with swollen axons (Fig. 4E). Oligodendrocytes had variable pathologic features ranging from intact nuclei and mildly swollen ER in the cytoplasm to peripheral clumping of coarse chromatin along the nuclear membrane (Fig. 4F). Oligodendrocytes undergoing apoptosis in the ischemic lesion were identified by irreg-

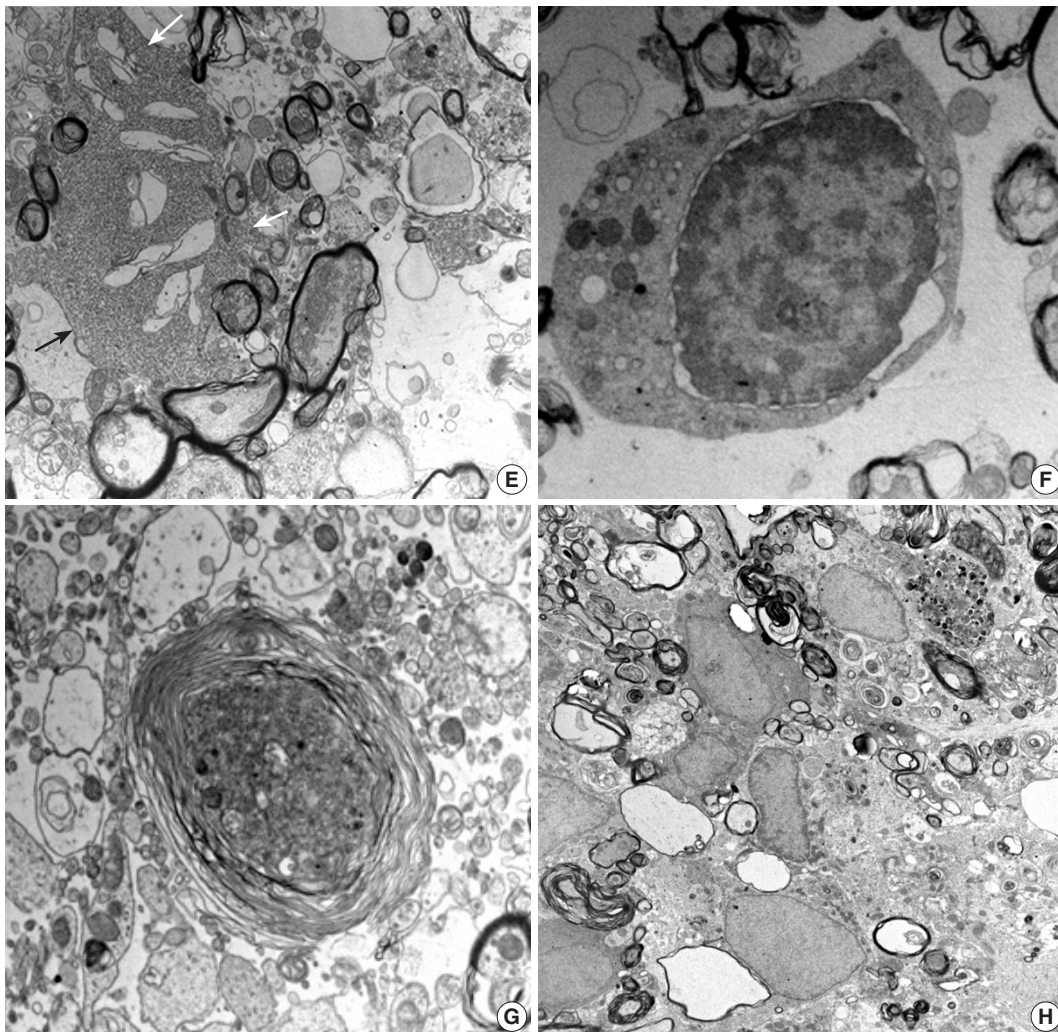


**Fig. 4.** (Continued from the previous page) Club-shaped processes of reactive astrocytes (arrows) intimately contacted swollen axons and organelles drifted from injured myelinated axons (E,  $\times 6,000$ ). Degenerative changes in an oligodendrocyte appear as an isolated cell with nuclear cytoplasmic dissociation by an irregular cleft, vesicles, and swollen mitochondria in the cytoplasm, and nuclear chromatin condensation along the nuclear membrane (F,  $\times 6,000$ ). Note the different stages of myelinated axon injury; from swollen axons filled with electron-dense organelles surrounded by a loosely arranged, laminating myelin sheath to demyelinated ghost axons formed by cystic vacuoles containing sparsely granular or myeloid debris (G,  $\times 6,000$ ). A series of myelinated axonal injury, from loosening myelin sheath to macrophages infiltration phagocytized myelin and other cellular debris, was present at 4 days post-ischemia (H,  $\times 6,000$ ).

ular clumping of coarse nuclear chromatin at the periphery of the nucleus, detachment of the nuclear membrane, and an electron-dense cytoplasm filled with swollen mitochondria and ER (Fig. 4F).

At 4 days post-ischemia, whorled myelinated axons were present though the pattern differed from those at 6 hours. The whorls were formed by swollen axons filled with cell organelles and electron-dense fine filamentous materials covered with whorled lamellae of myelin sheaths (Fig. 4G). Demyelinated ghost axons packed with edematous flooding were common. Macrophages had phagocytized degenerated and demyelinated axons and electron-dense bodies (Fig. 4H).

At 7 to 21 days post-ischemia, the exudative reaction subsided progressively. A number of unmyelinated or thinly myelinated axons were evident. Variably degenerated myelinated axons with an infiltration of scavenging macrophages were seen in the presence of hypertrophic astrocytes and oligodendrocytes. The ultrastructural features were compatible with a pseudocystic wall observed by light microscopy. The number of macrophages decreased with time, but hypertrophic astrocytes were still evident at 21 days post-ischemia.

Axon and myelin thickness was further separately assessed to identify their contributions to *g*-ratio changes. Axon diameter significantly decreased ( $p < .001$ ) at 3 hours to 6 hours post-ischemia. However, myelin thickness (calculated by nerve fiber diameter minus axon diameter) remarkably increased ( $p < .001$ ) at 3 to 6 hours, and then decreased at 24 hours post-ischemia. The increased axon diameter and decreased myelin thickness at 4 to 21 days post-ischemia contributed to an increased *g*-ratio in the experimental animals. *G*-ratios did not differ between sham subjects and the contralateral PLIC in the experimental group.

## DISCUSSION

In this experiment, a focal lesion in the PLIC was successfully created by laser light with a low intensity light source (814 mW/mm<sup>2</sup>) and a light delivery needle (28-gauge). The light scattering capacity is 44 times higher in the GM than in WM,<sup>27</sup> which might be a promising mechanism to induce a WM infarct in this study. This system created a focal infarct in the PLIC with a chronic loss of motor function, and minimized injury to the adjacent striatum and optic tract. Thus, unwanted neurological and behavioral manifestations did not occur during the experimental period. It was possible to study progressive histopathological changes in the ischemic infarct by light and electron

microscopy.

The human cerebrum is composed of 40% GM and 60% WM, and WM damage causes clinically significant neurological diseases including stroke and vascular dementia.<sup>12</sup> The main components of the WM; myelinated axons, astrocytes, and oligodendrocytes, were injured by photothrombotic ischemia and infarction. In this study, pathological features developed during the first 3-hour highlighted nodular loosening of the myelin sheaths with polygonal wrinkling or compression of the axons. The lesion might be caused by post-thrombotic edema of the WM, indicating that the myelin sheath is very vulnerable to ischemic injury. Concurrent decreases in axonal diameter and increases in myelin sheath thickness at 3 to 6 hours post-ischemia indicated that injury of the myelin sheath and axon were synchronized.

During the acute phase of ischemic injury, motor dysfunction developed through the damage to myelinated axons, observed by electron microscopy at first. Simultaneously, immediate reactive change of astrocytes, evidenced by increased GFAP immunopositivity in the lesion center, began to recover the damaged WM. Reactive astrocytes continuously presented at 21 days after the WM ischemia in this study. Traditionally, reactive astrogliosis were thought to be detrimental because they secreted inhibitory substrates and provided adverse mechanical barrier for the axonal and dendritic plasticity.<sup>28</sup> However, there were recent studies that reactive astrocytes might provide endogenous mechanisms to protect the ischemic injury and facilitate neural regeneration by releasing many trophic factors.<sup>29,30</sup> Experimental data of our on-going study, data not shown, proved by quantitative morphometric analysis that reactive astrocytes produce highly increased immunoreactivity for brain-derived neurotrophic factor (BDNF) and develop other cerebral lesion by neurotransmitter modification without direct focal ischemic injury, so called diaschisis.<sup>31</sup> BDNF-immunopositive reactive astrocytes facilitated to restore myelin integrity<sup>32</sup> and promoted oligodendroglial differentiation from oligodendroglial precursor cells (OPCs) after WM damage.<sup>33</sup> Intravenous injection of synthetic BDNF also assisted OPC maturation, oligodendrocyte replacement and WM remyelination in WM stroke model of rats.<sup>34</sup>

With the progression of injury to myelinated axons and oligodendrocytes, a focal cystic infarct lesion developed. Cystic infarct in WM were formed by swelling and rupture of myelinated axons, expansion of the extracellular space containing edema fluid, and subsequent loss of massively swollen cellular elements. Macrophages infiltrated the lesion at 4 days post-isch-

emic injury and phagocytized axon-myelin debris and fat globules. A number of cystic ghost axons also indicated simultaneous injury of axon and myelin sheath by ischemia. Infarct volumes did not differ between subjects in the MRG and PRG. Motor recovery in the two groups depended on the completeness of histopathological capsular injury induced by the ischemia. Subjects in the PRG had more complete thickness destruction of the fiber tract at the anterior PLIC, whereas those in the MRG had partial destruction of the IC in serial sections of the brain. The procedure was clinically well tolerated throughout the experimental period, which spanned from 3 hours to 21 days post-ischemia. These findings show that photothrombotic focal cerebral ischemia produce a highly reliable model of WM infarct in the PLIC.

The pathophysiological mechanisms of WM stroke were previously most comprehensively studied by ET-1 injection into rat brains.<sup>15-19</sup> The histopathological features differed according to the first component (axon or myelin) injured and experimental methods used. ET-1 impeded regional cerebral blood flow without disintegrating the blood-brain barrier and led to myelin disruption. Axonal injury was evident prior to any clear changes in myelin in the rat model of ET-1 induced WM ischemia, which is a hallmark of WM stroke.<sup>15</sup> Sozmen *et al.*<sup>35</sup> reported signs of early axonal damage that were observed through ultrastructural electron microscopy studies at 24 hours post-ischemia, whereas myelin sheaths appeared intact within the infarct. Strokes induced by ET-1 injection into the IC are characterized by a well-demarcated, focal, demyelinated lesion and necrosis after 14 days.<sup>16</sup> In this study involving photothrombotic ischemia, concomitant axonal and myelin damage were observed by light and electron microscopy. Although ultrastructural features of whorled myelin formation and polygonal wrinkling of axons appeared simultaneously in this study, edematous change of the myelin sheath was the first pathologic feature by WM ischemia. The photothrombotic model of WM ischemia was not comparable to the ET-1 model, but the histopathological features are significantly similar to those of human WM stroke.

The inflammatory response following photothrombotic focal ischemia in the GM and WM is contested. A previous study reported prominent neutrophilic infiltrations in the GM at 24 to 48 hours post-ischemia, and cuffing of macrophages surrounding the central necrosis at 4 days post-ischemia.<sup>15,16</sup> However, prominent macrophage infiltration without neutrophil infiltrations was present at 4 days post-ischemia. Even when the same amount of ET-1 was administered to rats, a prominent macrophage/microglia response without neutrophil recruitment

in the striatum at 3 days<sup>15</sup> and a proliferative inflammatory response of both neutrophil and mononuclear leukocytes at 1 day post-ET-1 injection have been reported.<sup>18</sup> The difference in inflammatory cell types might be related to cytokines released from the damaged WM and GM and should be studied further. Astrocyte activation occurred early and appeared consecutively with myelin and axonal injury after photothrombotic ischemia. However, increased GFAP staining for astrocyte activation occurred later (7 to 14 days) than the early axonal damage in ET-1-induced subcortical/WM stroke models.<sup>15</sup> In this experiment, increased GFAP staining indicated that the astrocyte response was limited to the PLIC lesion and appeared very early at 1 hour post-ischemia. The number of astrocytes did not change, and cell hypertrophy increased GFAP staining in the lesion. GFAP staining delineated the lesion site persistently during the experimental period. The GFAP-positive astrocyte response was similar to that in the photothrombotic and ET-1 induced WM strokes in rats. Increased the number of astrocytes with GFAP positivity also observed in the ET-1 mouse model.<sup>35</sup>

The AchA is a branch of the internal carotid artery,<sup>14</sup> and intraluminal occlusion of the AchA in rats resulted in variable infarct size in the IC and hypothalamus.<sup>36</sup> A study reported the comprehensive histopathology of IC lacunar infarcts by AchA occlusion in gyrencephalic brains of miniature pigs. The study defined the area of the ischemic lesion as the ischemic core (an irreversibly damaged area), peri-infarct area, and marginal zone.<sup>26</sup> Light and electron microscopy of the AchA occlusion model showed progressive histopathology of edema, disrupted axonal alignment, and aberrant myelin sheaths at 24 hours post-ischemia. GFAP-positive astrocytes in the peri-infarct area from early stages, infiltrated macrophages that phagocytized myelin debris and swollen axons, and several organelles within fragile myelin sheaths were also observed at 1 week post-ischemia. The most important finding from the ultrastructural analysis was that axonal damage resulted in myelin sheath instability and subsequent demyelination. These findings corresponded with the early and late histopathological changes found in the photothrombotic capsular infarct model used in this study. Ischemia disturbs ion homeostasis due to a loss of ATP, which results in Ca<sup>2+</sup> overload in axons and glia. This process is accelerated by glutamate-mediated over-activation of ionotropic receptors. An initial pathology of axon and myelin swelling in WM ischemia is caused by excess glutamatergic activation of the  $\alpha$ -amino-3-hydroxy-5-methyl-4-isoxazole propionic acid (AMPA) receptors in the axon, while excitotoxic activation of *N*-methyl-D-aspartate receptors is the initial event in GM ischemia.<sup>37</sup> Ischemia has also

been shown to induce excitotoxic damage to oligodendrocytes and astrocytes through AMPA receptors.<sup>29,38</sup>

In conclusion, cerebral WM is highly vulnerable to the effects of focal ischemia, among which myelinated axon is damaged first. Early and persistent increase of GFAP immunopositivity in astrocytes might be important for investigating the molecular mechanism of WM infarcts as well as the endogenous or exogenous neuroprotective responses involved. Future studies will be focused on biologic interactive mechanisms among neurons, myelinated axons, astrocytes, oligodendrocytes, and vascular endothelial cells in the experimental model.

### Conflicts of Interest

No potential conflict of interest relevant to this article was reported.

### Acknowledgments

This study was supported by a grant (CRI 13072-3) of the CNUH-GIST.

## REFERENCES

- Schneider AT, Kissela B, Woo D, *et al.* Ischemic stroke subtypes: a population-based study of incidence rates among blacks and whites. *Stroke* 2004; 35: 1552-6.
- Hachinski VC, Potter P, Merskey H. Leuko-araiosis. *Arch Neurol* 1987; 44: 21-3.
- Matsusue E, Sugihara S, Fujii S, Ohama E, Kinoshita T, Ogawa T. White matter changes in elderly people: MR-pathologic correlations. *Magn Reson Med Sci* 2006; 5: 99-104.
- Fu JH, Lu CZ, Hong Z, Dong Q, Luo Y, Wong KS. Extent of white matter lesions is related to acute subcortical infarcts and predicts further stroke risk in patients with first ever ischaemic stroke. *J Neurol Neurosurg Psychiatry* 2005; 76: 793-6.
- Kim GM, Park KY, Avery R, *et al.* Extensive leukoaraiosis is associated with high early risk of recurrence after ischemic stroke. *Stroke* 2014; 45: 479-85.
- Bailey EL, McCulloch J, Sudlow C, Wardlaw JM. Potential animal models of lacunar stroke: a systematic review. *Stroke* 2009; 40: e451-8.
- He SQ, Dum RP, Strick PL. Topographic organization of corticospinal projections from the frontal lobe: motor areas on the lateral surface of the hemisphere. *J Neurosci* 1993; 13: 952-80.
- Lee MC, Jin CY, Kim HS, *et al.* Stem cell dynamics in an experimental model of stroke. *Chonnam Med J* 2011; 47: 90-8.
- Song S, Park JT, Na JY, *et al.* Early expressions of hypoxia-inducible factor 1alpha and vascular endothelial growth factor increase the neuronal plasticity of activated endogenous neural stem cells after focal cerebral ischemia. *Neural Regen Res* 2014; 9: 912-8.
- Jang JW, Lee JK, Lee MC, Piao MS, Kim SH, Kim HS. Melatonin reduced the elevated matrix metalloproteinase-9 level in a rat photothrombotic stroke model. *J Neurol Sci* 2012; 323: 221-7.
- Liebigt S, Schlegel N, Oberland J, Witte OW, Redecker C, Keiner S. Effects of rehabilitative training and anti-inflammatory treatment on functional recovery and cellular reorganization following stroke. *Exp Neurol* 2012; 233: 776-82.
- Bush EC, Allman JM. The scaling of white matter to gray matter in cerebellum and neocortex. *Brain Behav Evol* 2003; 61: 1-5.
- Kudo T, Takeda M, Tanimukai S, Nishimura T. Neuropathologic changes in the gerbil brain after chronic hypoperfusion. *Stroke* 1993; 24: 259-64.
- He Z, Yamawaki T, Yang S, Day AL, Simpkins JW, Naritomi H. Experimental model of small deep infarcts involving the hypothalamus in rats: changes in body temperature and postural reflex. *Stroke* 1999; 30: 2743-51.
- Hughes PM, Anthony DC, Ruddin M, *et al.* Focal lesions in the rat central nervous system induced by endothelin-1. *J Neuropathol Exp Neurol* 2003; 62: 1276-86.
- Frost SB, Barbay S, Mumert ML, Stowe AM, Nudo RJ. An animal model of capsular infarct: endothelin-1 injections in the rat. *Behav Brain Res* 2006; 169: 206-11.
- Whitehead SN, Hachinski VC, Cechetto DF. Interaction between a rat model of cerebral ischemia and beta-amyloid toxicity: inflammatory responses. *Stroke* 2005; 36: 107-12.
- Souza-Rodrigues RD, Costa AM, Lima RR, Dos Santos CD, Picanco-Diniz CW, Gomes-Leal W. Inflammatory response and white matter damage after microinjections of endothelin-1 into the rat striatum. *Brain Res* 2008; 1200: 78-88.
- Tanaka Y, Imai H, Konno K, *et al.* Experimental model of lacunar infarction in the gyrencephalic brain of the miniature pig: neurological assessment and histological, immunohistochemical, and physiological evaluation of dynamic corticospinal tract deformation. *Stroke* 2008; 39: 205-12.
- Shibata M, Ohtani R, Ihara M, Tomimoto H. White matter lesions and glial activation in a novel mouse model of chronic cerebral hypoperfusion. *Stroke* 2004; 35: 2598-603.
- Kim HS, Kim D, Kim RG, *et al.* A rat model of photothrombotic capsular infarct with a marked motor deficit: a behavioral, histologic, and microPET study. *J Cereb Blood Flow Metab* 2014; 34: 683-9.
- Kim HS, Park MS, Lee JK, Kim HJ, Park JT, Lee MC. Time point

- expression of apoptosis regulatory proteins in a photochemically-induced focal cerebral ischemic rat brain. *Chonnam Med J* 2011; 47: 144-9.
23. Swanson RA, Morton MT, Tsao-Wu G, Savalos RA, Davidson C, Sharp FR. A semiautomated method for measuring brain infarct volume. *J Cereb Blood Flow Metab* 1990; 10: 290-3.
  24. Lee KH, Kang KJ, Moon KS, *et al.* Prognostic significance of neuronal marker expression in glioblastomas. *Childs Nerv Syst* 2012; 28: 1879-86.
  25. Kim JM, Lee TH, Lee MC, *et al.* Endoneurial microangiopathy of sural nerve in experimental vacor-induced diabetes. *Ultrastruct Pathol* 2002; 26: 393-401.
  26. Donovan V, Kim C, Anugerah AK, *et al.* Repeated mild traumatic brain injury results in long-term white-matter disruption. *J Cereb Blood Flow Metab* 2014; 34: 715-23.
  27. Bashkatov AN, Genina EA, Tuchin VV. Tissue optical properties. In: Boas DA, Pitris C, Ramanujam N, eds. *Handbook of biomedical optics*. Boca Raton: CRC Press, 2011; 67-100.
  28. Silver J, Miller JH. Regeneration beyond the glial scar. *Nat Rev Neurosci* 2004; 5: 146-56.
  29. Franke H, Verkhatsky A, Burnstock G, Illes P. Pathophysiology of astroglial purinergic signalling. *Purinergic Signal* 2012; 8: 629-57.
  30. Sato Y, Chin Y, Kato T, *et al.* White matter activated glial cells produce BDNF in a stroke model of monkeys. *Neurosci Res* 2009; 65: 71-8.
  31. Carrera E, Tononi G. Diaschisis: past, present, future. *Brain* 2014; 137(Pt 9): 2408-22.
  32. Fulmer CG, VonDran MW, Stillman AA, Huang Y, Hempstead BL, Dreyfus CF. Astrocyte-derived BDNF supports myelin protein synthesis after cuprizone-induced demyelination. *J Neurosci* 2014; 34: 8186-96.
  33. Miyamoto N, Maki T, Shindo A, *et al.* Astrocytes promote oligodendrogenesis after white matter damage via brain-derived neurotrophic factor. *J Neurosci* 2015; 35: 14002-8.
  34. Ramos-Cejudo J, Gutiérrez-Fernández M, Otero-Ortega L, *et al.* Brain-derived neurotrophic factor administration mediated oligodendrocyte differentiation and myelin formation in subcortical ischemic stroke. *Stroke* 2015; 46: 221-8.
  35. Sozmen EG, Kolekar A, Havton LA, Carmichael ST. A white matter stroke model in the mouse: axonal damage, progenitor responses and MRI correlates. *J Neurosci Methods* 2009; 180: 261-72.
  36. He Z, Yang SH, Naritomi H, *et al.* Definition of the anterior choroidal artery territory in rats using intraluminal occluding technique. *J Neurol Sci* 2000; 182: 16-28.
  37. Karadottir R, Cavalier P, Bergersen LH, Attwell D. NMDA receptors are expressed in oligodendrocytes and activated in ischaemia. *Nature* 2005; 438: 1162-6.
  38. Bakiri Y, Hamilton NB, Káradóttir R, Attwell D. Testing NMDA receptor block as a therapeutic strategy for reducing ischaemic damage to CNS white matter. *Glia* 2008; 56: 233-40.

# Overexpression of POSTN in Tumor Stroma Is a Poor Prognostic Indicator of Colorectal Cancer

Hyeon Jeong Oh<sup>1,2</sup> · Jeong Mo Bae<sup>2,3</sup>  
Xian-Yu Wen<sup>2</sup> · Nam-Yun Cho<sup>2</sup>  
Jung Ho Kim<sup>1,2</sup> · Gyeong Hoon Kang<sup>1,2</sup>

<sup>1</sup>Department of Pathology, Seoul National University College of Medicine, Seoul;  
<sup>2</sup>Laboratory of Epigenetics, Cancer Research Institute, Seoul National University College of Medicine, Seoul; <sup>3</sup>Department of Pathology, SMG-SNU Boramae Medical Center, Seoul, Korea

Received: October 11, 2016  
Revised: November 30, 2016  
Accepted: January 19, 2017

## Corresponding Author

Gyeong Hoon Kang, MD  
Department of Pathology, Seoul National University College of Medicine, 103 Daehak-ro, Jongno-gu, Seoul 03080, Korea  
Tel: +82-2-740-8263  
Fax: +82-2-765-5600  
E-mail: ghkang@snu.ac.kr

**Background:** Tumor microenvironment has recently drawn attention in that it is related with tumor prognosis. Cancer-associated fibroblast also plays a critical role in cancer invasiveness and progression in colorectal cancers. Periostin (POSTN), originally identified to be expressed in osteoblasts and osteoblast-derived cells, is expressed in cancer-associated fibroblasts in several tissue types of cancer. Recent studies suggest an association between stromal overexpression of POSTN and poor prognosis of cancer patients. **Methods:** We analyzed colorectal cancer cases for their expression status of POSTN in tumor stroma using immunohistochemistry and correlated the expression status with clinicopathological and molecular features. **Results:** High level of POSTN expression in tumor stroma was closely associated with tumor location in proximal colon, infiltrative growth pattern, undifferentiated histology, tumor budding, luminal necrosis, and higher TNM stage. High expression status of POSTN in tumor stroma was found to be an independent prognostic parameter implicating poor 5-year cancer-specific survival and 5-year progression-free survival. **Conclusions:** Our findings suggest that POSTN overexpression in tumor stroma of colorectal cancers could be a possible candidate marker for predicting poor prognosis in patients with colorectal cancers.

**Key Words:** Colorectal neoplasms; POSTN; Immunohistochemistry; Stromal overexpression; Clinicopathological characters; Prognosis

Colorectal cancer (CRC) is the third most common cancer in the world, with nearly 1.4 million new cases diagnosed in 2012, and South Korea is one of the countries with the highest incidence of CRC.<sup>1</sup> Although TNM staging of American Joint Committee on Cancer (AJCC) is the most powerful and reliable tool for prediction of prognosis and therapeutic decision making in CRC patients, the clinical outcome of CRC patients may vary even within the same cancer stage. Despite curative surgery and adjuvant chemotherapy and/or radiation therapy, approximately 17% of stage II CRCs and 33% of stage III CRCs will have a disease recurrence following primary therapy.<sup>2</sup> Identification of CRCs with a high risk of recurrence might give a chance of benefit from additional therapy. Many studies are trying to find factors that could more precisely stratify patients into different risk categories.

Recent studies find that tumor microenvironment and tumor-stroma interaction are critical in tumor behavior. In tumor microenvironment, cancer-associated fibroblasts have an impor-

tant role in tumor-stroma interaction and could affect prognosis.<sup>3-7</sup> However, there are no specific markers of cancer-associated fibroblasts that have been proven to be related with tumor prognosis. Periostin (POSTN) is a secreted extracellular matrix protein which is originally identified to be expressed in osteoblasts and osteoblast-derived cells. POSTN is normally expressed in not only collagen-rich fibrous connective tissues, including periosteum and periodontal ligament, but also fibroblasts of normal tissue, including stomach and colon.<sup>8</sup> POSTN is also expressed in cancer-associated fibroblasts of breast, colon, lung, pancreas, and stomach cancer.<sup>9,10</sup> POSTN binds integrins, including  $\alpha\beta3$ ,  $\alpha\beta5$ , and  $\alpha6\beta4$ , which leads to the activation of the Akt/protein kinase B and focal adhesion kinase signalling pathways.<sup>11-13</sup> POSTN-activated signalling pathways promote angiogenesis, cellular survival, and resistance to hypoxia-induced cell death.<sup>8,14</sup> POSTN is also involved in epithelial-mesenchymal transition of tumor.<sup>8</sup> Recent studies show that POSTN is associated with tumor invasiveness and poor prognosis in

several malignancies.<sup>15-17</sup>

In the present study, we analyzed 1,125 CRC cases for their expression status of POSTN using immunohistochemistry and correlated POSTN expression with molecular features of CRCs, including CpG island methylator phenotype (CIMP), microsatellite instability (MSI), and clinicopathological features of CRC, including survival of patients. We tried to identify whether POSTN expression in cancer-associated fibroblast can be a prognostic marker in CRC.

## MATERIALS AND METHODS

### Tissue samples

A consecutive series of CRC cases were retrieved from the surgical files of the Department of Pathology, Seoul National University Hospital, Seoul, Korea. Among the patients who underwent surgical resection for primary CRC from 2004 to 2007, we excluded those with neo-adjuvant treatment, non-invasive cancers, familial adenomatous polyposis, multiple or recurrent tumors, and a history of other malignancy within 5 years. Demographic data and clinicopathological information were retrieved from electronic medical records. Two pathologists (J.M.B. and G.H.K.) reviewed hematoxylin and eosin-stained tissue slides for the degree of histologic differentiation which was categorized as well-moderate versus poor (> 50% vs ≤ 50%, respectively). Staging was classified according to the sixth edition guidelines of the AJCC. Hematoxylin and eosin-stained slides were also reviewed for evaluation of tumor budding, which is defined to be present when five or more buddings are present at ×200 magnification. Status of tumor infiltrating lymphocytes was divided into high and low (≥ 8 at ×400 magnification and < 8 at ×400 magnification, respectively). The study was approved by Institutional Ethics Committee of Seoul National University Hospital which waived the requirement to obtain informed consent (approval No. 1502-029-647).

### Evaluation of POSTN expression

After reviewing the hematoxylin and eosin tissue slides, representative areas of the tumor invasive front were selected and marked. Two-millimeter-core tissues were harvested from individual paraffin-embedded colon cancer tissues and were arranged in a new recipient paraffin block using a trephine apparatus (Superbiochip Laboratories, Seoul, Korea). Immunohistochemical analysis was performed with commercially available antibody against POSTN (1:200, HPA012306, Sigma, St. Louis, MO, USA). Two pathologists (H.J.O. and J.M.B.) independently

evaluated POSTN immunohistochemistry. POSTN expression in tumor stroma showed homogeneous staining intensity and the level of POSTN expression was graded as 0 (negative), 1 (weak), 2 (moderate), and 3 (strong) (Fig. 1). Then, grades 0–2 and 3 were categorized as POSTN-low and POSTN-high, respectively.

### *BRAF* and *KRAS* mutation and microsatellite instability analysis

Through microscopic examination, representative tumor areas in each case were marked and microdissected. The dissected tissues were subject to incubation at 55°C with lysis buffer and proteinase K for 2 days. Allele specific polymerase chain reaction for *BRAF* codon 600 and direct sequencing of *KRAS* codons 12 and 13 were performed. The MSI status of each tumor tissue versus normal tissue was determined by five National Cancer Institute markers including BAT25, BAT26, D2S123, D5S346, and D17S250. High MSI status was defined as when tumor DNA had altered alleles compared to normal DNA in two or more markers. Low MSI status was defined as when tumor DNA had altered allele compared to normal DNA in one marker. Microsatellite stable was defined as when no altered allele was present in tumor DNA.

### CIMP analysis

CIMP status was examined by MethyLight assay. Bisulfite-modified DNA was subject to MethyLight assay which was performed as previously described.<sup>18</sup> Methylation statuses of eight CIMP-specific CpG islands (*CACNA1G*, *CDKN2A*, *CRABP1*, *IGF2*, *MLH1*, *NEUROG1*, *RUNX3*, and *SOC1*) were quantified. CIMP-high was defined as five or more markers methylated, and CIMP-low was defined as four or less markers methylated out of eight. CIMP-0 was defined as no methylated marker.

### Statistical analysis

SAS software (ver. 9.4 for Microsoft Windows, SAS Institute Inc., Cary, NC, USA) was used for the statistical analysis in our cohort. To compare clinicopathologic characteristics to stromal POSTN expression, we performed Pearson's chi-square test. The age of CRC group according to stromal POSTN expression was compared using Wilcoxon's rank-sum test. For the survival analysis, 5-year cancer-specific survival (CSS) and 5-year progression-free survival (PFS) were calculated using the log-rank test with a Kaplan-Meier curve. Hazard ratios (HRs) were calculated using the Cox proportional hazard model. The assumption of the proportional hazards was verified by plotting the  $\log[-\log\{S(t)\}]$

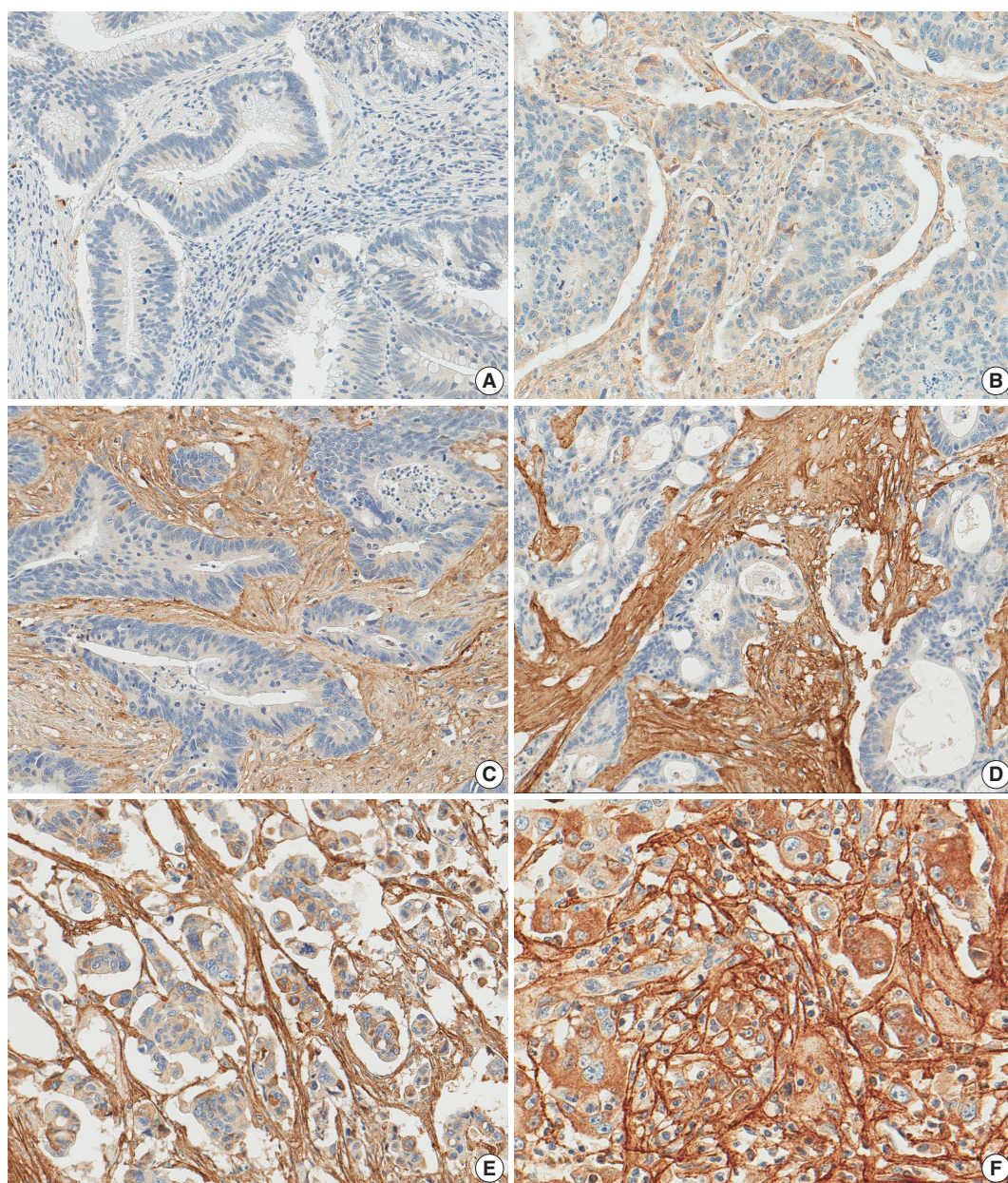


**Fig. 1.** Periostin expression in colorectal cancer. Grade 0 (A), grade 1 (B), grade 2 (C), and grade 3 (D) in moderately differentiated adenocarcinoma, grade 3 in poorly differentiated adenocarcinoma (E), grade 3 in high tumor budding area (F).

against the time of the study. In the modeling process, all variables that were associated with PFS with a  $p < .10$  were entered into an initial model; these variables were subsequently reduced by backward elimination. All statistical tests were two-sided, and statistical significance was defined as  $p < .05$ .

## RESULTS

### Patient characteristics

In a total of 1,135 CRC patients, the median age at diagnosis

was 62 years (range, 20 to 90 years). The male to female ratio was 1.49:1 (673 males and 452 females). Tumor location was proximal colon (proximal to splenic flexure) in 277 patients (24.6%), distal colon in 438 patients (38.9%), and rectum in 410 patients (36.4%). *KRAS* mutation and *BRAF* mutation were observed in 313 (27.8%) and 48 patients (4.3%), respectively. In microsatellite analysis, microsatellite stable, MSI-low, and MSI-high were observed in 964 (85.7%), 73 (6.5%), and 88 (7.8%) patients, respectively. In CIMP analysis, CIMP-0, CIMP-low, and CIMP-high were observed in 510 (45.3%), 553 (49.2%), and

62 (5.5%) patients, respectively. Median follow-up duration was 69.8 months (range, 0.3 to 150.2 months). Seven hundred seventy-nine patients received 5-fluorouracil (5-FU)-based adjuvant chemotherapy.

### Clinicopathological features of CRCs according to stromal POSTN expression

Of 1,125 CRC cases, 33 (2.9%), 296 (26.3%), 492 (43.7%), and 304 (27.0%) patients showed stromal POSTN expression

from grade 0 to 3, respectively. POSTN-low CRCs were 821 (73.0%) and POSTN-high CRCs were 304 (27.0%) (Table 1). CRCs with stromal POSTN-high expression were associated with proximal location (35.2% in POSTN-high group vs 20.7% in POSTN-low group,  $p < .001$ ), infiltrative growth pattern (44.7% vs 30.7%,  $p < .001$ ), advanced T, N, M category ( $p < .001$ ), frequent tumor budding (80.9% vs 68.2%,  $p < .001$ ) and luminal necrosis (94.4% vs 89.6%,  $p = .014$ ) compared with CRCs with stromal POSTN-low expression. In molecular aspect,

**Table 1.** Clinicopathologic characteristics of colorectal cancers according to the stromal POSTN expression

Variable		POSTN-low (n=821, 73.0%)	POSTN-high (n=304, 27.0%)	p-value
Age (yr)		62 (20–87)	62 (29–90)	.932
Sex	Male	500 (60.9)	173 (56.9)	.225
	Female	321 (39.1)	131 (43.1)	
Location	Proximal	170 (20.7)	107 (35.2)	< .001
	Distal	336 (40.9)	102 (33.5)	
	Rectum	315 (38.4)	95 (31.3)	
Growth pattern	Fungating	569 (69.3)	168 (55.3)	< .001
	Infiltrative	252 (30.7)	136 (44.7)	
T category	T1,2	192 (23.4)	18 (5.9)	< .001
	T3,4	629 (76.6)	286 (94.1)	
N category	N0	454 (55.3)	117 (38.5)	< .001
	N1,2	367 (44.7)	187 (61.5)	
M category	0	712 (86.7)	222 (73.0)	< .001
	1	109 (13.3)	82 (27.0)	
Stage	I, II	432 (52.6)	104 (34.2)	< .001
	III, IV	109 (13.3)	200 (65.8)	
Differentiation	Differentiated	802 (97.7)	284 (93.4)	.001
	Undifferentiated	19 (2.3)	20 (6.6)	
Tumor budding	Absent	261 (31.8)	58 (19.1)	< .001
	Present	560 (68.2)	246 (80.9)	
Dirty necrosis	Absent	85 (10.4)	17 (5.6)	.014
	Present	736 (89.6)	287 (94.4)	
Crohn-like reaction	Absent	703 (85.6)	251 (82.6)	.204
	Present	118 (14.4)	53 (17.4)	
Tumor-infiltrating lymphocytes	High ( $\geq 8$ /HPF)	599 (73.0)	233 (76.6)	.211
	Low ( $< 8$ /HPF)	222 (27.0)	71 (23.4)	
Serration	Absent	793 (96.6)	288 (94.7)	.155
	Present	28 (3.4)	16 (5.3)	
Mucin production	Absent	727 (88.5)	265 (87.2)	.525
	Present	94 (11.5)	39 (12.8)	
CIMP	CIMP-0	387 (47.1)	123 (40.5)	.030
	CIMP-low	396 (48.2)	157 (51.6)	
	CIMP-high	38 (4.6)	24 (7.9)	
MSI	MSS	702 (85.5)	262 (86.2)	.959
	MSI-low	54 (6.6)	19 (6.2)	
	MSI-high	65 (7.9)	23 (7.6)	
KRAS mutation	Wild type	602 (73.3)	210 (69.1)	.158
	Mutant	219 (26.7)	94 (30.9)	
BRAF mutation (n=1,124)	Wild type	791 (96.5)	285 (93.7)	.046
	Mutant	29 (3.5)	19 (6.3)	

Values are presented as median (range) or number (%).

POSTN, periostin; HPF, high-power field; CIMP, CpG island methylator phenotype; MSI, microsatellite instability.

CRCs with stromal POSTN-high expression showed higher frequency of CIMP-high (7.9% vs 4.6%,  $p = .030$ ) and *BRAF* mutation (6.3% vs 3.5%,  $p = .046$ ) compared with CRCs with stromal POSTN-low expression. However, the frequency of MSI-high and *KRAS* mutation were not statistically associated with stromal POSTN expression.

### Prognostic implication of stromal POSTN expression in CRCs

When we performed univariate survival analysis, CRCs with

stromal POSTN-high expression showed worse 5-year PFS (HR, 1.80; 95% CI, 1.47 to 2.20;  $p < .001$ ) (Fig. 2A) and worse 5-year CSS (HR, 2.00; 95% CI, 1.52 to 2.63;  $p < .001$ ) (Fig. 2B) compared with CRCs with stromal POSTN-low expression. In multivariate survival analysis, stromal POSTN-high expression was an independent prognostic indicator of poor 5-year CSS (HR, 1.50; 95% CI, 1.13 to 2.00;  $p = .006$ ) (Table 2) and poor 5-year PFS (HR, 1.38; 95% CI, 1.12 to 1.70;  $p = .003$ ) (Table 3).

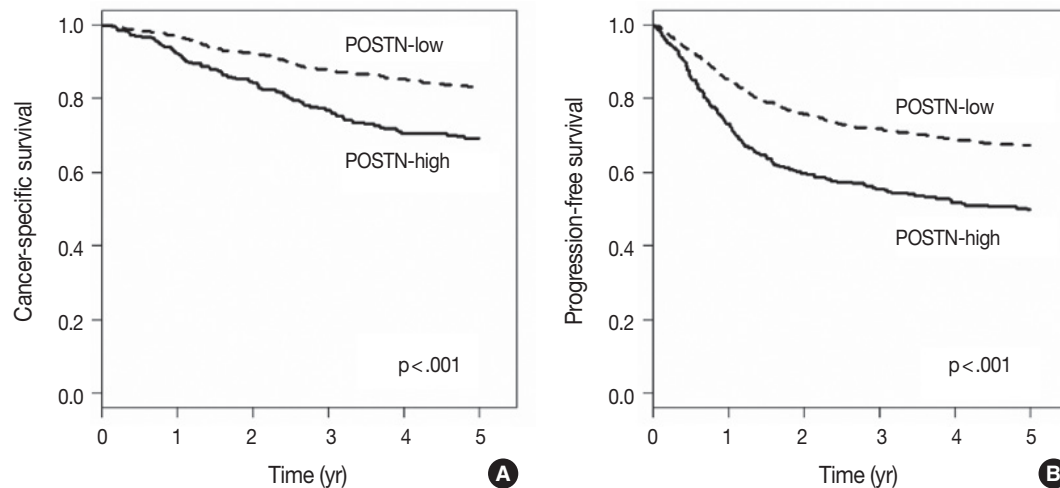


**Fig. 2.** Kaplan-Meier survival curves according to the stromal periostin (POSTN) expression. (A) Five-year cancer-specific survival. (B) Five-year progression-free survival.

**Table 2.** Univariate and multivariate analysis with respect to 5-year cancer-specific survival

Variable	Univariate		Multivariate	
	HR	p-value	HR	p-value
Gross (infiltrative/fungating)	1.87 (1.32–2.66)	< .001	1.64 (1.24–2.18)	.001
Stage (III, IV/I, II)	4.52 (3.26–6.26)	< .001	6.30 (4.27–9.29)	< .001
Differentiation (PD/WD, MD)	3.41 (2.05–5.67)	< .001	2.15 (1.27–3.62)	.013
<i>BRAF</i> (mutant/wild type)	1.92 (1.15–3.19)	.012	1.92 (1.11–3.34)	.041
Chemotherapy (treated/not-treated)	0.94 (0.71–1.25)	.655	0.38 (0.28–0.52)	< .001
POSTN (high/low)	2.00 (1.52–2.64)	< .001	1.50 (1.13–2.00)	.006
Tumor location (right/left)	1.56 (1.19–2.06)	.002	1.46 (1.09–1.96)	.011
Tumor-infiltrating lymphocytes (high/low)	0.69 (0.49–0.97)	.032	-	.051
Budding (present/absent)	1.90 (1.36–2.66)	< .001	-	.129
Crohn-like reaction (present/absent)	0.71 (0.48–1.06)	.095	-	.305
Age ( $\geq 65$ yr/ $< 65$ yr)	1.49 (1.15–1.93)	.003	-	.053
CIMP (CIMP-H/CIMP-0, L)	1.91 (1.21–3.02)	.006	-	.632
Sex (male/female)	1.04 (0.80–1.36)	.762	-	-
Necrosis (present/absent)	1.11 (0.70–1.78)	.652	-	-
Serration (present/absent)	1.42 (0.80–2.54)	.235	-	-
Mucin (present/absent)	1.32 (0.92–1.90)	.136	-	-
MSI (MSI-H/MSS, MSI-L)	0.82 (0.48–1.41)	.476	-	-
<i>KRAS</i> (mutant/wild type)	1.12 (0.84–1.49)	.440	-	-

HR, hazard ratio; PD, poorly differentiated; WD, well differentiated; MD, moderately differentiated; POSTN, periostin; CIMP, CpG island methylator phenotype; CIMP-H, CIMP-high; CIMP-L, CIMP-low; MSI, microsatellite instability; MSI-H, MSI-high; MSS, microsatellite stable; MSI-L, MSI-low.

**Table 3.** Univariate and multivariate analysis with respect to 5-year progression-free survival

Variable	Univariate		Multivariate	
	HR (95% CI)	p-value	HR (95% CI)	p-value
Gross (infiltrative/fungating)	1.96 (1.61–2.39)	<.001	1.43 (1.17–1.76)	.001
Stage (III, IV/I, II)	4.72 (3.71–6.02)	<.001	4.75 (3.63–6.23)	<.001
Differentiation (PD/WD, MD)	3.32 (2.28–4.85)	<.001	1.85 (1.26–2.71)	.002
<i>BRAF</i> (mutant/wild type)	1.61 (1.06–2.45)	.027	1.72 (1.12–2.63)	.013
Chemotherapy (treated/not-treated)	1.40 (1.11–1.76)	.004	0.59 (0.46–0.76)	<.001
POSTN (high/low)	1.80 (1.47–2.20)	<.001	1.40 (1.08–1.83)	.012
Budding (present/absent)	2.15 (1.66–2.79)	<.001	1.51 (1.15–1.97)	.003
Crohn-like reaction (present/absent)	0.72 (0.53–0.98)	.034	-	.302
Tumor-infiltrating lymphocytes (high/low)	0.70 (0.55–0.89)	.004	-	.089
Tumor location (right/left)	1.22 (0.98–1.51)	.080	-	.773
Age ( $\geq 6$ yr/ $< 65$ yr)	1.22 (1.00–1.49)	.046	-	.098
CIMP (CIMP-H/CIMP-0, L)	1.44 (0.98–2.12)	.061	-	.277
Sex (male/female)	0.94 (0.77–1.14)	.514	-	-
Necrosis (present/absent)	1.14 (0.80–1.62)	.463	-	-
Serration (present/absent)	1.32 (0.83–2.08)	.244	-	-
Mucin (present/absent)	1.12 (0.84–1.50)	.448	-	-
MSI (MSI-H/MSS, MSI-L)	0.80 (0.54–1.20)	.285	-	-
<i>KRAS</i> (mutant/wild type)	1.05 (0.85–1.31)	.633	-	-

HR, hazard ratio; CI, confidence interval; PD, poorly differentiated; WD, well differentiated; MD, moderately differentiated; POSTN, periostin; CIMP, CpG island methylator phenotype; CIMP-H, CIMP-high; MSI, microsatellite instability; MSI-H, MSI-high; MSS, microsatellite stable; MSI-L, MSI-low.

## DISCUSSION

Recent studies show POSTN is overexpressed in cancer stroma of various malignancies, including colorectal, breast, lung, pancreatic, ovarian, gastric, head and neck, thyroid and prostate cancer as well as in glioblastoma.<sup>19</sup> POSTN is thought to play important roles in tumorigenesis, such as invasiveness, metastasis, angiogenesis, lymphangiogenesis, and chemoresistance.<sup>8,15,20-24</sup> In this study, we found that POSTN is overexpressed in 304 (27.0%) out of 1,125 cases, which is consistent with the results of other studies in several malignancies.<sup>19</sup> Our study demonstrated that high POSTN expression is correlated with several aggressive clinicopathological features of CRCs. First, stromal POSTN expression was higher in CRCs of infiltrative growth pattern than CRCs of fungating growth pattern, which implies that POSTN is involved in infiltrative growth of tumor. Second, POSTN expression was correlated with T, N, or M category. These results suggest that POSTN might participate in tumor progression and nodal or distant metastasis, which is consistent with the results of a recent study that POSTN expression is higher in distant metastatic lesion than in matched primary colorectal lesion.<sup>17</sup> Cell line studies demonstrated that POSTN induces invasive activity and bestows a metastatic potential to HEK 293T cells which are tumorigenic but nonmetastatic.<sup>11,17</sup> These results support the idea that POSTN might contribute

to metastasis of tumor cells. Third, high tumor budding status was correlated with high POSTN expression. Several studies addressed that tumor budding should be regarded as a biomarker of poor prognosis, correlated with epithelial mesenchymal transition.<sup>25-28</sup> A cell line study has demonstrated that stable transfection of POSTN induced epithelial-mesenchymal transition and increased invasive activity in HEK 293T cells.<sup>11</sup> However, our present study has several limitations. First, this study is a retrospective study in a single institution. Second, stromal POSTN expression was evaluated in tissue microarray.

In our study, stromal POSTN expression was associated with CIMP-high and *BRAF* mutation. Because CIMP-high and *BRAF* mutation are hallmarks of molecular alterations in serrated neoplasia pathway, we can presume that stromal POSTN overexpression is associated with serrated neoplasia pathway. In a study by De Sousa *et al.*,<sup>29</sup> CCS3 subtype, which is related with serrated neoplasia pathway, showed overexpression of genes associated with epithelial mesenchymal transition and matrix remodeling. Recently, Fessler *et al.*<sup>30</sup> demonstrated the induction of a mesenchymal phenotype upon transforming growth factor  $\beta$  treatment in a genetically engineered organoid culture carrying *BRAF* V600E mutation. In serrated neoplasia pathway, three molecular groups are known to be involved. One is *BRAF*-mutant/CIMP-high/MSI-high subgroup, another is *BRAF*-mutant/CIMP-high/microsatellite stable (MSS) subgroup, and

the other is *KRAS*-mutant/CIMP-low/MSS subgroup.<sup>31,32</sup> In this study, stromal POSTN overexpression was related with *BRAF*-mutant/CIMP-high/MSS subgroup (data not shown). Moreover, some clinicopathological features associated with CIMP, such as right colon preponderance, poor differentiation, high rates of tumor budding, frequent lymphatic, vascular, or perineural invasion and nodal metastasis, were more frequently observed in POSTN-high colon cancer compared with POSTN-low colon cancer. Further molecular test is needed to elucidate the relation between high POSTN stromal expression and serrated neoplasia pathway.

An accumulating series of study results indicate that cancer-associated fibroblasts contribute to chemo-resistance and poor patient survival.<sup>15,17,28</sup> According to Xu *et al.*, medium to high stromal POSTN expression was an independent predictor of poor disease-free survival and disease-specific survival. They also presented the association of chemo-resistance and stromal POSTN expression in stage II CRCs and stage III CRCs with chemotherapy history. In *in vitro* study, SW480 and HT29 cells cultured in stromal POSTN-enriched media showed chemoresistance to 5-FU. Recombinant POSTN increased proliferation and phosphorylation of Akt in SW480 and HT29 cells. Furthermore, the proliferation and phosphorylation of Akt were inhibited by phosphoinositide 3-kinase inhibitor LY294002.<sup>17,24</sup> In our present study, stromal POSTN-high expression was an independent prognostic indicator of poor 5-year CSS and 5-year PFS. However, we could not confirm the chemo-resistance effect of stromal POSTN expression in our cohort (data not shown).

In conclusion, our findings suggest that immunohistochemical evaluation of stromal POSTN expression could be utilized for the identification of a subset of CRCs with poor prognosis. To determine whether stromal POSTN expression status is a prognostic marker of CRC, further studies are needed to validate this finding with an independent series of large-scaled CRC cases.

### Conflicts of Interest

No potential conflict of interest relevant to this article was reported.

### REFERENCES

1. Ferlay J, Soerjomataram I, Dikshit R, *et al.* Cancer incidence and mortality worldwide: sources, methods and major patterns in GLOBOCAN 2012. *Int J Cancer* 2015; 136: E359-86.
2. O'Connell MJ, Campbell ME, Goldberg RM, *et al.* Survival follow-

- ing recurrence in stage II and III colon cancer: findings from the ACCENT data set. *J Clin Oncol* 2008; 26: 2336-41.
3. Bozóky B, Savchenko A, Csermely P, *et al.* Novel signatures of cancer-associated fibroblasts. *Int J Cancer* 2013; 133: 286-93.
4. Chen WJ, Ho CC, Chang YL, *et al.* Cancer-associated fibroblasts regulate the plasticity of lung cancer stemness via paracrine signaling. *Nat Commun* 2014; 5: 3472.
5. Huang L, Xu AM, Liu S, Liu W, Li TJ. Cancer-associated fibroblasts in digestive tumors. *World J Gastroenterol* 2014; 20: 17804-18.
6. Hwang RF, Moore T, Arumugam T, *et al.* Cancer-associated stromal fibroblasts promote pancreatic tumor progression. *Cancer Res* 2008; 68: 918-26.
7. Pankova D, Chen Y, Terajima M, *et al.* Cancer-associated fibroblasts induce a collagen cross-link switch in tumor stroma. *Mol Cancer Res* 2016; 14: 287-95.
8. Morra L, Moch H. Periostin expression and epithelial-mesenchymal transition in cancer: a review and an update. *Virchows Arch* 2011; 459: 465-75.
9. Kikuchi Y, Kashima TG, Nishiyama T, *et al.* Periostin is expressed in pericryptal fibroblasts and cancer-associated fibroblasts in the colon. *J Histochem Cytochem* 2008; 56: 753-64.
10. Fukushima N, Kikuchi Y, Nishiyama T, Kudo A, Fukayama M. Periostin deposition in the stroma of invasive and intraductal neoplasms of the pancreas. *Mod Pathol* 2008; 21: 1044-53.
11. Yan W, Shao R. Transduction of a mesenchyme-specific gene periostin into 293T cells induces cell invasive activity through epithelial-mesenchymal transformation. *J Biol Chem* 2006; 281: 19700-8.
12. Gillan L, Matei D, Fishman DA, Gerbin CS, Karlan BY, Chang DD. Periostin secreted by epithelial ovarian carcinoma is a ligand for  $\alpha V\beta 3$  and  $\alpha V\beta 5$  integrins and promotes cell motility. *Cancer Res* 2002; 62: 5358-64.
13. Baril P, Gangeswaran R, Mahon PC, *et al.* Periostin promotes invasiveness and resistance of pancreatic cancer cells to hypoxia-induced cell death: role of the beta4 integrin and the PI3k pathway. *Oncogene* 2007; 26: 2082-94.
14. Bao S, Ouyang G, Bai X, *et al.* Periostin potently promotes metastatic growth of colon cancer by augmenting cell survival via the Akt/PKB pathway. *Cancer Cell* 2004; 5: 329-39.
15. Sung PL, Jan YH, Lin SC, *et al.* Periostin in tumor microenvironment is associated with poor prognosis and platinum resistance in epithelial ovarian carcinoma. *Oncotarget* 2016; 7: 4036-47.
16. Underwood TJ, Hayden AL, Derouet M, *et al.* Cancer-associated fibroblasts predict poor outcome and promote periostin-dependent invasion in oesophageal adenocarcinoma. *J Pathol* 2015; 235: 466-77.
17. Xu X, Chang W, Yuan J, *et al.* Periostin expression in intra-tumoral stromal cells is prognostic and predictive for colorectal carcinoma

- via creating a cancer-supportive niche. *Oncotarget* 2016; 7: 798-813.
18. Kim JH, Shin SH, Kwon HJ, Cho NY, Kang GH. Prognostic implications of CpG island hypermethylator phenotype in colorectal cancers. *Virchows Arch* 2009; 455: 485-94.
  19. Ratajczak-Wielgomas K, Dziegiel P. The role of periostin in neoplastic processes. *Folia Histochem Cytobiol* 2015; 53: 120-32.
  20. Kyutoku M, Taniyama Y, Katsuragi N, *et al.* Role of periostin in cancer progression and metastasis: inhibition of breast cancer progression and metastasis by anti-periostin antibody in a murine model. *Int J Mol Med* 2011; 28: 181-6.
  21. Shao R, Bao S, Bai X, *et al.* Acquired expression of periostin by human breast cancers promotes tumor angiogenesis through up-regulation of vascular endothelial growth factor receptor 2 expression. *Mol Cell Biol* 2004; 24: 3992-4003.
  22. Takanami I, Abiko T, Koizumi S. Expression of periostin in patients with non-small cell lung cancer: correlation with angiogenesis and lymphangiogenesis. *Int J Biol Markers* 2008; 23: 182-6.
  23. Wu G, Wang X, Zhang X. Clinical implications of periostin in the liver metastasis of colorectal cancer. *Cancer Biother Radiopharm* 2013; 28: 298-302.
  24. Xiao ZM, Wang XY, Wang AM. Periostin induces chemoresistance in colon cancer cells through activation of the PI3K/Akt/survivin pathway. *Biotechnol Appl Biochem* 2015; 62: 401-6.
  25. Dawson H, Lugli A. Molecular and pathogenetic aspects of tumor budding in colorectal cancer. *Front Med (Lausanne)* 2015; 2: 11.
  26. Zheng X, Carstens JL, Kim J, *et al.* Epithelial-to-mesenchymal transition is dispensable for metastasis but induces chemoresistance in pancreatic cancer. *Nature* 2015; 527: 525-30.
  27. Koelzer VH, Dawson H, Andersson E, *et al.* Active immunosurveillance in the tumor microenvironment of colorectal cancer is associated with low frequency tumor budding and improved outcome. *Transl Res* 2015; 166: 207-17.
  28. Ueno H, Shinto E, Shimazaki H, *et al.* Histologic categorization of desmoplastic reaction: its relevance to the colorectal cancer microenvironment and prognosis. *Ann Surg Oncol* 2015; 22: 1504-12.
  29. De Sousa EM, Wang X, Jansen M, *et al.* Poor-prognosis colon cancer is defined by a molecularly distinct subtype and develops from serrated precursor lesions. *Nat Med* 2013; 19: 614-8.
  30. Fessler E, Drost J, van Hooff SR, *et al.* TGFbeta signaling directs serrated adenomas to the mesenchymal colorectal cancer subtype. *EMBO Mol Med* 2016; 8: 745-60.
  31. Kim JH, Bae JM, Cho NY, Kang GH. Distinct features between MLH1-methylated and unmethylated colorectal carcinomas with the CpG island methylator phenotype: implications in the serrated neoplasia pathway. *Oncotarget* 2016; 7: 14095-111.
  32. Tsai JH, Cheng CH, Chen CC, *et al.* Traditional serrated adenoma with *BRAF* mutation is associated with synchronous/metachronous *BRAF*-mutated serrated lesions. *Histopathology* 2016; 68: 810-8.

# Comparison of Unsatisfactory Samples from Conventional Smear versus Liquid-Based Cytology in Uterine Cervical Cancer Screening Test

Hoiseon Jeong · Sung Ran Hong<sup>1</sup>  
Seoung-Wan Chae<sup>2</sup> · So-Young Jin<sup>3</sup>  
Hye Kyoung Yoon<sup>4</sup> · Juhie Lee<sup>5</sup>  
Eun Kyung Kim<sup>6</sup> · Sook Tai Ha<sup>7</sup>  
Sung Nam Kim<sup>8</sup> · Eun-Jung Park<sup>9</sup>  
Jong Jae Jung<sup>9</sup> · Sun Hee Sung<sup>10</sup>  
Sung-Chul Lim<sup>11</sup>

Department of Pathology, Korea University Ansan Hospital, Korea University College of Medicine, Seoul; <sup>1</sup>Department of Pathology, Cheil General Hospital and Women's Health Care Center, Dankook University College of Medicine, Seoul; <sup>2</sup>Department of Pathology, Kangbuk Samsung Hospital, Sungkyunkwan University School of Medicine, Seoul; <sup>3</sup>Department of Pathology, Soonchunhyang University Hospital, Soonchunhyang University College of Medicine, Seoul; <sup>4</sup>Department of Pathology, Inje University Busan Paik Hospital, Inje University College of Medicine, Busan; <sup>5</sup>Department of Pathology, Kyung Hee University School of Medicine, Seoul; <sup>6</sup>Department of Pathology, Eulji General Hospital, Seoul; <sup>7</sup>T&C Diagnostic Pathology Clinic, Seoul; <sup>8</sup>Samkwang Medical Laboratories, Seoul; <sup>9</sup>Foryou Pathology Laboratories, Gwangju; <sup>10</sup>Department of Pathology, Ewha Womans University Mokdong Hospital, Ewha Womans University School of Medicine, Seoul; <sup>11</sup>Department of Pathology, Chosun University School of Medicine, Gwangju, Korea

Received: December 22, 2016

Revised: March 9, 2017

Accepted: March 14, 2017

## Corresponding Author

Sung-Chul Lim, MD, PhD  
Department of Pathology, Chosun University School of Medicine, 309 Pilmun-daero, Dong-gu, Gwangju 61452, Korea  
Tel: +82-62-230-6343  
Fax: +82-62-226-5860  
E-mail: sclim@chosun.ac.kr

\*This study was presented at the 29th Annual Spring Meeting of the Korean Society for Cytopathologists, 2015 and the International Academy of Cytology 2016 at Yokohama.

**Background:** Cervical cytology for uterine cervical cancer screening has transitioned from conventional smear (CS) to liquid-based cytology (LBC), which has many advantages. The aim of this study was to compare the proportion of unsatisfactory specimens from CS versus LBC at multiple institutions including general hospitals and commercial laboratories. **Methods:** Each participating institution provided a minimum of 500 Papanicolaou (Pap) test results for analysis. Pap tests were classified according to the participating institution (commercial laboratory or general hospital) and the processing method (CS, ThinPrep, SurePath, or CellPrep). The causes of unsatisfactory results were classified as technical problems, scant cellularity, or complete obscuring factors. **Results:** A total of 38,956 Pap test results from eight general hospitals and three commercial laboratories were analyzed. The mean unsatisfactory rate of LBC was significantly lower than that of CS (1.26% and 3.31%,  $p = .018$ ). In the LBC method, samples from general hospitals had lower unsatisfactory rates than those from commercial laboratories (0.65% vs 2.89%,  $p = .006$ ). The reasons for unsatisfactory results were heterogeneous in CS. On the other hand, 66.2% of unsatisfactory results in LBC were due to the scant cellularity. **Conclusions:** Unsatisfactory rate of cervical cancer screening test results varies according to the institution and the processing method. LBC has a significantly lower unsatisfactory rate than CS.

**Key Words:** Papanicolaou test; Cervical cytology; Unsatisfactory; Liquid-based cytology; Conventional smear

Cervical cytology, known as Papanicolaou (Pap) test, was first introduced in Korea in the late 1950s and has since played an important role in the early detection of uterine cervical cancer.<sup>1</sup> Conventional smear (CS) is widely used for uterine cancer screening owing to its low cost and easy application. Liquid-based cytology (LBC) was developed in the early 2000s and has recently been increasingly used in Korea. Several LBC systems are commercially available in Korea, such as ThinPrep (Cytoc Corp., Boxborough, MA, USA), BD SurePath (BD Diagnostics, Burlington, NC, USA), and CellPrep (Biodyne, Seongnam, Korea).

In LBC, the sample is prepared by rinsing the sampling tool in liquid-based medium to make a cell suspension. The cell suspension is then used to prepare a slide with an evenly-distributed monolayer sheet of cells. LBC is being marketed on the basis of its advantages, such as low unsatisfactory rates, increased sensitivity in detecting cervical precancerous lesions, standardized and automated preparations, fast screening, availability of ancillary tests including a human papillomavirus DNA test, and facilitation of computer-assisted screening.<sup>2</sup>

A number of studies have compared the performance of LBC versus CS; however, the results have been conflicting. Some meta-analyses report that LBC has lower unsatisfactory rates and better performance in terms of sensitivity, specificity, and overall accuracy compared with CS.<sup>3-5</sup> Other studies report no evidence that LBC reduces unsatisfactory rates or detects high-grade lesions more accurately compared with CS.<sup>6-8</sup> An independent review also showed no significant difference between the two methods.<sup>9</sup>

Both CS and LBC are approved in Korea by the national cancer screening program as screening tests for uterine cervical cancer. However, there have been little data verifying the use of LBC in Korea, and no studies comparing the unsatisfactory rates of LBC versus that of CS in the country. To evaluate and compare the domestic use of CS and LBC, we compared the proportion of unsatisfactory tests from CS versus LBC at multiple Korean institutions including general hospitals and commercial laboratories.

## MATERIALS AND METHODS

This study spanned a 6-month period from July 2014 to January 2015. Each participating institution provided a minimum of 500 Pap test results for analysis. The Pap tests were classified according to the participating institution (commercial laboratory or general hospital) and by the processing method (CS, ThinPrep, SurePath, or CellPrep). The specimens were evaluated by cytotechnologists at each given institution during their routine screening work. When an unsatisfactory result was found, the

cause was evaluated using a checklist. Unsatisfactory slides were then reviewed and confirmed by cytopathologists.

The causes of unsatisfactory results were classified as either technical problems, scant cellularity, or complete obscuring factors,<sup>10</sup> and subdivided as shown in Table 1. Technical problems referred to cases of patchy cellularity, a halo effect, and/or thick preparations in which obscuring factors such as blood, bacteria, mucus, gel, and inflammation were not present.<sup>10</sup> Patchy cellularity referred to cases in which clear spaces formed on a slide owing to irregular loss of cells.<sup>10</sup> Halo effect referred to cases in which a rim of cells formed on the periphery of a slide, leaving an empty space in the center.<sup>10</sup> Thick preparation referred to cases in which the cellular details were obscured in >75% of the slide because of aggregation of squamous epithelial cells.<sup>10</sup> The Bethesda 2001 criteria were applied to evaluate cellularity. Regardless of the processing method, an adequate sample was defined as an estimated minimum of 5,000 well-preserved and well-visualized squamous epithelial cells.<sup>11</sup> Cases in which >75% of the cells were obscured were classified as unsatisfactory,<sup>11</sup> with the exception of cases with any abnormal cells.

Statistical analysis was performed with the SPSS statistical software package ver. 16.0 (SPSS Inc., Chicago, IL, USA), by using paired t tests and analysis of variance (ANOVA). Significance was defined as  $p < .05$ .

## RESULTS

We analyzed a total of 38,956 Pap test results from eight general hospitals (32,890 cases, 84.4%) and three commercial laboratories (6,066 cases, 15.6%). Total Pap test consisted of 15,872 (general hospital, 13,299; commercial laboratory, 2,573)

**Table 1.** Categorization of unsatisfactory samples according to the cause

Cause
Technical problems
Patch cellularity
Halo effect
Thick preparation
Scant cellularity
Scant cells in a clean background
Scant cells in a bloody background
Scant cells in a background of gel/inflammation/bacteria/mucus
Obscuring factors
Blood
Inflammation
Bacteria
Gel
Mucus

cases of CS (40.7%) and 23,084 (general hospital, 19,591; commercial laboratory, 3,493) cases of LBC (59.3%). LBC consisted of 5,309 cases of ThinPrep (23.0%), 15,868 cases of SurePath (68.7%), and 1,907 cases of CellPrep (8.3%) (Table 2). Each institution used CS in parallel with one type of LBC, with the exception of one general hospital that did not provide any CS data. The participating institutions provided data on the number of unsatisfactory samples and the total numbers of CS and LBC samples in the 6-month period. Unsatisfactory rates were calculated from the data and are shown in Table 3. The unsatisfactory rate of CS had a wide range of distribution from 0.1% to 11.2%, whereas that of LBC was between 0.0% and 4.4%. The mean unsatisfactory rates for CS and LBC were 3.31% and 1.26%, respectively (Table 4), showing that LBC had a significantly lower unsatisfactory rate than CS ( $p = .017$ ).

The unsatisfactory rates were then analyzed according to the participating institution: either commercial laboratory or general hospital (Table 4). In commercial laboratories, the unsatisfactory rates of CS ranged from 2.91% to 11.16% (mean, 6.04%), whereas those of LBC ranged from 1.63% to 4.37% (mean, 2.89%). In general hospitals, the unsatisfactory rates of CS ranged

from 0.14% to 5.20% (mean, 2.14%), whereas those of LBC ranged from 0% to 1.80% (mean, 0.65%). Regardless of the processing method, the general hospital group had a significantly lower unsatisfactory rate than the commercial laboratory group ( $p = .006$ ).

For the preparation of LBC, six institutions used ThinPrep, three used SurePath, and two used CellPrep. The unsatisfactory rates were analyzed according to the three LBC products used. The unsatisfactory rate for ThinPrep, which was used in most institutions, ranged from 0.1% to 4.4%, with a mean rate of 1.6%. The unsatisfactory rate for SurePath ranged from 0.0% to 0.8%, with a mean rate of 0.3%. Between the two institutions that used CellPrep, one reported an unsatisfactory rate of 1.6% whereas the other reported 1.8%; the mean unsatisfactory rate of CellPrep was 1.7%. Although SurePath (0.3%) had a lower mean unsatisfactory rate than ThinPrep (1.6%) or CellPrep (1.7%), ANOVA revealed no statistically significant difference among the three groups.

The causes of unsatisfactory results were heterogeneous in CS (Table 5). The most common reason was scant cellularity on a clean background, which was observed in 90 out of 287 unsatisfactory cases of CS (31.4%). The second most common reason was obscuring due to inflammation (84 cases, 29.3%). A considerable proportion of unsatisfactory cases showed scant cellularity on a background of gel/inflammation/blood/mucus (GIBM; 32 cases). Inflammation was the most common obscuring factor, occurring in 84 cases; while the other factors (blood, bacteria, gel, and mucus) occurred in a minority of cases. Within the cat-

**Table 2.** Composition of the samples

Method	General hospital	Commercial laboratory	Total
Liquid-based cytology	19,591	3,493	23,084 (59.3)
Conventional smear	13,299	2,573	15,872 (40.7)
Total	32,890 (84.4)	6,066 (15.6)	38,956 (100)

Values are presented as number (%).

**Table 3.** Unsatisfactory rate (%) of each participating institution

Method	Institution No. <sup>a</sup>											Total
	1	2	3	4	5	6	7	8	9	10	11	
	SurePath	SurePath	CellPrep	ThinPrep	ThinPrep	ThinPrep	SurePath	ThinPrep	ThinPrep	ThinPrep	CellPrep	
LBC	0/500 (0.0)	22/2,856 (0.8)	9/500 (1.8)	9/539 (1.7)	1/1,457 (0.1)	1/384 (0.3)	1/12,512 (0.0)	5/843 (0.6)	55/1,258 (4.4)	22/828 (2.7)	23/1,407 (1.6)	148/23,084 (0.6)
CS	4/531 (0.8)	51/1,155 (4.4)	26/500 (5.2)	23/658 (3.5)	19/2,975 (0.6)	16/4,670 (0.3)	4/2,810 (0.1)	No data	77/690 (11.2)	24/826 (2.9)	43/1,057 (4.1)	287/15,872 (1.8)

Values are presented as number (%).

LBC, liquid-based cytology; CS, conventional smear.

<sup>a</sup>1 to 8, general hospitals; 9 to 11, commercial laboratories.

**Table 4.** Comparison of unsatisfactory sample rate according to the processing method and institution

Method	Unsatisfactory sample rate					
	p-value	Institution		p-value		
		GH	CL			
LBC		1.26 ± 1.36	.017	0.65 ± 0.73	2.89 ± 1.38	.006
CS		3.31 ± 3.33		2.14 ± 2.15	6.04 ± 4.47	.088

Values are presented as mean ± standard deviation.

GH, general hospital; CL, commercial laboratory; LBC, liquid-based cytology; CS, conventional smear.

**Table 5.** Comparison of unsatisfactory samples in CS versus LBC

Category	CS	LBC	p-value
Technical problems			
Patchy	13 (4.5)	4 (2.7)	.06
Halo	3 (1.1)	18 (12.2)	.14
Thick	24 (8.4)	2 (1.4)	.17
Scant cellularity			
Clean	90 (31.4)	69 (46.6)	.39
Bloody	13 (4.5)	22 (14.9)	.15
GIBM <sup>a</sup>	32 (11.2)	7 (4.7)	.32
Obscuring factors			
Blood	15 (5.2)	10 (6.8)	.44
Inflammation	84 (29.3)	15 (10.1)	.09
Bacteria	5 (1.7)	1 (0.7)	-
Gel	2 (0.7)	0	-
Mucus	6 (2.1)	0	-
Total	287 (100)	148 (100)	

Values are presented as number (%).

CS, conventional smear; LBC, liquid-based cytology.

<sup>a</sup>Scant cells in a background of gel/inflammation/bacteria/mucus.

egory of technical problems, unsatisfactory cases due to a thick preparation had the largest proportion (24 cases).

Among 148 unsatisfactory LBC cases, 98 (66.2%) were due to scant cellularity. Of note, all of the unsatisfactory cases with SurePath were due to scant cellularity. Of the remaining unsatisfactory LBC cases, 26 (17.6%) were due to obscuring factors and 24 (16.3%) were due to technical problems. Within the scant cellularity category, most cases (69 cases, 46.6%) were on a clean background, analogous to CS cases. However, only seven LBC cases (4.7%) showed scant cellularity on a GIBM background, whereas a considerable proportion of CS cases with scant cellularity had a GIBM background. The number and proportion of unsatisfactory LBC cases with obscuring factors (26 cases, 17.6%) were much smaller than those of CS cases (112 cases, 39%). There was no unsatisfactory LBC case due to obscuring by gel or mucus. Obscuring inflammation, which was the second most common cause of unsatisfactory results in CS (84 cases, 29.3%), was much less prevalent in LBC cases (15 cases, 10.1%). Within the technical problem category, 18 out of 24 cases were due to a halo effect, 17 of which were reported in ThinPrep cases.

There was no statistically significant difference in the unsatisfactory rate according to processing method (CS vs LBC) (Table 5). The causes of unsatisfactory results in CS cases were thick preparation, scant cellularity on a clean or GIBM background, and obscuring inflammation. The causes of unsatisfactory results in LBC samples were scant cellularity on a clean or bloody background, halo effect, and obscuring inflammation. Of note, no LBC samples were reported as unsatisfactory due to obscuring by

gel or mucus; however, we were unable to verify this statistically.

## DISCUSSION

Estimating the unsatisfactory rate and overall accuracy of uterine cervical cancer screening tests can help in determining the optimal screening frequency, a management plan for abnormal results, and the need to apply new methods or conduct further studies.<sup>5</sup> A low unsatisfactory rate can decrease the chance of patient revisit, thereby lowering the overall cost of the screening program.<sup>12</sup> Studies have shown that a substantial fraction of false-negative Pap test results are in fact unsatisfactory results,<sup>13,14</sup> and false-negative results can lead to worse conditions than do false-positive results. Therefore, a low unsatisfactory rate is considered an important checkpoint before adopting a particular testing protocol into a large-scale screening program. In countries with nationalized health-care systems, such as England, cervical cancer screening programs have switched from CS to LBC methods, and a striking subsequent reduction in the proportion of unsatisfactory slides has been reported.<sup>9,12</sup> The Korean guideline for cervical cancer screening was established by the National Cervical Cancer Screening Guideline Development Committee and published in 2015.<sup>15</sup> One of the key questions forwarded by the committee was regarding the accuracy and insufficient sample rate of LBC compared with CS.<sup>15</sup> The results of the present study show that the unsatisfactory rate is significantly lower for LBC than for CS, in line with the results of previous studies.<sup>3,16-19</sup> Considering that the performance of LBC was not inferior to that of CS in published papers from Korea,<sup>5</sup> the lower unsatisfactory rate of LBC makes it a better screening test tool than CS. The current published Korean guideline for cervical cancer screening allows the use of both CS and LBC as screening tests.<sup>15</sup>

In Korea, >60% of cervical cancer screening tests conducted by primary health-care units are analyzed in commercial laboratories.<sup>1,20</sup> However, in most of the existing literature comparing CS and LBC, the specimens were analyzed in university hospitals.<sup>5</sup> Thus, the present study included three commercial laboratories among the 11 participating institutions. LBC had significantly lower unsatisfactory rates in the general hospital group than in the commercial laboratory group. In the case of CS, the general hospital group had lower unsatisfactory rates than the commercial laboratory group, although the difference was not statistically significant. Considering that many parts of the sample-processing procedure are standardized for LBC, the difference in unsatisfactory rate between commercial laboratories and general hospitals is believed to be due to differences in patient

characteristics. In general hospitals, patients who have been diagnosed as having atypical squamous cells of undetermined significance or higher cytologic atypia at their first screening are often referred to pathologists and reexamined. A precondition exists that there must be no atypical cells in a sample judged to be unsatisfactory; thus, the high fraction of patients with cytologic atypia likely contributes to the lower unsatisfactory rate in general hospitals than in commercial laboratories.

In terms of the particular LBC product used, six of the 11 participating institutions used ThinPrep, three used SurePath, and two used CellPrep. There was no significant difference in unsatisfactory rates for tests conducted using the three different LBC products, although SurePath tended to have a lower unsatisfactory rate compared to ThinPrep and CellPrep, which were similar to one another. These results are in line with a previous study showing that SurePath has a lower unsatisfactory rate than ThinPrep.<sup>21,22</sup> Of note, one confounding variable could be that all three institutions using SurePath were general hospitals.

The analysis revealed that in CS, unsatisfactory test results were caused by a variety of factors, whereas in LBC, two-thirds of unsatisfactory samples were caused by scant cellularity. This is consistent with a previous study concluding that LBC eliminates most sources of unsatisfactory tests with the exception of scant cellularity, which is the main reason for unsatisfactory LBC tests.<sup>23</sup> In particular, obscuring factors, which were the cause of a large proportion of the unsatisfactory CS test results, were found to be less frequent in the LBC method. It is noteworthy that we found no unsatisfactory LBC cases caused by gel or mucus obscuration. With regard to the technical problems, many unsatisfactory CS samples were caused by a thick smear, whereas those in LBC were caused by a halo effect. Of note, 17 of the 18 unsatisfactory samples caused by a halo effect were reported by institutions that used ThinPrep; the halo effect of ThinPrep is confirmed by another study.<sup>24</sup> However, there were no significant differences in causes of unsatisfactory results between CS and LBC.

In this study, we did not use the split-sample method in which a given sample is divided and processed using both CS and LBC to compare results. The processing method was chosen at the discretion of the patient and clinician, who were unaware of the study. We assumed that random assignment was made, though there may indeed have been selection bias. Furthermore, the study was conducted with data from various institutions, and although we provided guidance on determining unsatisfactory results and their causes, the possibility of interobserver variability cannot be ruled out. The lack of epidemiological

data is also a limitation of this study. In a multicenter study analyzing the effects of transitioning from CS to LBC on unsatisfactory Pap test results, an increased relative risk of unsatisfactory result was reported in women aged 50 years or older after transition to LBC.<sup>25</sup> A study of randomized clinical trials in Europe reported that there is a greater decrease in unsatisfactory results with LBC than with CS in younger women, and that this effect decreases with age.<sup>19</sup> However, in young women with obscuring elements, LBC seemed to have little or no effect on cervical atrophy and the consequent low cellularity problem.<sup>25</sup> Furthermore, in comparison with the large number of cervical cancer screening tests analyzed in commercial laboratories, our commercial laboratory group was small. Therefore, there is a limitation in that the results of this study may not accurately reflect the situation in Korea. Given that the commercial laboratory group tended to show a higher rate of unsatisfactory results than the general hospital group, the overall unsatisfactory rate of cervical cancer screening test may be higher than that presented in this study.

In summary, the unsatisfactory rate of uterine cervical Pap smear results was lower for LBC than for CS. Regardless of the processing method, lower rates of unsatisfactory results were observed in the general hospital group than in the commercial laboratory group. Furthermore, we confirmed the effect of using each of the three most common LBC products. Although SurePath tended to show a lower unsatisfactory rate than did ThinPrep or CellPrep, there was no statistically significant difference. The causes of the unsatisfactory results were heterogeneous in CS, whereas most (two-third) of the unsatisfactory LBC were due to scant cellularity.

We compared the unsatisfactory rates of CS and LBC for uterine cervical cancer screening tests in Korea through a cross-sectional study of approximately 39,000 Pap test results obtained during a 6-month period from 11 different institutions including both general hospitals and commercial laboratories. Our results suggest that LBC is the preferred method in Korea, and this was verified by comparing the unsatisfactory rates of Pap test results. This study provides the basic data necessary for evidence-based decision making in health-care policies such as the national cancer screening project.

---

### Conflicts of Interest

No potential conflict of interest relevant to this article was reported.

## Acknowledgments

This research was supported by The Korean Society for Cytopathologists Grant No. 2014-01.

## REFERENCES

- Park MH. Cervical cancer screening in Korea. *Korean J Cytopathol* 2003; 14: 43-52.
- Hoda RS, Loukeris K, Abdul-Karim FW. Gynecologic cytology on conventional and liquid-based preparations: a comprehensive review of similarities and differences. *Diagn Cytopathol* 2013; 41: 257-78.
- Bernstein SJ, Sanchez-Ramos L, Ndubisi B. Liquid-based cervical cytologic smear study and conventional Papanicolaou smears: a metaanalysis of prospective studies comparing cytologic diagnosis and sample adequacy. *Am J Obstet Gynecol* 2001; 185: 308-17.
- Abulafia O, Pezzullo JC, Sherer DM. Performance of ThinPrep liquid-based cervical cytology in comparison with conventionally prepared Papanicolaou smears: a quantitative survey. *Gynecol Oncol* 2003; 90: 137-44.
- Oh JK, Shin HR, Gong G, Sohn JH, Khang SK. Diagnostic accuracy of conventional Pap test, liquid-based cytology and human papillomavirus DNA testing in cervical cancer screening in Korea: a meta-analysis. *Korean J Epidemiol* 2008; 30: 178-87.
- Kituncharoen S, Tantbirojn P, Niruthisard S. Comparison of unsatisfactory rates and detection of abnormal cervical cytology between conventional Papanicolaou smear and liquid-based cytology (SurePath(R)). *Asian Pac J Cancer Prev* 2015; 16: 8491-4.
- Davey E, Barratt A, Irwig L, *et al*. Effect of study design and quality on unsatisfactory rates, cytology classifications, and accuracy in liquid-based versus conventional cervical cytology: a systematic review. *Lancet* 2006; 367: 122-32.
- Siebers AG, Klinkhamer PJ, Grefte JM, *et al*. Comparison of liquid-based cytology with conventional cytology for detection of cervical cancer precursors: a randomized controlled trial. *JAMA* 2009; 302: 1757-64.
- Obwegeser J, Schneider V. Thin-layer cervical cytology: a new meta-analysis. *Lancet* 2006; 367: 88-9.
- Rosa M, Pragasam P, Sareman J, Aoalin A, Graf W, Mohammadi A. The unsatisfactory ThinPrep Pap test: analysis of technical aspects, most common causes, and recommendations for improvement. *Diagn Cytopathol* 2013; 41: 588-94.
- Solomon D, Nayar R. The Bethesda system for reporting cervical cytology: definitions, criteria, and explanatory notes. 2nd ed. New York: Springer, 2004.
- Biro C, Hyne S, Roberts J, Thurloe J, Bowditch R. Liquid-based versus conventional cervical cytology. *Lancet* 2006; 367: 1481-2.
- Pairwuti S. False-negative Papanicolaou smears from women with cancerous and precancerous lesions of the uterine cervix. *Acta Cytol* 1991; 35: 40-6.
- van der Graaf Y, Vooijs GP, Gaillard HL, Go DM. Screening errors in cervical cytologic screening. *Acta Cytol* 1987; 31: 434-8.
- Min KJ, Lee YJ, Suh M, *et al*. The Korean guideline for cervical cancer screening. *J Gynecol Oncol* 2015; 26: 232-9.
- Ronco G, Cuzick J, Pierotti P, *et al*. Accuracy of liquid based versus conventional cytology: overall results of new technologies for cervical cancer screening: randomised controlled trial. *BMJ* 2007; 335: 28.
- Guidos BJ, Selvaggi SM. Use of the Thin Prep Pap test in clinical practice. *Diagn Cytopathol* 1999; 20: 70-3.
- Strander B, Andersson-Ellström A, Milsom I, Rådberg T, Ryd W. Liquid-based cytology versus conventional Papanicolaou smear in an organized screening program: a prospective randomized study. *Cancer* 2007; 111: 285-91.
- Castle PE, Bulten J, Confortini M, *et al*. Age-specific patterns of unsatisfactory results for conventional Pap smears and liquid-based cytology: data from two randomised clinical trials. *BJOG* 2010; 117: 1067-73.
- Lee HK, Kim SN, Khang SK, Kang CS, Yoon HK. Quality control program and its results of Korean Society for Cytopathologists. *Korean J Cytopathol* 2008; 19: 65-71.
- Moriarty AT, Clayton AC, Zaleski S, *et al*. Unsatisfactory reporting rates: 2006 practices of participants in the college of american pathologists interlaboratory comparison program in gynecologic cytology. *Arch Pathol Lab Med* 2009; 133: 1912-6.
- Fontaine D, Narine N, Naugler C. Unsatisfactory rates vary between cervical cytology samples prepared using ThinPrep and SurePath platforms: a review and meta-analysis. *BMJ Open* 2012; 2: e000847.
- Siebers AG, Klinkhamer PJ, Vedder JE, Arbyn M, Bulten J. Causes and relevance of unsatisfactory and satisfactory but limited smears of liquid-based compared with conventional cervical cytology. *Arch Pathol Lab Med* 2012; 136: 76-83.
- Song LH, Goh ES, Phang LC, Poh WT, Tay SK. Technical aspect of ThinPrep. *Singapore Med J* 2000; 41: 575-8.
- Owens CL, Peterson D, Kamineni A, *et al*. Effects of transitioning from conventional methods to liquid-based methods on unsatisfactory Papanicolaou tests: results from a multicenter US study. *Cancer Cytopathol* 2013; 121: 568-75.

## Unusual Histology of Eosinophilic Myenteric Ganglionitis: A Case Report

Hyekyung Lee · Dongwook Kang  
Heejin Kim<sup>1</sup> · Byungsun Cho<sup>2</sup>  
Jeho Jang<sup>2</sup>

Departments of Pathology, <sup>1</sup>Radiology, and  
<sup>2</sup>Surgery, Eulji University School of Medicine,  
Daejeon, Korea

Received: June 2, 2016

Revised: August 5, 2016

Accepted: September 7, 2016

### Corresponding Author

Jeho Jang, MD

Department of Surgery, Eulji University School of  
Medicine, 77 Gyeryong-ro 771beon-gil, Jung-gu,  
Daejeon 34824, Korea

Tel: +82-42-259-1272

Fax: +82-42-259-1111

E-mail: jhjang@eulji.ac.kr

Eosinophilic myenteric ganglionitis is a disorder characterized by infiltration of the Auerbach myenteric plexus by eosinophils. As a cause of chronic intestinal pseudo-obstruction (CIPO), eosinophilic myenteric ganglionitis has been rarely reported and the majority of the reported cases in the literature were children. We experienced a case of eosinophilic myenteric ganglionitis associated with CIPO in a 53-year-old female patient. Histologic examination of the resected descending colon showed moderate eosinophilic infiltrates with hypogangliosis in the myenteric plexus. Immunohistochemical study revealed increased number of CD4-positive lymphocytes and stronger but scantier glial fibrillary acid protein expression in the inflamed myenteric plexus.

**Key Words:** Eosinophils; Ganglionitis; Pseudo-obstruction

Chronic intestinal pseudo-obstruction (CIPO) represents a rare and highly morbid syndrome characterized by impaired gastrointestinal propulsion together with symptoms of bowel obstruction in the absence of any lesions occluding the gut lumen.<sup>1,2</sup> The diagnosis of CIPO is mainly clinical and confirmed by endoscopic or radiologic findings. Chronic intestinal pseudo-obstruction has many underlying causes and eosinophilic myenteric ganglionitis has rarely been reported as a cause of CIPO. Eosinophilic myenteric ganglionitis is known as a neuropathy which develops mainly in children and shows no degenerative pathologic findings such as neuronal loss, and no lymphocytic infiltrates.<sup>3,4</sup> We present a middle aged female patient with eosinophilic myenteric ganglionitis as the underlying cause of CIPO. In our case, we observed hypogangliosis with moderate eosinophilic infiltrates admixed with CD4-positive T cells, which has not been described before.

### CASE REPORT

A 53-year-old woman presented to the emergency department with a 2-week history of abdominal distention and constipation. She had a previous history of having undergone a myomectomy

15 years ago and has been under thyroid hormone replacement therapy for 10 years. She suffered severe constipation for a long time that was refractory to stool softeners. Seven years ago, she had visited our hospital due to the same symptoms. At the time, abdominopelvic computed tomography revealed markedly dilated entire colon with feces and tapered narrowing in the distal portion (Fig. 1A, B). Colonoscopic mucosal biopsy showed mild lymphoplasmacytic infiltrates in the mucosa without muscularis mucosa component. At this visit, laboratory findings were within normal limits except for a slightly decreased TSH level (0.48  $\mu$ IU/mL; normal range, 0.55 to 4.2). Serologic study of anti-Hu antibody, anti-Ri antibody, anti-Yo antibody, anti-neuromyelitis optica antibody, anti-antinuclear antibody, anti-thyroid-stimulating hormone receptor antibody, anti-thyroglobulin antibody, and anti-thyroid microsomal antibody were all negative. On abdominopelvic computed tomography, the entire colon was severely dilated and there was no significant difference between the previous and current images. Neither mural thickening nor any mass lesion was noted at the narrowed area.

The differential diagnoses included colonic obstruction due to stricture from inflammatory bowel disease or ischemic colitis and a mild form of congenital megacolon. Colonoscopic evalua-

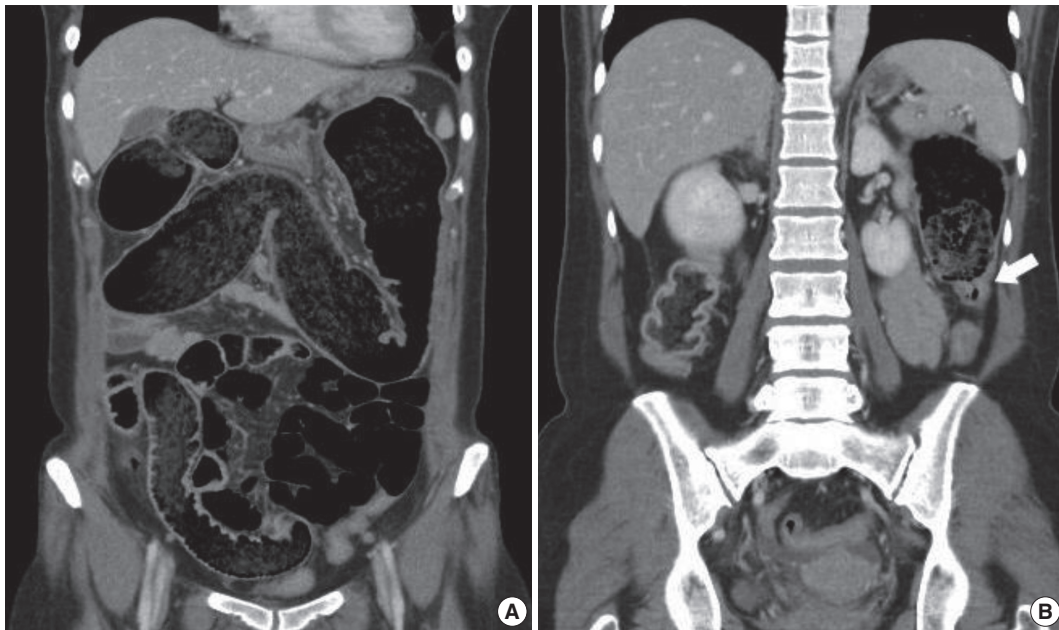


**Fig. 1.** Abdominopelvic computed tomography shows markedly dilated colon filled with feces (A). Transition point between the dilated proximal and collapsed distal colon is noted (B, arrow).

tion showed luminal narrowing in the descending colon without definite luminal obstructive lesions. Proximal advancement of the scope was not possible due to much fecal material and the patient's pain. After 3 days of conservative management with slow bowel preparation with polyethylene glycol solution, the distended abdomen was decompressed and the symptoms subsided. Colon transit time study showed a slow transit constipation pattern. Given concern for the possibility of intractable benign luminal stenosis due to adhesive structure or ischemic enteritis, segmental colectomy was performed laparoscopically. There was no evidence of adhesion or mechanical obstruction except for focal physiologic attachment between the visceral and parietal peritoneum. The patient's postoperative course was uncomplicated and the patient's symptoms resolved after the surgery.

### Pathologic features

A segment of descending colon measuring 12 cm in length was received. Approximately half of the colonic segment was dilated (Fig. 2). The wall thickness appeared even without regional differences between the dilated and the narrowed portions. Except for the luminal dilatation, the colon was grossly unremarkable. Histologic examination revealed mild lymphoplasmacytic infiltrates with scattered eosinophils in the mucosa. The average number of eosinophils was less than 4 per high power field (HPF). The muscularis mucosa was thickened up to 660  $\mu\text{m}$  in the dilated area in contrast to the thin muscularis



**Fig. 2.** Approximately half of the resected segment of the descending colon was dilated.

mucosa in the narrow area (Fig. 3A). Scattered mast cells were noted in the submucosa without significant eosinophilic infiltrates. The Meissner's plexuses were unremarkable. Intermuscular Auerbach's myenteric plexuses showed moderate eosinophilic infiltrates up to 22 per HPF (Fig. 3B) and hypogangliosis with atrophic reduction of the volume of nerve bundle, which became more evident with synaptophysin immunostain (Fig. 3C). The atrophic myenteric plexus was accompanied by increased fibrosis and admixed with some CD3 and CD4 dual positive lymphocytes (Fig. 3D) and a few CD8-positive lymphocytes on immunostain. Immunohistochemical study showed preserved positivity

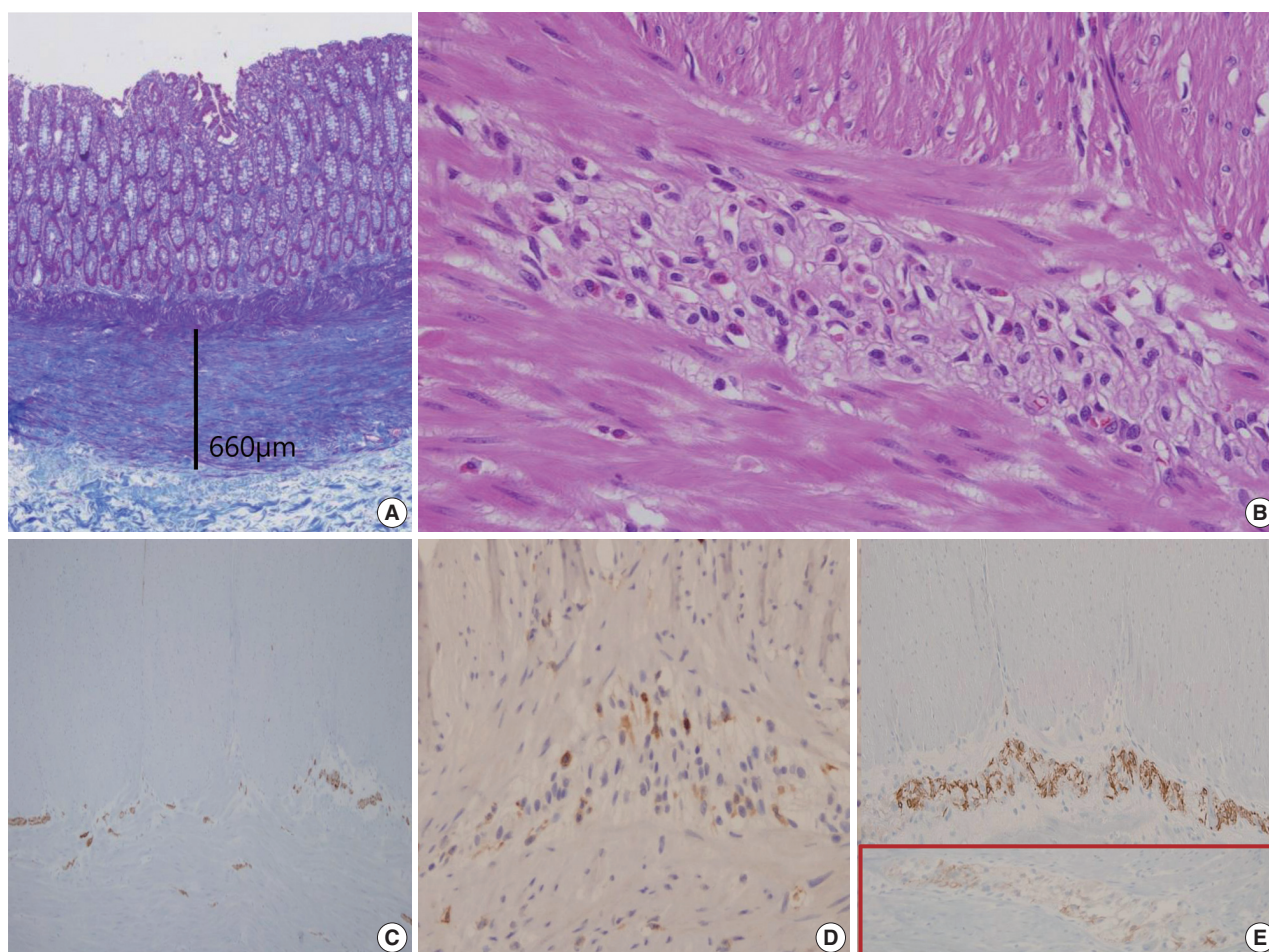


**Fig. 3.** Summary of histologic findings: thickened muscularis mucosa in the dilated colon (A), many eosinophils in Auerbach's myenteric plexus (B), hypogangliosis in synaptophysin immunostain (C), scattered CD4-positive lymphocytes in the affected myenteric plexus (D) and stronger but scantier glial fibrillary acidic protein positivity in our patient (E) in contrast to the control patient (in box).

of c-Kit and stronger but scantier glial fibrillary acidic protein (GFAP) reaction in the myenteric plexus when we compared the immunostain results with a comparable descending colon of a 60 year old female patient who received Hartmann's operation due to cancer (Fig. 3E). Bcl-2 stain for anti-apoptosis showed no definite difference between the two colons. There was no significant difference in the severity of the eosinophilic infiltrates in the myenteric plexus between the grossly dilated and narrow portions. However, there was regional difference in the eosinophilic infiltrates between the inner portion and the outer portion of the myenteric plexus. There was no eosinophilic infiltrates in the submucosa and the inner muscle proper in contrast to the increased number of eosinophils, lymphocytes, and histiocytes in the outer muscle layer, subserosa, and serosa. There was no evidence of peripheral blood eosinophilia. Based on these findings, a diagnosis of eosinophilic myenteric ganglionitis was made.

## DISCUSSION

Digestive motility, an important pathogenic factor of CIPO, is a highly coordinated process and depends on smooth muscle contractility and the related pacemaker activity evoked by the interstitial cells of Cajal (ICCs). Both of these mechanisms are finely tuned by the intrinsic enteric nervous system (ENS) and the extrinsic sympathetic and parasympathetic nerves, independently from the central and peripheral nervous systems. Based on histology, CIPO can be classified into three major entities depending on the predominant involvement of enteric neurons, ICCs, or smooth muscle cells: neuropathies, mesenchymopathies, and myopathies.

Neuropathy can be classified into two major forms: (1) inflammatory neuropathies in which a significant inflammatory response is identified within nerve tissue and (2) degenerative neuropathies characterized by evidence of neurodegenerative aspects in

the absence of an identifiable inflammatory response. Inflammatory neuropathy is also subdivided into lymphocytic and eosinophilic depending on the prominent infiltrating cells. Lymphocytic neuropathy is the main inflammatory neuropathy and eosinophilic neuropathy has rarely been reported.<sup>5</sup> Distinctive findings of eosinophilic neuropathy has mainly been reported in children showing no degenerative pathologic findings such as neuronal loss and no lymphocytic infiltrates. We report a case of eosinophilic myenteric ganglionitis which developed in a middle-aged female patient with the pathologic features of hypoganglionic and CD4-positive lymphocytic infiltrates. The pathogenesis of eosinophilic myenteric ganglionitis has not been clearly elucidated. However, interleukin 5 (IL-5), a well-known eosinophilic chemotactic factor, has been mentioned in eosinophilic myenteric ganglionitis.<sup>3</sup> Although we did not evaluate IL-5, the increased number of CD3 and CD4 dual positive cells may suggest the increased production of IL-5 from the infiltrating CD4-positive helper T cells for eosinophilic chemotaxis. A few scattered CD8-positive lymphocytes may be involved in the cytotoxic reaction of the nerve plexus resulting in hypoganglionic. Atrophic plexus and cell loss in neuroinflammatory disease were mentioned as the result of the activation of a caspase dependent mechanism;<sup>6</sup> however, immunoreactivity of Bcl-2 in our case showed no definite reduced positivity. The expression of GFAP in the myenteric plexus was an impressive finding. The myenteric plexus is composed of enteric neurons and enteric glial cells. Enteric glial cells are the main constituent of the ENS and the majority of the enteric glial cells are located in the myenteric plexus. Recently, the role of enteric glial cells as a neuroprotector and as an immune-modulator in inflammatory processes has been investigated<sup>7</sup> and the myenteric GFAP-expressing glial subpopulation was reported to be susceptible to systemic inflammation.<sup>8</sup> In our case, the stronger but scantier expression of GFAP seems to be related with the overproduction of GFAP by activated enteric glial cells for neuroprotection as a damaged myenteric plexus. The role of the myenteric plexus as an immune-modulator and barrier was evident in the findings of scarce inflammatory reaction in the inner muscle layer in contrast to mild to moderate inflammatory reaction in the outer muscle layer and the subserosa. This regional difference suggests the barrier function of the myenteric plexus to diffusible and systemic immune reactants supplied by the mesenteric bloods through the subserosal and outer muscular layer vessels. There being no difference in the eosinophilic infiltrates in the myenteric plexus between the dilated and narrow areas was also meaningful. Similarly, no difference in ENS abnormality between the affected and

the nonaffected areas in Crohn disease has been described.<sup>9</sup> This finding suggests the eosinophilic reaction as a systemic reaction, and the possible discrepancy between the pathologic findings and functional impairment. The pathologic findings such as eosinophilic infiltrates or neuronal loss can be the underlying causes of CIPO; however, the clinical functional impairment is more complex. Physiologic abnormality such as disturbed activity of neurotransmitters can be another factor to take into consideration. The increased number of mast cells in the submucosa may be the finding of the crosstalk between mast cells and eosinophils.<sup>10</sup> The thickened muscularis mucosa in the dilated colon can be a compensatory response to prolonged high luminal pressure. The therapeutic effect of surgery is limited since CIPO often involves the entire gastrointestinal tract with a progressive nature. As surgical approach can aggravate the underlying condition, it should be reserved for only carefully selected patients. If a confirmed diagnosis of ganglionitis is made through a full-thickness biopsy of the intestinal wall, the patient might benefit from an anti-inflammatory or immunosuppressive therapy before the surgical procedure. However, in the absence of a transmural tissue diagnosis, patients with enteric ganglionitis cannot be subject to these nonoperative treatment options.

In conclusion, we think this colonic lesion might have begun as a systemic immune reaction showing eosinophilic myenteric ganglionitis and progressed into a chronic inflammatory lesion showing atrophic myenteric plexus, reduced ganglion cells, thickened muscularis mucosa, and subserosal fibrosis. These abnormal findings can be the basis of the clinical symptoms of CIPO. The diagnosis of CIPO is mainly clinical, and the histopathology of CIPO has frequently been reported as a frustrating experience by pathologists due to limited experience. Further combined clinical and histopathological studies are needed in order to enrich the understanding and management CIPO.

### Conflicts of Interest

No potential conflict of interest relevant to this article was reported.

### REFERENCES

1. De Giorgio R, Sarnelli G, Corinaldesi R, Stanghellini V. Advances in our understanding of the pathology of chronic intestinal pseudo-obstruction. *Gut* 2004; 53: 1549-52.
2. Lee BH, Kim N, Kang SB, *et al.* Two cases of chronic idiopathic intestinal pseudo-obstruction with different clinical features. *J Neu-*

- rogastroenterol Motil 2010; 16: 83-9.
3. Schäppi MG, Smith VV, Milla PJ, Lindley KJ. Eosinophilic myenteric ganglionitis is associated with functional intestinal obstruction. *Gut* 2003; 52: 752-5.
  4. Chander B, Fiedler P, Jain D. Eosinophilic myenteric ganglionitis: a case of intestinal pseudo-obstruction in a 93-year-old female. *J Clin Gastroenterol* 2011; 45: 314-6.
  5. De Giorgio R, Camilleri M. Human enteric neuropathies: morphology and molecular pathology. *Neurogastroenterol Motil* 2004; 16: 515-31.
  6. De Giorgio R, Bovara M, Barbara G, *et al.* Anti-HuD-induced neuronal apoptosis underlying paraneoplastic gut dysmotility. *Gastroenterology* 2003; 125: 70-9.
  7. Lakhan SE, Kirchgessner A. Neuroinflammation in inflammatory bowel disease. *J Neuroinflammation* 2010; 7: 37.
  8. Rosenbaum C, Schick MA, Wollborn J, *et al.* Activation of myenteric glia during acute inflammation *in vitro* and *in vivo*. *PLoS One* 2016; 11: e0151335.
  9. De Giorgio R, Guerrini S, Barbara G, *et al.* Inflammatory neuropathies of the enteric nervous system. *Gastroenterology* 2004; 126: 1872-83.
  10. De Winter BY, van den Wijngaard RM, de Jonge WJ. Intestinal mast cells in gut inflammation and motility disturbances. *Biochim Biophys Acta* 2012; 1822: 66-73.

# Clear Cell Renal Cell Carcinoma with Intratumoral Granulomatous Reaction: A Case Report and Review of the Literature

Hayeon Kim · Jong Wook Kim<sup>1</sup>  
Aeree Kim · Hyeyoon Chang

Departments of Pathology and <sup>1</sup>Urology,  
Korea University Guro Hospital, Seoul, Korea

**Received:** July 4, 2016  
**Revised:** August 26, 2016  
**Accepted:** September 7, 2016

## Corresponding Author

Hyeyoon Chang, MD  
Department of Pathology, Korea University Guro  
Hospital, 148 Gurodong-ro, Guro-gu, Seoul 08308,  
Korea  
Tel: +82-2-2626-1470  
Fax: +82-2-2626-1481  
E-mail: breakfree83@hanmail.net

Granulomatous reaction associated with clear cell renal cell carcinoma (CCRCC) is a rare finding, and only a few cases have been described in the literature. It is postulated to occur due to cancer-related antigenic factors such as cancer cells themselves or soluble tumor antigens shed into the blood. Herein, we describe a case of a 56-year-old male patient diagnosed with CCRCC with intratumoral granulomatous inflammation.

**Key Words:** Carcinoma, renal cell; Granulomatous reaction; Kidney neoplasms

Granulomatous inflammation is a distinctive pattern of chronic inflammation composed of activated macrophages and T lymphocytes.<sup>1</sup> Central necrosis is often accompanied. Granulomatous reaction occurs in various noninfectious or infectious conditions. Leading causes of granulomatous inflammation include systemic sarcoidosis and tuberculosis.

Granulomatous reaction in tumor stroma is an uncommon phenomenon but well defined in several tumors.<sup>2</sup> Granulomatous reaction associated with tumor in patients without sarcoidosis or infection have been designated as tumor-related sarcoid-like reaction (SLR).<sup>3</sup> Tumor-related SLR has been found in association with various malignant lesions including the breast, lung, and kidney cancers and hematologic malignancy such as Hodgkin's and non-Hodgkin's lymphomas.<sup>2,4-6</sup> We present a unique case of a clear cell renal cell carcinoma (CCRCC) associated with extensive tumor-related SLR and a brief review of the literature.

## CASE REPORT

A 56-year-old male with a history of deep vein thrombosis located in left common iliac vein and hypertension underwent

thromboembolectomy in July 2015. Contrast-enhanced computed tomography (CT) scan revealed a renal cyst with internal enhancing structure in the upper pole of the right kidney, which measured 1.6 cm. On follow-up CT scan after 6 months, the largest diameter of the renal cyst increased to 5.6 cm. He complained of no specific symptom. Renal function test and urinalysis were unremarkable. The patient went through a partial nephrectomy on January 2016. He had an uneventful peri- and postoperative course. On a thorough clinical workup, he had no history, signs and clinical findings suggestive of sarcoidosis or tuberculosis.

Gross examination revealed a 5.3 cm × 4.0 cm × 2.8 cm-sized well-encapsulated cortical cyst. The cystic space was mainly filled with old blood but also displayed a tan-colored solid mass measuring 2.2 cm × 1.4 cm × 1 cm (Fig. 1). The renal capsule was grossly intact.

Histopathologic examination revealed a CCRCC of Fuhrman nuclear grade 2, without sarcomatoid differentiation. The tumor contained areas of hemorrhage and coagulative necrosis. The tumor was well-delineated from surrounding normal renal parenchyma. There was no discrete fibrous capsule around the tumor. Multiple non-necrotizing granulomas of various sizes with



**Fig. 1.** Cut surface of the tumor showing yellowish solid mass with surrounding hemorrhagic area.

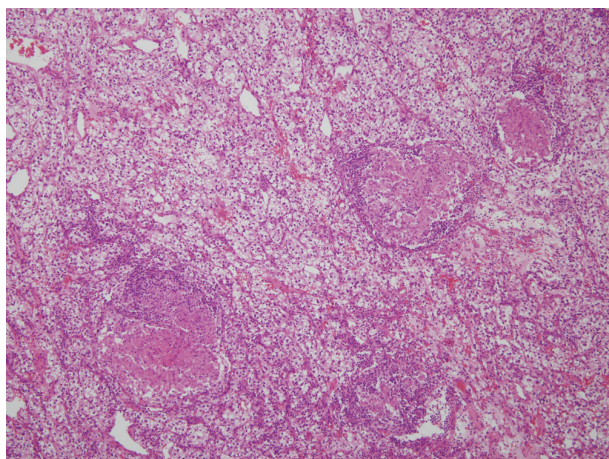


**Fig. 2.** Several epithelioid granulomas in the clear cell renal cell carcinoma.

multinucleated giant cells were scattered within the tumor stroma (Fig. 2). A few granulomas contained foci of coagulative necrosis, but they were devoid of caseation necrosis that is characteristic of tuberculosis (Fig. 3). Distribution of the granulomas showed no zonation pattern. Mild lymphocytic infiltration accompanied those granulomas.

As the performed procedure was a partial nephrectomy, evaluation of uninvolved renal parenchyma was limited. The parenchyma immediately surrounding the tumor showed no granulomatous reaction.

On Ziehl-Neelsen and Grocott's methenamine silver stains, no acid-fast bacteria or other microorganisms were identified. Polymerase chain reaction for *Mycobacterium* species yielded negative result.

On a follow-up CT scan taken 5 months after the operation,

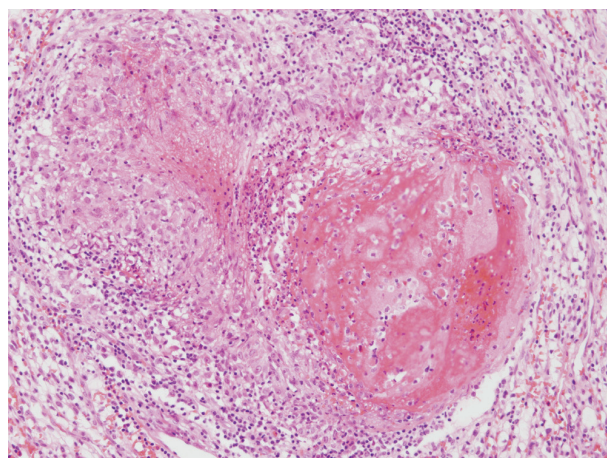


**Fig. 3.** A granuloma showing a focus of coagulative necrosis.

any evidence of recurrence was not detected.

## DISCUSSION

Tumor-related SLR is postulated to occur due to T cell-mediated reaction against various cancer-associated antigens.<sup>7</sup> Those antigenic factors are believed to be expressed directly by the cancer cells or shed as soluble antigen during tumor destruction. As those antigenic factors are conveyed by nearby lymphatic system, tumor-related SLR is most commonly identified in tumor-draining lymph nodes.<sup>8</sup> Kurata *et al.*<sup>9</sup> studied distribution of various kinds of inflammatory cells in lymph nodes with tumor-related SLR. In this study, tumor-related SLR mainly appeared in lymphoid sinuses and T-cell zones in a continuous growth pattern. This finding supports the hypothesis that tumor-related SLR occurs because of tumor-shed antigens drained into lymph nodes. Granulomas in lymph nodes may be observed without any evidence of metastasis.

The association of renal cell carcinoma and granulomatous reaction is a rare phenomenon. Only fewer than 15 cases have been reported in the English literature since early 1990s.<sup>3,7,8,10-13</sup> We reviewed the clinical and pathological characteristics of previously reported cases. Those clinicopathologic details are summarized in Table 1. Of the 13 cases reviewed, there was a male preponderance (9 males and 4 females). In reports which included the side of affected kidney, seven out of 10 cases occurred in the right kidney. Tumor size ranged from 2.3 to 9.5 cm. Most cases manifested as clear cell type, except for one case of sarcomatoid renal cell carcinoma.<sup>3</sup> Fuhrman nuclear grade ranged from 1 to 4, but there was only one case with grade 4 histology which was the sarcomatoid renal cell carcinoma case. Of 12 CCRCCs with

**Table 1.** Reported cases of granulomatous reaction associated with CCRCC

Source	Year	Age/Sex	Side	No. of cases	Locations of granulomas	Histologic type	Fuhrman grade	Tumor size (cm)	Follow-up period
Hes <i>et al.</i> <sup>7</sup>	2003	73–85 (mean 78.3)/2F, 1M	Unstated	3	Within tumor	Clear cell	1	2.3–7.0 (mean 4.4)	6 mo–4 yr
Kovacs <i>et al.</i> <sup>16</sup>	2004	62/F	Left	1	Within tumor and fibrous stroma surrounding the tumor	Clear cell	Not documented	6	15 mo
Piscioli <i>et al.</i> <sup>3</sup>	2008	70/M	Right	1	Periphery of the tumor	Sarcomatoid	4	7	Died of metastases after 6 mo
Shah <i>et al.</i> <sup>13</sup>	2010	62/M	Left	1	Within tumor	Clear cell	1	5	12 mo
Narasimhaiah <i>et al.</i> <sup>12</sup>	2011	44–65/3M	Right	3	Within tumor and fibrous stroma surrounding the tumor	Clear cell	1–3	3–7	Not documented
Ouellet <i>et al.</i> <sup>9</sup>	2012	62/M	Right	1	Peritumoral only, without intratumoral granulomas	Clear cell	3	3.5	30 mo
Burhan <i>et al.</i> <sup>11</sup>	2013	62/M	Right	1	Within tumor	Clear cell	3	9	Not documented
Khatua <i>et al.</i> <sup>10</sup>	2015	42/F	Left	1	Within tumor	Clear cell	2	9.5	1 yr
Present case	2016	56/M	Right	1	Within tumor	Clear cell	2	5.3	5 mo

CCRCC, clear cell renal cell carcinoma; F, female; M, male.

tumor-related SLRs, three cases had documented the absence of sarcomatoid component.<sup>8,10</sup> There was no mention of sarcomatoid differentiation in the rest of the cases.

All of the cases exhibited epithelioid granulomatous reaction related to the tumor. In the majority including this study (8 out of 13), granulomas existed only in tumor stroma. Four cases had granulomas both in the tumor stroma and fibrous stroma immediately surrounding the tumor. Piscioli *et al.*<sup>3</sup> reported a case of sarcomatoid renal cell carcinoma (RCC) containing granulomas only in the periphery of the neoplasm.

The follow-up period varied from 4 months to 4 years. The patient with sarcomatoid RCC in the report of Piscioli *et al.*<sup>3</sup> died from multiple disseminated metastatic disease 6 months after the diagnosis. Rest of the cases maintained disease-free status until the last follow-up.

Tumor-related SLR was reported to be associated with better prognosis or lower possibility of metastasis in Hodgkin's lymphoma, gastric adenocarcinoma<sup>2</sup> and breast cancer.<sup>4</sup> In contrast, Tomimaru *et al.*<sup>14</sup> found that sarcoid reaction identified in regional lymph nodes did not lead to better prognosis in lung cancer. As granulomatous reaction is thought to give protective function against infectious agents, tumor-related SLR might also aid in destruction of tumor cells. Activation of immune system is known to cause regression of tumors in various malignancies.<sup>15</sup> Likewise, tumor-related SLR may be a immunologic defense mechanism against tumor cells, decreasing the metastasis rate and expansion

of the tumor. However, tumor-related SLR may only be secondary phenomenon due to tumor-shed antigens. In Table 1, there is a case without recurrence or distant metastasis after a long follow-up period (4 years),<sup>7</sup> but this does not support the hypothesis that tumor-related SLR is associated with better prognosis. In the reviewed cases, only one patient died of distant metastases during the follow-up period (6 months).<sup>3</sup> However, that patient was diagnosed with a sarcomatoid RCC, which is known to show aggressive clinical course. Thus, the relationship between sarcoid reaction and tumor prognosis is yet to be defined.

In summary, we describe a rare case of CCRCC with intratumoral granulomatous reaction in a male patient, without evidence of systemic sarcoidosis or tuberculosis. We reviewed clinicopathologic findings of previously reported cases with similar histologic features. Further research is required to clarify the mechanism of tumor-related SLR and its impact on prognosis.

### Conflicts of Interest

No potential conflict of interest relevant to this article was reported.

### REFERENCES

1. Kumar V, Abbas AK, Aster JC. Robbins and Cotran pathologic basis of disease. 9th ed. Philadelphia: Elsevier/Saunders, 2015.

2. Brincker H. Sarcoid reactions in malignant tumours. *Cancer Treat Rev* 1986; 13: 147-56.
3. Pisciole I, Donato S, Morelli L, Del Nonno F, Licci S. Renal cell carcinoma with sarcomatoid features and peritumoral sarcoid-like granulomatous reaction: report of a case and review of the literature. *Int J Surg Pathol* 2008; 16: 345-8.
4. Pavic M, Debourdeau P, Vacelet V, Rousset H. Sarcoidosis and sarcoid reactions in cancer. *Rev Med Interne* 2008; 29: 39-45.
5. Bassler R, Birke F. Histopathology of tumour associated sarcoid-like stromal reaction in breast cancer: an analysis of 5 cases with immunohistochemical investigations. *Virchows Arch A Pathol Anat Histopathol* 1988; 412: 231-9.
6. Okumura N, Teramachi M, Okada K, Itoh M, Inoue R, Kobayashi K. A case report of lung cancer with sarcoid-like reaction in the primary tumor and regional lymph nodes. *Nihon Kyobu Shikkan Gakkai Zasshi* 1987; 25: 360-4.
7. Hes O, Hora M, Vanecek T, *et al.* Conventional renal cell carcinoma with granulomatous reaction: a report of three cases. *Virchows Arch* 2003; 443: 220-1.
8. Ouellet S, Albadine R, Sabbagh R. Renal cell carcinoma associated with peritumoral sarcoid-like reaction without intratumoral granuloma. *Diagn Pathol* 2012; 7: 28.
9. Kurata A, Terado Y, Schulz A, Fujioka Y, Franke FE. Inflammatory cells in the formation of tumor-related sarcoid reactions. *Hum Pathol* 2005; 36: 546-54.
10. Khatua S, Bose K, Bandyopadhyay A, Banerjee A. A rare association of sarcoid-like granuloma with renal cell carcinoma. *J Cancer Res Ther* 2015; 11: 1033.
11. Burhan W, Al Rowaie Z, Rajih E, Akhtar M. Sarcoid-like granulomatous reaction in renal cell carcinoma: report of a case with review of the published reports. *Ann Saudi Med* 2013; 33: 614-8.
12. Narasimhaiah DA, Manipadam MT, Aswathaman K, Krishnamoorthy S. Renal cell carcinoma associated with granulomatous reaction. *Saudi J Kidney Dis Transpl* 2011; 22: 1211-4.
13. Shah VB, Sharma P, Pathak HR. Conventional clear renal cell carcinoma with granulomatous reaction. *Indian J Pathol Microbiol* 2010; 53: 379-80.
14. Tomimaru Y, Higashiyama M, Okami J, *et al.* Surgical results of lung cancer with sarcoid reaction in regional lymph nodes. *Jpn J Clin Oncol* 2007; 37: 90-5.
15. Ricci SB, Cerchiari U. Spontaneous regression of malignant tumors: importance of the immune system and other factors (review). *Oncol Lett* 2010; 1: 941-5.
16. Kovacs J, Varga A, Bessenyei M, Gomba S. Renal cell cancer associated with sarcoid-like reaction. *Pathol Oncol Res* 2004; 10: 169-71.

# Human Papillomavirus Infection—Associated Adenoid Cystic Carcinoma of the Hard Palate

Arthur Minwoo Chung · Dong Il Sun<sup>1</sup> · Eun Sun Jung · Youn Soo Lee

Departments of Hospital Pathology and <sup>1</sup>Otorhinolaryngology, College of Medicine, The Catholic University of Korea, Seoul, Korea

Adenoid cystic carcinoma (ACC) is a rare tumor of the head and neck region. It accounts for less than 1% of all head and neck malignancies and approximately 4%–10% of all salivary gland tumors.<sup>1</sup> Unlike squamous cell carcinoma, p16 protein overexpression is not a common feature of ACC, especially with a co-existing human papillomavirus (HPV) infection.<sup>2</sup> Here, we present a case of ACC of the hard palate associated with HPV infection.

## CASE REPORT

A 55-year-old male patient presented with a 3.9-cm mass in the right hard palate, which appeared 3 months ago and had increased in size over time. The patient was otherwise healthy without a remarkable medical history. He was a nonsmoker and did not have a history of alcohol or other substance use disorders. Magnetic resonance imaging revealed a lobular contoured mass in the right hard palate, extending to the retromolar trigone and involving the pterygoid muscle and plates. The patient underwent a right inferior maxillectomy. The cut surface of the resected specimen showed a whitish gray and firm mass with irregular margins, measuring 3.9 cm in diameter (Fig. 1). The mass was involving the maxillary bone. Microscopically, the lesion showed poorly circumscribed infiltrates of tumor cells forming a cribriform pattern (Fig. 2A). There was no squamous dysplasia of the overlying surface epithelium. Small to medium bland cells with scant cytoplasm surrounded pseudocysts, and mitotic

figures were rarely seen. Perineural invasion was commonly seen, as was venous invasion. Approximately 75% of tumor cells were positive for p16 (RTU, Roche, Branford, CT, USA) (Fig. 2B) on immunohistochemistry. The ductal cells were positive for CD117 (1:400, DAKO, Glostrup, Denmark) (Fig. 2C), whereas the myoepithelial cells were strongly positive for p63 (1:200, DAKO) (Fig. 2D). HPV detection and genotyping were performed using the BMT HPV 9G DNA kit provided by Biometrix Technology Inc. (Chuncheon, Korea). DNA was isolated from the tissue using the DNA extraction kit, and amplification was performed with a polymerase chain reaction mixture consisting of extracted target DNA, the primer set, and polymerase chain reaction premix. Hybridization was performed using an HPV DNA chip at room temperature for 30 minutes. HPV DNA hybridization was detected using the DNA Chip Scanner (ScanArray Gx, Perkin-Elmer Life and Analytical Science, Boston, MA, USA). In this case, the tumor tissue DNA was positive for HPV type 16. The resection margins were free of tumor. On the basis of these findings, the histopathological diagnosis was HPV-associated ACC. After discussion with the head and neck multidisciplinary team, the patient underwent postoperative radiation therapy. No recurrence was evident at 6-month follow-up.

## DISCUSSION

HPV has been shown to be etiologically related to the development of 20%–25% of head and neck carcinomas. It has a strong predilection for the oropharynx, as up to 80% of nonkeratinizing oropharyngeal squamous cell carcinomas are related to HPV infection.<sup>3</sup> The likelihood of detecting HPV outside of the oropharynx is very low, especially in the nasal cavity.<sup>4</sup> Using

### Corresponding Author

Arthur Minwoo Chung, MD  
Department of Hospital Pathology, College of Medicine, The Catholic University of Korea, 222 Banpo-daero, Seocho-gu, Seoul 06591, Korea  
Tel: +82-2-2258-1613, Fax: +82-2-2258-1628, E-mail: minu0731@gmail.com

Received: April 5, 2016 Revised: June 10, 2016

Accepted: July 7, 2016

an HPV DNA chip, we report the first case of ACC of the hard palate associated with HPV infection.

Although p16 protein overexpression can be detected in ACC of the head and neck, the staining pattern of p16 is mostly focal

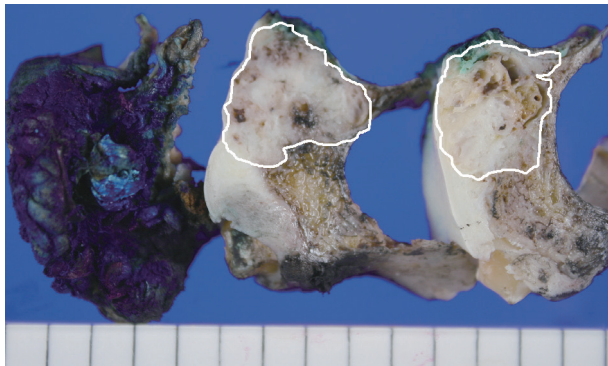


**Fig. 1.** On cut sections, an ill-defined, whitish gray mass (white circle), measuring 3.9 cm in diameter, involves the maxillary bone.

(less than 75% of cells are stained), and the presence of co-existing HPV infection is rare.<sup>2,3</sup> Even though p16 protein overexpression was observed in our case, we used an HPV DNA chip for confirmation.

The most important differential diagnosis to consider is HPV-related carcinoma with adenoid cystic-like features due to its morphologic and immunohistochemical features. Its morphologic resemblance to ACC is based on architectural patterns, a dual population of cells, and immunohistochemical expression of myoepithelial markers. However, HPV-related carcinoma with adenoid cystic-like features has a predominantly solid growth pattern, and it is associated with squamous dysplasia of the overlying surface epithelium.<sup>1</sup> Furthermore, HPV 33 is the most common high-risk HPV type in HPV-related carcinoma; however, HPV type 16 was detected in our case.

Because of their overlapping morphological features, basaloid squamous cell carcinoma must be distinguished from ACC. Un-

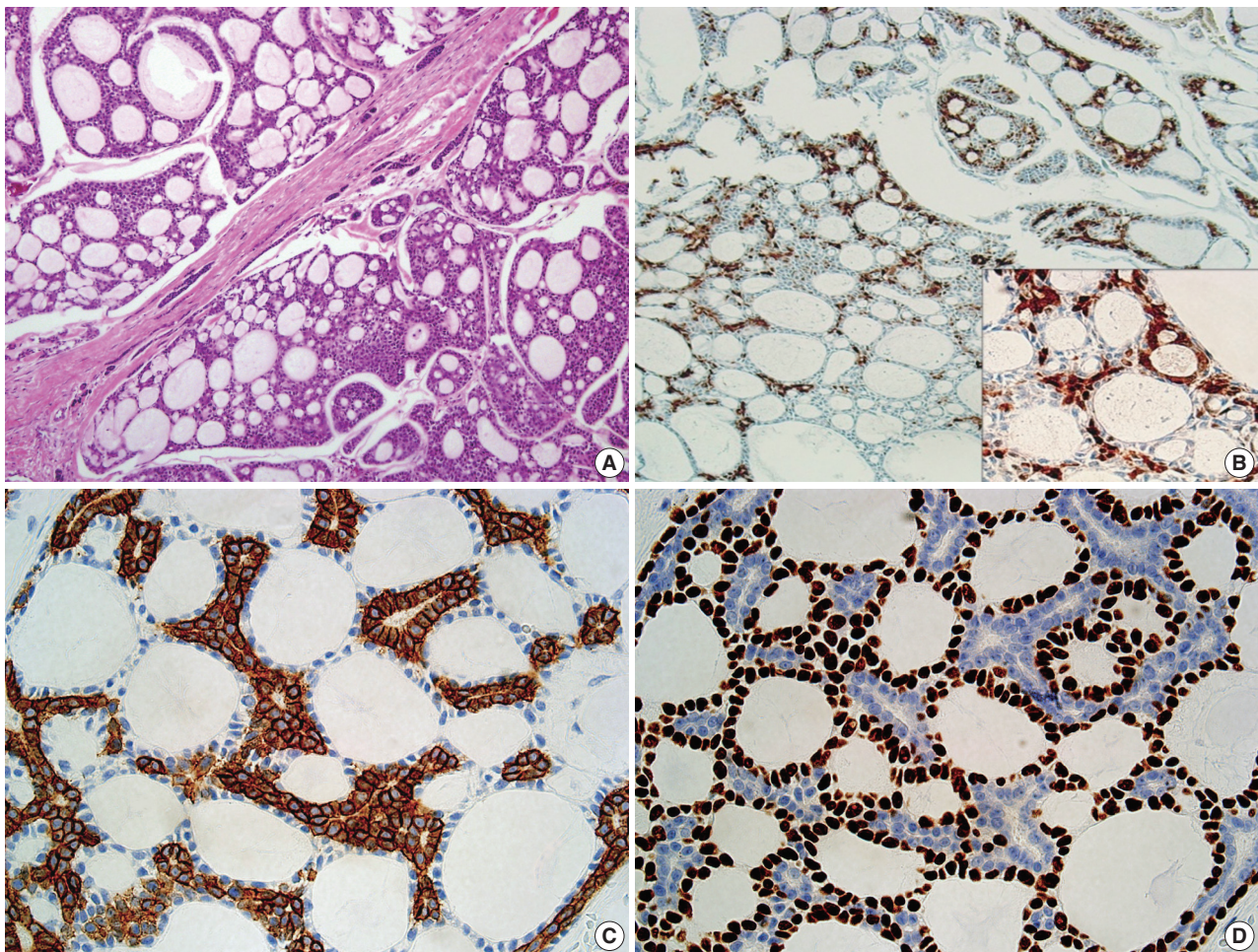


**Fig. 2.** Microscopic findings of the adenoid cystic carcinoma of the hard palate. (A) Adenoid cystic carcinoma with a cribriform pattern. (B) p16 protein expression is seen in 75% of cells. The ductal cells are positive for CD117 (C), and the myoepithelial cells are positive for p63 (D).

like basaloid squamous cell carcinoma, ACC usually lacks squamous differentiation. The most important differentiating characteristic of ACC is the presence of a myoepithelial cell component. In our case, the tumor has this dual population.

In summary, we present an HPV-associated ACC of the hard palate. HPV-associated ACC is extremely rare, and only two cases of HPV-related ACC arising in the nasal cavity have been reported. Here, we report the first documented case of ACC in the hard palate with the presence of p16 protein expression and co-existent HPV type 16 infection.

---

### Conflicts of Interest

No potential conflict of interest relevant to this article was reported.

### REFERENCES

1. Hwang SJ, Ok S, Lee HM, Lee E, Park IH. Human papillomavirus-related carcinoma with adenoid cystic-like features of the inferior turbinate: a case report. *Auris Nasus Larynx* 2015; 42: 53-5.
2. Boland JM, McPhail ED, Garcia JJ, Lewis JE, Schembri-Wismayer DJ. Detection of human papilloma virus and p16 expression in high-grade adenoid cystic carcinoma of the head and neck. *Mod Pathol* 2012; 25: 529-36.
3. Bishop JA, Guo TW, Smith DF, *et al.* Human papillomavirus-related carcinomas of the sinonasal tract. *Am J Surg Pathol* 2013; 37: 185-92.
4. Bishop JA, Ogawa T, Stelow EB, *et al.* Human papillomavirus-related carcinoma with adenoid cystic-like features: a peculiar variant of head and neck cancer restricted to the sinonasal tract. *Am J Surg Pathol* 2013; 37: 836-44.
5. Maruya S, Kurotaki H, Shimoyama N, Kaimori M, Shinkawa H, Yagihashi S. Expression of p16 protein and hypermethylation status of its promoter gene in adenoid cystic carcinoma of the head and neck. *ORL J Otorhinolaryngol Relat Spec* 2003; 65: 26-32.

## A Rare Case of Nodular Mucinosis of the Breast

Hyun Min Koh · Young Hee Maeng<sup>1</sup> · Bo Geun Jang<sup>1</sup> · Jae Hyuk Choi<sup>2</sup> · Chang Lim Hyun<sup>1</sup>

Department of Pathology, Jeju National University Hospital, Jeju; Departments of <sup>1</sup>Pathology and <sup>2</sup>Surgery, Jeju National University Hospital, Jeju National University College of Medicine and Graduate School of Medicine, Jeju, Korea

Nodular mucinosis of the breast is an extremely rare stromal lesion described as a nerve sheath myxoma by Wee *et al.*<sup>1</sup> in 1989, which was the first report of its kind. To the best of our knowledge, the English literature contains few examples of this lesion. In this report, we describe a case of nodular mucinosis characterized by abundant myxoid tissue with scattered spindle cells without epithelial components.

### CASE REPORT

A 22-year-old previously healthy woman visited our hospital complaining of a soft mass on her right breast that had been present for a year. Recently, the lesion had gradually increased in size. She had no other complaints, such as pain or nipple discharge. There was no relevant family or personal medical history. She had never been pregnant and had never taken exogenous hormones or any drugs. The patient showed no evidence of Carney complex. Upon physical examination, a well-demarcated, protruding and movable cystic nodule was present at 10 o'clock on the areola of her right breast. The skin surface covering the nodule exhibited no specific changes and the nipple was unremarkable. Ultrasonography of the breast revealed a 1-cm ovoid cystic nodule located in the dermal layer, which was presumed to be a benign lesion. Surgical resection was carried out without other diagnostic tests, such as fine needle aspiration or mammography.

Grossly, the specimen was an ovoid cystic nodule measuring 1.1 × 0.6 × 0.6 cm and was covered by an ellipse of normal skin.

#### Corresponding Author

Chang Lim Hyun, MD, PhD  
Department of Pathology, Jeju National University School of Medicine, 15 Aran 13-gil, Jeju 63241, Korea  
Tel: +82-64-754-8818, Fax: +82-64-717-1131, E-mail: venisua@jejunu.ac.kr

Received: May 27, 2016 Revised: July 20, 2016

Accepted: July 25, 2016

The outer surface of the nodule was smooth and glistening. Upon sectioning, the cyst was well circumscribed, but not encapsulated (Fig. 1A) and was filled with pale tan, gelatinous material surrounded by grayish white fibrous tissue (Fig. 1B). Histologically, the lesion consisted of abundant myxoid tissue with a few scattered spindle cells and had a slightly multilobular appearance with fibrocollagenous stroma. Capillaries and thin-walled vessels were noted within the nodule (Fig. 1C). Rare histiocytes, lymphocytes, and plasma cells were seen in the nodule. Neither mammary ducts nor epithelial elements were observed. Spindle cells showed bland-looking nuclei and elongated amphophilic cytoplasm with no atypia or mitosis. The myxoid tissue was analyzed via Alcian blue staining (pH 2.5) and periodic acid-Schiff (PAS) testing. Alcian blue stained the myxoid stroma bright blue (Fig. 1D) and PAS was negative, indicating the existence of acidic mucopolysaccharides. The spindle cells showed reactivity to vimentin (Fig. 1E) but were nonreactive to smooth muscle actin (Fig. 1F). Based on these findings, we confirmed nodular mucinosis of the breast. Postoperative status was good, and the patient has been in remission for 3 years since the surgery.

### DISCUSSION

Nodular mucinosis of the breast is an extraordinary entity that has been reported fewer than 10 times in the English literature since the first case was described in 1989 (Table 1).<sup>1-7</sup> Several common clinical and pathologic features were observed in previous reports. Nodular mucinosis of the breast is predominantly found in young women ranging from 15 to 72 years.<sup>2-6</sup> The typical clinical manifestation is a soft mass under the nipple or in the subareolar region that gradually increases in size, and occasionally presents with nipple discharge or pain.<sup>2-6</sup> Ultrasonography usually reveals a well-circumscribed, lobulated, homoge-

nous, hypoechoic mass and mammography shows a round-lobular, radiopaque mass without microcalcifications or spicula formation.<sup>2-5</sup> Fine needle aspiration typically reveals mucin without epithelial elements or malignant evidence.<sup>2,4,5</sup> The treatment of choice is surgical excision, which usually leads to a successful outcome without residual disease. Nodular mucinosis of the breast does not have an established link with Carney complex,<sup>5</sup> which is an autosomal dominant syndrome charac-

terized by multiple neoplasias, including myxomas at various sites, endocrine tumors, and lentiginosis related to genetic defects.<sup>8</sup>

Grossly, the lesion is usually a small, ovoid protruding nodule, ranging from 0.9 to 3.2 cm in diameter.<sup>2-6</sup> The cut surface demonstrates a well-circumscribed but not encapsulated, multinodular lesion that is grayish-white, grayish-pink, or yellow-to-tan in color<sup>2-6</sup> and has a myxoid, mucinous or gelatinous consistency.<sup>3-6</sup>

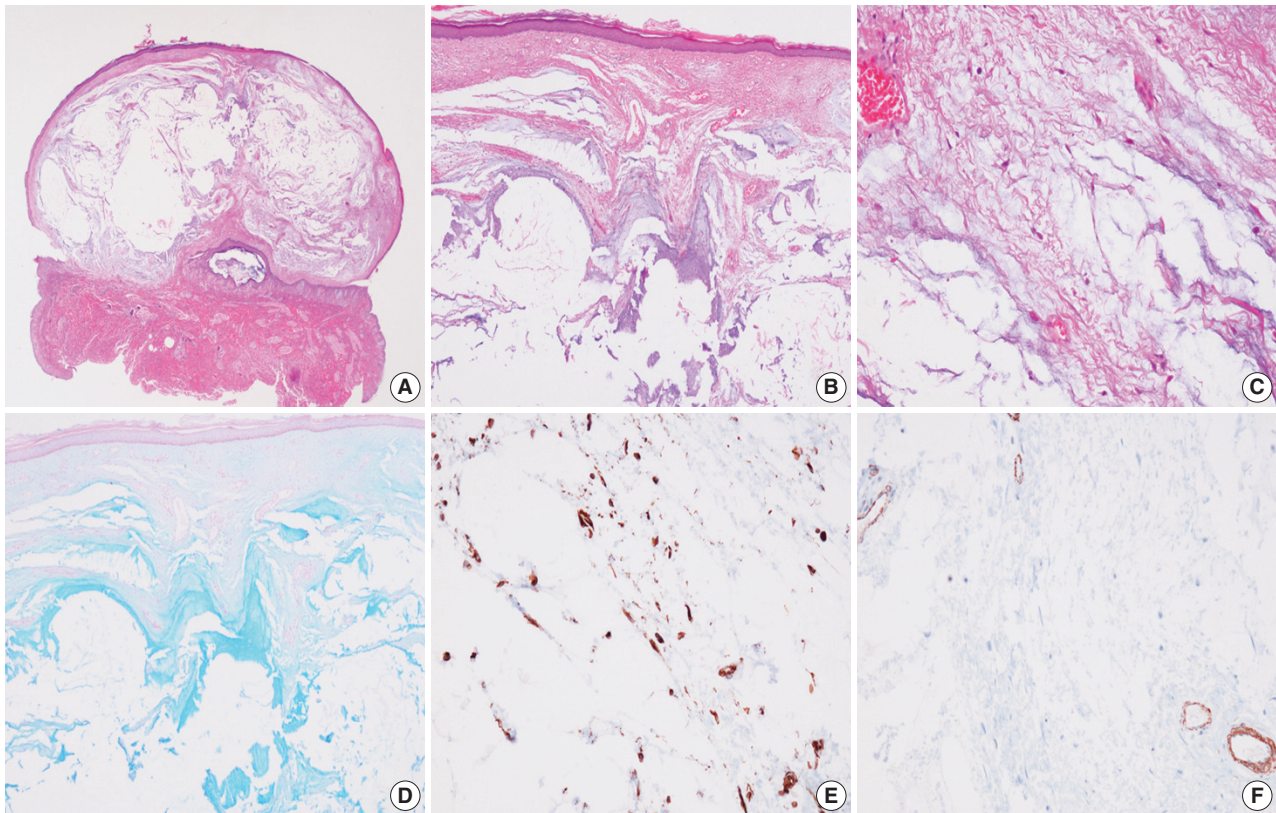


**Fig. 1.** Histopathologic findings. (A) The lesion is a well-circumscribed cyst showing a slightly multilobular appearance. (B) The lesion is filled with basophilic myxoid substance. (C) The lesion consists of scattered spindle cells with thin walled vessels and capillaries. (D) Alcian blue stains the myxoid material in bright blue. (E) The spindle cells are reactive to vimentin. (F) The spindle cells show nonreactivity to smooth muscle actin.

**Table 1.** Clinical features of nine reported cases of nodular mucinosis of the breast (including the present case)

Reference	Age (yr)	M/F	Location	Size (cm)	Follow-up	Prognosis
Michal <i>et al.</i> <sup>6</sup> (1998)	40	M	Left nipple	2 × 1.5 × 1.5	6 yr	No recurrence
	28	F	Right nipple	1.5 × 1.5 × 1	3 yr	No recurrence
	29	F	Right nipple	2.5 × 2.5 × 2	6 mo	No recurrence
Koide <i>et al.</i> <sup>5</sup> (2002)	30	F	RUO to N	2.9 × 2.1	NA	NA
Sanati <i>et al.</i> <sup>4</sup> (2005)	21	F	Left nipple	1.5 × 0.9 × 0.8	NA	NA
Chisholm <i>et al.</i> <sup>3</sup> (2010)	72	F	Right subareolar	0.9 × 0.8 × 0.3	4 mo	No recurrence
Manglik <i>et al.</i> <sup>2</sup> (2010)	15	F	Right subareolar (supernumerary nipple)	1 × 1 × 0.5	NA	NA
Bulut <i>et al.</i> <sup>7</sup> (2015)	37	F	Right subareolar	3.2 × 2.5 × 1.7	29 mo	No recurrence
Our case	22	F	Right subareolar	1.1 × 0.6 × 0.6	3 yr	No recurrence

M, male; F, female; RUO to N, right upper outer to nipple; NA, not available.

The histological features of nodular mucinosis of the breast include a multinodular myxoid or mucinous lesion separated by fibrocollagenous stroma.<sup>2-6</sup> The lesion consists of sparse spindle cells, which have bland and elongated nuclei, scant and/or pale cytoplasm, and indistinct cell borders.<sup>2,4,5</sup> Rarely histiocytes, lymphocytes, plasma cells, and/or mast cells can be seen within and around the nodules,<sup>2-6</sup> and some capillaries or small vessels are seen within the lesions.<sup>3,5,6</sup> The lesion neither contains nor invades the breast parenchyma.<sup>2-4,6</sup> Also, no epithelial components can be identified.<sup>2-6</sup> Myxoid or mucinous areas are stained intensely with Alcian blue and Hale colloidal iron, but are negative on PAS, proving the existence of acid mucopolysaccharide.<sup>2-6</sup> The spindle cells are positive for calponin, vimentin, and smooth muscle actin and negative for cytokeratin, smooth muscle myosin, and S-100, probably arising from myofibroblasts.<sup>2-5</sup>

Clinicians need to be able to differentiate nodular mucinosis of the breast from other myxoid and mucinous lesions such as mucinous carcinoma, micropapillary carcinoma *in situ* with excessive mucin, fibroadenoma with myxomatous stroma and mucocele-like lesions.<sup>2-5</sup> Nodular mucinosis exhibits mucin with no epithelial elements or malignant evidence on fine needle aspiration.<sup>2,4,5</sup> The presence of an epithelial cell component in the mucin suggests other myxoid and mucinous lesions.<sup>4,7</sup> In addition, cytologically mucocele-like lesions are characterized by abundant mucin and monolayer clusters or sheets of epithelial cells without nuclear atypia and is usually associated with microcalcifications, which is a feature not typical of nodular mucinosis.<sup>4</sup> Mucin in mucocele-like lesions is usually stained with PAS but appears negative on Alcian blue and Hale colloidal iron staining.<sup>4,7</sup>

Considering that nodular mucinosis has no epithelial components in acidic mucin pools, differentiation is not a major challenge, so long as spindle cells are not mistaken for epithelial cells.

We have discussed a very rare case of nodular mucinosis of the breast. Although this entity is benign, it is imperative that it be distinguished from other lesions that occur near the nipple, es-

pecially mucinous carcinoma, via pathologic examination after surgical excision.

---

### Conflicts of Interest

No potential conflict of interest relevant to this article was reported.

### REFERENCES

1. Wee A, Tan CE, Raju GC. Nerve sheath myxoma of the breast: a light and electron microscopic, histochemical and immunohistochemical study. *Virchows Arch A Pathol Anat Histopathol* 1989; 416: 163-7.
2. Manglik N, Berlingeri-Ramos AC, Boroumand N, Eltorkey M. Nodular mucinosis of the breast in a supernumerary nipple: case report and review of the literature. *J Cutan Pathol* 2010; 37: 1178-81.
3. Chisholm C, Greene JF Jr. Nodular mucinosis of the breast: expanding our understanding with an unusual case. *Am J Dermatopathol* 2010; 32: 187-9.
4. Sanati S, Leonard M, Khamapirad T, Eltorkey MA. Nodular mucinosis of the breast: a case report with pathologic, ultrasonographic, and clinical findings and review of the literature. *Arch Pathol Lab Med* 2005; 129: e58-61.
5. Koide N, Akashi-Tanaka S, Fukutomi T, Nanasawa T, Hasegawa T. Nodular mucinosis of the breast: a case report with clinical and imaging findings. *Breast Cancer* 2002; 9: 261-4.
6. Michal M, Ludvíková M, Zámecnik M. Nodular mucinosis of the breast: report of three cases. *Pathol Int* 1998; 48: 542-4.
7. Bulut T, Celik B, Nassar A, Yalcin AD. Nodular mucinosis of breast: a case report. *J Med Cases* 2015; 6: 457-9.
8. Stratakis CA, Carney JA, Lin JP, et al. Carney complex, a familial multiple neoplasia and lentiginosis syndrome: analysis of 11 kindreds and linkage to the short arm of chromosome 2. *J Clin Invest* 1996; 97: 699-705.

# Cerebellar Liponeurocytoma: Relevant Clinical Cytogenetic Findings

Alexander Tucker · Kritsanapol Boon-Unge<sup>1</sup> · Nancy McLaughlin · Hassana Ibrahim<sup>2</sup>  
Nagesh Rao<sup>3</sup> · Neil Martin · Richard Everson · Négar Khanlou<sup>1</sup>

Department of Neurosurgery, <sup>1</sup>Division of Neuropathology, Department of Pathology and Laboratory Medicine, <sup>2</sup>Division of Neuroradiology, Department of Radiological Sciences, <sup>3</sup>Division of Clinical and Molecular Cytogenetics, Department of Pathology and Laboratory Medicine, University of California-Los Angeles, Los Angeles, CA, USA

Cerebellar liponeurocytoma (cLNC) is a glioneuronal tumor first described in 1978.<sup>1</sup> Histologically, the lesion is similar to medulloblastoma and many pathologists incorrectly describe cLNC as “lipomatous medulloblastoma.” Various other nomenclatures have been used to describe cLNC, such as lipomatous glioneurocytoma and lipidized mature neuroectodermal tumor of the cerebellum.<sup>2</sup> To date, over 40 cases have been reported in the literature, including supratentorial variants. Recent studies have shown that cLNC lesions contain *NEUROG1* transcripts (expressed in progenitor cells of the cerebellar ventricular zone) and that they lack *ATOH1* or *OTX2* transcripts (expressed in progenitor cells of the external granule cell layer). These findings suggest that cLNC cells may originate from GABAergic neurons of the cerebellar ventricular zone.

Ultrastructural analysis of cLNC has demonstrated the presence of lipidized neurocytic cells rather than mature adipocytes.<sup>3</sup> In 2000, World Health Organization (WHO) changed its classification to include “cerebellar liponeurocytoma,” emphasizing the tumor’s neurocytic differentiation. Furthermore, in the current classification, cLNC was classified in the category of glioneuronal tumors and upgraded to grade II due to the results of long-term follow-up studies revealing a higher recurrence rate than was originally thought.<sup>4</sup> For most cases, immunohistochemical and molecular profiling of the tumor is essential in the diagnosis of cLNC. While a typical cytogenetic abnormality is not assigned to cLNC, absence of the molecular hallmarks of

high grade tumors (e.g., *MYC* rearrangements as seen in medulloblastoma) are valuable negative findings in the diagnostic work-up. Clinically, pathological diagnosis of cLNC remains challenging with many tumors misdiagnosed for histologic mimics with high-grade potential such as oligodendroglioma and medulloblastoma. In this case report, we describe the clinical, radiographic, and pathological features of a patient with newly diagnosed cLNC. By demonstrating the complete cytogenetic profile of cLNC, we hope to improve recognition and proper diagnosis of this rare entity.

## CASE REPORT

A 41-year-old, right-handed woman without significant past medical or family history presented for evaluation of intermittent, positional headaches for 1 year. These symptoms progressed and became associated with nausea. The patient denied any postural instability, tremor, changes in gait, vision changes, dysphonia, weakness, or sensory disturbance. There was no associated neck or back pain.

Examination at presentation revealed that the patient was awake, alert, and fully oriented. Visual fields were full to confrontation and fundoscopic examination showed no papilledema. The patient had normal facial sensation and facial movement. Tongue and palate were along the midline. Bilateral finger-to-nose testing was normal. Strength was full and no pronator drift was detected. Sensation was intact to light touch throughout. No hyperreflexia was noted nor were there signs of lower extremity clonus. An equivocal Babinski sign was noted on the right side, but toes were downgoing on the left. Her gait appeared smooth and Romberg sign was negative.

Magnetic resonance imaging (MRI) of the brain with and

### Corresponding Author

Alexander Tucker, MD  
Department of Neurosurgery, University of California-Los Angeles, Suite 562 5th Floor, Wasserman Building, 300 Stein Plaza, Los Angeles, CA 90095-6901, USA  
Tel: +1-310-794-7362, Fax: +1-310-267-2707, E-mail: atucker@mednet.ucla.edu

Received: June 10, 2016 Revised: July 20, 2016

Accepted: July 25, 2016

without contrast was obtained and showed a 4.5×5.2×3.6 cm (anterior-posterior×transverse×cranial-caudal) heterogeneously enhancing mass in the right cerebellar hemisphere. The lesion was hypointense on T1 and hyperintense on T2, and it had minimal surrounding edema (Fig. 1A–D). The presence of flow voids on T2 imaging indicated possible high vascularity. It was not entirely clear if the tumor was intra- or extra-axial. Moderate mass effect was evident, resulting in tonsillar herniation of approximately 1.6 cm into the foramen magnum and compression of the fourth ventricle. Resultant obstructive hydrocephalus was mild, and transependymal transudation was noted on T2 imaging. Complete spine MRI did not show any abnormality.

Suboccipital craniotomy was performed and microsurgical total resection of the tumor was achieved. Grossly, the tumor appeared to be intra-axial with an exophytic component and it was red/yellow-colored, not hemorrhagic, and well-circumscribed. It originated within the medial aspect of the right cerebellar hemisphere in the region of the vermis underlying the arachnoid (Fig. 1E). It did not involve the dura. Superficially, the tumor had a clearly defined margin with a clean plane between the lesion and the adjacent cerebellar tissue. In the deep aspect of the tumor, however, the interface between the tumor and healthy parenchyma was not as sharply defined.

### Histopathology and molecular studies

Histologic examination of the permanent sections showed a moderately cellular biphasic neoplasm. Areas of tumor cells were

characterized by round to elongated nuclei with scant cytoplasm arranged in sheets (Fig. 2A). Foci of oligodendroglia-like tumor cells with central round nuclei and perinuclear halos were arranged in nests, separated by thin branching vessels (Fig. 2B). In other areas, nuclear palisading, perivascular rosetting, and rare Homer-Wright rosettes were seen (Fig. 2C). Nuclear pleomorphism and atypia were minimal. Clusters of lipidized tumor cells reminiscent of mature adipocytes were easily identified within the tumor (Fig. 2D). Mitoses were inconspicuous. Rare microfoci of necrosis were seen whereas pseudopalisading necrosis was absent. Prominent vascular channels with hyalinization and occasional complex vessels were noted within the tumor. Classic microvascular endothelial hyperplasia was not identified.

Immunohistochemistry using antibodies to glial fibrillary acidic protein (GFAP), a glial marker, and synaptophysin, a neuronal marker, were performed. Neoplastic cells showed diffuse and strong immunoreactivity with synaptophysin (Fig. 3A), but failed to react with GFAP. Staining for GFAP and CD34 highlighted background reactive gliosis and blood vessels, respectively (Fig. 3B). Inhibin, CD99, and neurofilament immunoreactions were negative in tumor cells. The proliferative rate based on Ki-67 nuclear labeling index was estimated at 3%–5% (Fig. 3C). Although overall morphologic and immunohistochemical profile did not favor a high grade tumor, select molecular studies were performed.

Fluorescent *in-situ* hybridization (FISH) studies showed no evidence of 1p/19q co-deletion, *N-MYC* or epidermal growth fac-

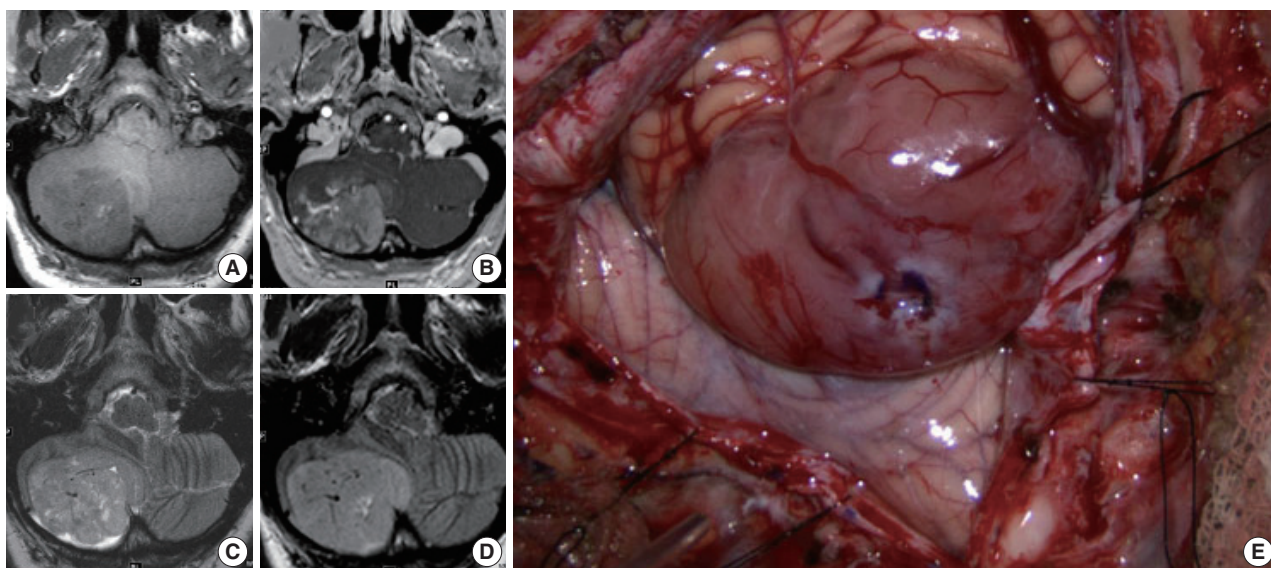


**Fig. 1.** Radiographic and gross appearance. Magnetic resonance imaging of heterogeneously-enhancing right cerebellar hemisphere mass. Axial T1-weighted precontrast (A), T1-weighted postcontrast (B), T2-weighted (C), and fluid attenuated inversion recovery (D) images through the posterior fossa. Intraoperative photograph of tumor and surrounding cerebellum (E).

tor receptor (*EGFR*) amplification, *MYC* or *EWSR1* rearrangements, or *PTEN* deletion. However, these studies detected three to six copies each of chromosomes 1, 2, 7, 8q, 10, 19, and 22q in 50%–80% ([151–247]/300) of nuclei examined (Fig. 3D).

## DISCUSSION

The case described here highlights the main clinical, radiographic and pathologic features of cLNC. With its histologic similarity to many other neoplasms, surgical pathologists must include cLNC in the differential diagnoses of lesions of the posterior fossa with a clear cell morphology (oligodendroglioma, hemangioblastoma, and clear cell ependymoma), neuroectodermal tumors (medulloblastoma), and tumors with possible lipidized component (glioblastoma and meningioma). Without a clear diagnostic rubric, most histologic and molecular studies aim to exclude tumors of high-grade potential, rendering the diagnosis of cLNC as a diagnosis of exclusion. The importance of accurate diagnosis cannot be overstated, as it used to guide further therapeutic intervention and determination of the patient's prognosis.

Histologically, cLNC appears as monotonous sheets of clear cells or oligodendroglia-like cells, as well as characteristic lipidized cells. Biphasic patterns of dense cellularity alternating with clear cell areas, such as in this case, have also been reported.<sup>3</sup> Nuclear palisading, true rosette formation and perivascular arrangements were also noted in our case; however, this is not typical. Areas of high cellularity and rosette formation may prompt some pathologists to consider the diagnosis of glioblastoma or ependymoma; however, unlike these entities, cLNC is rarely mitotically active. Features such as necrosis and vascular endothelial hyperplasia, when present, are not correlated with malignant transformation or rapid regrowth and have no effect on overall prognosis. Conversely, there are a few reports describing aggressive clinical tumor behavior in the absence of the classic high-grade features, although this evidence is limited.<sup>5</sup>

The most common alternative diagnosis considered by pathologists reviewing cases of cLNC is medulloblastoma. Medulloblastoma is the most prevalent primary malignancy of the posterior fossa, seen most commonly in children and young adults. In contrast, cLNC is typically diagnosed in adults. Histologically, medulloblastoma has a more primitive or embryonal appear-

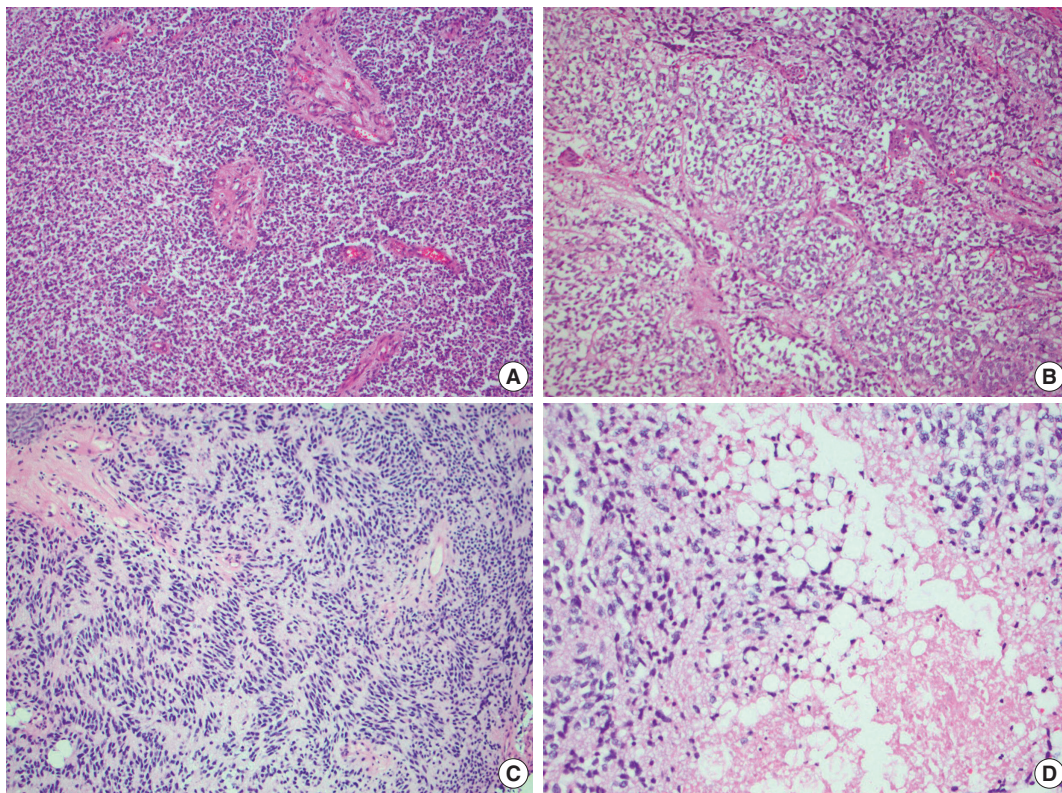


**Fig. 2.** Hematoxylin and eosin staining. (A) Areas of dense cellularity and scattered prominent vascular channels. (B) Oligodendroglial-like areas demonstrating cells with distinct perinuclear halos and a chicken wire vascular pattern. (C) Region of palisading tumor nuclei reminiscent of ependymoma. (D) Foci of lipidized cells.

ance than the neurocytic morphology observed in the cLNC. Similarly, anaplasia, nuclear crowding, and high proliferation rates are more common in medulloblastoma than in cLNC. In addition, clear cell morphology and lipidized cells are not typical

findings in medulloblastoma, but are seen in cLNC.

Other tumors that are considered part of the differential diagnosis for cLNC include oligodendroglioma and clear cell ependymoma. In general, the diagnosis of oligodendroglioma in the

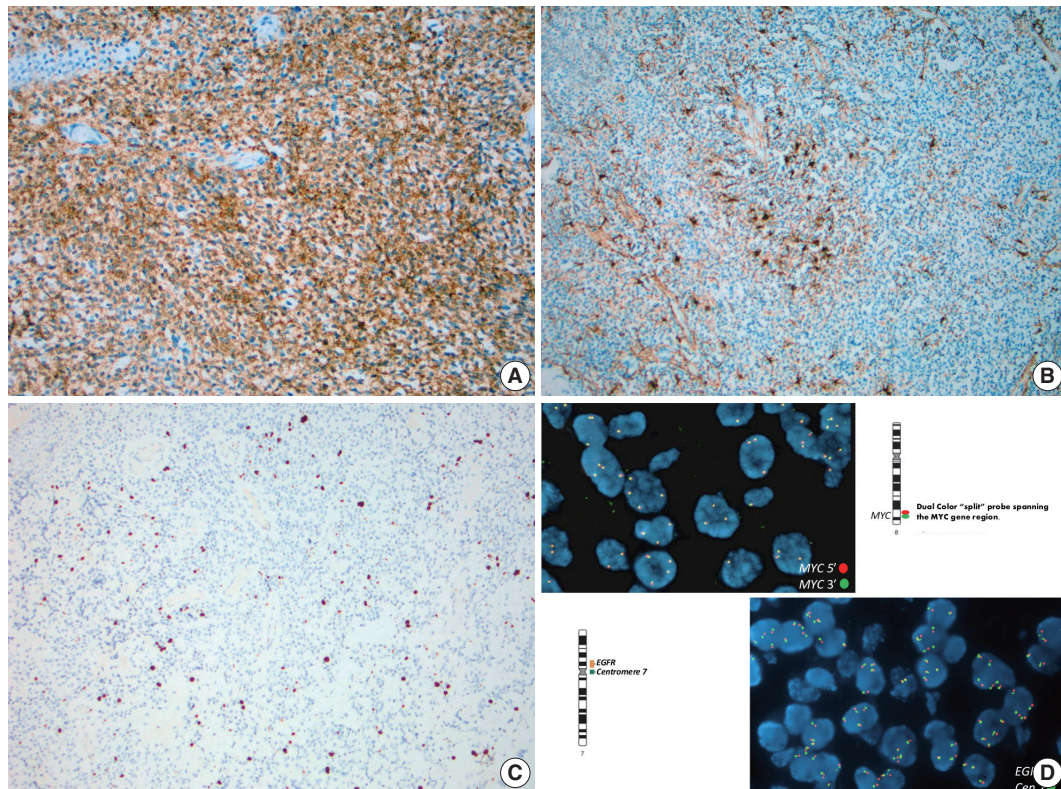


**Fig. 3.** Immunohistochemistry and fluorescent *in-situ* hybridization. (A) Diffuse synaptophysin immunoreactivity within the tumor. (B) Reactive gliosis on glial fibrillary acidic protein immunohistochemistry, but no tumor immunoreactivity. (C) Low Ki-67 nuclear labeling index, estimated at 3%–5%. (D) Fluorescent *in-situ* hybridization demonstrating lack of epidermal growth factor receptor (*EGFR*) amplification or *MYC* rearrangement.

**Table 1.** Demographic and pathologic comparison of cLNC and central neurocytoma, clear cell ependymoma, oligodendroglioma, and medulloblastoma

	Cerebellar liponeurocytoma	Central neurocytoma	Clear cell ependymoma	Oligodendroglioma	Medulloblastoma
Age of diagnosis (yr)	50–60	20–40	1–20	30–50	5–30
WHO grade	II	II	II	II or III	IV
Histology	Neurocytic clear cells in sheets with lipidized cells	Clear cells, modest cytoplasm, salt and pepper chromatin	Clear cells, round nuclei, perinuclear halos, perivascular rosettes	Clear cells, dark nuclei, "chicken wire" vasculature	Highly cellular, small, round, primitive/embryonal cells
High grade features	Uncommon	Uncommon	Common	Common	Common
IHC hallmark	Synaptophysin + GFAP +/- Ki-67 <5%	Synaptophysin + GFAP - Ki-67 <5%	GFAP + EMA + (dot-like) Vimentin ++ Ki-67 <5%	IDH-1 (R132H) +/- Olig2 + Synaptophysin +/- Ki-67 variable	Synaptophysin ++ NSE ++ Vimentin ++ Ki-67 high (>20%)
Genetic hallmark	Preserved <i>MYC</i> status, no 1p/19q loss, no <i>IDH1</i> mutation, possible <i>TP53</i> mutation	Gain of chromosome 7	Loss of chromosome 22	Dual 1p/19q loss	Isochromosome 17q, <i>MYC</i> rearrangement

cLNC, cerebellar liponeurocytoma; WHO, World Health Organization; IHC, immunohistochemistry; GFAP, glial fibrillary acidic protein; EMA, epithelial membrane antigen; IDH-1, isocitrate dehydrogenase 1; NSE, neuron-specific enolase.

cerebellum should be approached cautiously and cLNC should always be included in its differential diagnosis. Despite clear cell morphology, oligodendroglioma lacks the extensive neuronal differentiation or lipidization that is found in cLNC. Similarly, clear cell ependymoma is generally strongly immunoreactive to GFAP, lacks lipid-laden cells, and histologically presents with higher-grade nuclear features.

When studied with immunohistochemistry, cLNC is immunoreactive with the most commonly used neuronal markers (i.e., neuron-specific enolase, synaptophysin, Neu-N, chromogranin A, and MAP-2). Glial differentiation and GFAP expression when present are limited. Cases with skeletal muscle differentiation, albeit uncommon, may show desmin expression.<sup>6</sup> The Ki-67 proliferation index for cLNC is generally significantly lower than that for medulloblastoma and other high grade mimics, typically <5%.<sup>7</sup> In many cases a low mitotic rate and low Ki-67 proliferation index can be used to exclude medulloblastoma as a likely consideration when histological diagnosis is less clear.

Although current literature tends to use histologic and molecular markers for neurocytomas to classify cLNC, recent studies question this practice and suggest that cLNC may have an alternative genetic pathogenesis. In central neurocytoma, polysomic gain of chromosome 7 is found frequently and isolated loss of 1p and 19q have also been reported.<sup>8</sup> In extraventricular neurocytomas, dual 1p/19q loss and particularly t(1;19)(q10;p10), is observed and has been associated with atypical histologic features and increased mitotic activity.<sup>9</sup> It should be noted that dual 1p/19q loss is considered the genetic hallmark of oligodendroglioma and is not seen in central neurocytoma. In contrast to central and extraventricular neurocytoma, there are no detailed cytogenetic reports of cLNC tumors.

In the case presented here, there was no evidence of 1p/19q co-deletion, *N-MYC* or *EGFR* amplification, *MYC* or *EWSR1* rearrangements, or *PTEN* deletion. Cytogenetic studies detected three to six copies each of chromosomes 1, 2, 7, 8q, 10, 19, and 22q. In addition to preserved *MYC* status, detailed cluster DNA analyses was used to distinguish cLNC from medulloblastoma. Typically cLNC lacks isochromosome 17 or mutations of the beta-catenin (*CTNNB1*), *PTCH* or adenomatous polyposis coli (*APC*) genes which are often found in medulloblastoma.<sup>2,10</sup> Unlike astrocytic tumors, *IDH1* mutation is not commonly present in cLNC and there was no *IDH1* mutation in codon 132 in the case presented here. *TP53* mutations are seen in 20% of the cLNC cases, although not in the case described above, which is a higher rate than in medulloblastoma and usually not found in central neurocytoma.<sup>10</sup> Recent data show the upregulation of

*FABP4*, a gene primarily expressed in adipocytes and macrophages. Unfortunately most of these molecular markers are not available to clinical testing. The specificity or prognostic significance of these finding remains to be determined, although it appears likely that cLNC is a genetically distinct entity from other forms of neurocytoma. We recommend that role of FISH studies in the diagnosis of cLNC is to test for clinically relevant genetic abnormalities known to be associated with histologic mimics of cLNC as their absence could be of tremendous diagnostic and prognostic value (Table 1).

According to the WHO classification, cLNC is considered a low-grade lesion; however, long-term follow-up of patients diagnosed with this tumor is imperative. Recent research suggests that the recurrence rate for cLNC may be much higher than previously believed-as high as 40% within 12 years for patients treated surgically.<sup>2</sup> Currently, the standard of care for treating these tumors involves surgical resection and serial neuroimaging. Although evidence is limited, some clinicians advocate adjuvant radiotherapy in cases of subtotal resection or recurrence if reoperation is not possible.<sup>5</sup> Like most primary intracranial neoplasms, extra cranial metastasis is rare and only one case of distant metastases has been reported in the literature. There are currently no accepted histologic features of cLNC that can be relied on to indicate a more aggressive nature of increased likelihood of recurrence. Atypical features including high proliferative index, necrosis, high mitotic activity, and prominent vascular hyperplasia may warrant a close clinical follow-up, although these findings have not yet been correlated with clinical outcome. It remains to be elucidated whether these atypical features are truly predictive of a more malignant biologic behavior since some tumors recur in the absence of atypical histopathology.

This case report is the first complete description of the clinical, radiographic, histologic, immunohistochemical and genetic findings of cLNC. Although no one immunohistochemical marker, genetic profile or histologic feature distinguishes cLNC, a constellation of findings from multiple modalities can be used to correctly diagnosis this lesion. Further study of cLNC will be required to better understand its pathophysiology, identify a unique diagnostic indicator and perhaps find a cure for this rare brain tumor.

### Conflicts of Interest

No potential conflict of interest relevant to this article was reported.

## REFERENCES

1. Bechtel JT, Patton JM, Takei Y. Mixed mesenchymal and neuroectodermal tumor of the cerebellum. *Acta Neuropathol* 1978; 41: 261-3.
2. Nishimoto T, Kaya B. Cerebellar liponeurocytoma. *Arch Pathol Lab Med* 2012; 136: 965-9.
3. George DH, Scheithauer BW. Central liponeurocytoma. *Am J Surg Pathol* 2001; 25: 1551-5.
4. Louis DN, Ohgaki H, Wiestler OD, et al. The 2007 WHO classification of tumours of the central nervous system. *Acta Neuropathol* 2007; 114: 97-109.
5. Jenkinson MD, Bosma JJ, Du Plessis D, et al. Cerebellar liponeurocytoma with an unusually aggressive clinical course: case report. *Neurosurgery* 2003; 53: 1425-7.
6. Gonzalez-Campora R, Weller RO. Lipidized mature neuroectodermal tumour of the cerebellum with myoid differentiation. *Neuropathol Appl Neurobiol* 1998; 24: 397-402.
7. Oudrhiri MY, Raouzi N, El Kacemi I, et al. Understanding cerebellar liponeurocytomas: case report and literature review. *Case Rep Neurol Med* 2014; 2014: 186826.
8. Taruscio D, Danesi R, Montaldi A, Cerasoli S, Cenacchi G, Giangaspero F. Nonrandom gain of chromosome 7 in central neurocytoma: a chromosomal analysis and fluorescence in situ hybridization study. *Virchows Arch* 1997; 430: 47-51.
9. Rodriguez FJ, Mota RA, Scheithauer BW, et al. Interphase cytogenetics for 1p19q and t(1;19)(q10;p10) may distinguish prognostically relevant subgroups in extraventricular neurocytoma. *Brain Pathol* 2009; 19: 623-9.
10. Horstmann S, Perry A, Reifenberger G, et al. Genetic and expression profiles of cerebellar liponeurocytomas. *Brain Pathol* 2004; 14: 281-9.

